Function and Regulation of TRPP2 and TRPP3, and identification of pore gates of TRP channels

by

Wang Zheng

A thesis submitted in partial fulfillment of the requirements for the degree of

Doctor of Philosophy

Department of Physiology
University of Alberta

ABSTRACT

The transient receptor potential (TRP) superfamily of cation channels is composed of eight subfamilies, TRPC/V/M/P/ML/A/N/Y, and play distinct sensory roles in response to various environmental stimuli. TRPP2, or polycystin-2, is mutated in autosomal dominant polycystic kidney disease (ADPKD). Recent studies have shown that protein dosage alterations play a critic role in cyst formation and disease progression, but mechanisms controlling TRPP2 expression remain incompletely characterized. TRPP3, or polycystin-L, is a homologue of TRPP2 but itself is not involved in ADPKD. It is a cation channel activated by calcium and protons. How TRPP3 channel function is regulated remains poorly understood. Despite structures of several TRP channels have recently been determined, how their pore gates, which control pore opening or closing, function and whether they share conserved gate residues(s) have remained elusive.

In Chapter 2, we found that TRPP2 is translationally up-regulated by endoplasmic reticulum (ER) stress. Using cultured mammalian cells, we first showed that TRPP2 protein expression is up-regulated by ER stress which increases phosphorylation of eukaryotic initiation factor 2α (P-eIF2α). Increasing and reducing P-eIF2α was then found to increase TRPP2 expression and suppress ER stress-induced TRPP2 up-regulation, respectively. PCR and polysome-binding assays showed that ER stress does not affect the TRPP2 mRNA level but increases its binding to ribosomes. By mutation analyses, we found that an upstream open reading frame in the 5'-untranslated region (5'UTR) of TRPP2 mRNA represses TRPP2 translation and mediates ER stress-induced up-regulation.

In Chapter 3, we identified far upstream element-binding protein 1 (FUBP1) that binds the 3'UTR of TRPP2 mRNA and suppresses its translation. Using dual-luciferase assays, we first

identified nucleotides 691-1044 (called 3FI, located in the 3'UTR of TRPP2 mRNA) that represses the expression of luciferase. Using pull-down assays and mass spectrometry we identified FUBP1 as a 3FI-binding protein. *In vitro* over-expression of FUBP1 reduced the expression of TRPP2 protein but not mRNA. In embryonic zebrafish, FUBP1 knock-down by morpholino injection increased TRPP2 expression and alleviated tail curling caused by morpholino-mediated knock-down of TRPP2. Conversely, FUBP1 over-expression by mRNA injection significantly increased pronephric cyst occurrence and tail curling. Furthermore, FUBP1 binds directly to eIF4E-binding protein 1, indicating a link to the translation initiation complex.

In Chapter 4, we identified a novel TRPP3 C-terminal domain critical for its trimerization and channel function. By SDS-PAGE, blue native PAGE and mutagenesis we first identified a novel C-terminal domain, called C1 (K575-T622), involved in stronger homo-trimerization of TRPP3 than the non-overlapping C-terminal coiled-coil 2 (CC2) domain which was reported to be important for TRPP3 trimerization. By electrophysiology and *Xenopus* oocyte expression, we found that C1, but not CC2, is critical for TRPP3 channel function. Co-immunoprecipitation and dynamic light scattering experiments further supported involvement of C1 in trimerization. Further, C1 acted as a blocking peptide that inhibits TRPP3 trimerization as well as TRPP3 and TRPP3/PKD1L3 channel function.

In Chapter 5, we found that TRPP3 channel function is regulated by N-terminal domain palmitoylation and phosphorylation. By *Xenopus* oocyte electrophysiology, we first found that Cys-38 residue is functionally important. We then found that TRPP3 channel activity was inhibited by the palmitoylation inhibitor 2-bromopalmitate and rescued by the palmitoylation substrate palmitic acid. By acyl-biotin exchange assays, we showed that TRPP3, but not mutant

C38A, is indeed palmitoylated. When Thr-39 was mutated to Asp or Glu to mimic phosphorylation, TRPP3 function was significantly reduced. Furthermore, TRPP3 N-terminus displayed double bands in which the upper band was abolished by λ phosphatase treatment or T39A mutation.

In Chapter 6, we investigated gate residues within the distal fragment of helix S6 of TRPV/P/M/C channels based on *Xenopus* oocyte electrophysiology and hydrophobic gate theory. We found that channel activity drastically increases when TRPV6-Ala616, -Met617, TRPP3-Leu557 or -Ala558, but not any of their proximate residues, was changed to hydrophilic residues. Further mutation studies showed that channel activity strongly correlates with hydrophilicity and inversely with size of residues at these sites, suggesting that TRPV6-Ala616/-Met617 and TRPP3-Leu557/-Ala558 serve as gate residues. Similar studies only identified a single-residue gate in TRPP2(Leu677), TRPM8(Val976) and TRPC4(Iso617). Our identified double consecutive or single gate residues were all hydrophobic and were within motif "LIAM".

In summary, our studies constitute valuable contributions to understanding the function and regulation of TRPP2 and TRPP3, and the nature of TRP channel gates.

PREFACE

Chapter 2 of this thesis has been published as 'Translational up-regulation of polycystic kidney disease protein PKD2 by endoplasmic reticulum stress' in ***FASEB Journal***, 27, 4998-5009, 2013

Jungwoo Yang, Wang Zheng, Qian Wang, Carlos Lara, Shaimaa Hussein and Xing-Zhen Chen

Jungwoo Yang and I contributed equally to this paper;

In this paper, I performed the end-point RT-PCR and real-time RT-PCR experiments, the polysome assays, luciferase plasmids contruction and dual-luciferase assays. I also actively participated in the writing of the first version of the manuscript and in preparation of revisions. Conceived and designed the experiments: JWY, WZ and XZC. Performed the experiments: JWY, WZ, QW, CL and SH. Analyzed the data: JWY, WZ, QW, CL and SH and XZC. Wrote the paper: JWY, WZ and XZC.

Chapter 3 of this thesis has been published as 'Far upstream element-binding protein 1 binds the 3' untranslated region of PKD2 and suppresses its translation' in ***Journal of the American Socity of Nephrology***, 27, 2645-2657, 2016

Wang Zheng, Fan Shen, Ruikun Hu, Birbickram Roy, Jungwoo Yang, Qian Wang, Fan Zhang, Jennifer C. King, Consolato Sergi, Song-Mei Liu, Emmanuelle Cordat, Jingfeng Tang, Ying Cao, Declan Ali and Xing-Zhen Chen

I and Fan Shen contributed equally to this paper;

In this paper, I designed and performed the major parts of the experiments, including all the luciferase plasmids contruction and dual-luciferase assays, RNA pull-down assay and mass spectrometry to identify FUBP1, RNA-protein immunoprecipitation, GST pull-down,

participation in zebrafish experiments, and wrote the first version of the manuscript and was deeply involved in revisions

Conceived and designed the experiments: WZ, CS, SML, EC, TY, DA and XZC. Performed the experiments: WZ, FS, RKH, BR, JWY, QW, FZ and JCK. Analyzed the data: WZ, CS, SML, EC, TY, DA and XZC. Wrote the paper: WZ and XZC

Chapter 4 of this thesis has been published as 'A novel PKD2L1 C-terminal domain critical for trimerization and channel function' in ***Scientific Reports***, 5:9460. Doi: 10.1038/srep09460, 2015 Wang Zheng, Shaimaa Hussein, Jungwoo Yang, Jun Huang, Fan Zhang, Samuel Hernandez-Anzaldo, Carlos Fernandez-Patron, Ying Cao, Hongbo Zeng, Jingfeng Tang and Xing-Zhen Chen

I and Shaimaa Hussein contributed equally to this paper;

In this paper, I conceived the main idea that C1 is functionally important to TRPP3 trimerization, designed and performed parts of the experiments, including all the non-reducing SDS-PAGE, blue-native SDS-PAGE, co-immunoprecipitation, C-terminal peptide expression and purification from E. *coli*, dynamic light scattering experiment, plasmid contruction for blocking peptide expression, wrote the first version of the manuscript and was deeply involved in revisions.

Conceived and designed the experiments: WZ, CFP, YC, HBZ, JFT and XZC. Performed the experiments: WZ, SH, JWY, JH, FZ and SHA. Analyzed the data: WZ, CFP, YC, HBZ, JFT and XZC. Wrote the paper: WZ and XZC.

Chapter 5 of this thesis has been published as 'Regulation of TRPP3 channel function by N-terminal domain palmitoylation and phosphorylation' in ***Journal of Biological Chemistry***, 291, 25678-25691

Wang Zheng, Jungwoo Yang, Erwan Beauchamp, Ruiqi Cai, Shaimaa Hussein, Laura Hofmann, Qiang Li, Veit Flockerzi, Luc G. Berthiaume, Jingfeng Tang and Xing-Zhen Chen

In this paper, Jungwoo and I first identified C38, but not any of other cysteine residues located in extracellular or intracellular parts, to be functionally important. Then, Shaimma reminded me that C38 could be a palmitoylation site. Fllowing the suggestion, I designed and performed the experiments involving 2BP and PA treatment s. I also designed and performed parts of experiments, including acyl-biotin exchange assay, confocal immunofluorescence, T39 phosphorylation and the relationship between C38 palmitoylation and T39 phosphorylation. Besides, I wrote the first version of the manuscript and was deeply involved in revisions.

Conceived and designed the experiments: WZ, VF, JT, LB and XZC. Performed the experiments: WZ, JY, EB, RQC, SH, LH and QL. Analyzed the data: WZ, VF, JT, LB and XZC. Wrote and revised the paper: WZ and XZC.

Chapter 6 of this thesis is ready to be submitted as 'Unconventianal double-residue pore gates in transient receptor potential channels'

Wang Zheng, Ruiqi Cai, Laura Hofmann, Qiaolin Hu, Jingfegn Tang, Veit Flockerzi, and Xing-Zhen Chen

In this paper, I first conceived the idea that TRP channels contain conserved hydrophobic gate. As the project goes on, Dr. Chen and I coined the concept of double-residue gate. The experiments I designed and performed includes generation of most mutants, two-electrode voltage clamp, biotinylation assay. Besides, I wrote the first version of the manuscript and was involved in revisions.

Conceived and designed the experiments: WZ, JT, VF and XZC. Performed the experiments: WZ, RC, LH and QH. Analyzed the data: WZ, JT, VF and XZC. Wrote the paper: WZ and XZC.

ACKNOWLEDGMENTS

I am very lucky to get so much help and inspiration from all the people around me during my PhD studies. I want to give them my warmest thanks.

First of all, I would like to thank my supervisor, Dr. Xing-Zhen Chen, for all his great help and support during my research. I learned so much through our enjoyful discussions. Also, he offers me extremely encouragement during my toughest time. Most importantly, he gives me enough freedom to explore what I am truly interested in, which builds my aspiration to be a scientist. Without this, it would have been impossible for me to attain these achievements. In addition, he has always been helpful in my personal life.

I also want to specially thank my supervisory committee members, Dr. James Young and Dr. Emmanuelle Cordat. They are always helpful and encourageous throughout my PhD studies. My thanks also go to Dr. Peter Light and Dr. Christophe Altier, my external examiners, for their effort and support to my thesis defense.

I also would like to thank my previous and current lab members, including Jungwoo Yang, Carlos Lara, Shaimaa Hussein, Qian Wang, Ruiqi Cai, Qiaolin Hu, Xiong Liu, for their help and friendship. I enjoyed every invaluable discussion with them. In addition, I want to thank Deb O'Neill. She was always there for help and advice whenever I needed it.

Besides, I want to thank all supporting staff in our department, including Dr. Greg Funk, Debbie O'Neill, Sharon Orescan, Kim Sawada, Donna Simpson, and Dominique Burlot. I am also very grateful to have been part of the membrane protein disease research group (MPDRG) for the past six years.

Last but not the least, I am extremely grateful to my wife for all her love and support.

TABLE OF CONTENTS

LIST OF FIGURES

LIST OF ABBREVIATIONS

2-ME	2-mercaptoethanol
3'UTR	3' untranslated region
4EBP	eIF4E-binding proteins
5'UTR	5' untranslated region
ADPKD	autosomal dominant polycystic kidney disease
ADPR	adenosine diphosphate ribose
APT	acyl-protein thioesterase
ASIC	acid sensing ion channel
ATF4	activating transcription factor 4
ATF6	activating transcription factor 6
Bicc1	bicaudal C 1
BN- PAGE	blue native PAGE
BSA	bovine serum albumin
CC2	coiled-coil 2
CHOP	C/EBP homologous protein
Co-IP	co-immunoprecipitation
cryo-EM	cryo-electron microscopy
CT	C-terminus
Ctrl	control
DHHC	Asp-His-His-Cys
DLS	dynamic light scattering
DMEM	dulbecco's modified Eagle's medium

DMSO	dimethyl sulphoxide
dpf	day post-fertilization
DTT	dithiothreitol
EGTA	ethylene glycol tetraacetic acid
eIF2α	eukaryotic translation initiation factor 2α
eIF4E	eukaryotic translation initiation factor 4E
eIF4G	eukaryotic translation initiation factor 4G
ER	endoplasmic reticulum
ESRD	end stage renal disease
FBS	fetal bovine serum
FIR	FUBP-interacting repressor
FUBP1	far upstream element-binding protein 1
FUSE	far upstream element
GADD34	growth arrest and DNA damage-inducible protein
GAP43	growth-associated protein 43
GCN4	general control protein 4
GFP	green fluorescence protein
GPS	G protein-coupled receptor proteolytic site
HEK293	human embryonic kidney 293
hpf	hour post-fertilization
hr	hour
IRE1	inositol-requiring kinase 1
JEV	Japanese encephalitis virus

KD	knockdown
KH	K-homology
KO	knockout
MDCK	madin-darby canine kidney
MEF	mouse embryonic fibroblast
MO	morpholino
NEM	N-ethylmaleimide
NLS	nuclear localization sequence
NMDG	N-methyl-D-glucamine
NPM	nucleophosmin
NT	C-terminus
PABP	poly(A)-binding protein
PC1	polycystin-1
PC2	polycystin-2
PERK	protein kinase-like ER kinase
PM	plasma membrane
RBP	RNA-binding protein
RIP	RNA immunoprecipitation
RT-PCR	reverse transcription polymerase chain reaction
SCAM	substituted-cysteine accessibility method
SEM	standard error of the mean
STAT-1	signal transducer and activator of transcription-1
TM	transmembrane

TRAF2	TNF receptor-associated factor 2
TRP	transient receptor potential
uORF	upstream open reading frame
UPR	unfolded protein response
WB	western blot
WT	wild-type
XBP1	X-box binding protein 1

LIST OF MUTANTS USED IN THIS THESIS

TRPP3		**TRPP2**	**TRPV6**	**TRPM8**	**TRPC4**
ΔNT	L552N	F676N	L613N	L971S	L612N
ΔCT	L553N	L677N	L614N	V972S	L613N
4xC-A	M555N	A678N	I615N	L974S	M615N
3xC-A	F556N	I679N	A616N	L975S	L616N
C38A	L557N	F604P	M617N	V976S	I617N
ΔC1	A558N	L677K	M618N	A977S	A618N
ΔCC2	I559N	L677R	G619N	M978S	M619N
ΔC1/ΔCC2	I560N	L677D	M610S	F979S	M620N
ΔNT/ΔCT	L557K	L677E	L611S	G980S	G503S
ΔNT/T622X	L557R	L677S	L613S	V976Q	I617D
V670X	L557E	L677G	L614S	V976D	I617K
T622X	L557D	L677A	I615S	V976R	I617G
S581X	L557Q	L677V	A616S	V976A	I617A
Δ1-20	L557S	L677F	M617S	V976F	I617F
Δ1-41	L557T	L677W	M618S	V976W	I617W
Δ1-60	L557G	L678Q	G619S		G503S/I617N
Δ1-81	L557A	L678S	A616K		G503S/I617D
Δ1-95	L557V	L678T	A616E		G503S/I617K
Δ1-30	L557I	F604P/L677G	A616Q		G503S/I617A
Δ1-36	L557F	F604P/L677D	A616S		G503S/I617F
Δ1-38	L557W	F604P/L677K	A616T		G503S/I617W
Δ1-40	A558K	F604P/L677R	A616G		
V37A	A558E	F604P/L677F	A616V		
C38A	A558Q	F604P/L677Y	A616I		
V37A/C38A	A558S	F604P/L677W	A616F		
C69A/C70A	A558T		A616Y		
C74A	A558G		A616W		
C210A	A558V		M617K		
C223A	A558I		M617E		
C512A	A558L		M617Q		
T34E	A558F		M617S		
S41E/S42E/T43E	A558W		M617T		
T39E	L557N/A558W		M617G		
T39D	L557W/A558N		M617A		
T39A			M617W		
C38A/T39A			A616N/M617W		
C38A/T39E			A616W/M617N		

CHAPTER 1

INTRODUCTION

1.1 Transient receptor potential (TRP) superfamily

The discovery of TRP channels was related to a channelopathy in fruit fly, *Drosophila melanogaster*. When studying phototransduction events, Cosens and Manning (1969) identified a spontaneously occurring *Drosophila* mutant with an abnormal response to light stimuli [1], e.g., the photoreceptor potential shows a transient response during prolonged illumination, which is in contrast to the sustained response in wild-type (WT) flies. This mutant strain was therefore called *trp* standing for transient receptor potential. After twenty years, this finding lead to the molecular indentification of the first TRP ion channel from *Drosophila* [2]. Later, the vertebrate counterparts were identifed with ubiquitous expression in various tissues and cell types. Accumulated evidence have showed that TRPs mostly forms non-selective cation channels and are involved in various sensory physiology, including detection of changes in light, pH, osmolarity, tempetature, tastants, pheromones and mechanical stimuli [3,4]. Mutations in TRP genes or abnormal expressions of TRP proteins have been found to linked to various human disease states, including neurodegenerative, kidney, cardiac, skeletal and chronic pain diseases [5-8].

TRP channels are predominantly found in animals. In mammals, the TRP family contains nearly 30 members divided into six subfamilies according to sequence and function similarities [9]: TRPA (ankyrin), TRPC (canonical), TRPM (melastatin), TRPML (mucolipin), TRPP (polycystin), TRPV (vanilloid). TRPN (no mechanoreceptor potential C) can be only found in non-mammals, such as worms and fish. In addition, a new TRP channel, constitutes a new subfamily known as TRPY (yeast), has been identified in yeast and other fungi [10]. The homology of TRP superfamily members is illustrated below (Fig. 1-1).

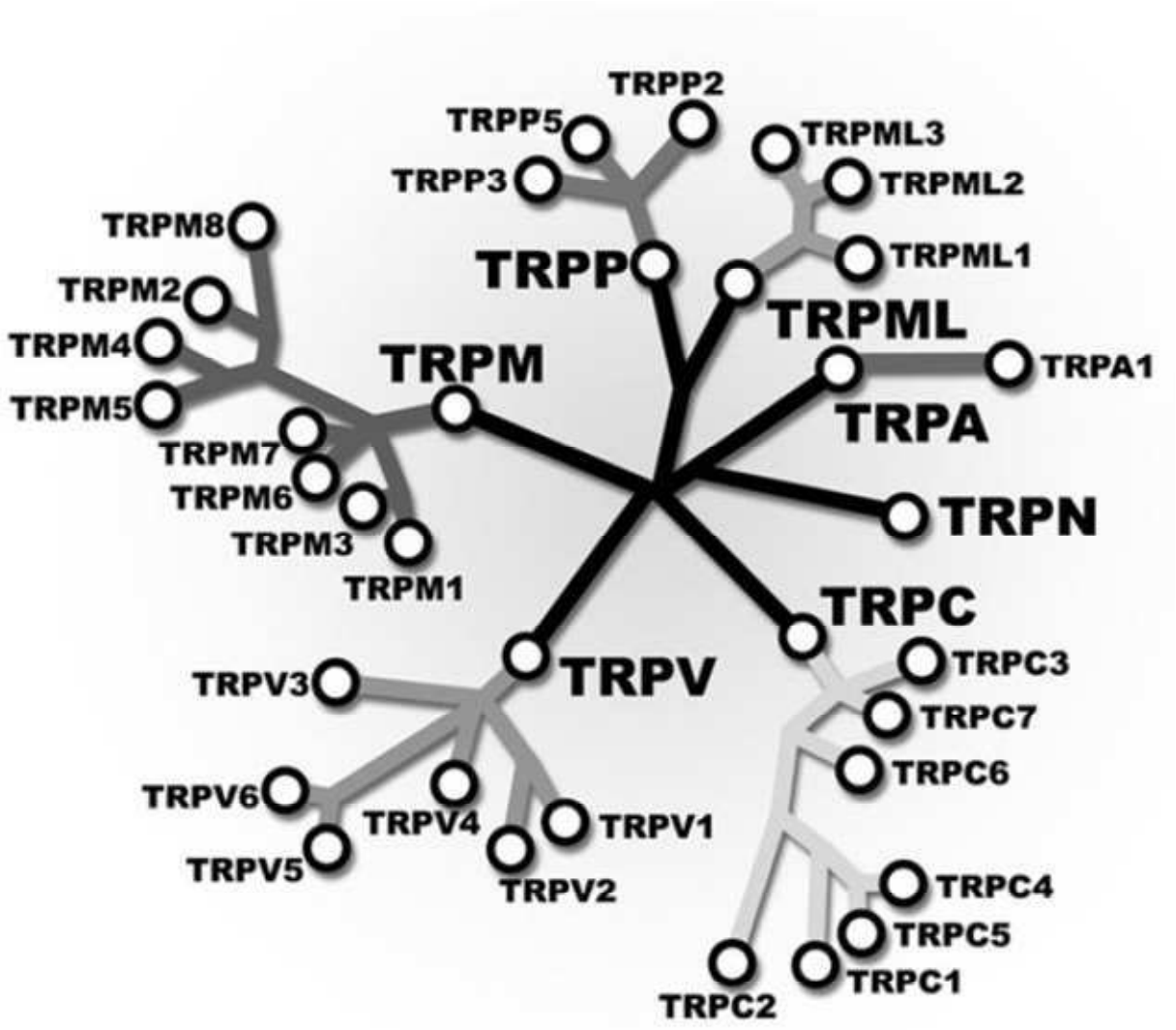

Fig. 1-1. Phylogeny of TRP channels. The phylogenetic tree shows the relationship between different TRP subfamilies. TRPN channels have only been identified in non-mammals. Adapted with permission from Latorre *et al*., *Q. Rev. Biophys.*, 2009 [11].

1.1.1 Structural features of TRP channels

As a general property, TRP channels contain six transmembrane segments (S1-S6) with intracellular N- and C-termini and a pore-forming loop between S5 and S6 (Fig. 1-2). They are different regarding the sizes or functional domains of N- and/or C-terminus [12]. A variable number of ankyrin repeats can be found in TRP channels from several subfamilies, including TRPCs (3 or 4), TRPVs (6), TRPAs (14 or 15), and TRPNs (29) [13]. TRPMs have a unique TRPM homology domain, composed of four consecutive amino acids, in the N-terminus. In subfamilies of TRPVs, TRPCs and TRPMs, a highly conserved TRP domain in the C-terminus contributes to channel gating and PIP2 regulation [14,15]. Some TRP channels contain a C-terminal enzyme domain and are also called 'chenzyme'. For instance, a nudix hydrolase domain was found in the C-terminus of TRPM2 which can function as an adenosine diphosphate ribose (ADPR) pyrophosphatase [16]. TRPM6 and TRPM7 both contain an atypical α-kinase domain at the C-terminus [17,18].

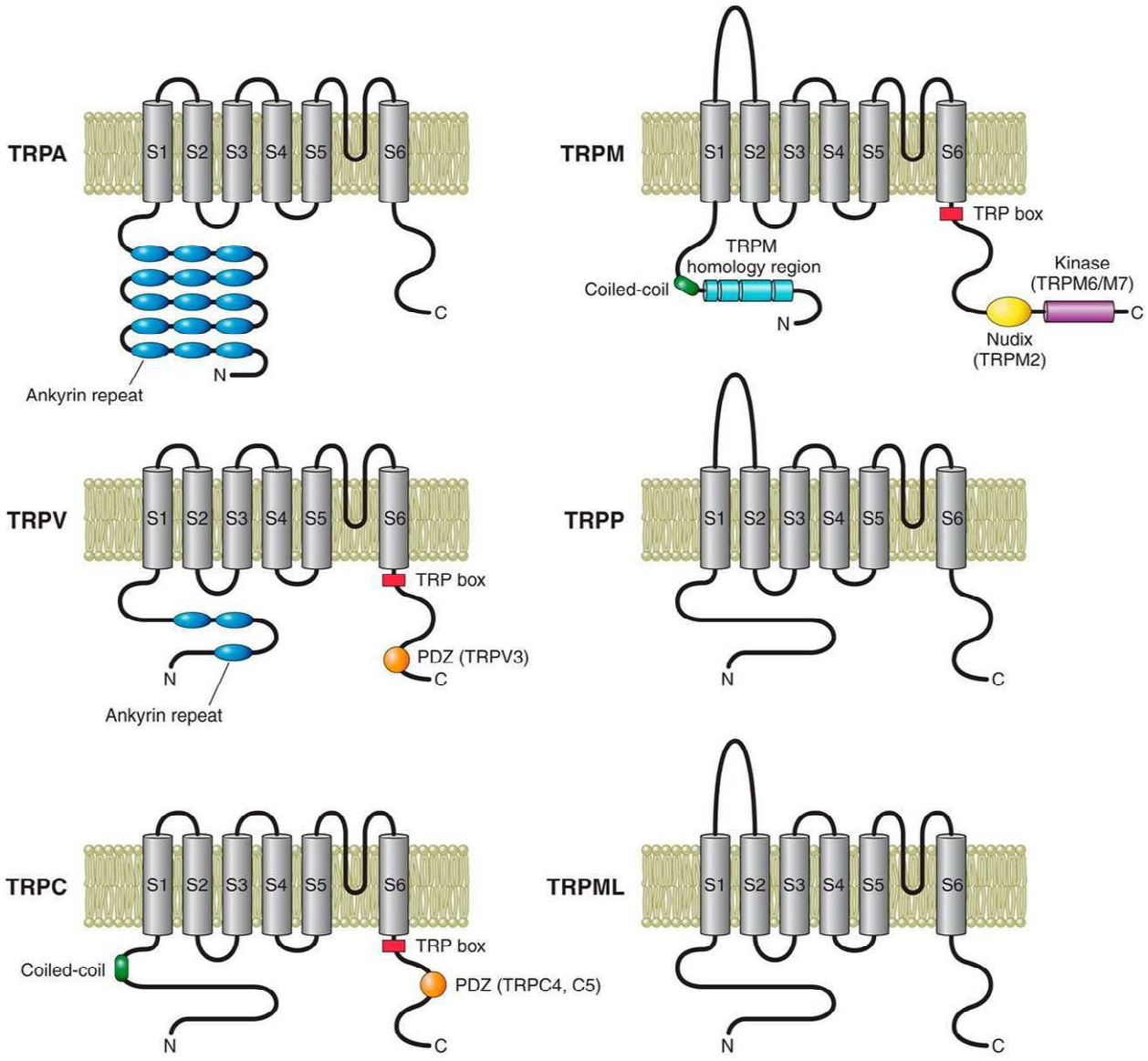

Fig. 1-2. Membrane topology and functional domains of N- and C-termini of mammalian TRP channels. All TRP channels share the same membrane topology with six transmembrane segments and intracellular N- and C-termini. The putative pore region is localized between S5 and S6. From Earley and Brayden, *Physiol Rev.*, 2015 [19] (permission is not required for this figure to be reused in a thesis).

1.1.2 Homo- and heterotetramerization

Although most TRP channels function as homotetramers, they can also form heterotetramers to fullfil different functions [20]. In TRPC subfamily, for example, TRPC4 or TRPC5 forms heterotetramers with TRPC1 [21] and TRPC3/6/7 is found in the same complex channel [22]. Moreover, TRPC3/4/5/6 form a heteromeric channels when TRPC1 is present [21]. Within the TRPV subfamily, two close homologues TRPV5 and TRPV6 can form a functional heterotetramer and TRPV1-4 assemble into heteromeric channel complexes [23]. In TRPM subfamily, TRPM6 and TRPM7 form a heteromeric channel complex which exhibits distinct biophysical and pharmacological properties compared to TRPM6 or TRPM7 homomeric channel [24]. The interaction between intracellular channels TRPML1 and TRPML3 leads to the lysosome localization of TRPML3 [25].

1.1.3 Activation mechanisms

Once being activated, TRP channels allow cations to pass across the membrane, leading to various downstream cellular responses through either depolarizing cells or initiating Ca^{2+} signaling pathways. Unlike voltage-gated cation channels, TRP channels are not responsive to voltage since they do not contain a typical voltage sensor in S4 [26]. However, TRP channels are gated by thermal, mechanical, chemical, nociceptive, and local cellular environmental stimuli in a polymodal activation manner [3,4]. While TRPV1-4 and TRPM3 are gated by high temperature, TRPM8, TRPA1, and TRPC5 are responsive to low temperature [8,27,28]. TRPC channels activation requires stimulation of phospholipase C pathway which directly activats TRPC2, TRPC3, TRPC6 and TRPC7 through diaglycerol or indirectly activated TRPC4, and TRPC5 through a mechanism yet to be determined [29,30]. Although TRPV5 and TRPV6 are considered to be

constitutively open when heterologously over-expressed, it is unknown whether endogenous TRPV5 and TRPV6 are gated by some unidentified agonists [8]. While some TRPM channels, such as TRPM6 and TRPM7, can be activated by decrease in intracellular Mg^{2+} concentration [31,32], an increase in intracellular Ca^{2+} ($[Ca^{2+}]_i$) can activate several other TRPM channels, including TRPM4 [33], TRPM5 [34] and TRPM2 [35], and TRPA1 [36]. TRPM2 is also gated by other stimuli ranging from ADPR, nicotinamide adenine dinucleotide, and oxidative stress [37-39]. Except for high temperature, various stimuli including hypo-osmotic cell swelling, rises in $[Ca^{2+}]_i$, D-erythro-sphingosine can also activate TRPM3 [40-43]. The diverse activation mechanisms of TRPs confer their various functions under physiological and pathological conditions.

1.1.4 High-resolution structures

Thanks to breakthroughs in technique of cryo-electron microscopy (cryo-EM), we have gained lots of insights into the molecular mechanisms of TRP channel gating and regulation during the past four years with structural analysis. High-resolution structures of several full-length TRP members have been determined, including TRPV1 [44-46], TRPA1 [47], TRPV2 [48,49], TRPV6 [50] and TRPP2 [51]. More TRP structures are believed to come in the future. TRPV1 is the first mammalian ion channel whose full-length structure has been resolved with resolution within 3.5 Å using cryo-EM (Fig. 1-3A) [44], which opens an exciting new ear for structural studies of membrane proteins. Similar to voltage-gated potassium channels, TRPV1 forms a tetramer with S1-S4 reside in the peripheral to support the central pore domain formed by S5-loop-S6 (Fig. 1-3B). The C-terminal conserved TRP domain was unexpectedly revealed to interact with both pre-S1 domain and S4-S5 linker (Fig. 1-3C) and these intramolecular interactions are necessary for conformational changes leading to the pore open induced by agonists.

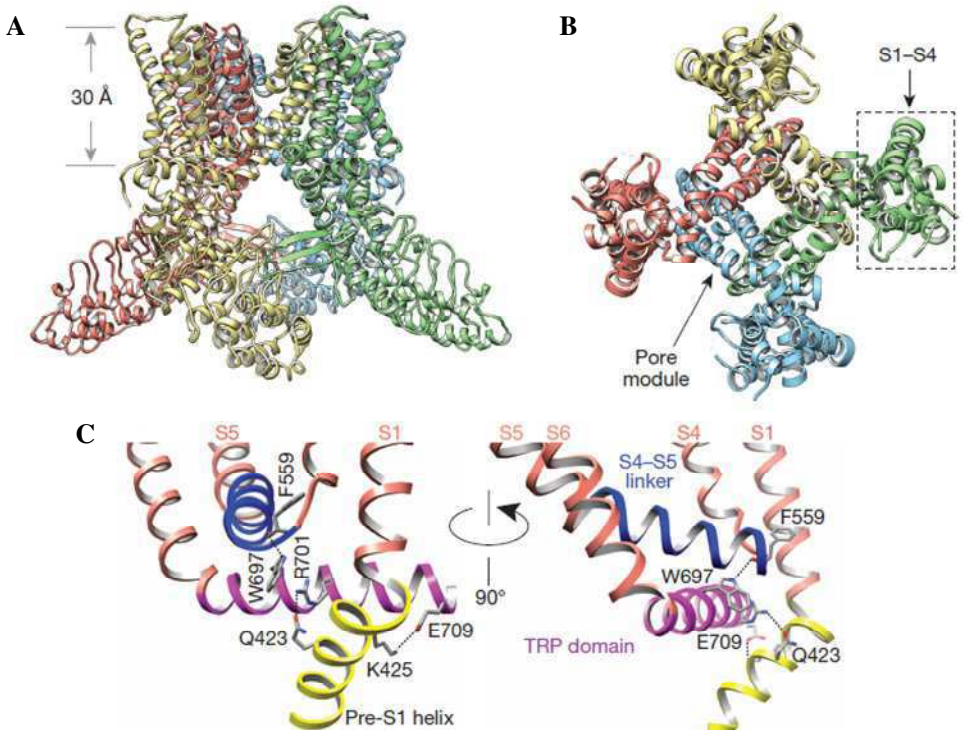

Fig. 1-3. Diagram of overall rat TRPV1 structure and interactions among TRP domain, pre-S1 domain and S4-S5 linker. Reused, with permission, from Liao *et al*., *Nature*, 2013 [44]

1.1.5 TRP channelopathy

Traditionally, channelopathies are diseases caused by mutations in the genes encoding ion channels which lead to altered functions of channel proteins. To date, only a few TRP channelopathies have been established if following this definition, such as segmental glomerular sclerosis (TRPC6) [52], autosomal dominant polycystic kidney disease (ADPKD, TRPP2) [53], and scapuloperoneal spinal muscular atrophy (TRPV4) [54]. However, accumulated genetic evidences have showen that most TRP members are involved in various diseases, including chronic pain and overactive bladder (TRPV1), chronic cough (TRPA1 and TRPV1), diabetes (TRPV1 and TRPM4), obesity (TRPV4 and TRPM5), chronic obstructive pulmonary disease (TRPV4),

cardiac hypertrophy (TRPC6), familial Alzheimer's disease (TRPM7), Olmsted syndrome (TRPV3) and cancer (TRPC6, TRPV2 and TRPM8) [5,6,55].

1.1.6 Mice models deficient in TRP channels

Although channel functions of TRP channels have been thoroughly studies with heterologous expression systems, including *Xenopus laevis* oocytes and mammalian cell lines, and provided valuable clues about their physiological functions, the exact *in vivo* functions of most individual TRP channels, if not all, still remains elusive. Mice deficient in most individual TRP channels do not exhibit obvious phenotype (see [56] for a detailed review). This is probably because many TRP channels have overlapping functions and thus form a complex conpensatory network. Therefore, it would be interesting to generate double knockout or even triple knockout mice with deficiency of functionally related TRP channels. Besides, since lots of gain-of-function mutations in TRP genes have been identified to be linked to human diseases [5,6], it would provide meaningful information by generating knockin mice containing well-studied gain-of-function mutations using recently developed CRISPR-cas9 technology.

1.2 ADPKD

ADPKD is one of the most common genetic diseases affecting 0.2% population worldwide [53,57]. ADPKD is characterized by fluid-filled cyst formation in both kidneys which leads to a gradual decline in renal function and ultimately approximately 50% patients develop end stage renal disease (ESRD) around the age of 55 years which accounts for up to 10% of the ESRD cases [58]. The disease is a systematic disease with hypertension, cardiac valvular abnormalities, cerebral aneurysms and cysts in liver and pancreas as extra-renal manifestations [59]. There is no effective drug been approved so far for ADPKD treatment by U.S. Food and Drug Administration.

1.2.1 Genetics of ADPKD

85% of ADPKD is caused by mutations in the *PKD1* gene, encoding the protein polycystin-1 (PC1, also called PKD1). The remaining 15% of the disease is caused by mutations in the *PKD2* gene, encoding polycystin-2 (PC2, also called PKD2 or TRPP2) [60-62]. The *PKD1* gene, containing 46 exons, is located on chromosome 16 and transcripted into a large 14.1 kb mRNA. In comparison, *PKD2* gene is composed of 15 exons and encodes a relatively short mRNA transcript of 5.1 kb. Pathogenic mutations have been identified throughout the entire gene of *PKD1* and *PKD2* and no mutation hot spot has been found [63].

1.2.2 Polycystin proteins

PC1 protein is a transmembrane protein of 4303 amino acids containing a large extracellular N-terminus, 11 transmembrane segments and a short intracellular C-terminus (Fig. 1-4) [64]. Many functional domains have been identified in the extracellular N-terminal domain

and some are shown to be implicated in protein-protein interactions. A G protein-coupled receptor proteolytic site is identified in the N-terminus and its cleavage is required to induce tubulogenesis *in vitro* [65]. The structure of the last six transmembrane segments resembles that of TRP channels. A coiled-coil domain in the cytoplasmic C-terminus of PC1 was proposed to interact with PC2 [66]. In addition, the C-terminus has also been shown to contain two cleavage sites which, once cleaved, generate two products to regulate gene expression through interacting with transcription factors, β-catenin or STAT6 and translocation into the nucleus [67,68].

PC2, also called PKD2 or TRPP2, is a membrane protein of 968 amino acids. It is the founding member of polycystin subfamily of TRPs and acts as a nonselective cation channel permeable to Ca^{2+}, K^{+} and Na^{+} [69,70]. Similar to other TRP channels, TRPP2 contains six putative transmembrane segments and cytoplasmic N- and C-termini. The C-terminus contains a coiled-coil domain to interact with PC1 (Fig. 1-4) [65].

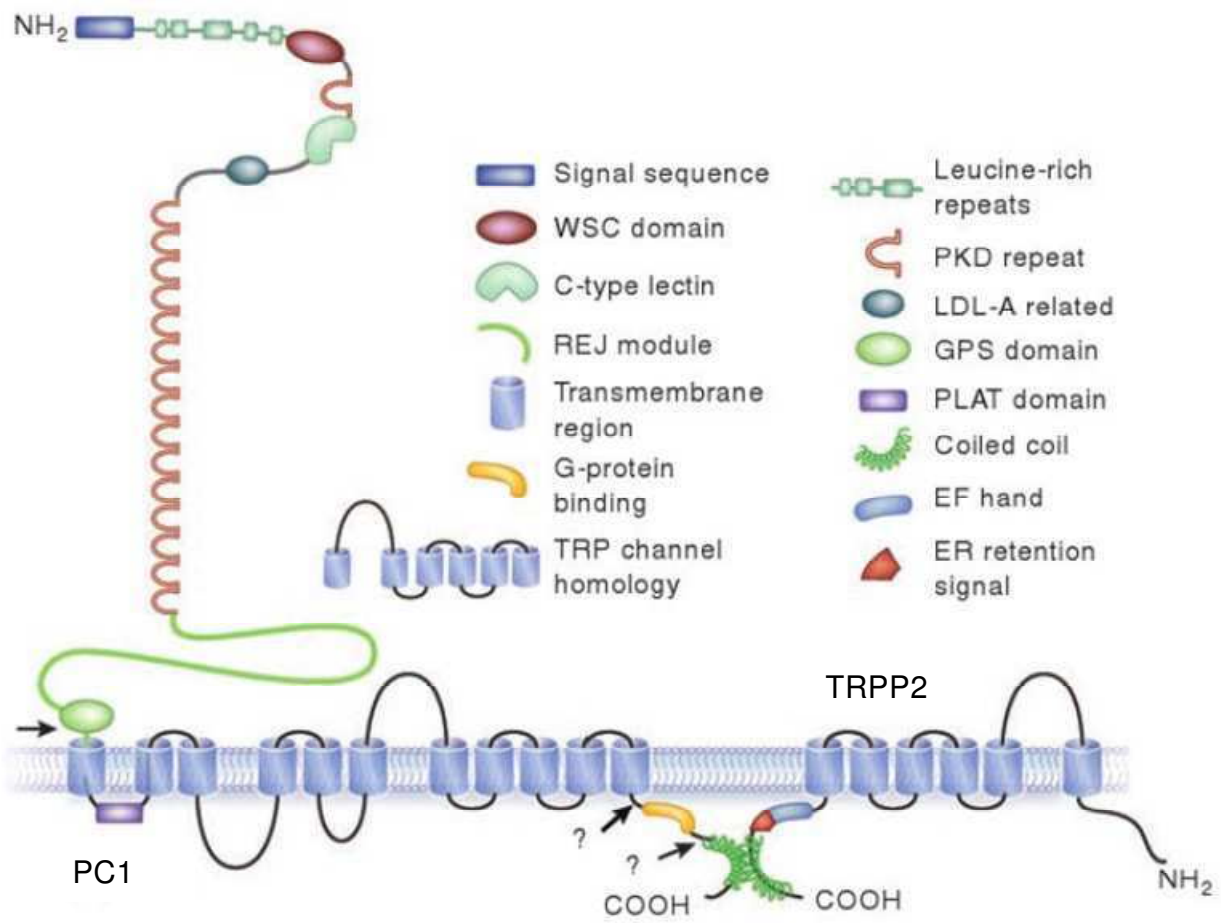

Fig. 1-4. Diagram of the PC1 and TRPP2 proteins. PC1 and TRPP2 are assumed to form a complex through coiled-coil domains in the C-terminus. Functional domains in N- and C-termini and regions of homology are shown. The arrows indicate the cleavage sites in the N-terminus (GPS site) and C-terminus of PC1. Adapted with permission from Torres and Harris, *Kidney Int.*, 2009 [71].

Although not identical, the tissue expression of PC1 and TRPP2 proteins is largely over-lapping [72,73]. At cellular level, both proteins are highly expressed in renal tubular epithelial cells in which PC1 is mainly localized in the plasma membrane (PM) and TRPP2 is found in both the PM and endoplasmic reticulum (ER) [72,74,75]. Besides, both PC1 and TRPP2 are found in the primary cilium which is a special cellular organelle protruding from the PM of non-dividing cells and exists in almost all cell types [76,77]. It is thought that the primary cilium of renal epithelial

cells protrudes into the tubule lumen to sense fluid flow , and PC1 and TRPP2 are proposed to form a channel complex to act as a mechanosensor here [78], which seems to nicely explain why mutations in either *PKD1* or *PKD2* could result in similar ADPKD phenotypes. PC1/TRPP2 complex mediates a Ca^{2+} influx upon bending of the cilium induced by fluid flow. How the influxing Ca^{2+} induces further cellular evens still remains elusive. It is worthy to note that dysfunctions of many ciliary proteins all result in renal cyst formation, suggesting that ADPKD may be a ciliapathy [79].

1.2.3 Mechanisms of cyst formation

In general, ADPKD patients carry mutations in only one allele of *PKD1* or *PKD2* gene inherited from their parents (germ-line mutation, also called 'first-hit'). The other allele functions normally. It is thought that the 50% protein level reduction of functional PC1 or TRPP2 is not enough to initiate cyst formation. Cysts can only be induced when the functional PC1 or TRPP2 level falls below the cystogenic threshold (called 'second-hit') [80,81]. This 'two-hit' model (Fig. 1-5) is supported by the fact that cysts only afftact 1% of the nephrons [82]. Although somatic mutations inactivating the normal allele were thought to be the 'second hit', they have only been identified in 20-43% of the analyzed *PKD1* or *PKD2* kidney cysts [83-86]. Over the past decade, accumulated evidence has established a "dosage" model that suggests cystogenesis is induced when the functional PC1 or TRPP2 protein expression is reduced below a threshold level by some environmental factors [87-89]. This threshold may vary in terms of species type, developmental stage, nephron segment or cell type [90-92]. In mice, 60% reduction in functional PC1 protein level only induces slowly progressive cyst formation, but 80% reduction can lead to rapidly progressive disease, supporting the correlation of polycystins dosage with disease

severity [93]. Therefore, approaches designed to promote the functional polycystin protein level may slow cyst progression. Ths is especially important considering the fact that recent clinical trials aiming to slow the cyst growth based on reported PC1 or TRPP2 signaling pathways have not been successful. Therefore, it is critical to unveil mechanisms underlying regulation of PC1 or TRPP2 expression and identify new therapeutic targets and approaches for treatment of ADPKD.

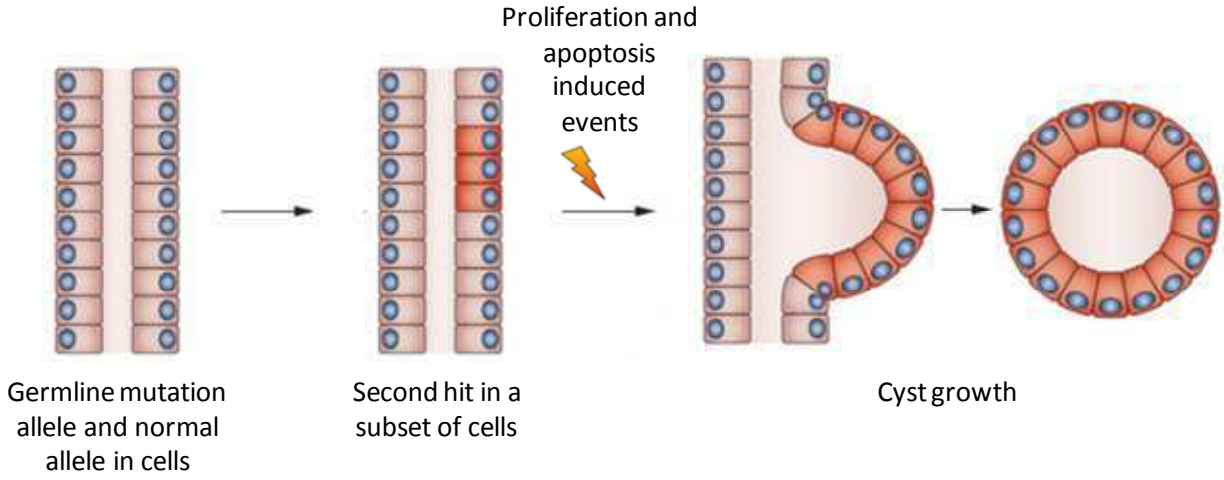

Fig. 1-5. Schematic illustration of the 'two-hit' model of cyst formation in ADPKD. All renal tubular epithelial cells contain one inheritedly mutated *PKD1* or *PKD2* allele ('first-hit') and one unaffected allele. During later life stage, a subset of cells experienced a 'second hit' (orange, either the somatic mutations resulting in inactivation of the unaffected allele or reduction of protein levels of functional PC1 and/or TRPP2), leading to aberrant regulation of many signalling pathways related to cell proliferation and apoptosis, which initiates cyst formation. Adapted with permission from Happe and Peters, *Nat. Rev. Nephrol.*, 2014 [94].

1.2.4 Molecular signaling pathways involved in ADPKD

In the cellular level, two key hallmarks of ADPKD are the increased proliferation and apoptosis of cystic cells [95-97]. Both PC1 and TRPP2 are expressed in several cellular membranes where they form homotetramer or heterotetramer complex to modulate signaling pathways

controling cell proliferation, apoptosis, adhesion, and differentiation [98]. Many abnormal signaling pathways contribute to cyst growth, including cAMP accumulation, reduced Ca^{2+} influx, activation of Ras/Raf/ERK, mTOR, PI3-kinase, and Jak2-STAT1/3 signaling (Fig. 1-6) [99-103]. Most drugs are currently designed to target to one of these signaling pathways (Fig. 1-6).

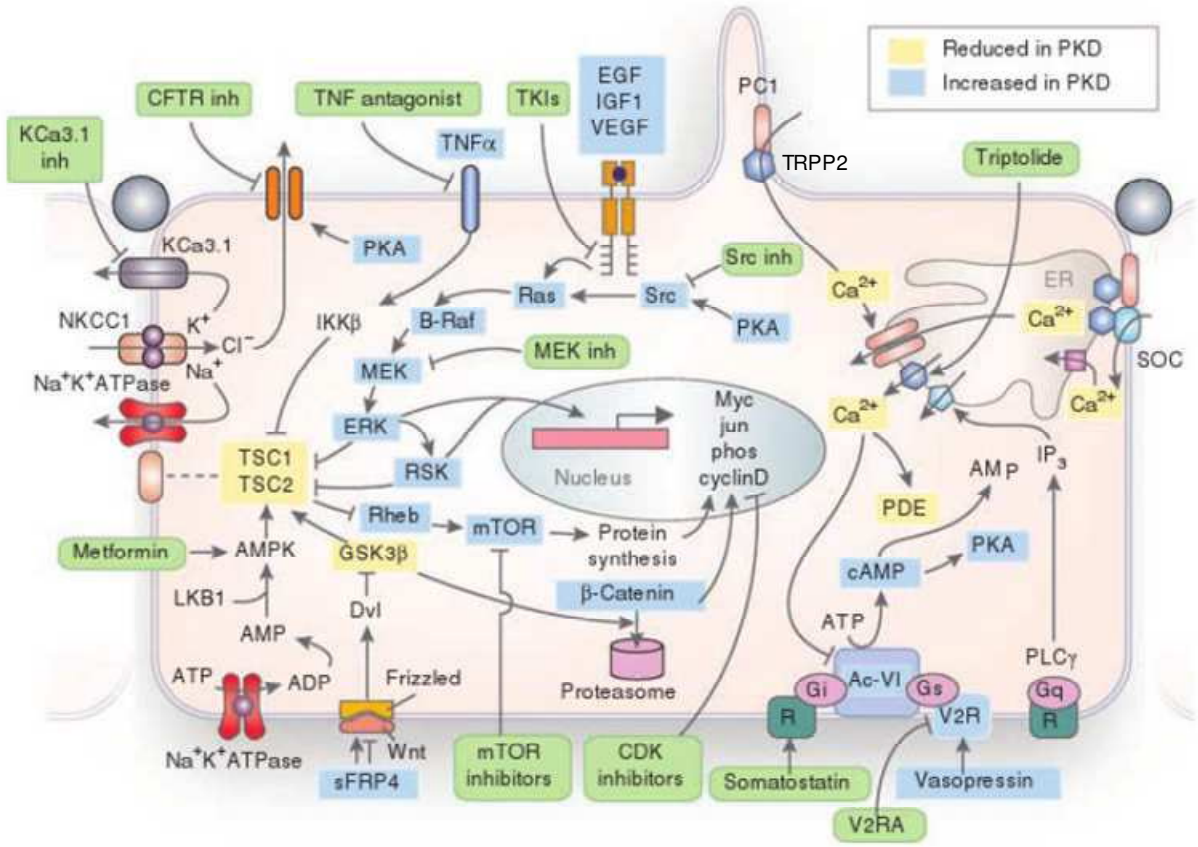

Fig. 1-6. Diagram of putative signaling pathways up- or down-regulated in ADPKD. Rationale for treatment with V2 receptor antagonists, somatostatin, triptolide, tyrosine kinase, src, MEK, TNFα, mTOR, or CDK inhibitors; metformin, and CFTR or KCa3.1 inhibitors (green boxes) are shown. Adapted with permission from Torres and Harris, *Kidney Int.*, 2009 [71].

1.3 Regulation of TRPP2 expression

During embryonic development, TRPP2 expression is tightly regulated. When examining TRPP2 expression in staged mouse embryos, Glen *et al.* [104] found that staining for TRPP2 was observed in the embryonic ectoderm and endoderm as early as on the 6th embryonic day (day E6) and at E12.5, low-intensity staining was seen in the metanephric ureteric bud. Embryos at E15.5 showed TRPP2 expression resembling the adult pattern, with low staining in proximal tubules and high level in distal tubules. Extra-renal expression sites were also observed, including multiple endocrine organs, cardiac, skeletal, and smooth muscle, and multiple mesenchymal tissues. This change of TRPP2 expression in mouse embryos supports its important role in development. To date, little is known about how TRPP2 expression is regulated during embryonic development.

Recently, some evidence suggested that expression of TRPP2 is also regulated in the adult kidney under certain circumstances. During ischemic acute renal failure, TRPP2 protein level was shown to be substantially up-regulated in damaged cells [105]. Also, when renal ischaemic injury was induced in mouse, Yan *et al.* [106] found that TRPP2 expression is increased by up to 5-fold in the post-ischaemic kidney, with the highest expression observed at 48 h post-reperfusion. In 2009, Sony *et al.* [107] reported that following ischemia reperfusion injury, cellular repair responses is influenced by TRPP2 dosage. All these data suggest that TRPP2 plays an important role in cellular repair following ischemic injury. Of note, ischemia leads to several types of cellular stresses, e.g., ER stress.

Protein level regulation takes place transcriptionally and/or translationally. With computational analysis, Irma *et al.* [108] identifed several putative binding sites in the promoter region of TRPP2 for transcription factors E2F, EGRF, ETS, MZF1, SP1 and ZBP-89. To date,

however, little experimental data has been reported about transcription factors regulating expression of TRPP2. In comparison, some reports showed that TRPP2 is translationally regulated by several mechanisms. In 2009, Huan *et al.* [109] found that microRNA-17 binds to TRPP2 mRNA 3'UTR and dow-regulates its translation. Interestingly, *Xenopus* and mice showed cystic phenotype with transgenic over-expression of microRNA-17 [110]. In 2010, Tran *et al.* [111] showed that expression of TRPP2 is regulated at the translational level by the RNA binding protein bicaudal C 1 (Bicc1), which competes with microRNA-17 for binding to the same site. Therefore, studies of TRPP2 expression regulation will provide us with novel insights into roles of TRPP2 dosage in ADPKD occurrence and might suggest new strategies for treatment of ADPKD.

1.4 Translational regulation

Compared with thoroughly studied transcriptional regulation, translational regulation has gained increasing attention. In fact, more than two thirds of genes show no direct correlation between mRNA and protein levels [112]. Translational regulation has been well established to play a critical role during development in which a specific subgroup of mRNAs is tightly controlled to be translated during a particular stage with no change in the majority of mRNAs [113-115]. Translational regulation is generally mediated by *trans*-regulatory factors (e.g., RNA-binding proteins (RBP) and non-coding RNAs) which interacts with *cis*-regulatory elements located mostly in 5' or 3' untranslated regions (UTRs). The importance of UTRs in regulating protein expression is highlighted by the findings that mutations in UTRs is involved in lots of human diseases [116].

1.4.1 5'UTR-mediated translational regulation

Generally, 5'UTR is short with nucleotides of around 100 to 220 across species [117]. Regulatory elements in 5'UTR include high GC content, secondary structure, and upstream open reading frames (uORFs). The uORF is a major regulatory element in 5'UTR and is defined by start and stop codons upstresm of the main ORF. Although uORFs generally function to inhibit protein expression of main ORF under normal conditions dur to their inhibitory effects on the scanning of ribosomes along the transcripts [118-120], it can also up-regulate protein synthesis under certain conditions. A classical example of uORF-mediated regulation comes from yeast (Fig. 1-7A). The general control protein 4 (GCN4) acts as a sensor for amino acid starvation via four uORFs in its 5'UTR. No matter what the nutritional condition is, the first uORF is always efficiently translated. Under normal codition, uORFs 2-4 are allowed to be translated since

ribosomes and initiation cofactors can be rapidly reloaded following translation of uORF1, which leads to inhibit the translation of the main ORF. During amino acid starvation in which eukaryotic translation initiation factor 2α (eIF2α) is phosphorylated (functional initiation complex is thus scarce), reloading of ribosomes is decelerated and a functional initiation complex is reassembled only when the scanning process proceeds to the main ORF, thus GCN4 is expressed. The fast feature of this translational regulation allows a rapid response to nutritional stress [121,122]. Another similar example of regulation via uORF is the Carnitine Palmitoyltransferase 1C (CPT1C) which regulates metabolism in the brain in conditions of energy surplus. The uORF in the 5'UTR of CPT1C suppresses its expression under normal condition, but in the presence of stress stimuli induced by glucose depravation or palmitate-BSA treatment, the uORF mediates up-regulation of CPT1C expression [123]. uORFs were also found to play an important role in ER stress (Fig. 1-7B). Under normal condition with low elF2α phosphorylation, uORFs function as a barrier to prevent the translation of the main ORF in mRNAs of some ER-stress induced proteins, like activating transcription factor 4 (ATF4), C/EBP homologous protein (CHOP), and growth arrest and DNA damage-inducible protein (GADD34). However, under ER stress conditions, enhanced elF2α phosphorylation facilitates the ribosome to bypass the uORF, and to translate the main genes. This quick translational regulation is critical for cells to survive during ER stress [124-126].

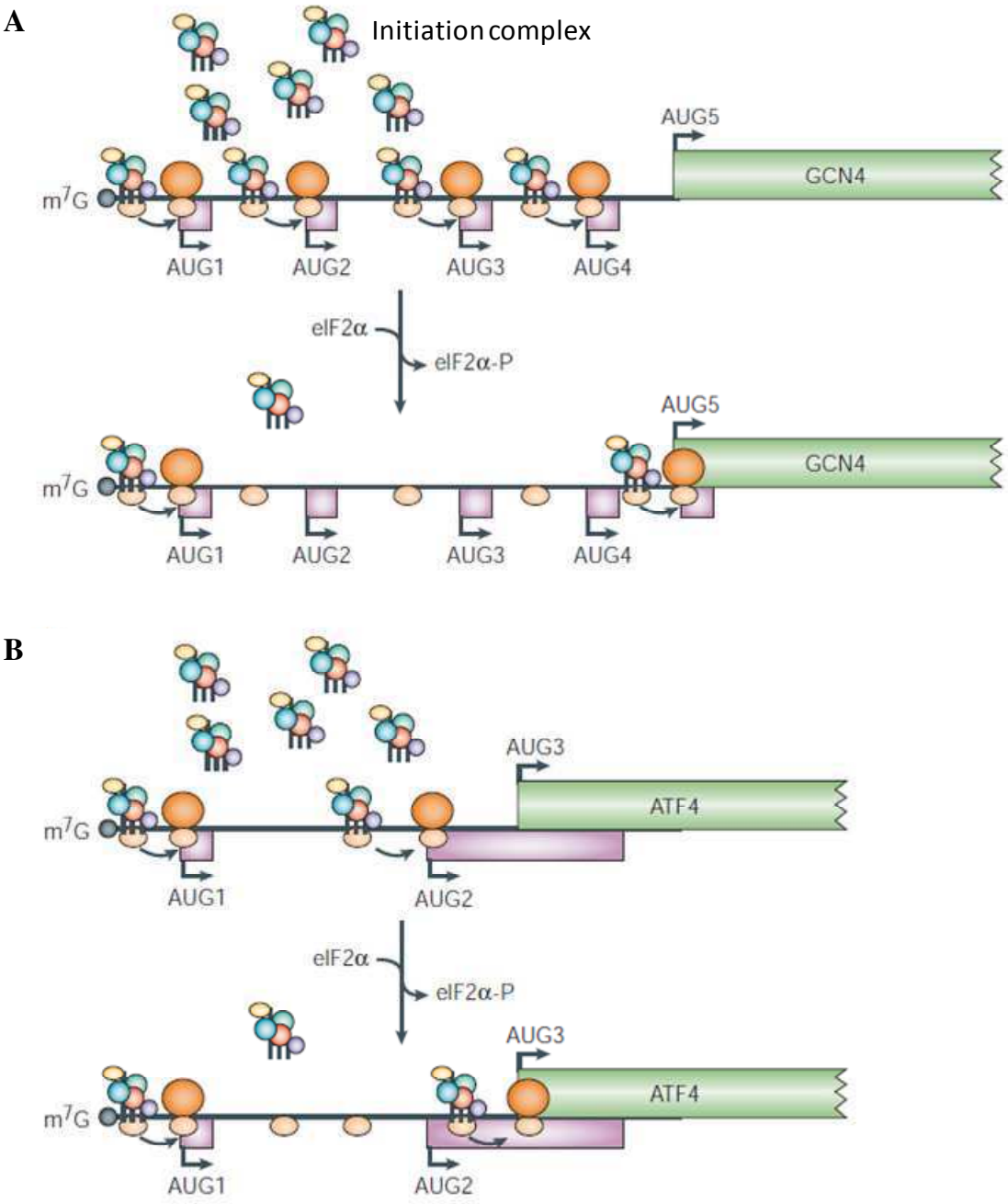

Fig. 1-7. Translational regulation by uORF in 5'UTR of mRNA. (**A**) Translational regulation of GCN4 by four uORFs. Under normal conditions in which eIF2α phosphorylation level is low and the initiation complex is abundant, part of ribosomes resume scanning to reinitiate at uORF2-4 once finishing the uORF1 translation. Therefore, few ribosomes will arrive at the initiation site of GCN4 ORF. In contrast, under amino acid starvation conditions in which eIF2α phosphorylation is largely increased and the abundance of the initiation complex is low, the reinitiation at uORF 2-4 becomes less frequent, allowing ribosomes scanning to reinitiate at GCN4 ORF. (**B**) Translational regulation of ATF4 by two uORFs. Similar to the regulation of

GCN4, under normal conditions when the eIF2α phosphorylation is low, the ribosomes frequently reinitiate at uORF2, thus ATF4 ORF translation is suppressed. During ER stress, eIF2α is phosphorylated and the level of the initiation complex is reduced, the scanning ribosomes pass uORF2 and reinitiate at the ATF4 ORF. Protein coding regions are shown as green rectangles; uORF are shown as purple rectangles; 5'UTR are indicated as black thin lines; initiation codons (AUG) are shown with arrows and ribosomes are shown in orange oval (dark orange, 60S subunit; light orange, 40S subunit). M^7G, cap structure. Reused, with permission, from Holcik and Sonenberg, *Nat. Rev. Mol. Cell Biol.*, 2005 [127].

1.4.2 3'UTR-mediated translational regulation

Compared with 5' UTR, 3'UTR are generally much longer, indicating a significant potential for regulation. Translational regulation by 3'UTR is mainly mediated by two *trans*-acting factors, RNA-binding proteins and micro-RNAs. Based on their relevance to the research described in this thesis, only the RNA-binding proteins are discussed here. Usually, RNA-binding proteins recognize and bind to nucleotide motifs located in 3'UTR. After binding, a RNA-binding protein can regulate the translational initiation in the distant 5' cap of the mRNA. The question is how this regulation can happen at the distant 5' terminus? It is generally accepted that mRNAs show a 'closed-loop' through interaction between the 'head' and 'tail', in other words, the 3' and 5' ends are spatially proximate [128,129]. This circularization is mainly mediated by the interaction between the initiation factor eIF4G, associated with 5' cap in the head, and poly(A)-binding protein (PABP), bound to poly(A) sequence in the tail (Fig. 1-8A). Actually, this circularization can facilitate direct recycling of 40S ribosomal subunit from 3' to 5' terminus, thus increasing efficiency of translation [130]. A general mechanism of translational initiation control by a 3'UTR-binding protein was then proposed in several studies (Fig. 1-8B) [131-135]. According to this mechanism, when binding to the 3'UTR motif, the 3'UTR-binding protein could disassemble or inactivate the initiation complex at the 5' head through an

intermediate protein, such as eIF4E-binding proteins (4EBPs), which prevents the formation of initiation complex by competing with eIF4G for binding to eIF4E.

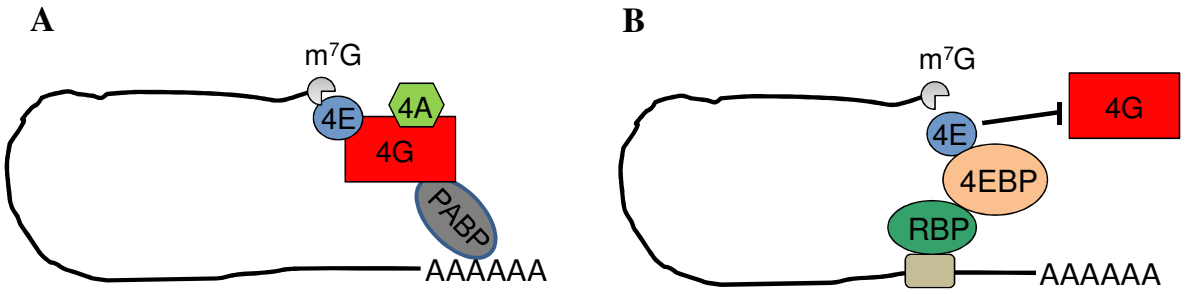

Fig. 1-8. Translational regulation by RNA-binding proteins (RBPs) and 3'UTR of mRNA. (**A**) Circularization of mRNAs mediated by interaction between the initiation factor eIF4G and poly(A)-binding protein (PABP). eIF4G is linked to 5' cap through another initiation factor eIF4E. (**B**) Mechanism of translational regulation by an RBP and sequence motif in 3'UTR. In this mechanism, an intermediate protein, such as eIF4E-binding protein (4EBP), is recruited by the RBP to a target mRNA. 4EBP then interacts with eIF4E, causing its dissociation with eIF4G, which prevents the formation of initiation complex and thus translation. M^7G, cap structure. Adapted with permission from Kong and Lasko, *Nat. Rev. Genet.*, 2012 [135].

1.5 ER stress

In eukaryotic cells, the ER is an organelle mainly involved in protein folding, calcium storage, and lipid biosynthesis [136]. Proteins are folded into functional conformations in the ER with post-translational modifications, such as glycosylation and disulfide bond formation [137,138]. The folded proteins undergo quality control, and only those properly folded are exported to the Golgi complex. Misfolded or unfolded proteins will be retained in the ER to either complete the folding processes or be targeted for degradation [139]. Any disruption of these processes leading to accumulation of misfolded proteins will induce ER stress. A number of disturbing factors that cause ER stress include ER Ca^{2+} depletion, altered protein glycosylation, gene mutations, abnormal nutrient levels, hypoxia, oxidative stress, and over-expression of normal and/or incorrectly folded proteins [140]. The resulting ER stress triggers an evolutionarily conserved series of signal transduction events, the so-called unfolded protein response (UPR) [140]. These signalling events aim to attenuate global protein translation to mitigate misfolded protein load and ameliorate the accumulation of unfolded proteins by increasing ER resident chaperones. However, cell apoptosis will be initiated if the stress is severe or sustained, which involves induction of the proapoptotic transcriptional factor CHOP, activation of c-Jun amino-terminal kinase, and cleavage of caspase-12 [141].

ER stress is associated with numerous diseases, such as neurodegeneration including Parkinson's and Alzheimer's diseases, inflammation, cancer and diseases in heart, kidney, liver, lung and pancreas [142-145]. ER stress and several UPR factors are induced by ischemic injury in brain and heart, leading to CHOP-dependent neuron apoptosis and cardiomyocyte degeneration [146].

1.5.1 UPR signaling

When ER stress is induced, three ER transmembrane sensors are activated to initiate adaptive responses, protein kinase-like ER kinase (PERK), inositol-requiring kinase 1 (IRE1), and activating transcription factor 6 (ATF6) (Fig. 1-9) [147]. They are localized in ER membrane with N-terminus inside ER lumen and C-terminus in the cytosol. Under normal condition, their N-termini interact with ER lumen protein BiP (also called glucose-regulated protein 78 kDa) to maintain them in an inactivated state. [148]. However, during ER stress, accumulated unfolded proteins bind with Bip, leading BiP to be relaeased from these sensors to allow their activation through oligomerization, thus inducing the UPR [148].

PERK is a serine/threonine kinase to phosphorylate eIF2α upon activation to lower global protein translation, thereby reducing the protein load to the ER [149,150]. However, phosphorylation of eIF2α can selectively enhance the translation of several proteins involved in UPR [151,152], such as transcriptional factor ATF4, which helps to reduce misfolded protein in the ER [126].

IRE1 is highly conserved in eukaryotic cells, suggesting it may be the first evolutionally appeared ER stress sensor [153,154]. Upon activation, endoribonulease activity of IRE1 is elicited to specifically cleave the mRNA encoding the transcriptional factor X-box binding protein 1 (XBP1) which is then be able to induce a variety of UPR-related genes [147]. This cleavage is required for translation of XBP1 proteins [155].

ATF6 is a transcriptional factor that regulates transcription of UPR-related genes through binding to ER stress response elements in the promoter region. ER stress induces translocation of ATF6 from the ER to the Golgi apparatus where it is proteolytic cleaved by S1P and S2P to generate a fragment which is transcriptionally active. ATF6 can activate a number of UPR-related genes, including XBP1 [140,156]. The three branches of the UPR (ATF4, XBP1, and ATF6)

coordinately regulate the expression of proteins, such as ER chaperones and folding enzymes, with effort to matigate the overload of misfolded proteins in ER.

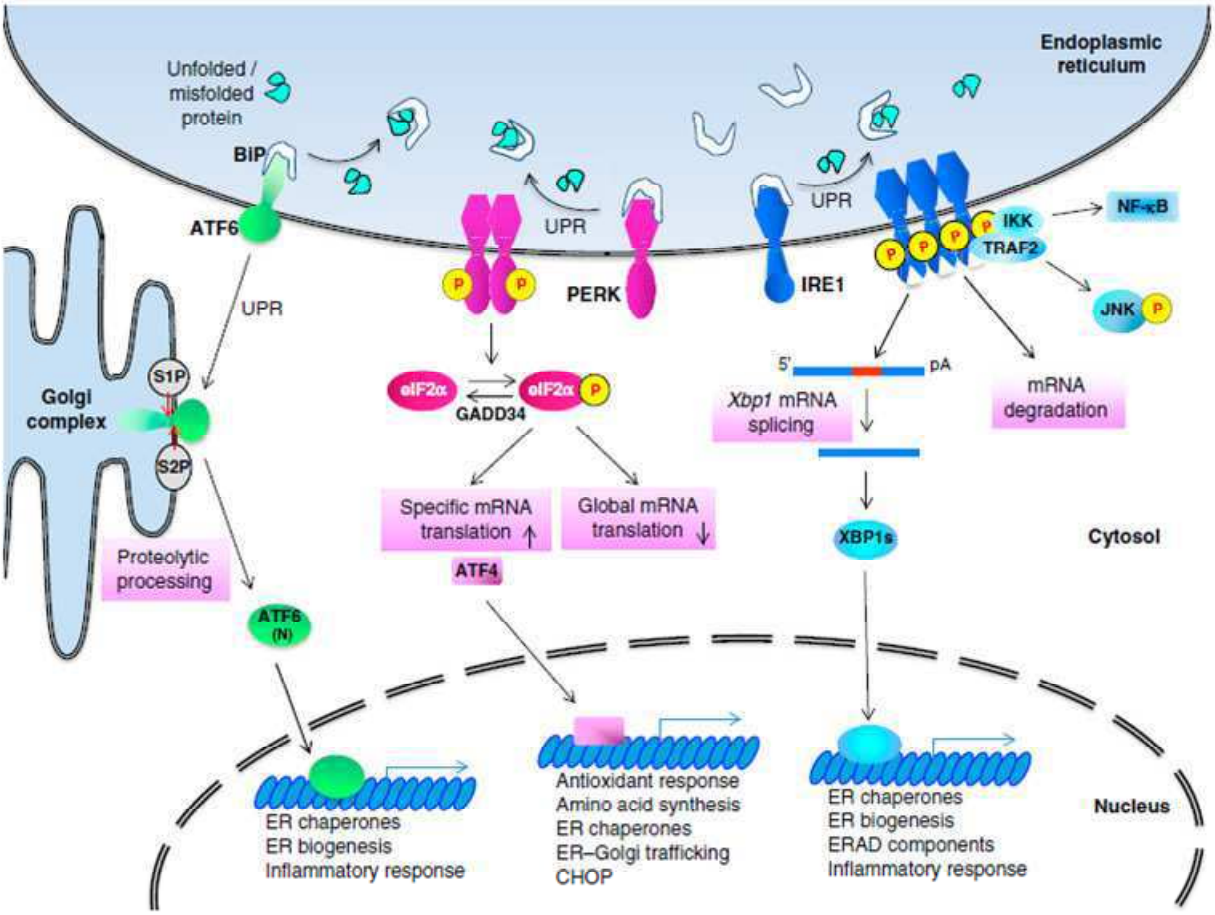

Fig. 1-9. Three URP branch transduction pathways during ER stress. PERK/eIF2α pathway ameliorates global protein tranlastion while selectively up-regulates translation of specific proteins. IRE1 functions as an endoribonuclease to cleave XBP1 mRNA and increase its expression which in turn induces transcription of various ER stress related genes. ATF6 is cleaved and activated by S1P and S2P. Cleaved ATF6 translaocates to nucleus and functions as a transcription factor. Reused, with permission, from Cao and Kaufman, *Curr. Biol*., 2012 [157]

1.5.2 ER-initiated apoptotic signaling

ER-initiated apoptotic signaling is induced when the UPR fails to restore the proper protein folding in the ER [141], but it remains unclear how the cell makes a decision between survival and death. Three ER sensor proteins are identified to be responsible for ER-initiated apoptotic signaling. Interestingly, they are also involved in the UPR.

IRE1-dependent apoptotic signaling occurs via diverse pathways. IRE1 interacts with the adaptor protein TNF receptor-associated factor 2 (TRAF2). IRE1 and TRAF2 then interact with a mitogen-activated protein kinase, ASK1, which subsequently phosphorylates JNK [158,159].

CHOP is one of the most thoroughly investigated molecules among those involved in ER-initiated apoptotic signaling. CHOP is a pro-apoptotic transcriptional factor that is mainly regulated by ATF4- and ATF6-dependent pathways [160,161].

caspase-12 has been reported to be processed during ER stress [160,161]. ER stress induces cleavage and activation of pro-caspase 12, which in turn activates caspase-9 and caspase-3, leading to mitochondria-independent cell death.

1.6 Far upstream element-binding protein 1 (FUBP1)

Human FUBP homologs (FUBP1 to 3) are 600-711 amino acid DNA-/RNA-binding proteins and share sequence similarity of 61-81% [162]. They also share common structural features such as four K-homology (KH) domains that bind with DNA or RNA (Fig. 1-10) [162]. All three FUBPs are present in multiple tissues including kidney, liver, pancreas, thymus, ovary and skin [163,164]. FUBP1 was initially identified as a DNA-binding protein that up-regulates the transcription of proto-oncogene *c-Myc* through binding to the far upstream element (FUSE) located 1.5 kb upstream of the transcription start site in the promoter region [165]. More recently, FUBP1 was found to be able to function as an RNA-binding protein to regulate translation efficiency or stability of several cellular and viral mRNAs [166]. The importance of FUBP1 study has been highlighted by the evidence suggesting that FUBP1 plays a key role in carcinogenesis. Mutations of the *FUBP1* gene or abnormal expression of FUBP1 protein have been documented in a number of malignant tissues [167-171]. Besides, FUBP1 also plays a important role in the development of lung [172], brain and neural networks [167,173].

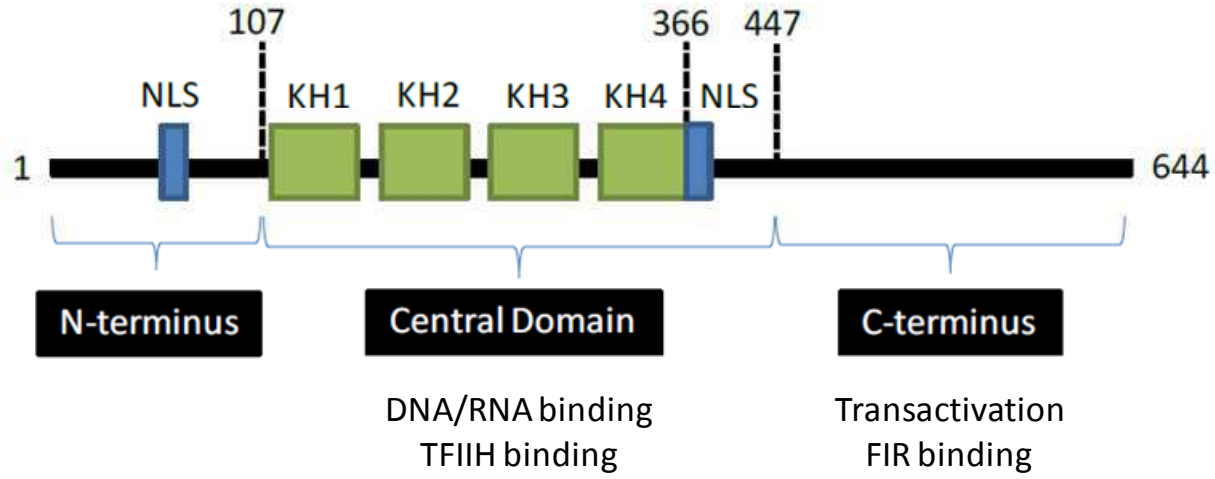

Fig. 1-10. Schematic structure of human FUBP1 protein. The N-terminus is composed of amino acid residues 1-106. The central domain contains residues 107-447 and posseses four KH domains for DNA/RNA binding. Amino acid residues 448-644 constitute the C-terminus responsible for FUBP1-interacting repressor (FIR) binding and transcription activation. The well-defined nuclear localization sequence (NLS) at the N-terminus and the central domain are illustrated. Adapted, with permission, from Zhang and Chen, *Oncogene*, 2013 [166]

1.6.1 FUBP1 as a DNA-binding protein

FUBP1 up-regulates transcription of *c-Myc* through binding to the FUSE [165] which is also a binding target of FUBP-interacting repressor (FIR) [174]. The transcription of *c-Myc* gene relays on the interplay among FUBP1, FIR and FUSE [174]. FUBP1 recognizes and interacts FUSE core sequence 5'- TATATTCCCTCGGGATTTTTTATTTTGTG-3' through its KH3 and KH4 domains [175]. However, this interaction is not sufficient for *c-Myc* optimal transcription which also needs additional *cis*-elements and and *trans*-factors [176]. Liu *et al* [177] showed that after binding with FUSE, FUBP1 interacts with transcription factor TFIIH bound with *c-Myc* transcription start site, which leads to formation of a promoter loop. This loop will bring FUBP1 close to the RNA polymerase II complex at the transcription start site where FUBP1 activates TFIIH helicase and subsequently promotes transcription of *c-Myc* gene.

1.6.2 FUBP1 as an RNA-binding protein

More recently, FUBP1 has been found to function as an RNA-binding protein interacting with several cellular mRNAs or viral RNAs [178]. Such interactions affect either RNA stabilization or translation efficiency. FUBP1 translationally down-regulates expression of growth-associated protein 43 (GAP43), a neuroprotein involved in axonal growth and regeneration, to contribute neural development [179]. This regulation is mediated by interaction between FUBP1 and a 26-

necleotides AU-rich region, about 300 nucleotides downstream from the stop codon, within the GAP43 mRNA 3'UTR [167] which has been reported to important for stablility of its mRNA [180]. Therefore, it could be that FUBP1 reduces GAP43 protein level through promoting its mRNA degradation once binding with the AU-rech region [167]. Nucleophosmin (NPM) is a regulator of cell proliferation and genomic instability due to association with nucleolar ribonecleoproteins [181,182]. FUBP1 has been found to bind to the 3'UTR of the NPM mRNA and inhibits NPM mRNA translation through inhibiting translation initiation. When FUBP1 was knocked down by siRNA, more NPM mRNA was bound with the polysomes which are the indicator for active translation [183]. Conversely, FUBP1 over-expression resulted in a shift of the NPM mRNA from polysome-bound to mono-ribosome-bound states, suggesting a decreased translation of NPM protein [183]. In addition to regulating stability and translation efficiency of cellular mRNAs, FUBP1 has also been shown to binding several viral RNAs to regulate their replication in human cells. One example is the Japanese encephalitis virus (JEV) which is the major cause for encephalitis in Asia [184]. FUBP1 binds to 3'UTR of the JEV RNA [184]. JEV replication was enhanced with FUBP1 knock-down and was inhibited with FUBP1 over-expression in HeLa cells [184].

1.7 TRPP3

TRPP3, also called PCL or PKD2L1, was the first described TRPP2 homologue. Another TRPP2 homologue is TRPP5, also called PKD2L2. TRPP2, -3 and -5 form the TRPP subfamily. Unlike TRPP2, TRPP3 is not involved in ADPKD. Similar to TRPP2, TRPP3 functions as a Ca^{2+} permeable non-selective cation channel.

1.7.1 Structural properties of TRPP3

TRPP3 is composed of 805 animo acids and show 50% sequence identity and 71% similarity to TRPP2. TRPP3 possesses a membrane topology similar to TRPP2, with six transmembrane segments, intracellular N- and C-termini and a pore loop between S5 and S6 (Fig. 1-11). A large extracellular loop between S1 and S2, only exists in members of TRPP and TRPML subfamilies, is likely to serve as a sensor domain for unidentified stimuli. The TRPP3 C-terminus contains an EF-hand domain proposed for Ca^{2+} binding and a coiled-coil domain contributing to oligomerization. [185,186], but both domains are not a determinant of channel function [187]. Although TRPP3 are predicted to contain sites for glycosylation and phosphorylation, no post-translational mofidifications have been experimentally documented.

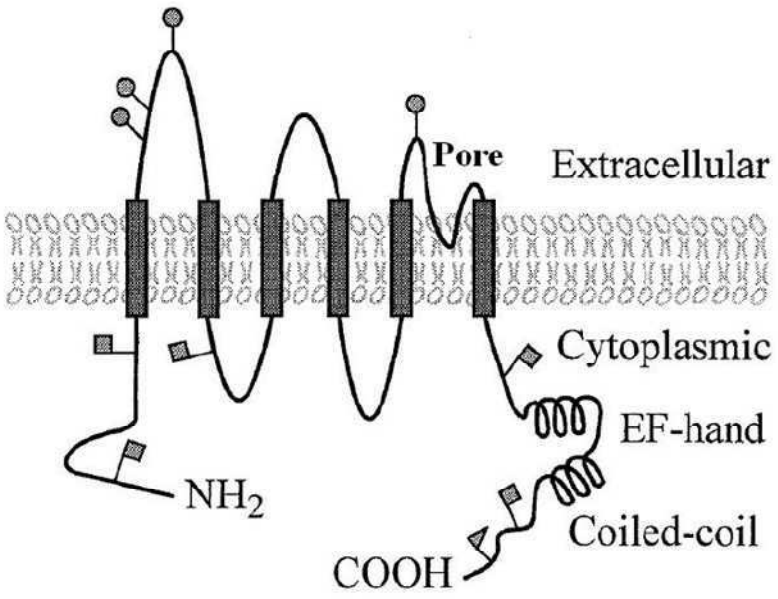

Fig. 1-11. Schematic membrane topology of TRPP3. Predicted N-glycosylation, PKA-phosphorylation and PKC-phosphorylation sites are indicated with circles, triangles and squares, respectively. C-terminal EF-hand and coiled-coil domains are shown. Resued, with permission, from Chen *et al.*, *Nature*, 1999 [188].

1.7.2 TRPP3 homomeric channel – Ca^{2+} response

Among TRPP members, TRPP3 was the first one shown to form an ion channel. In 1999, Chen *et al.* [188] demonstrated that, when expressed in *Xenopus* oocytes, human TRPP3 forms a ion channel activated by extracellular Ca^{2+} and is conducting to cations, including Na^{+}, K^{+} and Ca^{2+}, with no preference, but not negatively charged ions. This Ca^{2+}-induced activation is followed by a subsequent inactivation which the underlying mechanism remains elusive. When oocytes were pre-injected with Ca^{2+} chelator ethylene glycol tetraacetic acid (EGTA) to eliminate any free intracellular Ca^{2+}, extracellular Ca^{2+} can no longer induce TRPP3 activation, suggesting that Ca^{2+} entry leading to increase of intracellular free Ca^{2+} is required for channel activation. A Ca^{2+}-binding domain EF-hand in TRPP3 C-terminus was initially thought to mediate its activation/inactivation behavior. However, a truncation mutant lacking the EF-hand

still exhibited a similar multi-phasic behavior as WT channels [187]. To date, the exact mechanisms underlying the TRPP3 multi-phasic activation and inactivation is still needed to be determined.

1.7.3 TRPP3/PKD1L3 heteromeric channel – off response

Different from the PM targeting of TRPP3 in *Xenopus* oocytes, when heterologously expressed in mammalian cells, e.g., human embryonic kidney 293 (HEK293) cells, TRPP3 is mainly localized in the ER membrane with unknown channel function. However, co-expression with PKD1L3, a homologue of PC1 protein, leads TRPP3 to substantially traffick to PM where the two form a heteromeric channel complex activated by acids in an so-called off-response manner, e.g., activation is induced only when extracellular acid is removed [189,190]. Subsequent studies suggested TRPP3/PKD1L3 as the sour taste receptor [191,192]. Both weak and strong acids are able to induce TRPP3/PKD1L3 off-response whose current amplitude is determined by the difference between the stimulating pH and the washing pH, but independent of time of acid application [189]. Different from TRPP3 on-response in *Xenopus* oocytes, TRPP3/PKD1L3 off-response can be repeated and does not exhibit inactivation [189]. TRPP3/PKD1L3 channel complex is Ca^{2+} permeable and two negatively charged residues D523 [193] and D525 [194] in the TRPP3 S5-S6 pore loop have been identified to affect the Ca^{2+} permeation, suggesting they may be the determinants of the channel complex selectivity. To date, the exact mechanism underlying the off-response still remains elusive.

1.7.4 TRPP3 physiological function

TRPP3 is expressed in various tissues, including kidney, tongue, brain, testis and cardiac tissue [195,196]. To date, the TRPP3 physiological function has remained elusive; no obvious phenotype has been identified in TRPP3 knockout mice. Since the TRPP3/PKD1L3 complex shows an off-response to acid, the complex was proposed to be a candidate receptor for sour taste sensation. This hypothesis received strong support from early evidence: 1) TRPP3 and PKD1L3 are co-expressed in a subset of taste receptor cells in specific taste areas responsible for sour tastes [197]; 2) when cells expressing TRPP3 have been eliminated by induced expression of attenuated diphtheria toxin in mice, sour taste sensation is completely abolished, with no influence on ability to taste salty, sweet, bitter, and umami flavors [198]. However, subsequent discoveries using knockout mice challenged this hypothesis: 1) mice with PKD1L3 deletion exhibit no abnormality in sour taste [191]; 2) mice with targeted TRPP3 deletion only show 25-45% of reduction in responses to sour tastants [191]. All these together suggest that PKD1L3 is not directly involved in sour tastes and that TRPP3 is involved in only some part of this sensation with unknown mechanism. In 2009, two Japanese people were reported to experience acquired sour taste aguesia (inability to response to sour stimuli) and interestingly, mRNAs of PKD1L3, TRPP3 and acid sensing ion channels (ASICs) were not detectable in lingual fungiform papillae tissues containing taste cells [199], suggesting ASICs, in addition to TRPP3, is also involved in sour detection. Our laboratory recently reported that TRPP3 itself, without PKD1L3, is capable of showing an off-response in *Xenopus* oocytes [200], suggesting that TRPP3 may be involved in sour taste independent of PKD1L3. Whether and how PKD1L3 plays a role in sour taste are needed to be determined.

1.7.5 TRPP3 Homo- and hetero-tetrameric assembly

Compared with other TRP channels, TRPP2 and TRPP3 from the TRPP subfamily were extensively reported to form heteromeric channel complexes with proteins from the PC1 family, including PC1, PKD1L1, PKD1L2, PKD1L3 and PKDREJ, which share a similar membrane topology (see a summary in Fig. 1-12). The most studied complexes were TRPP2/PC1 and TRPP3/PKD1L3, both reported to be with 3:1 stoichiometry, e.g., one TRPP2 (or TRPP3) trimer paired with one PC1 (or PKD1L3) monomer [194,201]. Although the composition information for other reported complexes, such as TRPP3/PC1 and TRPP3/PKD1L1, is not available, they are probably organized with the same stoichiometry. Since TRP channels are generally considered to form homotetramer through dimerization domains in terms of the symmetry, this 3:1 stoichiometry of TRPP/PKD complex gives rise to an interesting question as to whether homo-trimerization is a required process for TRPP2 or TRPP3 hetero- and homo-tetrameric assemblies. The identification of a functionally important trimerization domain would be critical to this question.

PC1 protein	PC1	PKD1L1		PKD1L2	PKD1L3	PKDREJ
Binding partner	TRPP2	TRPP2	TRPP3	??	TRPP3	TRPP2 and -3
Localization	Cilia, cell surface, exosomes	Embryonic node cilia	Cilia	Skeletal muscle	Taste buds	Sperm
Role	Cilia sensor, mechanosensor?	Establishes left–right asymmetry	Cilia calcium concentration	Neuromuscular disease: mouse overexpression	Sour (H^+) detector	Regulating acrosome reaction

Fig. 1-12. Heteromeric complex between proteins from PC1 and TRPP families. Adapted, with permission, from Ong and Harris, *Kidney Int.*, 2015 [202].

Indeed, a C-terminal coiled-coil 2 domain (CC2) in TRPP3 (G699-W743) and TRPP2 (R844-K876) was found to homotrimerize *in vitro* and be important for both TRPP3 homomeric and TRPP3/PKD1L3 heteromeric assembly [185,186,194]. However, our previous study showed that

TRPP3 truncation mutants lacking CC2 retains similar Ca^{2+}-activated channel activity as WT TRPP3 [187]. Also, HEK cells co-expressing WT PKD1L3 and TRPP3 truncation mutant lacking CC2 still exhibit normal off-response to acid, but little response was observed when the entire TRPP3 C-terminus is truncated, although cell surface expression was not affected by this truncation mutation [203]. These data challenged the involvement of the CC2 domain in functional TRPP3 homo- and hetero-tetrameric channel assembly.

1.8 Palmitoylation

Palmitoylation is a post-translational modification which covantly adds 16-carbon chain fatty acid palmitic acid to cytoplasmic cysteine residues [204], thus palmitoylation increases the hydrophobicity of cytoplasmic proteins, leading to their association with the surface of membranes. Different from other lipid modifications, palmitoylation is reversible, which makes it an important dynamic mechanism to regulate protein functions [205,206]. To date, abnormal regulation of protein palmitoylation has been found to be involved in a number of human disases, such as cancer, X-linked mental retardation, and schizophrenia [207-209]. With the technique advances in proteomic methodology, an unexpected range of proteins have been revealed to be modified by palmitoylation, including an growing list of ion channels [210,211].

1.8.1 Palmitoyltransferases

Protein palmitoylation is mostly catalyzed by a family of palmitoyltransferases containing the signature DHHC (Asp-His-His-Cys) motif, of which there are 23 in humans [204], about 20 in worms and flies and 7 in yeast [212]. To date, it remains largely unclear what is the particular function of individual DHHC enzyme and what the substrate specificity of these enzymes is [213,214]. Even though some online algorithms are developed to predict the protein palmitoylation sites, no consensus sequence motif has been identified surrounds the palmitoylated cysteine residues. DHHC enzymes are membrane proteins with four transmembraen segments and the conserved DHHC cysteine-rich catalytic domain is on the cytosolic face. Although many DHHC enzymes are found to be localized in the membranes of ER and Golgi, some of them are also found in the PM or membranes of endocytic vesicles [215]. So far, it is largely unknown regarding the regulation of DHHC proteins expression and trafficking.

1.8.2 Thioesterases

As mentioned above, the palmitoylation process is reversible. The de-palmitoylation is mediated by so-called acyl-protein thioesterases (APTs), of which three have been identified, APT1, APT2 and APT1-like [216,217]. Although they are thought to play critical roles in palmitoylation-depalmitoylation cycle to control protein functions spatiotemporally, we know very limited information about them, compared with DHHC enzymes. APT1 was shown to mediate de-palmitoylation of Gα proteins [218,219] and APT2 is involved in de-palmitoylation of growth-associated protein-43 [216,220]. Both APT1 and APT2 are found to depalmitoylate Ras [220]. Besides, the calcium-activated large potassium channel (BK) was shown to be de-palmitoylated by APT1 and APT1-like [221].

1.8.3 Ion channel regulation by protein palmitoylation

While palmitoylation of soluble cytoplasmic proteins allows them to attach to membranes, the effects of palmitoylation on transmembrane proteins, e.g., ion channels, remain more enigmatic. Since the first palmitoylated ion channel, rodent voltage-gated Na channel, was characterized in 1987 [222], more than 50 different ion channels have been experimentally documented to be palmitoylated to date [211]. Accumulated evidence has indicated that palmitoylation can control either the the number of channel molecules on a membrane, through regulating their trafficking, or the single channel activity, through regulating channel kinetics.

1.9 Hydrophobic gate theory

Ion channels are membrane proteins forming a pore to allow ions to pass through the cell membranes. There are two fundamental properties of ion channels, 1) they are selective to different types of ions; 2) they switch between a closed state (non-conducting to ions) and an open state (ion conducting). Generally, the switch between closed and open states is determined by the presence of external stimuli, including transmembrane voltage, chemical ligands, temperature, mechanical force, which is termed gating. The gate is defined as the region along the pore to prevent ion species from passing through the pore when the channel is in the closed state. During the channel activation, the pore is widened to be open with the gate conformational movement which is induced when the stimulous signals act to the channel sensor, the region for detection of stimuli, e.g., the binding pocket for a ligand. Although the gate and sensor are directly linked on functional level, they are not necessary to be close to each other physically. Rather, they are usually in different channel parts, typically many nanometers away. The gating process often starts from sensing the signal (by sensor domains), through transdecution of the signal (via linker domains), and ends with movement of the gate to open the pore.

Molecular dynamics (MD) simulation studies on nanopore models showed that when water molecules are confined within a hydrophobic pore in the same scale with the biological ion channels, they show very distinct behaviors described as liquid-vapor transitions (Fig. 1-13A) due to the unfavorable interaction between the water molecules, which is hydrophilic, and the lining of the hydrophobic pore. The liquid states are 'wetted' and conductive to ions, whereas the the vapor states are devoid of water within part of the pore, called 'dewetted', exerting an energetic barrier to ion conduction, which was later termed 'hydrophobic gating' [223-225]. MD

studies showed that hydrophobic gating occurs when the diameter of the hydrophobic pore is less than 14 Å, the diameter of one water molecule is assumed to be around 3 Å (Fig. 1-13B).

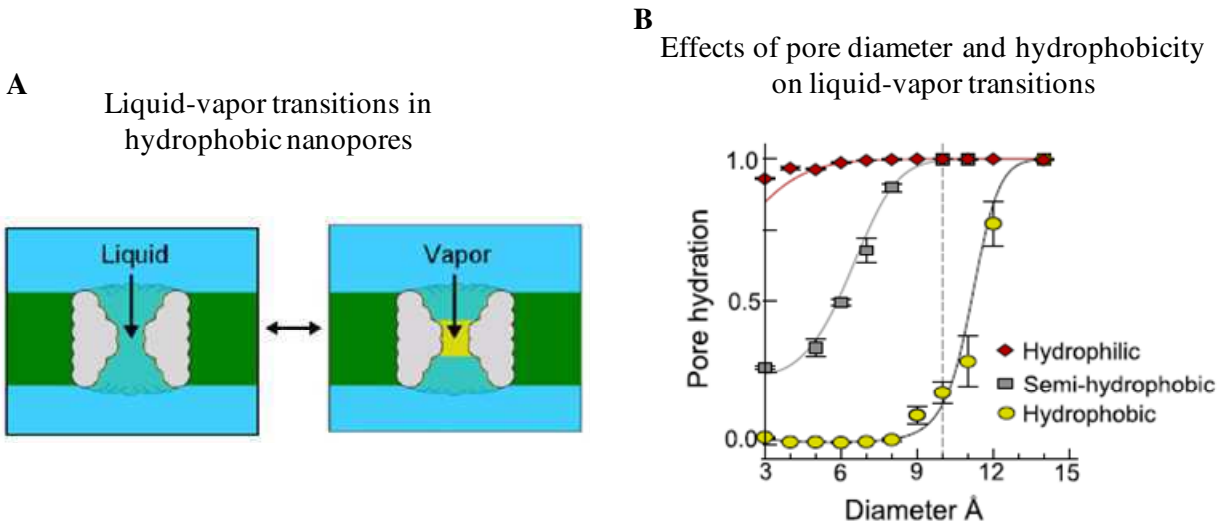

Fig. 1-13. Principles of hydrophobic gating. (**A**) Schematic illustration of liquid-vapor transitions within a hydrophobic nanopore. Hydrophobic surfaces and the membrane are indicated in white and green, respectively. The dewetted vapor state (yellow) represents an energetic barrier ion permeation. (**B**) The hydration rate of the pore is determined not only by the pore diameter but also the hydrophobicity of atoms lining the pore. Adapted from Aryal *et al*., *J. Mol. Biol.*, 2015 [226] (permission is not required for this figure to be reused in a thesis).

According to the hydrophobic gate theory, a hydrophobic gate closes the pore through liquid-vapor transition of water molecules within the pore rather than through physical occlusion of the pore. Conformational changes of pore-lining helices, e.g., following binding of an agonist, enlarge the pore size thereby increasing the channel's open probability. The pore hydration rate is close to zero (e.g., no ion is eligible to pass through) when the pore gate has a physical diameter of less than 9 Å and dramatically increases to the maximum when it reaches 12-13 Å in a strong sigmoidal dependence (Fig. 1-13B) [226]. Therefore, the ion conduction ($\propto$ hydration rate x pore

surface area) is able to be substantially increased when the change of pore diameter is within this dynamic range (9-13 Å), which is highly advantageous for ion channels whose functions are to control substantial ion movement with relatively small conformational change. The hydrophobic gating theory is strongly supported by the observed pore sizes of the crystallized bacterial small conductance mechano-sensitive channel MscS in closed (8 Å) and open (13 Å) states [227,228]. Also, the open-state pore sizes of TRP channels characterized so far were all found to be within the 11-13 Å range [229-233]. Since the the hydrophbic pore is not physically occluded when ion channels are in closed state with the absense of agonists, one way to lead to pore conducting without conformational change, as suggested by the simulation studies, is to change the gate region from hydrophobic to hydrophilic (Fig. 1-13B) [226]. Thus, channels could be placed in the open state by two approaches: 1) increasing the pore diameter (via conformational changes induced by stimuli); 2) replacing the hydrophobic gate residues with hydrophilic ones (via mutation) [226]. The later one is verified and approved in the TWIK-1 K2P potassium channel and MscL mechano-sensitive channel in which channel activities are strongly correlated with the hydrophilicity of the gate residue [234-236].

1.10 Objective, hypothesis and rationale

1.10.1 Objective

The main purpose of this study is to gain a better understanding of protein dosage regulation of TRPP2 and functional regulation of TRPP3 ion channel, and pore gates of TRPs. For this, my specific objectives are 1) to investigate molecular mechanisms underlying the regulation of TRPP2 protein translation by ER stress and its mRNA 5'UTR; 2) to investigate molecular mechanisms underlying the regulation of TRPP2 protein translation by FUBP1 and its mRNA 3'UTR; 3) to study roles of the TRPP3 C-terminus in TRPP3 channel activity and oligomerization; 4) to study rolesTRPP3 N-terminus in TRPP3 channel activity and post-translational modifications; 5) to investigate the gate residues of TRP channels from different subfamilies.

1.10.2 Hypothesis

Our hypotheses are that 1) ER stress and P-eIF2α translationally up-regulates TRPP2 protein expression through acting on the 5'UTR uORF of its mRNA; 2) FUBP1 translationally down-regulates TRPP2 protein expression through binding to its 3'UTR; 3) the TRPP3 C-terminus contains domain (K575-T622) that is critical for both channel function and trimerization; 4) TRPP3 channel function is regulated by palmitoylation and phosphorylation at the N-terminal residues Cys-38 and Thr-39, respectively; 5) TRP channels share conserved hydrophobic amino acid residues as their pore gates.

1.10.3 Rationale

A "two hit" model was first proposed in 1992 to illustrate a possible mechanism underlying the cystogenesis of ADPKD [237]. This hypothesis suggested that the occurrence of a somatic mutation in the remaining normal allele initiated cyst formation in the affected cells. This model received support from the identification of somatic mutations that inactivated the normal allele only in 20-43% of the analyzed *PKD1* or *PKD2* renal cysts [83-86]. However, no somatic mutation was found in the remaining analyzed cysts. Over the past decades, evidence has been accumulating in support of a "dosage" model that suggests that renal cystogenesis can be initiated when the functional PC1 or TRPP2 protein level is reduced below a threshold level in the absence of a somatic mutation [87-89]. Therefore, it became important to elucidate how PC1 and TRPP2 protein expression is regulated in order to ultimately develop new therapeutic targets and approaches, especially as the outcomes of previous clinical trials are rather negative. Cultured mammalian cells are good models to study molecular mechanisms of TRPP2 translational regulation since they are easy to be maintained and manipulated. Well-established molecular and biochemical techniques in our lab are ready to be used for cultured cell lines, including RT-PCR, dual-luciferase assay, polysome analysis, western blot, co-immunoprecipitation, and protein over-expression and knockdown. However, there are limitations about cultured cell models. For example, they cannot mimic the physiological contexts in which TRPP2 functions. The molecular mechanisms unveiled may not apply to TRPP2 in its native expression tissues. Therefore, we also employed the *in vivo* zebrafish model to verify the results obtained from culture cells. The rapid development and ease of gene manipulation make zebrafish a perfect model to study gene function and regulation. Gene knock-down by morpholino injection into fertilized zebrafish eggs within 1 hour post-fertilization has

been effective and widely used. Embryos with TRPP2 morpholino knock-down develop renal cysts and tail dorsal curvature 2-3 days post-fertilization. Thus, larval zebrafish of 2-5 days post-fertilization have become an excellent model for studying disorders associated with altered TRPP2 dosage. Since zebrafish are distant from human species, mice could be a better model for further confirmation if results are promising from zebrafish experiments.

Compared with *Xenopus laevis* oocytes, mammalian cells would be better models to study TRPP3 channel function and regulation. However, when over-expressed alone in common cultured mammalian cells, including HEK and MDCK cells, TRPP3 is mainly localized in ER membranes. For some unknown reason, TRPP3 substantially trafficks to PM when expressed in *Xenopus laevis* oocytes where it shows well-documented Ca^{2+}-activated channel activity. Our lab has established *Xenopus laevis* oocytes system to TRPP3 channel function for many years. Taken together, *Xenopus* oocytes are particularly appropriate for structure-function relationship study of TRPP3.

One of the basic properties of ion channels is that their activities are controlled by specific stimuli through opening or closing a gate, e.g., the so-called gating. Understanding the nature of the gate would provide insights into molecular mechanisms of how ion channels work and help design drugs aiming to modulate channel activities. TRPs gates have benn much less studied compared with voltage-gated ion channels. Residues defining the narrowest region along the ion-conducting pore were revealed as the gate based upon recently resolved high-resolution structures of several TRPs. However, it is unknown as to whether and how these gate residues are functioning in the native lipid bilayer membrane environment. *Xenopus* oocytes provide an excellent model to functionally study gates of TRP channels in native environments. It allows us to easily over-express various functional TRP channels, and thus to systemically study gates in

TRPs from different subfamilies with electrophysiology approaches together with mutagenesis and biochemical approaches.

1.11 REFERENCES

1. Cosens, D. J. & Manning, A. Abnormal electroretinogram from a Drosophila mutant. *Nature* **224**, 285-287 (1969).

2. Montell, C. & Rubin, G. M. Molecular characterization of the Drosophila trp locus: a putative integral membrane protein required for phototransduction. *Neuron* **2**, 1313-1323 (1989).

3. Venkatachalam, K. & Montell, C. TRP channels. *Annu. Rev. Biochem.* **76**, 387-417 (2007).

4. Clapham, D. E. TRP channels as cellular sensors. *Nature.* **426**, 517-524 (2003).

5. Nilius, B., Owsianik, G., Voets, T. & Peters, J. A. Transient receptor potential cation channels in disease. *Physiol Rev.* **87**, 165-217 (2007).

6. Nilius, B. & Owsianik, G. Transient receptor potential channelopathies. *Pflugers Arch.* **460**, 437-450 (2010).

7. Julius, D. TRP channels and pain. *Annu. Rev. Cell Dev. Biol.* **29**, 355-384 (2013).

8. Nilius, B. TRP channels in disease. *Biochim. Biophys. Acta* **1772**, 805-812 (2007).

9. Montell, C. The TRP superfamily of cation channels. *Sci. STKE.* **2005**, re3 (2005).

10. Moiseenkova-Bell, V. & Wensel, T. G. Functional and structural studies of TRP channels heterologously expressed in budding yeast. *Adv. Exp. Med. Biol.* **704**, 25-40 (2011).

11. Latorre, R., Zaelzer, C. & Brauchi, S. Structure-functional intimacies of transient receptor potential channels. *Q. Rev. Biophys.* **42**, 201-246 (2009).

12. Wu, L. J., Sweet, T. B. & Clapham, D. E. International Union of Basic and Clinical Pharmacology. LXXVI. Current progress in the mammalian TRP ion channel family. *Pharmacol. Rev.* **62**, 381-404 (2010).

13. Nilius, B. & Owsianik, G. The transient receptor potential family of ion channels. *Genome Biol.* **12**, 218 (2011).

14. Nilius, B., Owsianik, G. & Voets, T. Transient receptor potential channels meet phosphoinositides. *EMBO J.* **27**, 2809-2816 (2008).

15. Rohacs, T., Lopes, C. M., Michailidis, I. & Logothetis, D. E. PI(4,5)P2 regulates the activation and desensitization of TRPM8 channels through the TRP domain. *Nat. Neurosci.* **8**, 626-634 (2005).

16. Perraud, A. L. *et al.* ADP-ribose gating of the calcium-permeable LTRPC2 channel revealed by Nudix motif homology. *Nature* **411**, 595-599 (2001).

17. Nadler, M. J. *et al.* LTRPC7 is a Mg.ATP-regulated divalent cation channel required for cell viability. *Nature* **411**, 590-595 (2001).

18. Runnels, L. W., Yue, L. & Clapham, D. E. TRP-PLIK, a bifunctional protein with kinase and ion channel activities. *Science* **291**, 1043-1047 (2001).

19. Earley, S. & Brayden, J. E. Transient receptor potential channels in the vasculature. *Physiol Rev.* **95**, 645-690 (2015).

20. Cheng, W., Sun, C. & Zheng, J. Heteromerization of TRP channel subunits: extending functional diversity. *Protein Cell* **1**, 802-810 (2010).

21. Strubing, C., Krapivinsky, G., Krapivinsky, L. & Clapham, D. E. Formation of novel TRPC channels by complex subunit interactions in embryonic brain. *J. Biol. Chem.* **278**, 39014-39019 (2003).

22. Hofmann, T., Schaefer, M., Schultz, G. & Gudermann, T. Subunit composition of mammalian transient receptor potential channels in living cells. *Proc. Natl. Acad. Sci. U. S. A* **99**, 7461-7466 (2002).

23. Hellwig, N., Albrecht, N., Harteneck, C., Schultz, G. & Schaefer, M. Homo- and heteromeric assembly of TRPV channel subunits. *J. Cell Sci.* **118**, 917-928 (2005).

24. Li, M., Jiang, J. & Yue, L. Functional characterization of homo- and heteromeric channel kinases TRPM6 and TRPM7. *J. Gen. Physiol* **127**, 525-537 (2006).

25. Venkatachalam, K., Hofmann, T. & Montell, C. Lysosomal localization of TRPML3 depends on TRPML2 and the mucolipidosis-associated protein TRPML1. *J. Biol. Chem.* **281**, 17517-17527 (2006).

26. Ramsey, I. S., Delling, M. & Clapham, D. E. An introduction to TRP channels. *Annu. Rev. Physiol.* **68:619-47.**, 619-647 (2006).

27. Zimmermann, K. *et al.* Transient receptor potential cation channel, subfamily C, member 5 (TRPC5) is a cold-transducer in the peripheral nervous system. *Proc. Natl. Acad. Sci. U. S. A* **108**, 18114-18119 (2011).

28. Vriens, J. *et al.* TRPM3 is a nociceptor channel involved in the detection of noxious heat. *Neuron* **70**, 482-494 (2011).

29. Venkatachalam, K., Zheng, F. & Gill, D. L. Regulation of canonical transient receptor potential (TRPC) channel function by diacylglycerol and protein kinase C. *J. Biol. Chem.* **278**, 29031-29040 (2003).

30. Hofmann, T. *et al.* Direct activation of human TRPC6 and TRPC3 channels by diacylglycerol. *Nature* **397**, 259-263 (1999).

31. Li, M. *et al.* Molecular determinants of Mg2+ and Ca2+ permeability and pH sensitivity in TRPM6 and TRPM7. *J. Biol. Chem.* **282**, 25817-25830 (2007).

32. Li, M., Jiang, J. & Yue, L. Functional characterization of homo- and heteromeric channel kinases TRPM6 and TRPM7. *J. Gen. Physiol* **127**, 525-537 (2006).

33. Launay, P. *et al.* TRPM4 is a Ca2+-activated nonselective cation channel mediating cell membrane depolarization. *Cell* **109**, 397-407 (2002).

34. Prawitt, D. *et al.* TRPM5 is a transient Ca2+-activated cation channel responding to rapid changes in [Ca2+]i. *Proc. Natl. Acad. Sci. U. S. A* **100**, 15166-15171 (2003).

35. Du, J., Xie, J. & Yue, L. Intracellular calcium activates TRPM2 and its alternative spliced isoforms. *Proc. Natl. Acad. Sci. U. S. A* **106**, 7239-7244 (2009).

36. Zurborg, S., Yurgionas, B., Jira, J. A., Caspani, O. & Heppenstall, P. A. Direct activation of the ion channel TRPA1 by Ca2+. *Nat. Neurosci.* **10**, 277-279 (2007).

37. Hara, Y. *et al.* LTRPC2 Ca2+-permeable channel activated by changes in redox status confers susceptibility to cell death. *Mol. Cell* **9**, 163-173 (2002).

38. Sano, Y. *et al.* Immunocyte Ca2+ influx system mediated by LTRPC2. *Science* **293**, 1327-1330 (2001).

39. Perraud, A. L. *et al.* ADP-ribose gating of the calcium-permeable LTRPC2 channel revealed by Nudix motif homology. *Nature* **411**, 595-599 (2001).

40. Vriens, J. *et al.* TRPM3 is a nociceptor channel involved in the detection of noxious heat. *Neuron* **70**, 482-494 (2011).

41. Grimm, C., Kraft, R., Schultz, G. & Harteneck, C. Activation of the melastatin-related cation channel TRPM3 by D-erythro-sphingosine [corrected]. *Mol. Pharmacol.* **67**, 798-805 (2005).

42. Lee, N. *et al.* Expression and characterization of human transient receptor potential melastatin 3 (hTRPM3). *J. Biol. Chem.* **278**, 20890-20897 (2003).

43. Grimm, C., Kraft, R., Sauerbruch, S., Schultz, G. & Harteneck, C. Molecular and functional characterization of the melastatin-related cation channel TRPM3. *J. Biol. Chem.* **278**, 21493-21501 (2003).

44. Liao, M., Cao, E., Julius, D. & Cheng, Y. Structure of the TRPV1 ion channel determined by electron cryo-microscopy. *Nature.* **504**, 107-112 (2013).

45. Cao, E., Liao, M., Cheng, Y. & Julius, D. TRPV1 structures in distinct conformations reveal activation mechanisms. *Nature* **504**, 113-118 (2013).

46. Gao, Y., Cao, E., Julius, D. & Cheng, Y. TRPV1 structures in nanodiscs reveal mechanisms of ligand and lipid action. *Nature* **534**, 347-351 (2016).

47. Paulsen, C. E., Armache, J. P., Gao, Y., Cheng, Y. & Julius, D. Structure of the TRPA1 ion channel suggests regulatory mechanisms. *Nature.* **520**, 511-517 (2015).

48. Zubcevic, L. *et al.* Cryo-electron microscopy structure of the TRPV2 ion channel. *Nat. Struct. Mol. Biol.* **23**, 180-186 (2016).

49. Huynh, K. W. *et al.* Structure of the full-length TRPV2 channel by cryo-EM. *Nat. Commun.* **7**, 11130 (2016).

50. Saotome, K., Singh, A. K., Yelshanskaya, M. V. & Sobolevsky, A. I. Crystal structure of the epithelial calcium channel TRPV6. *Nature* **534**, 506-511 (2016).

51. Shen, P. S. *et al.* The Structure of the Polycystic Kidney Disease Channel PKD2 in Lipid Nanodiscs. *Cell* **167**, 763-773 (2016).

52. Winn, M. P. *et al.* A mutation in the TRPC6 cation channel causes familial focal segmental glomerulosclerosis. *Science* **308**, 1801-1804 (2005).

53. Igarashi, P. & Somlo, S. Genetics and pathogenesis of polycystic kidney disease. *J. Am. Soc. Nephrol.* **13**, 2384-2398 (2002).

54. uer-Grumbach, M. *et al.* Alterations in the ankyrin domain of TRPV4 cause congenital distal SMA, scapuloperoneal SMA and HMSN2C. *Nat. Genet.* **42**, 160-164 (2010).

55. Kaneko, Y. & Szallasi, A. Transient receptor potential (TRP) channels: a clinical perspective. *Br. J. Pharmacol.* **171**, 2474-2507 (2014).

56. Desai, B. N. & Clapham, D. E. TRP channels and mice deficient in TRP channels. *Pflugers Arch.* **451**, 11-18 (2005).

57. Wilson, P. D. Polycystic kidney disease. *N. Engl. J. Med.* **350**, 151-164 (2004).

58. Gabow, P. A. Autosomal dominant polycystic kidney disease. *N. Engl. J. Med.* **329**, 332-342 (1993).

59. Gabow, P. A. Autosomal dominant polycystic kidney disease--more than a renal disease. *Am. J. Kidney Dis.* **16**, 403-413 (1990).

60. Mochizuki, T. *et al.* PKD2, a gene for polycystic kidney disease that encodes an integral membrane protein. *Science* **272**, 1339-1342 (1996).

61. The polycystic kidney disease 1 gene encodes a 14 kb transcript and lies within a duplicated region on chromosome 16. The European Polycystic Kidney Disease Consortium. *Cell* **78**, 725 (1994).

62. Peters, D. J. & Sandkuijl, L. A. Genetic heterogeneity of polycystic kidney disease in Europe. *Contrib. Nephrol.* **97**, 128-139 (1992).

63. Tan, Y. C., Blumenfeld, J. & Rennert, H. Autosomal dominant polycystic kidney disease: genetics, mutations and microRNAs. *Biochim. Biophys. Acta* **1812**, 1202-1212 (2011).

64. Nims, N., Vassmer, D. & Maser, R. L. Transmembrane domain analysis of polycystin-1, the product of the polycystic kidney disease-1 (PKD1) gene: evidence for 11 membrane-spanning domains. *Biochemistry* **42**, 13035-13048 (2003).

65. Qian, F. *et al.* Cleavage of polycystin-1 requires the receptor for egg jelly domain and is disrupted by human autosomal-dominant polycystic kidney disease 1-associated mutations. *Proc. Natl. Acad. Sci. U. S. A* **99**, 16981-16986 (2002).

66. Qian, F. *et al.* PKD1 interacts with PKD2 through a probable coiled-coil domain. *Nat. Genet.* **16**, 179-183 (1997).

67. Lal, M. *et al.* Polycystin-1 C-terminal tail associates with beta-catenin and inhibits canonical Wnt signaling. *Hum. Mol. Genet.* **17**, 3105-3117 (2008).

68. Low, S. H. *et al.* Polycystin-1, STAT6, and P100 function in a pathway that transduces ciliary mechanosensation and is activated in polycystic kidney disease. *Dev. Cell* **10**, 57-69 (2006).

69. Vassilev, P. M. *et al.* Polycystin-2 is a novel cation channel implicated in defective intracellular Ca(2+) homeostasis in polycystic kidney disease. *Biochem. Biophys. Res. Commun.* **282**, 341-350 (2001).

70. Koulen, P. *et al.* Polycystin-2 is an intracellular calcium release channel. *Nat. Cell Biol.* **4**, 191-197 (2002).

71. Torres, V. E. & Harris, P. C. Autosomal dominant polycystic kidney disease: the last 3 years. *Kidney Int.* **76**, 149-168 (2009).

72. Foggensteiner, L. *et al.* Cellular and subcellular distribution of polycystin-2, the protein product of the PKD2 gene. *J. Am. Soc. Nephrol.* **11**, 814-827 (2000).

73. Ong, A. C. *et al.* Coordinate expression of the autosomal dominant polycystic kidney disease proteins, polycystin-2 and polycystin-1, in normal and cystic tissue. *Am. J. Pathol.* **154**, 1721-1729 (1999).

74. Cai, Y. *et al.* Identification and characterization of polycystin-2, the PKD2 gene product. *J. Biol. Chem.* **274**, 28557-28565 (1999).

75. Wilson, P. D., Geng, L., Li, X. & Burrow, C. R. The PKD1 gene product, "polycystin-1," is a tyrosine-phosphorylated protein that colocalizes with alpha2beta1-integrin in focal clusters in adherent renal epithelia. *Lab Invest* **79**, 1311-1323 (1999).

76. Yoder, B. K., Hou, X. & Guay-Woodford, L. M. The polycystic kidney disease proteins, polycystin-1, polycystin-2, polaris, and cystin, are co-localized in renal cilia. *J. Am. Soc. Nephrol.* **13**, 2508-2516 (2002).

77. Pazour, G. J., San Agustin, J. T., Follit, J. A., Rosenbaum, J. L. & Witman, G. B. Polycystin-2 localizes to kidney cilia and the ciliary level is elevated in orpk mice with polycystic kidney disease. *Curr. Biol.* **12**, R378-R380 (2002).

78. Nauli, S. M. *et al.* Polycystins 1 and 2 mediate mechanosensation in the primary cilium of kidney cells. *Nat. Genet.* **33**, 129-137 (2003).

79. Ong, A. C. & Wheatley, D. N. Polycystic kidney disease--the ciliary connection. *Lancet* **361**, 774-776 (2003).

80. Raj, A., Rifkin, S. A., Andersen, E. & van, O. A. Variability in gene expression underlies incomplete penetrance. *Nature* **463**, 913-918 (2010).

81. Ong, A. C. *et al.* Polycystin-1 expression in PKD1, early-onset PKD1, and TSC2/PKD1 cystic tissue. *Kidney Int.* **56**, 1324-1333 (1999).

82. Qian, F., Watnick, T. J., Onuchic, L. F. & Germino, G. G. The molecular basis of focal cyst formation in human autosomal dominant polycystic kidney disease type I. *Cell* **87**, 979-987 (1996).

83. Cornec-Le, G. E., Audrezet, M. P., Le, M. Y., Chen, J. M. & Ferec, C. Genetics and pathogenesis of autosomal dominant polycystic kidney disease: 20 years on. *Hum. Mutat.* **35**, 1393-1406 (2014).

84. Koptides, M., Hadjimichael, C., Koupepidou, P., Pierides, A. & Constantinou, D. C. Germinal and somatic mutations in the PKD2 gene of renal cysts in autosomal dominant polycystic kidney disease. *Hum. Mol. Genet.* **8**, 509-513 (1999).

85. Brasier, J. L. & Henske, E. P. Loss of the polycystic kidney disease (PKD1) region of chromosome 16p13 in renal cyst cells supports a loss-of-function model for cyst pathogenesis. *J. Clin. Invest* **99**, 194-199 (1997).

86. Pei, Y. *et al.* Somatic PKD2 mutations in individual kidney and liver cysts support a "two-hit" model of cystogenesis in type 2 autosomal dominant polycystic kidney disease. *J. Am. Soc. Nephrol.* **10**, 1524-1529 (1999).

87. Jiang, S. T. *et al.* Defining a link with autosomal-dominant polycystic kidney disease in mice with congenitally low expression of Pkd1. *Am. J. Pathol.* **168**, 205-220 (2006).

88. Lantinga-van, L., I *et al.* Lowering of Pkd1 expression is sufficient to cause polycystic kidney disease. *Hum. Mol. Genet.* **13**, 3069-3077 (2004).

89. Kim, I. *et al.* Polycystin-2 expression is regulated by a PC2-binding domain in the intracellular portion of fibrocystin. *J. Biol. Chem.* **283**, 31559-31566 (2008).

90. Fedeles, S. V. *et al.* A genetic interaction network of five genes for human polycystic kidney and liver diseases defines polycystin-1 as the central determinant of cyst formation. *Nat. Genet.* **43**, 639-647 (2011).

91. Raphael, K. L. *et al.* Inactivation of Pkd1 in principal cells causes a more severe cystic kidney disease than in intercalated cells. *Kidney Int.* **75**, 626-633 (2009).

92. Piontek, K., Menezes, L. F., Garcia-Gonzalez, M. A., Huso, D. L. & Germino, G. G. A critical developmental switch defines the kinetics of kidney cyst formation after loss of Pkd1. *Nat. Med.* **13**, 1490-1495 (2007).

93. Hopp, K. *et al.* Functional polycystin-1 dosage governs autosomal dominant polycystic kidney disease severity. *J. Clin. Invest* **122**, 4257-4273 (2012).

94. Happe, H. & Peters, D. J. Translational research in ADPKD: lessons from animal models. *Nat. Rev. Nephrol.* **10**, 587-601 (2014).

95. Lanoix, J., D'Agati, V., Szabolcs, M. & Trudel, M. Dysregulation of cellular proliferation and apoptosis mediates human autosomal dominant polycystic kidney disease (ADPKD). *Oncogene* **13**, 1153-1160 (1996).

96. Woo, D. Apoptosis and loss of renal tissue in polycystic kidney diseases. *N. Engl. J. Med.* **333**, 18-25 (1995).

97. Nadasdy, T. *et al.* Proliferative activity of cyst epithelium in human renal cystic diseases. *J. Am. Soc. Nephrol.* **5**, 1462-1468 (1995).

98. Harris, P. C. & Torres, V. E. Polycystic kidney disease. *Annu. Rev. Med.* **60**, 321-337 (2009).

99. Shillingford, J. M. *et al.* The mTOR pathway is regulated by polycystin-1, and its inhibition reverses renal cystogenesis in polycystic kidney disease. *Proc. Natl. Acad. Sci. U. S. A* **103**, 5466-5471 (2006).

100. Boca, M. *et al.* Polycystin-1 induces resistance to apoptosis through the phosphatidylinositol 3-kinase/Akt signaling pathway. *J. Am. Soc. Nephrol.* **17**, 637-647 (2006).

101. Yamaguchi, T. *et al.* Cyclic AMP activates B-Raf and ERK in cyst epithelial cells from autosomal-dominant polycystic kidneys. *Kidney Int.* **63**, 1983-1994 (2003).

102. Bhunia, A. K. *et al.* PKD1 induces p21(waf1) and regulation of the cell cycle via direct activation of the JAK-STAT signaling pathway in a process requiring PKD2. *Cell* **109**, 157-168 (2002).

103. Arnould, T. *et al.* The polycystic kidney disease 1 gene product mediates protein kinase C alpha-dependent and c-Jun N-terminal kinase-dependent activation of the transcription factor AP-1. *J. Biol. Chem.* **273**, 6013-6018 (1998).

104. Markowitz, G. S. *et al.* Polycystin-2 expression is developmentally regulated. *Am. J. Physiol.* **277**, F17-F25 (1999).

105. Obermuller, N. *et al.* Altered expression pattern of polycystin-2 in acute and chronic renal tubular diseases. *J. Am. Soc. Nephrol.* **13**, 1855-1864 (2002).

106. Zhao, Y., Haylor, J. L. & Ong, A. C. Polycystin-2 expression is increased following experimental ischaemic renal injury. *Nephrol. Dial. Transplant.* **17**, 2138-2144 (2002).

107. Prasad, S., McDaid, J. P., Tam, F. W., Haylor, J. L. & Ong, A. C. Pkd2 dosage influences cellular repair responses following ischemia-reperfusion injury. *Am. J. Pathol.* **175**, 1493-1503 (2009).

108. Lantinga-van, L., I *et al.* Common regulatory elements in the polycystic kidney disease 1 and 2 promoter regions. *Eur. J. Hum. Genet.* **13**, 649-659 (2005).

109. Sun, H. *et al.* MicroRNA-17 post-transcriptionally regulates polycystic kidney disease-2 gene and promotes cell proliferation. *Mol. Biol. Rep.* **37**, 2951-2958 (2010).

110. Patel, V. *et al.* miR-17~92 miRNA cluster promotes kidney cyst growth in polycystic kidney disease. *Proc. Natl. Acad. Sci. U. S. A* **110**, 10765-10770 (2013).

111. Tran, U. *et al.* The RNA-binding protein bicaudal C regulates polycystin 2 in the kidney by antagonizing miR-17 activity. *Development.* **137**, 1107-1116 (2010).

112. Araujo, P. R. *et al.* Before It Gets Started: Regulating Translation at the 5' UTR. *Comp. Funct. Genomics.* **2012:475731. Epub@2012 May 28.**, 475731 (2012).

113. Gebauer, F. & Hentze, M. W. Molecular mechanisms of translational control. *Nat. Rev. Mol. Cell Biol.* **5**, 827-835 (2004).

114. Sonenberg, N. & Hinnebusch, A. G. Regulation of translation initiation in eukaryotes: mechanisms and biological targets. *Cell.* **136**, 731-745 (2009).

115. Jackson, R. J., Hellen, C. U. & Pestova, T. V. The mechanism of eukaryotic translation initiation and principles of its regulation. *Nat. Rev. Mol. Cell Biol.* **11**, 113-127 (2010).

116. Conne, B., Stutz, A. & Vassalli, J. D. The 3' untranslated region of messenger RNA: A molecular 'hotspot' for pathology? *Nat. Med.* **6**, 637-641 (2000).

117. Pesole, G. *et al.* Structural and functional features of eukaryotic mRNA untranslated regions. *Gene.* **276**, 73-81 (2001).

118. Matsui, M., Yachie, N., Okada, Y., Saito, R. & Tomita, M. Bioinformatic analysis of post-transcriptional regulation by uORF in human and mouse. *FEBS. Lett.* **581**, 4184-4188 (2007).

119. Vogel, C. *et al.* Sequence signatures and mRNA concentration can explain two-thirds of protein abundance variation in a human cell line. *Mol. Syst. Biol.* **6:400.**, 400 (2010).

120. Calvo, S. E., Pagliarini, D. J. & Mootha, V. K. Upstream open reading frames cause widespread reduction of protein expression and are polymorphic among humans. *Proc. Natl. Acad. Sci. U. S. A.* **106**, 7507-7512 (2009).

121. Mueller, P. P. & Hinnebusch, A. G. Multiple upstream AUG codons mediate translational control of GCN4. *Cell.* **45**, 201-207 (1986).

122. Hinnebusch, A. G. Translational regulation of GCN4 and the general amino acid control of yeast. *Annu. Rev. Microbiol.* **59:407-50.**, 407-450 (2005).

123. Lohse, I., Reilly, P. & Zaugg, K. The CPT1C 5'UTR contains a repressing upstream open reading frame that is regulated by cellular energy availability and AMPK. *PLoS. One.* **6**, e21486 (2011).

124. Lee, Y. Y., Cevallos, R. C. & Jan, E. An upstream open reading frame regulates translation of GADD34 during cellular stresses that induce eIF2alpha phosphorylation. *J. Biol. Chem.* **284**, 6661-6673 (2009).

125. Palam, L. R., Baird, T. D. & Wek, R. C. Phosphorylation of eIF2 facilitates ribosomal bypass of an inhibitory upstream ORF to enhance CHOP translation. *J. Biol. Chem.* **286**, 10939-10949 (2011).

126. Vattem, K. M. & Wek, R. C. Reinitiation involving upstream ORFs regulates ATF4 mRNA translation in mammalian cells. *Proc. Natl. Acad. Sci. U. S. A* **101**, 11269-11274 (2004).

127. Holcik, M. & Sonenberg, N. Translational control in stress and apoptosis. *Nat. Rev. Mol. Cell Biol.* **6**, 318-327 (2005).

128. Gallie, D. R. A tale of two termini: a functional interaction between the termini of an mRNA is a prerequisite for efficient translation initiation. *Gene.* **216**, 1-11 (1998).

129. Varani, G. Delivering messages from the 3' end. *Proc. Natl. Acad. Sci. U. S. A.* **98**, 4288-4289 (2001).

130. Gingras, A. C., Raught, B. & Sonenberg, N. eIF4 initiation factors: effectors of mRNA recruitment to ribosomes and regulators of translation. *Annu. Rev. Biochem.* **68:913-63.**, 913-963 (1999).

131. Mazumder, B. & Fox, P. L. Delayed translational silencing of ceruloplasmin transcript in gamma interferon-activated U937 monocytic cells: role of the 3' untranslated region. *Mol. Cell Biol.* **19**, 6898-6905 (1999).

132. Mazumder, B., Seshadri, V., Imataka, H., Sonenberg, N. & Fox, P. L. Translational silencing of ceruloplasmin requires the essential elements of mRNA circularization: poly(A) tail, poly(A)-binding protein, and eukaryotic translation initiation factor 4G. *Mol. Cell Biol.* **21**, 6440-6449 (2001).

133. Ostareck, D. H., Ostareck-Lederer, A., Shatsky, I. N. & Hentze, M. W. Lipoxygenase mRNA silencing in erythroid differentiation: The 3'UTR regulatory complex controls 60S ribosomal subunit joining. *Cell.* **104**, 281-290 (2001).

134. Ostareck, D. H. *et al.* mRNA silencing in erythroid differentiation: hnRNP K and hnRNP E1 regulate 15-lipoxygenase translation from the 3' end. *Cell.* **89**, 597-606 (1997).

135. Kong, J. & Lasko, P. Translational control in cellular and developmental processes. *Nat. Rev. Genet.* **13**, 383-394 (2012).

136. Schroder, M. & Kaufman, R. J. ER stress and the unfolded protein response. *Mutat. Res.* **569**, 29-63 (2005).

137. Fewell, S. W., Travers, K. J., Weissman, J. S. & Brodsky, J. L. The action of molecular chaperones in the early secretory pathway. *Annu. Rev. Genet.* **35**, 149-191 (2001).

138. Kornfeld, R. & Kornfeld, S. Assembly of asparagine-linked oligosaccharides. *Annu. Rev. Biochem.* **54**, 631-664 (1985).

139. Ellgaard, L., Molinari, M. & Helenius, A. Setting the standards: quality control in the secretory pathway. *Science* **286**, 1882-1888 (1999).

140. Shen, X., Zhang, K. & Kaufman, R. J. The unfolded protein response--a stress signaling pathway of the endoplasmic reticulum. *J. Chem. Neuroanat.* **28**, 79-92 (2004).

141. Schroder, M. & Kaufman, R. J. The mammalian unfolded protein response. *Annu. Rev. Biochem.* **74**, 739-789 (2005).

142. Wang, S. & Kaufman, R. J. The impact of the unfolded protein response on human disease. *J. Cell Biol.* **197**, 857-867 (2012).

143. Doyle, K. M. *et al.* Unfolded proteins and endoplasmic reticulum stress in neurodegenerative disorders. *J. Cell Mol. Med.* **15**, 2025-2039 (2011).

144. Dickhout, J. G., Carlisle, R. E. & Austin, R. C. Interrelationship between cardiac hypertrophy, heart failure, and chronic kidney disease: endoplasmic reticulum stress as a mediator of pathogenesis. *Circ. Res.* **108**, 629-642 (2011).

145. Kitamura, M. Endoplasmic reticulum stress and unfolded protein response in renal pathophysiology: Janus faces. *Am. J. Physiol Renal Physiol* **295**, F323-F334 (2008).

146. Minamino, T. & Kitakaze, M. ER stress in cardiovascular disease. *J. Mol. Cell Cardiol.* **48**, 1105-1110 (2010).

147. Ron, D. & Walter, P. Signal integration in the endoplasmic reticulum unfolded protein response. *Nat. Rev. Mol. Cell Biol.* **8**, 519-529 (2007).

148. Bertolotti, A., Zhang, Y., Hendershot, L. M., Harding, H. P. & Ron, D. Dynamic interaction of BiP and ER stress transducers in the unfolded-protein response. *Nat. Cell Biol.* **2**, 326-332 (2000).

149. Scheuner, D. & Kaufman, R. J. The unfolded protein response: a pathway that links insulin demand with beta-cell failure and diabetes. *Endocr. Rev.* **29**, 317-333 (2008).

150. Harding, H. P., Zhang, Y., Bertolotti, A., Zeng, H. & Ron, D. Perk is essential for translational regulation and cell survival during the unfolded protein response. *Mol. Cell* **5**, 897-904 (2000).

151. Ron, D. Translational control in the endoplasmic reticulum stress response. *J. Clin. Invest* **110**, 1383-1388 (2002).

152. Harding, H. P., Zhang, Y. & Ron, D. Protein translation and folding are coupled by an endoplasmic-reticulum-resident kinase. *Nature* **397**, 271-274 (1999).

153. Wang, X. Z. *et al.* Cloning of mammalian Ire1 reveals diversity in the ER stress responses. *EMBO J.* **17**, 5708-5717 (1998).

154. Tirasophon, W., Welihinda, A. A. & Kaufman, R. J. A stress response pathway from the endoplasmic reticulum to the nucleus requires a novel bifunctional protein kinase/endoribonuclease (Ire1p) in mammalian cells. *Genes Dev.* **12**, 1812-1824 (1998).

155. Yoshida, H., Matsui, T., Yamamoto, A., Okada, T. & Mori, K. XBP1 mRNA is induced by ATF6 and spliced by IRE1 in response to ER stress to produce a highly active transcription factor. *Cell* **107**, 881-891 (2001).

156. Haze, K., Yoshida, H., Yanagi, H., Yura, T. & Mori, K. Mammalian transcription factor ATF6 is synthesized as a transmembrane protein and activated by proteolysis in response to endoplasmic reticulum stress. *Mol. Biol. Cell* **10**, 3787-3799 (1999).

157. Cao, S. S. & Kaufman, R. J. Unfolded protein response. *Curr. Biol.* **22**, R622-R626 (2012).

158. Nishitoh, H. *et al.* ASK1 is essential for endoplasmic reticulum stress-induced neuronal cell death triggered by expanded polyglutamine repeats. *Genes Dev.* **16**, 1345-1355 (2002).

159. Urano, F. *et al.* Coupling of stress in the ER to activation of JNK protein kinases by transmembrane protein kinase IRE1. *Science* **287**, 664-666 (2000).

160. Ron, D. & Walter, P. Signal integration in the endoplasmic reticulum unfolded protein response. *Nat. Rev. Mol. Cell Biol.* **8**, 519-529 (2007).

161. Kaufman, R. J. Orchestrating the unfolded protein response in health and disease. *J. Clin. Invest* **110**, 1389-1398 (2002).

162. vis-Smyth, T., Duncan, R. C., Zheng, T., Michelotti, G. & Levens, D. The far upstream element-binding proteins comprise an ancient family of single-strand DNA-binding transactivators. *J. Biol. Chem.* **271**, 31679-31687 (1996).

163. Weber, A. *et al.* The FUSE binding proteins FBP1 and FBP3 are potential c-myc regulators in renal, but not in prostate and bladder cancer. *BMC. Cancer* **8**, 369 (2008).

164. Lu, J. Y. & Schneider, R. J. Tissue distribution of AU-rich mRNA-binding proteins involved in regulation of mRNA decay. *J. Biol. Chem.* **279**, 12974-12979 (2004).

165. Duncan, R. *et al.* A sequence-specific, single-strand binding protein activates the far upstream element of c-myc and defines a new DNA-binding motif. *Genes Dev.* **8**, 465-480 (1994).

166. Zhang, J. & Chen, Q. M. Far upstream element binding protein 1: a commander of transcription, translation and beyond. *Oncogene* **32**, 2907-2916 (2013).

167. Irwin, N., Baekelandt, V., Goritchenko, L. & Benowitz, L. I. Identification of two proteins that bind to a pyrimidine-rich sequence in the 3'-untranslated region of GAP-43 mRNA. *Nucleic Acids Res.* **25**, 1281-1288 (1997).

168. Bettegowda, C. *et al.* Mutations in CIC and FUBP1 contribute to human oligodendroglioma. *Science* **333**, 1453-1455 (2011).

169. Rabenhorst, U. *et al.* Overexpression of the far upstream element binding protein 1 in hepatocellular carcinoma is required for tumor growth. *Hepatology* **50**, 1121-1129 (2009).

170. Malz, M. *et al.* Overexpression of far upstream element binding proteins: a mechanism regulating proliferation and migration in liver cancer cells. *Hepatology* **50**, 1130-1139 (2009).

171. Zubaidah, R. M. *et al.* 2-D DIGE profiling of hepatocellular carcinoma tissues identified isoforms of far upstream binding protein (FUBP) as novel candidates in liver carcinogenesis. *Proteomics.* **8**, 5086-5096 (2008).

172. Kim, M. J. *et al.* Downregulation of FUSE-binding protein and c-myc by tRNA synthetase cofactor p38 is required for lung cell differentiation. *Nat. Genet.* **34**, 330-336 (2003).

173. Williams, B. Y., Hamilton, S. L. & Sarkar, H. K. The survival motor neuron protein interacts with the transactivator FUSE binding protein from human fetal brain. *FEBS Lett.* **470**, 207-210 (2000).

174. Liu, J. *et al.* The FUSE/FBP/FIR/TFIIH system is a molecular machine programming a pulse of c-myc expression. *EMBO J.* **25**, 2119-2130 (2006).

175. Braddock, D. T., Louis, J. M., Baber, J. L., Levens, D. & Clore, G. M. Structure and dynamics of KH domains from FBP bound to single-stranded DNA. *Nature* **415**, 1051-1056 (2002).

176. Benjamin, L. R. *et al.* Hierarchical mechanisms build the DNA-binding specificity of FUSE binding protein. *Proc. Natl. Acad. Sci. U. S. A* **105**, 18296-18301 (2008).

177. Liu, J. *et al.* The FBP interacting repressor targets TFIIH to inhibit activated transcription. *Mol. Cell* **5**, 331-341 (2000).

178. Valverde, R., Edwards, L. & Regan, L. Structure and function of KH domains. *FEBS J.* **275**, 2712-2726 (2008).

179. Kusik, B. W., Hammond, D. R. & Udvadia, A. J. Transcriptional regulatory regions of gap43 needed in developing and regenerating retinal ganglion cells. *Dev. Dyn.* **239**, 482-495 (2010).

180. Nishizawa, K. & Okamoto, H. Mutation analysis of the role for the carboxy-terminus encoding region in NGF-induced stabilization of GAP-43 mRNA. *Biochem. Biophys. Res. Commun.* **205**, 1380-1385 (1994).

181. Colombo, E., Alcalay, M. & Pelicci, P. G. Nucleophosmin and its complex network: a possible therapeutic target in hematological diseases. *Oncogene* **30**, 2595-2609 (2011).

182. Grisendi, S. *et al.* Role of nucleophosmin in embryonic development and tumorigenesis. *Nature* **437**, 147-153 (2005).

183. Olanich, M. E., Moss, B. L., Piwnica-Worms, D., Townsend, R. R. & Weber, J. D. Identification of FUSE-binding protein 1 as a regulatory mRNA-binding protein that represses nucleophosmin translation. *Oncogene* **30**, 77-86 (2011).

184. Chien, H. L., Liao, C. L. & Lin, Y. L. FUSE binding protein 1 interacts with untranslated regions of Japanese encephalitis virus RNA and negatively regulates viral replication. *J. Virol.* **85**, 4698-4706 (2011).

185. Molland, K. L., Paul, L. N. & Yernool, D. A. Crystal structure and characterization of coiled-coil domain of the transient receptor potential channel PKD2L1. *Biochim. Biophys. Acta.* **1824**, 413-421 (2012).

186. Molland, K. L., Narayanan, A., Burgner, J. W. & Yernool, D. A. Identification of the structural motif responsible for trimeric assembly of the C-terminal regulatory domains of polycystin channels PKD2L1 and PKD2. *Biochem. J.* **429**, 171-183 (2010).

187. Li, Q., Liu, Y., Zhao, W. & Chen, X. Z. The calcium-binding EF-hand in polycystin-L is not a domain for channel activation and ensuing inactivation. *FEBS Lett.* **516**, 270-278 (2002).

188. Chen, X. Z. *et al.* Polycystin-L is a calcium-regulated cation channel permeable to calcium ions. *Nature.* **401**, 383-386 (1999).

189. Inada, H. *et al.* Off-response property of an acid-activated cation channel complex PKD1L3-PKD2L1. *EMBO Rep.* **9**, 690-697 (2008).

190. Ishimaru, Y. *et al.* Transient receptor potential family members PKD1L3 and PKD2L1 form a candidate sour taste receptor. *Proc. Natl. Acad. Sci. U. S. A.* **103**, 12569-12574 (2006).

191. Horio, N. *et al.* Sour taste responses in mice lacking PKD channels. *PLoS. One.* **6**, e20007 (2011).

192. Nelson, T. M. *et al.* Taste function in mice with a targeted mutation of the pkd1l3 gene. *Chem. Senses.* **35**, 565-577 (2010).

193. Fujimoto, C. *et al.* The single pore residue Asp523 in PKD2L1 determines Ca2+ permeation of the PKD1L3/PKD2L1 complex. *Biochem. Biophys. Res. Commun.* **404**, 946-951 (2011).

194. Yu, Y. *et al.* Molecular mechanism of the assembly of an acid-sensing receptor ion channel complex. *Nat. Commun.* **3**, 1252 (2012).

195. Li, Q. *et al.* Direct binding of alpha-actinin enhances TRPP3 channel activity. *J. Neurochem.* **103**, 2391-2400 (2007).

196. Basora, N. *et al.* Tissue and cellular localization of a novel polycystic kidney disease-like gene product, polycystin-L. *J. Am. Soc. Nephrol.* **13**, 293-301 (2002).

197. Lopezjimenez, N. D. *et al.* Two members of the TRPP family of ion channels, Pkd1l3 and Pkd2l1, are co-expressed in a subset of taste receptor cells. *J. Neurochem.* **98**, 68-77 (2006).

198. Huang, A. L. *et al.* The cells and logic for mammalian sour taste detection. *Nature.* **442**, 934-938 (2006).

199. Huque, T. *et al.* Sour ageusia in two individuals implicates ion channels of the ASIC and PKD families in human sour taste perception at the anterior tongue. *PLoS. One.* **4**, e7347 (2009).

200. Hussein, S. *et al.* Acid-induced off-response of PKD2L1 channel in Xenopus oocytes and its regulation by Ca(2.). *Sci. Rep.* **5**, 15752 (2015).

201. Yu, Y. *et al.* Structural and molecular basis of the assembly of the TRPP2/PKD1 complex. *Proc. Natl. Acad. Sci. U. S. A.* **106**, 11558-11563 (2009).

202. Ong, A. C. & Harris, P. C. A polycystin-centric view of cyst formation and disease: the polycystins revisited. *Kidney Int.* 10 (2015).

203. Ishimaru, Y. *et al.* Interaction between PKD1L3 and PKD2L1 through their transmembrane domains is required for localization of PKD2L1 at taste pores in taste cells of circumvallate and foliate papillae. *FASEB J.* **24**, 4058-4067 (2010).

204. Fukata, Y. & Fukata, M. Protein palmitoylation in neuronal development and synaptic plasticity. *Nat. Rev. Neurosci.* **11**, 161-175 (2010).

205. Baekkeskov, S. & Kanaani, J. Palmitoylation cycles and regulation of protein function (Review). *Mol. Membr. Biol.* **26**, 42-54 (2009).

206. Linder, M. E. & Deschenes, R. J. Palmitoylation: policing protein stability and traffic. *Nat. Rev. Mol. Cell Biol.* **8**, 74-84 (2007).

207. el-Husseini, A. & Bredt, D. S. Protein palmitoylation: a regulator of neuronal development and function. *Nat. Rev. Neurosci.* **3**, 791-802 (2002).

208. Yeste-Velasco, M., Linder, M. E. & Lu, Y. J. Protein S-palmitoylation and cancer. *Biochim. Biophys. Acta.* **1856**, 107-120 (2015).

209. Raymond, F. L. *et al.* Mutations in ZDHHC9, which encodes a palmitoyltransferase of NRAS and HRAS, cause X-linked mental retardation associated with a Marfanoid habitus. *Am. J. Hum. Genet.* **80**, 982-987 (2007).

210. Blaskovic, S., Blanc, M. & van der Goot, F. G. What does S-palmitoylation do to membrane proteins? *FEBS J.* **280**, 2766-2774 (2013).

211. Shipston, M. J. Ion channel regulation by protein S-acylation. *J. Gen. Physiol.* **143**, 659-678 (2014).

212. Roth, A. F. *et al.* Global analysis of protein palmitoylation in yeast. *Cell* **125**, 1003-1013 (2006).

213. Nadolski, M. J. & Linder, M. E. Molecular recognition of the palmitoylation substrate Vac8 by its palmitoyltransferase Pfa3. *J. Biol. Chem.* **284**, 17720-17730 (2009).

214. Varner, A. S. *et al.* Characterization of human palmitoyl-acyl transferase activity using peptides that mimic distinct palmitoylation motifs. *Biochem. J.* **373**, 91-99 (2003).

215. Ohno, Y., Kihara, A., Sano, T. & Igarashi, Y. Intracellular localization and tissue-specific distribution of human and yeast DHHC cysteine-rich domain-containing proteins. *Biochim. Biophys. Acta* **1761**, 474-483 (2006).

216. Tomatis, V. M., Trenchi, A., Gomez, G. A. & Daniotti, J. L. Acyl-protein thioesterase 2 catalyzes the deacylation of peripheral membrane-associated GAP-43. *PLoS. One.* **5**, e15045 (2010).

217. Zeidman, R., Jackson, C. S. & Magee, A. I. Protein acyl thioesterases (Review). *Mol. Membr. Biol.* **26**, 32-41 (2009).

218. Siegel, G. *et al.* A functional screen implicates microRNA-138-dependent regulation of the depalmitoylation enzyme APT1 in dendritic spine morphogenesis. *Nat. Cell Biol.* **11**, 705-716 (2009).

219. Duncan, J. A. & Gilman, A. G. A cytoplasmic acyl-protein thioesterase that removes palmitate from G protein alpha subunits and p21(RAS). *J. Biol. Chem.* **273**, 15830-15837 (1998).

220. Rusch, M. *et al.* Identification of acyl protein thioesterases 1 and 2 as the cellular targets of the Ras-signaling modulators palmostatin B and M. *Angew. Chem. Int. Ed Engl.* **50**, 9838-9842 (2011).

221. Tian, L., McClafferty, H., Knaus, H. G., Ruth, P. & Shipston, M. J. Distinct acyl protein transferases and thioesterases control surface expression of calcium-activated potassium channels. *J. Biol. Chem.* **287**, 14718-14725 (2012).

222. Schmidt, J. W. & Catterall, W. A. Palmitylation, sulfation, and glycosylation of the alpha subunit of the sodium channel. Role of post-translational modifications in channel assembly. *J. Biol. Chem.* **262**, 13713-13723 (1987).

223. Rasaiah, J. C., Garde, S. & Hummer, G. Water in nonpolar confinement: from nanotubes to proteins and beyond. *Annu. Rev. Phys. Chem.* **59**, 713-740 (2008).

224. Beckstein, O. & Sansom, M. S. Liquid-vapor oscillations of water in hydrophobic nanopores. *Proc. Natl. Acad. Sci. U. S. A* **100**, 7063-7068 (2003).

225. Hummer, G., Rasaiah, J. C. & Noworyta, J. P. Water conduction through the hydrophobic channel of a carbon nanotube. *Nature* **414**, 188-190 (2001).

226. Aryal, P., Sansom, M. S. & Tucker, S. J. Hydrophobic gating in ion channels. *J. Mol. Biol.* **427**, 121-130 (2015).

227. Bass, R. B., Strop, P., Barclay, M. & Rees, D. C. Crystal structure of Escherichia coli MscS, a voltage-modulated and mechanosensitive channel. *Science* **298**, 1582-1587 (2002).

228. Wang, W. *et al.* The structure of an open form of an E. coli mechanosensitive channel at 3.45 A resolution. *Science* **321**, 1179-1183 (2008).

229. Jeon, J. P. *et al.* Activation of TRPC4beta by Galphai subunit increases Ca2+ selectivity and controls neurite morphogenesis in cultured hippocampal neuron. *Cell Calcium* **54**, 307-319 (2013).

230. Yeh, B. I., Kim, Y. K., Jabbar, W. & Huang, C. L. Conformational changes of pore helix coupled to gating of TRPV5 by protons. *EMBO J.* **24**, 3224-3234 (2005).

231. Chen, J. *et al.* Pore dilation occurs in TRPA1 but not in TRPM8 channels. *Mol. Pain* **5**, 3 (2009).

232. Gees, M., Colsoul, B. & Nilius, B. The role of transient receptor potential cation channels in Ca2+ signaling. *Cold Spring Harb. Perspect. Biol.* **2**, a003962 (2010).

233. Chung, M. K., Guler, A. D. & Caterina, M. J. TRPV1 shows dynamic ionic selectivity during agonist stimulation. *Nat. Neurosci.* **11**, 555-564 (2008).

234. Aryal, P., bd-Wahab, F., Bucci, G., Sansom, M. S. & Tucker, S. J. A hydrophobic barrier deep within the inner pore of the TWIK-1 K2P potassium channel. *Nat. Commun.* **5**, 4377 (2014).

235. Yoshimura, K., Batiza, A., Schroeder, M., Blount, P. & Kung, C. Hydrophilicity of a single residue within MscL correlates with increased channel mechanosensitivity. *Biophys. J.* **77**, 1960-1972 (1999).

236. Ou, X., Blount, P., Hoffman, R. J. & Kung, C. One face of a transmembrane helix is crucial in mechanosensitive channel gating. *Proc. Natl. Acad. Sci. U. S. A* **95**, 11471-11475 (1998).

237. Reeders, S. T. Multilocus polycystic disease. *Nat. Genet.* **1**, 235-237 (1992).

CHAPTER 2

RESULTS #1

Translational up-regulation of polycystic kidney disease protein PKD2 by endoplasmic reticulum stress

2.1 ABSTRACT

Autosomal dominant polycystic kidney disease (ADPKD) is caused by mutations in PKD1 or PKD2, and affects over 10 million people worldwide. It is characterized by cyst formation in kidney, liver and pancreas. Dosage changes in PKD1/PKD2 are important in ADPKD pathogenesis; therefore their expression/function has to be strictly regulated. However, how they are regulated remain poorly understood. Recent studies have linked PKD2 regulation to endoplasmic reticulum (ER) stress that is implicated in neuronal, cardiac and renal diseases. One major ER stress downstream is phosphorylation of eukaryotic initiation factor eIF2α by kinase PERK, which attenuates global protein translation and enhances translation of selected proteins. Here we showed that PKD2 protein expression is up-regulated by different stresses that all increase phosphorylated eIF2α (P-eIF2α) in several mammalian cells. Increasing P-eIF2α by over-expression or inhibiting the phosphatase activity resulted in increased PKD2. PCR and polysome-binding assays showed that ER stress does not affect the PKD2 mRNA level but increase its binding with ribosomes, indicating that P-eIF2α translationally up-regulates PKD2. By mutation analysis we found that the upstream open reading frame (uORF) in the 5'-untranslated region of PKD2 mRNA represses PKD2 translation. Thus, ER stress and P-eIF2α translationally up-regulates PKD2 through bypassing the inhibitory uORF.

2.2 INTRODUCTION

Autosomal dominant polycystic kidney disease (ADPKD) is an inherited genetic disorder, characterized by cyst formation in kidney, liver and pancreas. ADPKD originates from mutations in the PKD1 gene encoding PKD1 (~85%) or the PKD2 gene encoding PKD2 (~15%) in one allele and cysts form when the remaining PKD1 or PKD2 undergoes a somatic pathogenic mutation or dosage reduction [1]. The cystogenesis can be recapitulated by gene mutation or solely dosage reduction in rodent and fish models [2-5]. Interestingly, cystogenesis may derive from gain-of-function of PKD1 or PKD2 as well [6,7]. Thus, too much or too little PKD1/PKD2 are both cystogenic, and their expression/function has to be strictly regulated. At the cellular level, ADPKD is associated with several abnormalities, such as cell over-proliferation, apoptosis and de-differentiation. While PKD1 is a large membrane receptor-like protein, PKD2, composed of 968 amino acids, is a Ca^{2+}-permeable non-selective cation channel, mainly localized on the endoplasmic reticulum (ER) membrane but also on the plasma and primary cilia membranes [8,9]. Regulation of PKD1 and PKD2 function is connected to pathways involving renal primary cilia, Ca^{2+} signaling, mammalian target of rapamycin (mTOR) and the vasopressin receptor [10]. Based on these connections, anti-proliferative drugs aimed at slowing growth of cysts have been tested recently in clinical trials, of which the results have however been disappointing [11-13]. Thus, it is important to explore novel pathways and mechanisms.

In fact, recent studies have shown that PKD2 is involved in cell proliferation and apoptosis through cross-talk with cellular pathways related to ER stress or ER Ca^{2+} homeostasis [14-16]. ER stress refers to cellular states in which misfolded or unfolded proteins accumulate in the ER, and induces unfolded protein response (UPR) to restore homeostasis, or lead to apoptosis in the presence of prolonged stress [17,18]. PKD2 inhibits cell proliferation and protein synthesis

through promoting the phosphorylation of eukaryotic initiation factor 2α (P-eIF2α) by pancreatic ER-resident eIF2α kinase (PERK) which itself is activated by ER stress [14]. It was also reported that PKD2 inhibits cell proliferation and functions as an anti-apoptotic channel protein through modulating ER Ca^{2+} homeostasis [15,16].

Reversely, abnormal cellular or tissue conditions regulate PKD2 expression. For example, prolonged application of tunicamycin (Tm) in culture cell lines, which induces prolonged ER stress, down-regulates PKD2 expression through ER-associated degradation (ERAD) [19]. Also, PKD2 expression is substantially increased following ischemia-reperfusion (I/R) injury in adult rat kidney and it is interesting to note that I/R-induced PKD2 expression is primarily on the ER membrane [20]. In general, the I/R condition in cells simultaneously induces different cellular stresses including oxidative stress, ER stress and amino acid depletion [21]. However, it is still not clearly understood as to how PKD2 expression is regulated and what the role of PKD2 is in cellular stress conditions. ER stress and UPR are associated with numerous human diseases, such as neuronal, cardiac and renal diseases, as well as inflammation and cancer [22,23]. Indeed, ER stress is associated with a number of renal diseases, such as membranous nephropathy, glomerular disease, and tubular disease induced by ischemic injury, heavy metal or other agents [24-26].

As part of UPR, PERK kinase is activated and phosphorylates eIF2α at serine 51. As a translation initiation inhibitor, phosphorylated eIF2α (P-eIF2α) rapidly represses global protein synthesis, which prevents further accumulation of misfolded proteins in the ER [27]. In mammals, eIF2α can also be phosphorylated by three other kinases, heme regulated inhibitor (HRI) induced by oxidative stress, dsRNA-induced protein kinase (PKR) induced by viral infection, and general control nonderepressible-2 (GCN2) induced by nutrient depletion [28]. The reprogramming of gene

expression through P-eIF2α during several cellular stresses plays a pivotal role in determining cell survival or apoptosis [18]. Interestingly, P-eIF2α also translationally and/or transcriptionally up-regulates some selective genes, such as activating transcription factor 4 (ATF4), C/EBP homologous protein (CHOP), and growth arrest and DNA damage-inducible protein (Gadd34) that are critical for efficiently coping with cellular stress conditions [29]. These genes share a common feature in that in the 5' untranslated region (UTR) of their mRNAs there is an upstream open reading frame (uORF) that is inhibitory for the translation of the main ORF under normal, non-stress condition. The mechanism of inhibition is not fully understood but one possibility is that under non-stress condition the translated short peptide from uORF somehow inhibits the translation of the main ORF. Under stress conditions elevated P-eIF2α delays the initiation of scanning ribosomes, which bypasses the translation of uORF and enhances the translation of the main ORF [30].

In the present study, we examined how ER stress, P-eIF2α, and uORF of PKD2 mRNA mediate translational up-regulation of PKD2 protein expression, using commercial mammalian culture cell lines as well as those from PKD2 knockout (KO) mouse collecting duct (MCD) cells and PERK KO mouse embryonic fibroblast (MEF) cells, in combination with Western blotting (WB), reverse transcription polymerase chain reaction (RT-PCR), real-time PCR, ribosome binding analysis, luciferase reporter, gene knockdown (KD), and over-expression.

2.3 METHODS

Cell culture, plasmid constructs and gene transfection

Henrietta Lacks (HeLa), Madin-Darby canine kidney (MDCK) and human embryonic kidney 293T (HEK293T) cells were cultured in Dulbecco's modified Eagle's medium (DMEM) supplemented with L-glutamine, penicillin-streptomycin, and 10% fetal bovine serum (FBS) at 37˚C and 5% CO_2. *PERK*$^{+/+}$ and *PERK*$^{-/-}$ MEF cells and MCD D3 (*PKD2*$^{+/-}$) and B2 (*PKD2*$^{-/-}$) were provided by Dr. Guanqing Wu (Vanderbilt University) and maintained as described previously [31,32]. Plasmids pEGFP-C2-PKD2, pcDNA3.1(+)-PERK, pcDNA3.1(+)-PERK K618A, pcDNA3.1(+)-PERK ΔC (a C-terminus truncated mutant), pFLAG-CMV-2-Gadd34, pcDNA3.CD2-eIF2α and pcDNA3.CD2-eIF2α S51A were described previously [33-36]. Luciferase vector BI16 is a gift from Dr. Grabczyk (Louisiana State University) and it contains both Firefly and Renilla luciferase gene sequences sharing a bidirectional promoter [37]. A BamHI-NheI DNA fragment encoding the 5'UTR of the human PKD2 mRNA, along with the initiation codon of the PKD2 coding region, was inserted between the same restriction cutting sites in the BI16. Primer sequences used in this construct were as follows: sense 5'-GTCGGATCCCCGGGAAGAAAGGAACATG-3', and antisense 5'-CTGGCTAGCACCATCGCGGTCACTGGCGTC-3'. The resulting BI16-PKD2-5'UTR plasmid contains this 5'UTR sequence of PKD2 fused to the upstream of Renilla luciferase reporter gene. BI16-PKD2-ΔuORF and BI16-PKD2-ATG-to-TTG (with mutation of ATG initiation codon of PKD2 uORF to TTG) were generated using site II directed mutagenesis kit (Stratagene, La Jolla, CA, USA) following the manufacturer's instruction. In order to check the effect of recognition of uORF ATG initiation codon on the translation of downstream gene, the Kozak consensus surrounding the initiation codon was mutated to produce BI16-PKD2-KR (full-

length 5'UTR: GGAACA**ATG**GCTCC, KR: GGTACA**ATG**TCTCC). All plasmids were sequenced to ensure that there were only desired changes. Transient transfection was performed using Lipofectamine 2000 (Invitrogen, Carlsbad, CA, USA) following manufacturer's recommendation to HeLa and HEK293T cells at ~70% confluency.

Antibodies

Rabbit antibodies against PKD2, ATF4 and eIF2α, mouse antibodies against β-actin, green fluorescent protein (GFP) and heat shock protein 60 (HSP60), and goat antibodies against immunoglobulin heavy-chain binding protein (BiP, also called GRP78) and FLAG were purchased from Santa Cruz Biotech (Santa Cruz, CA, USA). Rabbit anti-P-eIF2α (on residue Ser 51) and mouse anti-c-Myc were purchased from Cell Signaling Technology (Pickering, ON, USA). Goat anti-PERK and rabbit anti-P-PERK for human cell lines were from R&D Systems (Minneapolis, MN, USA) and BioLegend (San Diego, CA, USA), respectively. Goat anti-PERK and rabbit anti-P-PERK for mouse cell lines were from Santa Cruz Biotech (Santa Cruz, CA, USA) and Cell Signaling Technology (Beverly, MA, USA), respectively. Secondary antibodies were purchased from GE Healthcare (Baie d'Urfe, QC, Canada).

RT-PCR and real-time RT-PCR

HeLa cells were treated with stress inducer thapsigargin (Tg) for 0.5, 1, 3, 6, or 12 hour (hr), respectively, and DMSO treatment was used as a control. Total cellular RNA was prepared using Trizol reagent (Invitrogen, Carlsbad, CA, USA) according to the instruction manual. Contaminating DNA was digested with RNase-free DNase (Promega, Madison, WI, USA). Single strand cDNA synthesis was carried out using Superscript III reverse transcriptase

(Invitrogen, Carlsbad, CA, USA) according to the manufacturer's instructions. PKD2, BiP, CHOP, and homocysteine-induced endoplasmic reticulum protein (herp) relative mRNA levels were determined by PCR using 28 cycles which was proved to be optimal. β-actin was used as loading control. The oligonucleotide primers for each gene were as follows: β-actin (sense 5'-CCTGGCACCCAGCACAAT-3' and antisense 5'-GGGCCGGACTCGTCATACT-3'), PKD2 sense 5'-GTATGACGGCTCACGCCTGTAATCC-3' and antisense 5'-AGAGATGGAGTTTCGCCACATTGCC-3'), CHOP (sense 5'-CCACTCTTGACCCTGCTTC-3' and antisense 5'-CCACTCTGTTTCCGTTTCC-3'), BiP (sense 5'-GAACACAGTGGTGCCTACCAAG-3' and antisense 5'-GGTGACTTCAATCTGTGGGACC-3') and Herp (sense 5'-CAATCAGAATGCTGCTCCTCAAG-3' and antisense 5'-GGTCCAATCCAACCAATCTCG-3'). Real-time PCR was performed using 7900HT Fast Real-Time PCR System (Applied Biosystems, Carlsbad, CA, USA) with the same primers. Quantitation of target genes was normalized using the reference β-actin. 7900HT Fast Real-Time PCR System software (version 2.4.1) was used to perform quantification and to generate Ct values. Values are a representation of three independent experiments, with standard errors as indicated.

Knockdown by small interfering RNA (siRNA)

Knockdown of human eIF2α by siRNA was performed using oligonucleotides at 100 nM with Lipofectamine 2000 according to the manufacturer's instructions. Oligonucleotides were purchased from Shanghai Gene Pharma Co, Shanghai, China: eIF2α (sense 5'-GGGUCUUUGAUGACAAGUATT-3', and antisense 5'-GGGUCUUUGAUGACAAGUATT-3'), its specific control siRNA (sense 5'-UUCUCCGAACGUGUCACGUTT-3' and antisense

5'-ACGUGACACGUUCGGAGAATT-3'). PKD2 knockdown by siRNA was described previously [33]. The efficiency of the siRNA knockdown was assessed by immunoblotting.

Sucrose gradient centrifugation and polysome analysis

HeLa cells were cultured as described above and treated with 1 μM Tg or DMSO for 3 hr. 15 min prior to harvesting, cells were treated with 100 μg/ml cycloheximide. Cells were washed three times with 1 × cold phosphate-buffered saline, and harvested directly on the plate using lysis buffer (20 mM HEPES-KOH, pH 7.4, 15 mM MgCl2, 200 mM KCl, 1% Triton X-100 (v/v), 100 μg/mL cycloheximide, 2 mM DTT, and 1 mg/mL heparin). Cell lysates were passed though a 23-gauge needle three times and then incubated on ice for 10 min. Nuclei and cell debris were cleared by centrifugation at 12, 000 × g for 10 min at 4℃ and the resulting supernatant was loaded onto a 7%-47% sucrose gradient solution containing 20 mM Tris-HCL (pH 7.4), 140 mM KCl, 5 mM MgCl2, 0.5 mM DTT, 0.1 mg/ml cycloheximicde, 0.2 mg/ml heparin. The sucrose gradients were then subjected to centrifugation in a Beckman SW-41 rotor for 4 hr at 25, 000 r.p.m. Fractions were collected from the top to bottom. To prevent degradation of RNA, equal volume of GulTC (6 M guanidium thiocyanate, 0.25 M sodium acetate) was added into each fractions and mix well. Equal volume isopropanol was used to precipitate RNA, and then resuspended in the same volume water for each fraction. Then the same volume of each fraction RNA was used to synthesize single-stranded cDNA using Superscript III reverse transcriptase (Invitrogen, Carlsbad, CA, USA) according to the manufacturer's instructions. Prepared cDNA was used to determine the relative mRNA levels for PKD2, CHOP, and β-actin with PCR. Oligonucleotide primers used in PCR were as follows: PKD2 (sense 5'-GTATGACGGCTCACGCCTGTAATCC-3' and antisense 5'-

AGAGATGGAGTTTCGCCACATTGCC-3'), CHOP (sense 5'-CCACTCTTGACCCTGCTTC-3' and antisense 5'-CCACT CTGTTTCCGTTTCC-3') and β-actin (sense 5'-CCTGGCACCCAGCACAAT-3' and antisense 5'-GGG CCGGACTCGTCATACT-3').

Dual luciferase assay

HeLa cells were cultured and plasmids transfections were performed as described above using BI16 (empty vector), PKD2-5'UTR, -ATG-to-TTG, -ΔuORF and -KR. 12 hr after transfection, cells were collected and dual luciferase assays were carried out with Dual-Luciferase® Reporter Assay System (Promega, Madison, WI, USA) according to the instruction manual. Values are a measure of a ratio of Renilla versus firefly luciferase units (relative light units) and represent the mean values of three independent transfections, with standard errors as indicated. Firefly luciferase values did not change significantly in the dual reporter assays.

Glycosylation analysis

Cell extracts were prepared by solubilization in cell lysis reagent (CelLytic™ M, Sigma-Aldrich, St. Louis, MO, USA) supplemented with a Halt™ protease inhibitor cocktail (Thermo Scientific, Waltham, MA, USA). Total proteins (60 μg) were denatured following manufacturer's protocols (New England BioLabs, Ipswich, MA, USA), and incubated with non-treated enzyme, 1000 units of endoglycosidase H (Endo H), or 1000 units of peptide N-glycosidase F (PNGase F) for 1 hr at 37℃ in buffer (50 μl). The reaction products were separated by SDS-PAGE and analyzed by WB.

Data analysis

Signals were quantified by Gel-Pro Analyzer (Sigma-Aldrich, St. Louis, MO, USA) and data were analyzed and plotted using SigmaPlot 12 (Systat Software, San Jose, CA, USA), and expressed as mean ± s.e.m. (N), where s.e.m. represents the standard error of the mean and N indicates the number of experimental repeats. A probability value (P) of less than 0.05 and 0.01 was considered significant and very significant, respectively.

2.4 RESULTS

Effects of ER stress induced by Tg or tunicamycin (Tm) on PKD2 protein and mRNA expression

It was previously reported that renal ischemia/reperfusion, which induces several cellular stress conditions among many other alterations, substantially increases PKD2 expression, notably PKD2 on the ER membrane [20,21]. However, we reported in 2008 that prolonged application of Tm, for 8 or more hr, results in decreased PKD2 expression due to ERAD through the ubiquitin-proteasome system [19]. Thus we wanted to study how cellular stresses, notably ER stress, regulate PKD2 protein expression, using culture cell models. For this we first induced ER stress using known ER stress inducers Tg, an ER Ca^{2+} ATPase inhibitor that depletes ER Ca^{2+} store, and Tm, an inhibitor of protein glycosylation, as they both lead to accumulation of unfolded proteins in the ER lumen [38-40]. WB experiments revealed that endogenous PKD2 protein expression in HEK293T cells treated with Tg (0.5 μM) for 1 hr increases by 81 ± 18% (P = 0.008, N = 7) (Fig. 2-1A). Similar results were obtained in HeLa cells treated with Tg for 1 or 3 hr (Fig. 2-1B). In average, endogenous PKD2 expression increased by 86 ± 20% (P = 0.005, N = 8) following 1 hr Tg treatment (Fig. 2-1B). Tm treatment for up to 6 hr in HEK293T cells also similarly increased PKD2 expression (Fig. 2-1C). However, longer treatment resulted in a decrease in PKD2 expression from the plateau value reached at 3-6 hr, consistent with our previous report that prolonged Tm treatment induces ERAD of PKD2 through the ubiquitin-proteasome system [19]. In contrast, PKD2 expression continued to increase even after 24 hr Tg treatment (Fig. 2-1D).

We next utilized Endo H and PNGase F to examine whether PKD2 proteins undergo subcellular redistribution during ER stress. Endo H cuts high mannose N-glycans of ER resident

PKD2 proteins while PNGase F cuts both high mannose N-glycans and complex N-glycans of PKD2 proteins of early- to mid-Golgi [8]. We found that all detected PKD2 proteins are ER residents in HeLa cells, in agreement with previous reports [8]), and that ER stress does not alter its ER predominant localization (Fig. 2-1E).

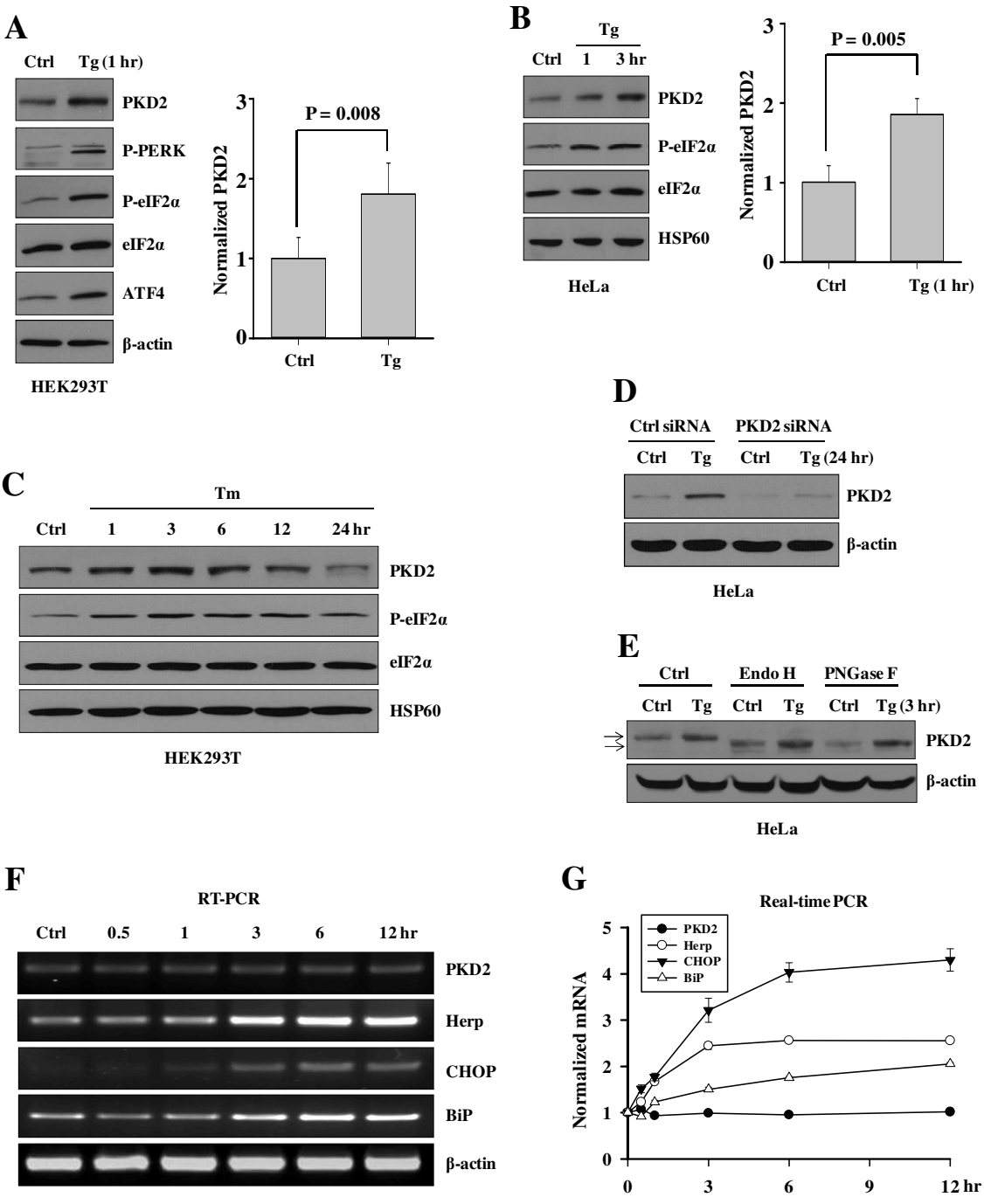

Fig. 2-1. PKD2 protein expression is induced by ER stress. (**A**) HEK293T cells were collected after treated with DMSO (Ctrl) or Tg (0.5 μM) for 1 hr. Blots were probed with the indicated antibodies and quantified by Gel-Pro Analyzer. Data were obtained from the same conditions as in A and averaged to compare PKD2 protein levels between treatment of DMSO (Ctrl) and Tg for 1 hr in HEK293T cells after normalization by β-actin (N = 7). (**B**) HeLa cells were collected after DMSO (Ctrl) or Tg (0.5 μM) treatment for 1 or 3 hr. Blots were probed with the indicated antibodies. Data were obtained from the same conditions as in B and averaged to compare PKD2 protein levels between treatment of DMSO (Ctrl) and Tg for 3 hr in HeLa cells after normalization by β-actin (N = 8). (**C**) HEK293T cells were collected after DMSO (Ctrl) or Tm (2 μg/ml) treatment for 1, 3, 6, 12, or 24 hr. Blots were probed with the indicated antibodies. (**D**) HeLa cells transfected with PKD2 siRNA or Ctrl siRNA were treated with DMSO (Ctrl) or Tg (1 μM) for 24 hr. Cell lysates were prepared for probing PKD2 and β-actin with corresponding antibodies. (**E**) HeLa cells were collected after DMSO (Ctrl) or Tg (1 μM) treatment for 3 hr and then treated with enzyme buffer (Ctrl), Endo H or PNGase F. Blots were probed with the indicated antibodies. Upper and lower bands indicate glycosylated and deglycosylated PKD2, respectively. β-actin was used as loading control. (**F**) Total RNAs from HeLa cells were prepared after DMSO (Ctrl) or Tg (1 μM) treatment for indicated durations. mRNAs levels were determined using RT-PCR.G) Synthesized cDNAs from (F) were also used as templates to determine the mRNAs levels using real-time PCR. Shown data are averages from three.

Because changes in the PKD2 level are due to PKD2 protein synthesis or degradation, and 1 hr Tg or Tm treatment is relatively short for significantly degrading PKD2 protein or changing PKD2 mRNA we reasoned that ER stress may have enhanced the PKD2 synthesis rate. In fact, only about 20% PKD2 would be degraded at 1 hr [41], which cannot account for the 80% increase by Tg for 1 hr. Also, by RT-PCR and real-time PCR assays, we found that PKD2 mRNA remains rather unchanged during ER stress for up to 24 hr (Fig. 2-1F and G), indicating that PKD2 protein expression is translationally up-regulated by ER stress.

Effects of PERK and other kinases on PKD2 protein expression

We next wanted to examine the mechanism of how PKD2 is rapidly (i.e. translationally) up-regulated by ER stress that activates numerous downstream processes. In general, when it comes to rapid up-regulation of protein translation during cellular stresses, P-eIF2α is one of a

few strong candidates to test. P-eIF2α was known to selectively enhance the synthesis of a subset of cellular factors including ATF4, Gadd34 and CHOP, which are essential for cells to cope with stress conditions. We first over-expressed PERK in HEK293T cells to increase P-eIF2α, which does not trigger ER stress [35], and indeed found that PKD2 protein expression significantly augments and positively correlates with an increase in P-eIF2α (Fig. 2-2A and B). Interestingly, the stimulatory effect of PERK over-expression persisted in the presence of ER stress induced by Tm or Tg. To determine whether PERK kinase activity is required for its effect we compared PERK with mutants PERK K618A and PERK ΔC that have no kinase activity due to loss of auto-phosphorylation [35,42]. Indeed, unlike PERK, either kinase dead mutant was unable to increase the PKD2 or P-eIF2α expression (Fig. 2-2C), indicating that PERK kinase activity is required under this condition. To provide further documentations we utilized PERK KO (*PERK*$^{-/-}$) MEF cell line and found that PKD2 expression in *PERK*$^{-/-}$ MEF cells, as opposed to WT (*PERK*$^{+/+}$) MEF cells, remains unchanged by Tg treatment (Fig. 2-2D). These data together showed that PKD2 up-regulation induced by ER stress depends on PERK kinase activity or one of its downstream factors, and that PKD2 expression positively correlates with that of P-eIF2α.

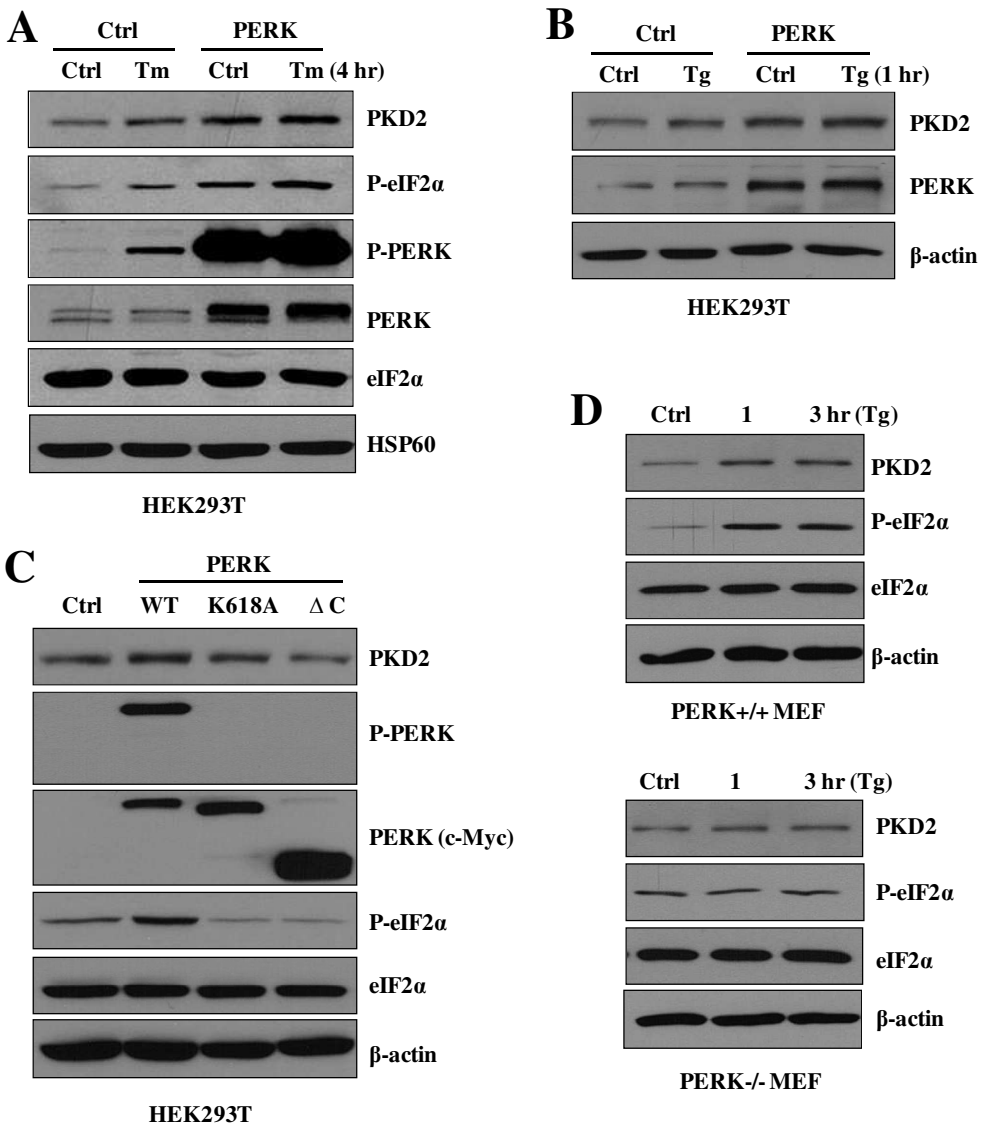

Fig. 2-2. PKD2 expression by ER stress is dependent on PERK activity. (**A**, **B**) HEK293T cells were transiently transfected with 500 ng of c-Myc-PERK fusion expression construct or empty vector (Ctrl) and treated with DMSO (Ctrl) or Tm (2 μg/ml) for 4 hr in (A) or Tg (0.5 μM) for 1 hr in (B). After treatment, cells were collected and blots were probed with the indicated antibodies. (**C**) HEK293T cells were transiently transfected with 500 ng of c-Myc-PERK, K618A or ΔC fusion expression constructs or empty vector (Ctrl) and then cell lysates were prepared for immunoblotting with the indicated antibodies. (**D**) $PERK^{+/+}$ or $PERK^{-/-}$ MEF cells were treated with DMSO (Ctrl) or Tg (0.5 μM) for 1 or 3 hr, and then cell lysates were prepared for immunoblotting with PKD2, P-eIF2α, eIF2α or β-actin antibodies.

We next examined whether and how other kinases of P-eIF2α regulate PKD2 expression. For this we activated eIF2α by arsenite (As) which induces oxidative stress and activates kinase HRI [43], and by polyinosinic:polycytidylic acid (poly IC) which mimics viral infection and activates kinase PKR [44]. Indeed, treatment with As or poly IC up-regulated PKD2 expression in both HEK293T and HeLa cells (Fig. 2-3A and B). Furthermore, PKD2 expression in *PERK*$^{-/-}$ MEF cells was induced by As and poly IC but not Tg (Fig. 2-3C). These data strongly indicate that P-eIF2α mediates the regulation. In particular, WB experiments revealed that in HeLa cells treated with As, PKD2 expression increases by 82 ± 11% (P = 0.005, N = 4) (Fig. 2-3D). Of note, putting together data obtained from using different stress conditions, we found that the P-eIF2α and PKD2 levels are not linearly correlated (Fig. 2-3B), suggesting that factors other than P-eIF2α may have also contributed to regulating PKD2.

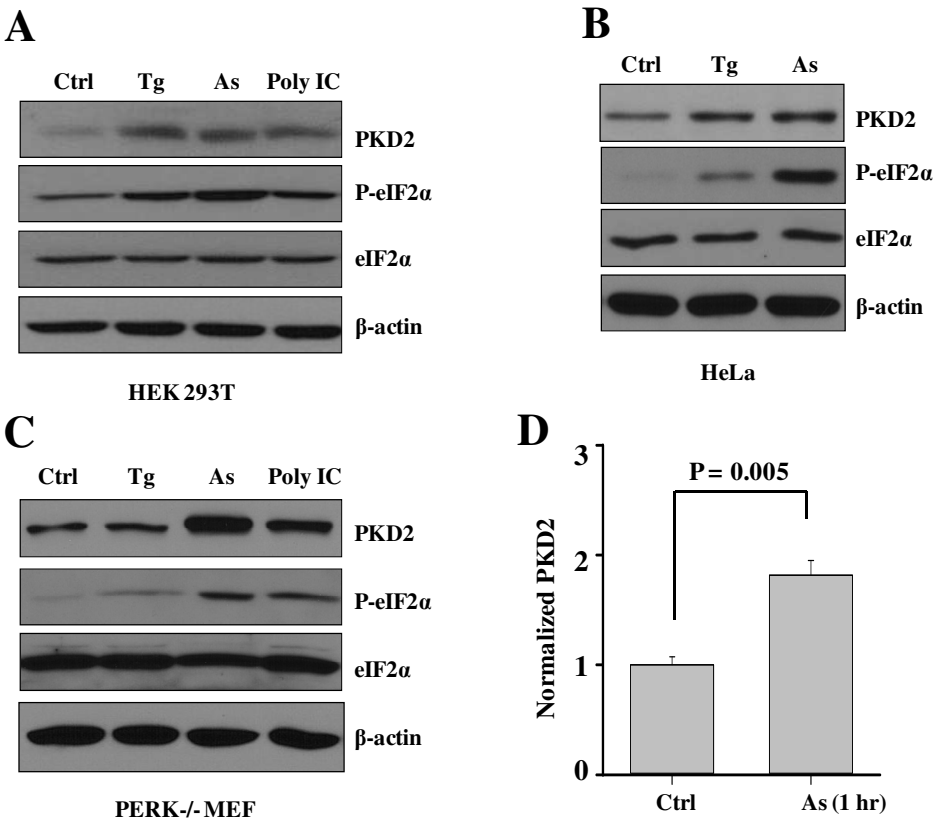

Fig. 2-3. PKD2 protein expression is induced by different stresses. (**A**) HEK293T cells were collected after DMSO (Ctrl), Tg (0.5 μM) or As (100 μM) treatment for 1 hr, or Poly IC (20 μg/ml) treatment for 18 hr. Blots were then probed with the indicated antibodies. (**B**) HeLa cells were collected after DMSO (Ctrl), Tg (0.5 μM) or As (100 μM) treatment for 1 hr. Blots were then probed with the same antibodies. (**C**) $PERK^{-/-}$ MEF cells were treated with the same procedures as HEK293T cells in (A) and detected with the indicated antibodies. (**D**) Bar graph showing the difference of PKD2 protein levels between treatments with DMSO (Ctrl) and As for 1 hr in HeLa cells after normalization by β-actin (N = 4).

Effects of salubrinal and Gadd34 on PKD2 protein expression

Further, because different stress conditions may affect common downstream factors (other than P-eIF2α) that may have regulated PKD2, we wanted to further document the effect of P-eIF2α on PKD2 expression. For this we treated cells with salubrinal which inhibits protein phosphatase 1 that is normally in complex with Gadd34 to de-phosphorylate P-eIF2α [36] thereby increasing P-eIF2α without activating cellular stress or eIF2α kinases [45]. In HEK293T, HeLa, MDCK, MEF and MCD D3 cells treated with salubrinal at various concentrations, PKD2 expression augmented in a dose-dependent manner, in correlation with expected increases in P-eIF2α, and, as expected, without altering PERK expression (Fig. 2-4). WB experiments showed that in HEK293T cells treated with salubrinal (50 μM), PKD2 expression increases by 199 ± 55% (P = 0.01, N = 3) (Fig. 2-4A). On the other hand, we also examined the effect of Gadd34 on PKD2 expression. Over-expression of Gadd34 significantly decreased P-eIF2α and abolished ER stress- and salubrinal-induced up-regulation of PKD2, but in the absence of ER stress and salubrinal treatment, the level of PKD2 expression remained unaffected (Fig. 2-5), presumably because low P-eIF2α in this condition has two opposite effects cancelling each other: one is to up-regulate the global translation and the other is to reduce PKD2 expression.

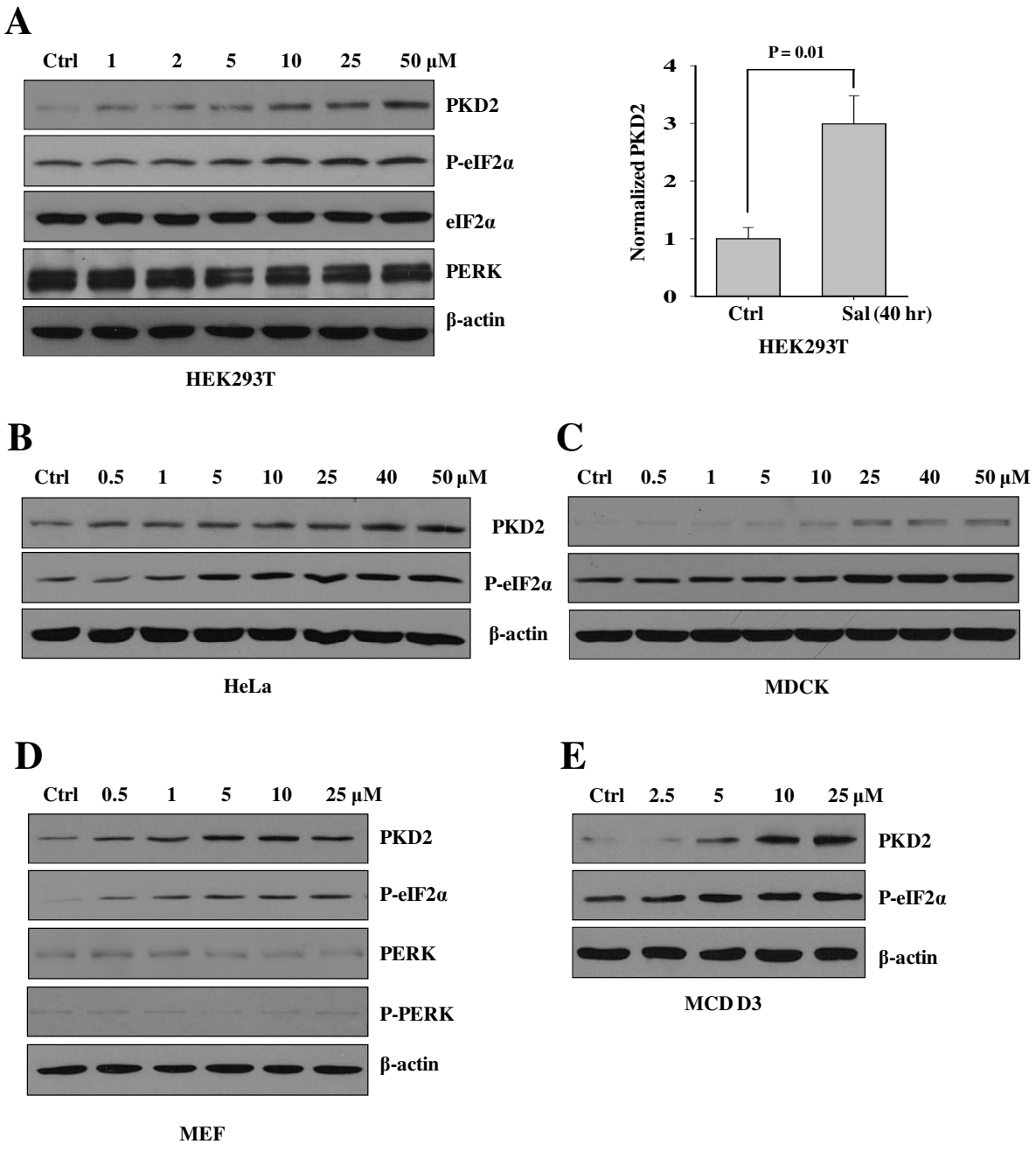

Fig. 2-4. PKD2 protein expression is induced by salubrinal. (**A**) HEK293T, (**B**) HeLa, (**C**) MDCK, (**D**) MEF and (**E**) MCD D3 cells were treated with DMSO (Ctrl) or salubrinal (Sal) for 40 hr at indicated concentrations. Cell lysates were then prepared and blots probed with the indicated antibodies. Right panel in (A), bar graph (N = 3) comparing PKD2 protein levels between treatment of DMSO (Ctrl) and salubrinal (50 μM) for 40 hr in HEK293T cells after normalization by β-actin.

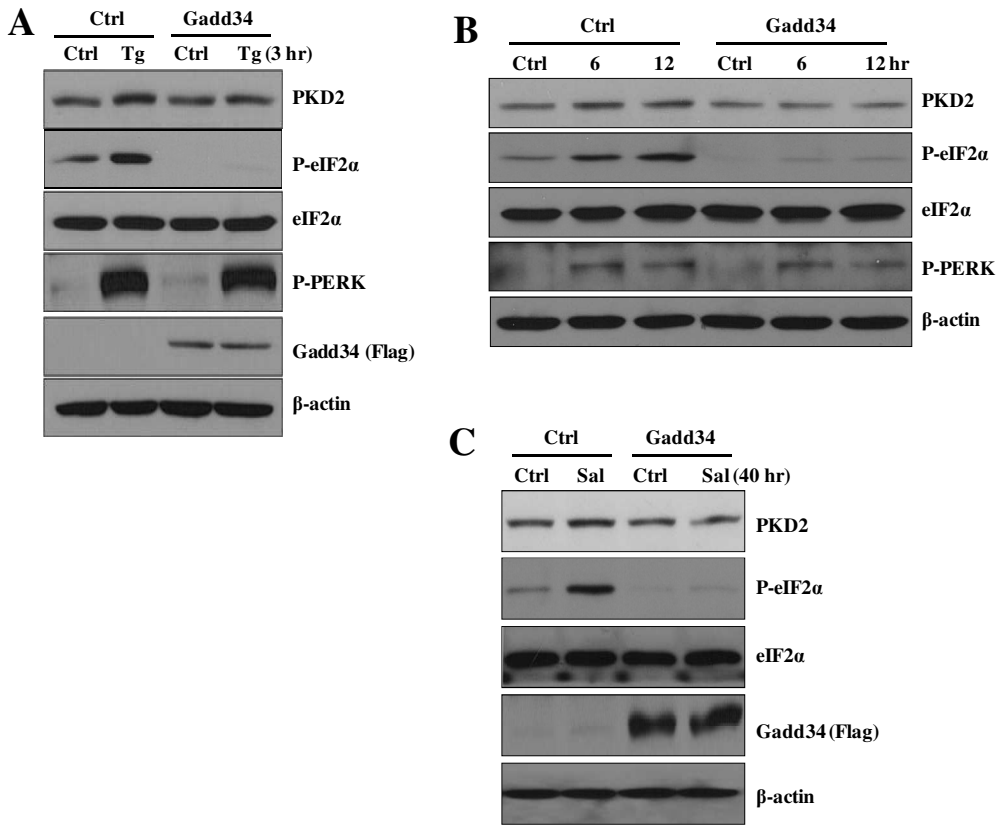

Fig. 2-5. Induction of PKD2 protein expression by ER stress is abolished by Gadd34. (**A-C**) HeLa cells were transiently transfected with 500 ng of Flag-Gadd34 fusion expression construct or empty vector (Ctrl). 40 hr after transfection, cells were treated with DMSO (Ctrl) or Tg (0.5 μM) for 3 hr in (A), Tg (0.5 μM) for 6 or 12 hr in (B), or salubrinal (50 μM) for 40 hr in (C). Cell lysates were then prepared for immunoblotting with the indicated antibodies.

Effect of P-eIF2α on PKD2 protein expression

So far, in all performed experiments, changes in P-eIF2α were made through indirect induction, which may result in other changes that may affect PKD2 expression. Thus we next examined the role of P-eIF2α through direct eIF2α over-expression and KD. We found that over-expression of WT eIF2α, but not the phosphorylation dead S51A mutant, increases P-eIF2α and up-regulates PKD2 in HeLa and HEK293T cells (Fig. 2-6A and B). Combination of eIF2α over-expression and Tg treatment exhibited the most pronounced increases in PKD2 expression,

compared with eIF2α over-expression or Tg treatment alone (Fig. 2-6C and D). On the other hand, eIF2α KD by siRNA in HeLa cells abolished the response of PKD2 to Tg treatment (Fig. 2-6E). Consistent with data shown in Fig. 2-5, the level of PKD2 remained unaffected by reduced P-eIF2α in the absence of ER stress (Fig. 2-6E).

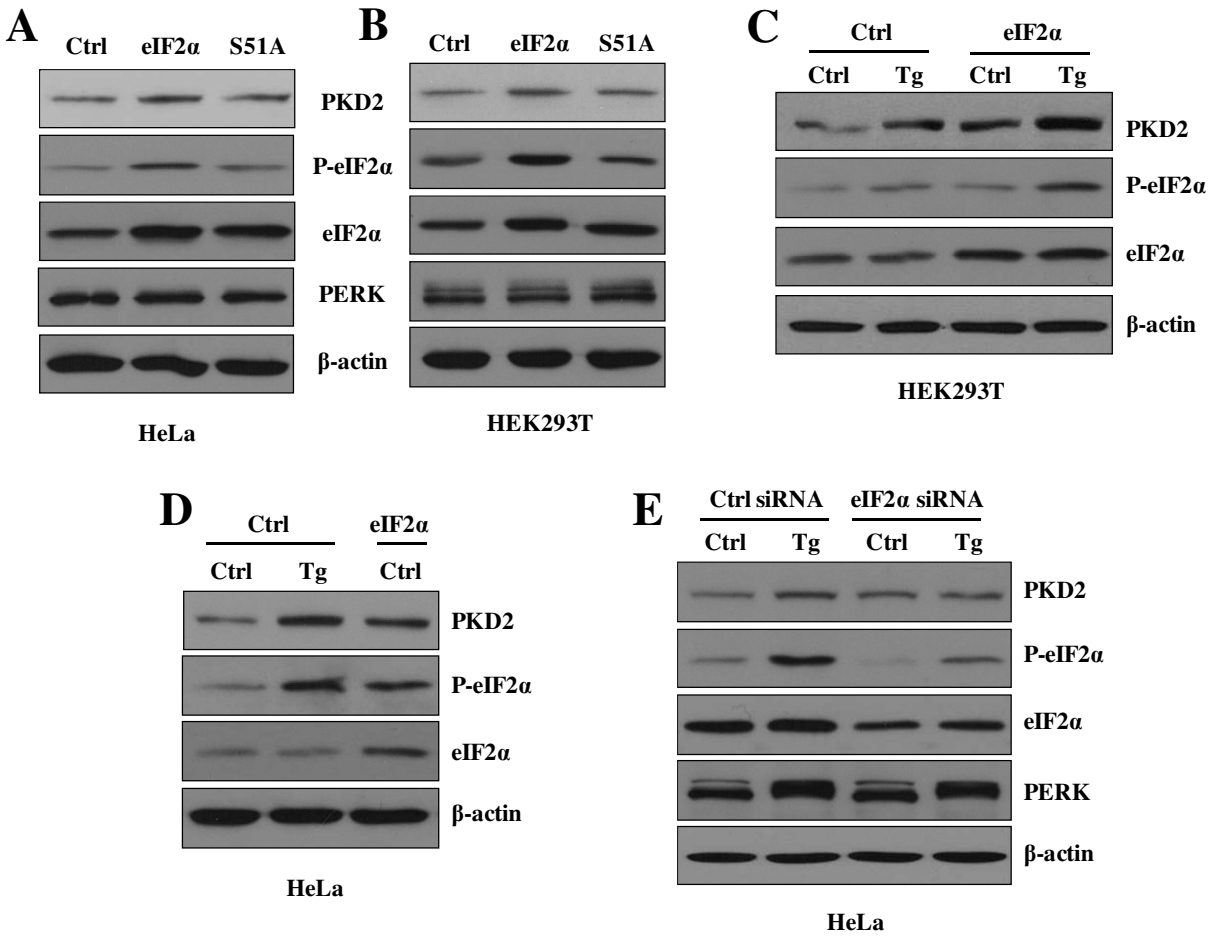

Fig. 2-6. PKD2 protein expression is regulated by phosphorylation of eIF2α. (**A**) HeLa and (**B**) HEK293T cells were transiently transfected with 500 ng of eIF2α or eIF2α S51A expression constructs or empty vector (Ctrl). 40 hr after transfection, cells were collected for immunoblotting with the indicated antibodies. (**C**) HEK293T and (**D**) HeLa cells were transiently transfected with 500 ng of eIF2α expression construct or empty vector (Ctrl). 40 hr after transfection, cells were treated with DMSO (Ctrl) or Tg (0.5μM) for 1 hr and then collected for immunoblotting with the indicated antibodies. (**E**) HeLa cells were transfected with eIF2α siRNA or Ctrl siRNA. 40 hr after transfection, cells were treated with DMSO (Ctrl) or Tg (0.5 μM) for 1 hr and then cell lysates were prepared and subjected to immunoblotting with PKD2, P-eIF2α, eIF2α, PERK or β-actin antibodies.

Effect of ER stress on the PKD2 mRNA binding with ribosomes

During ER stress, mRNAs encoding proteins such as ATF4, CHOP and Gadd34 that are translationally up-regulated by P-eIF2α were found to bind more ribosomes. We thus also employed polysome binding analysis for PKD2 in the presence and absence of ER stress. For this, mRNAs within sucrose density gradient fractions were extracted and then prepared for RT-PCR. In HeLa cells treated with DMSO (non-stress condition), β-actin mRNA (negative control) primarily sedimented to the high polysome-binding fractions 12, 13, and 14, indicating that β-actin mRNAs are actively translated (Fig. 2-7A and B). Tg treatment resulted in a significant portion of β-actin mRNAs shifted to lower polysome-binding fractions 10 and 11, indicating that β-actin translation is repressed during ER stress. On the contrary, CHOP mRNA (positive control) sedimented to higher polysome-binding fractions under ER stress condition (Tg) compared to non-stress condition (DMSO) (Fig. 2-7A and D), consistent with the fact that CHOP translation is induced by ER stress and P-eIF2α [46]. Similar to CHOP, by Tg treatment, significant portion of PKD2 mRNAs shifted from fractions 6 and 7 to fractions 7 and 8 (Fig. 2-7A and C), indicating that PKD2 synthesis is augmented under ER stress condition.

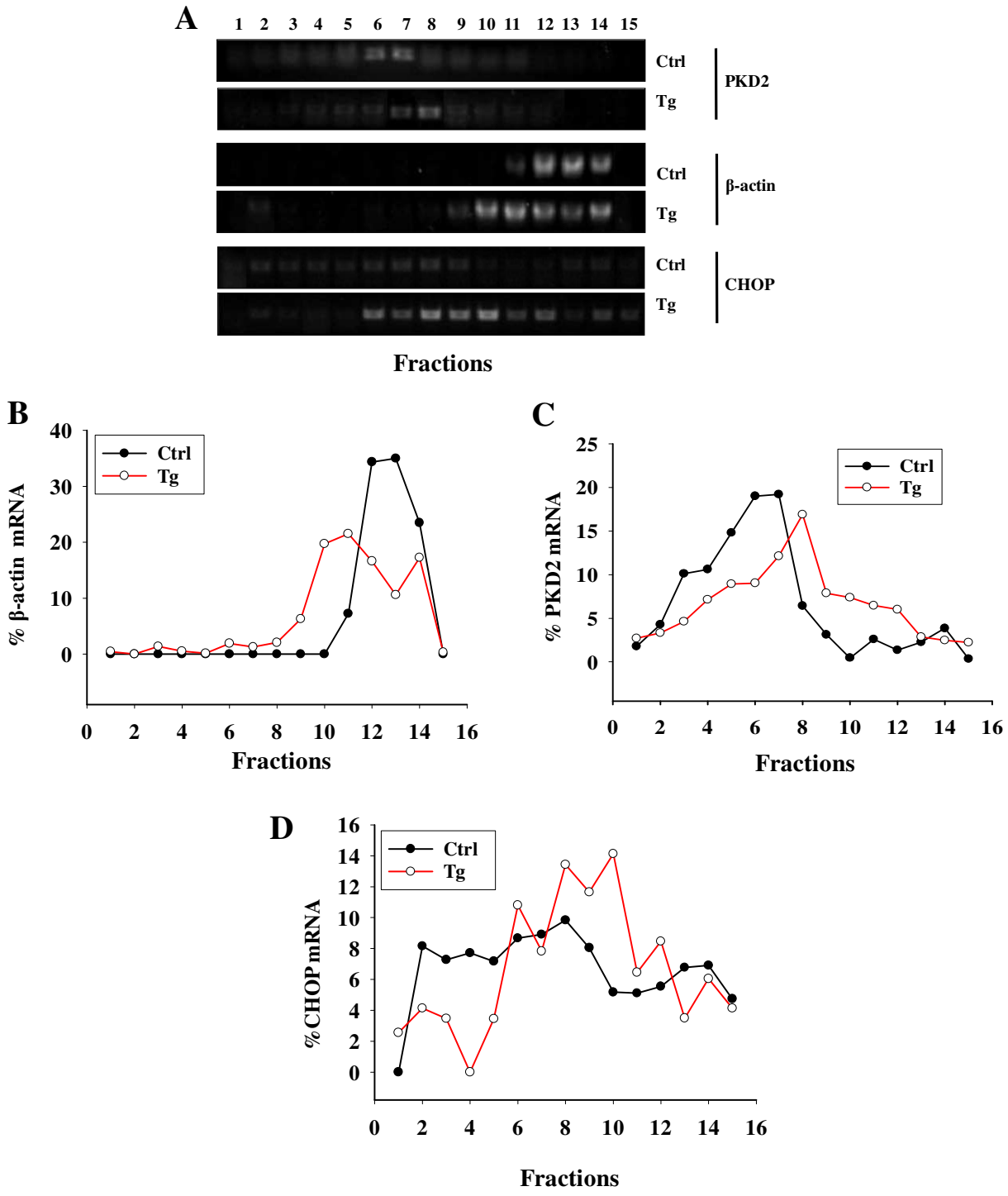

Fig. 2-7. Translation efficiency of PKD2 mRNA is enhanced by ER stress. (**A**) HeLa cells were treated with DMSO (Ctrl) or Tg (0.5 μM) for 3 hr and then cell lysates were fractionated by sucrose gradient centrifugation. Fractions were then collected from top to bottom and named from fraction 1 to fraction 15. RT-PCR was used to detect the mRNA levels of PKD2, β-actin (negative Ctrl) or CHOP (positive Ctrl). PCR products were then subjected to 1% agarose gel electrophoresis and quantified by Gel-Pro Analyzer. (**B-D**) Line graphs comparing polysome

distribution of β-actin, PKD2 or CHOP between DMSO (Ctrl) and Tg (0.5 μM) treatments for 3 hr in HeLa cells. Each fraction is presented as a percentage of the total density from all fractions within each sucrose gradient.

Role of uORF of PKD2 mRNA in the up-regulation of PKD2 synthesis by ER stress

A Bypass Model was recently proposed in an effort to account for how CHOP is translationally up-regulated by P-eIF2α and assumes that a uORF(s) present in the 5'UTR of a mRNA sequence mediates the translational regulation of the protein encoded by the main ORF of the mRNA by P-eIF2α and cellular stresses [46]. The model further assume that, under non-stress condition, either the synthesized peptide (from the uORF) inhibits the translation of the main ORF or the inhibitory function of the uORF causes dissociation of ribosomes from the mRNA at the end of uORF translation, possibly though preventing translation elongation or termination [46]. When P-eIF2α is high, eg, during stress conditions, due to delayed initiation, scanning ribosomes bypass the uORF and increase the translation of the main ORF. An analysis of annotated human, mouse, monkey and pig PKD2 mRNAs revealed one non-over-lapping uORF (Fig. 2-8A). To elucidate whether the PKD2 uORF is involved in the translational up-regulation of PKD2 by P-eIF2α, we constructed DNA plasmids harboring the mouse PKD2-5'UTR DNA (with full-length 5'UTR) or PKD2-ΔuORF DNA (with deleted uORF) for transfection into HeLa cells. Indeed we found that transfection of PKD2-ΔuORF produces significantly higher PKD2 expression compared to transfection of PKD2-5'UTR (Fig. 2-8B), while their mRNA levels are similar (Fig. 2-8C). Also, PKD2 protein expression from PKD2-5'UTR, but not that from PKD2-ΔuORF, was responsive to Tg treatment and eIF2α phosphorylation (Fig. 2-8B). Further, mutating the uORF start codon ATG to GGG abolished the responsiveness to Tg treatment (Fig. 2-8D and E).

Further, to confirm the inhibitory effect of uORF on the synthesis of PKD2 found by WB experiments, we performed dual-luciferase assays with a reporter plasmid harboring both Firefly and Renilla luciferase genes, which share a bidirectional promoter. Full-length 5'UTR or 5'UTR with uORF deletion, start codon ATG-to-TTG mutation, or Kozak sequence KR mutation (GGAAC**ATG**GCTCC to GGTAC**ATG**TCTCC) was inserted upstream of the Renilla luciferase gene. Firefly luciferase served as an internal control. We transfected the reporter plasmids into HeLa cells and found that full-length 5'UTR insertion inhibits luciferase activity while uORF deletion or ATG-to-TTG mutation significantly reduced the inhibition (Fig. 2-8F), indicating that the uORF in the 5'UTR mediates the inhibitory effect on luciferase activity (ie, PKD2 protein translation). We also tested the role of the PKD2 Kozak sequence and interestingly found that the KR mutation also significantly reduced the inhibitory effect of 5'UTR (Fig. 2-8F), consistent with the expected effect of a Kozak sequence, ie, through enhancing the translation of uORF to reduce the synthesis of luciferase. Our data together demonstrated that ER stress and P-eIF2α up-regulates PKD2 protein translation, through bypassing the uORF in the 5'UTR of PKD2 mRNA.

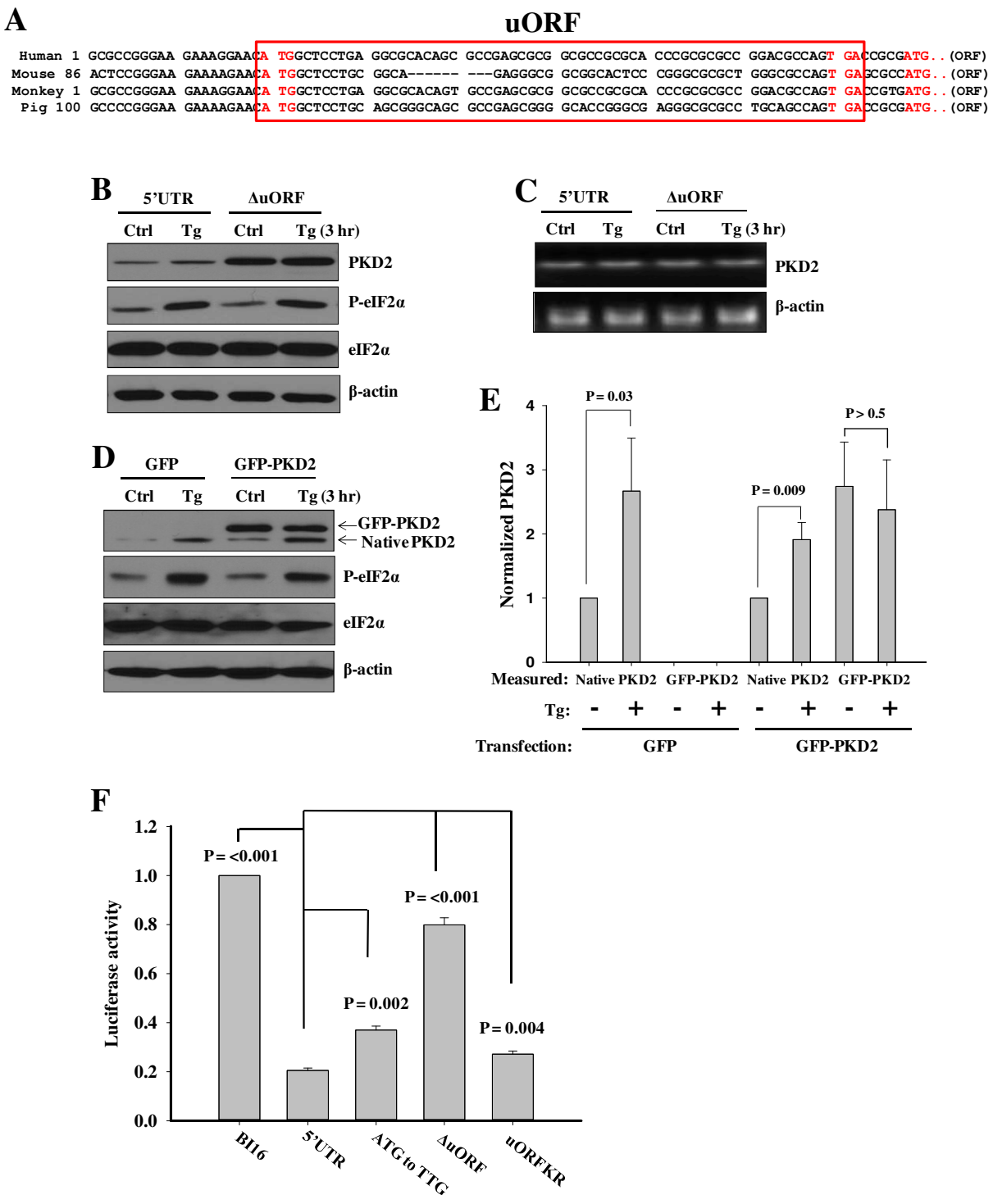

Fig. 2-8. PKD2 expression induction by ER stress is mediated by uORF in 5'UTR of its mRNA. (**A**) An alignment of annotated human, mouse, monkey and pig 5'UTRs of PKD2 mRNA. (**B**, **C**) HeLa cells were transiently transfected with 10 ng of mouse PKD2-5'UTR or PKD2-ΔuORF expression constructs or empty vector (Ctrl). 12 hr after transfection, cells were

collected after DMSO (Ctrl) or Tg (1 μM) treatment for 3 hr and subjected to immunoblot for protein detection or RT-PCR for mRNA detection. (**D**) HeLa cells were transiently transfected with 10 ng of GFP-PKD2 fusion expression construct or empty vector pEGFP-C2. 12 hr after transfection, Cells were treated with DMSO (Ctrl) or Tg (1μM) for 3 hr, and then cells were collected for immunoblotting. (**E**) Bar graph (N = 3) showing PKD2 protein relative levels under different conditions in HeLa cells after normalization by β-actin. (**F**) HeLa cells were transiently transfected with 80 ng of BI16, PKD2-5'UTR, ATG-to-TTG, ΔuORF or uORF KR luciferase constructs. 12 hr after transfection, cell lysates were prepared and luciferase activities measured. The bar graph (N = 3) shows Renilla luciferase relative activity after normalization by firefly luciferase.

2.5 DISCUSSION

By RT-PCR and real-time PCR, we have shown that the up-regulation does not occur through increasing PKD2 mRNA. Then, using PERK over-expression, induction of other stress conditions, salubrinal treatment, Gadd34 and eIF2α over-expression, together with WB and polysome analyses, we have accumulated extensive indirect as well as direct data that together have firmly established that P-eIF2α mediates PKD2 up-regulation. Finally, through WB and luciferase analyses we have shown that this up-regulation by P-eIF2α is through bypassing the translation of the inhibitory uORF in the 5'UTR of PKD2 mRNA (Fig. 2-9).

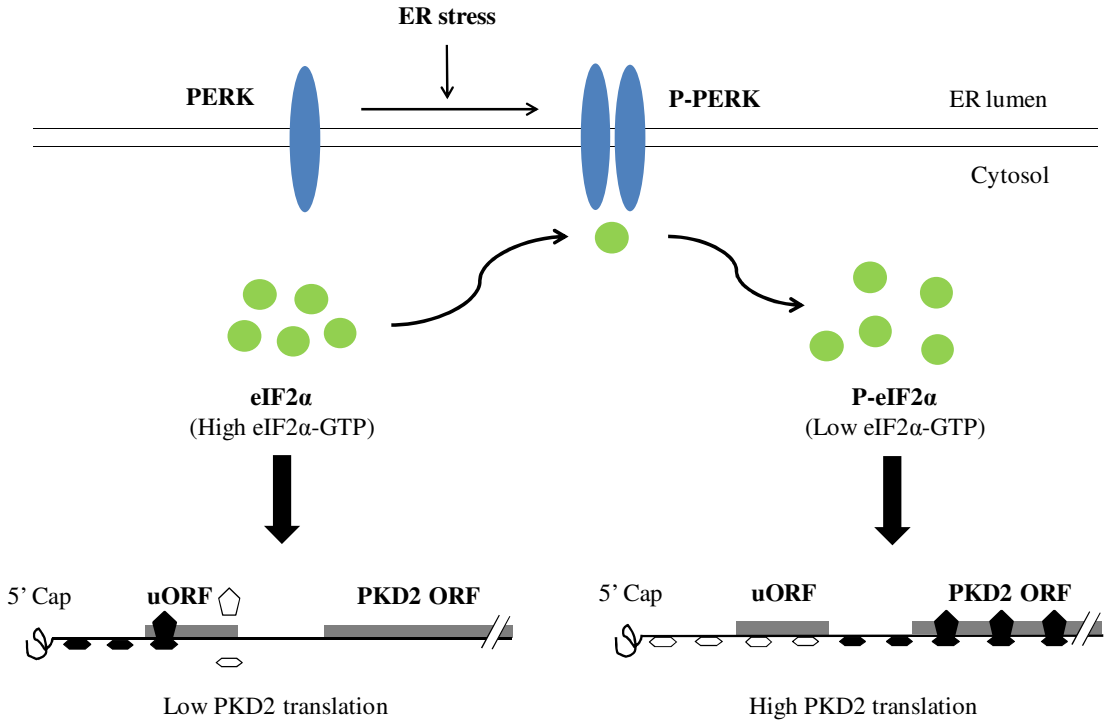

Fig. 2-9. Schematic illustration of the effect of ER stress on the translational regulation of PKD2. In the absence of stress, P-eIF2α is low and eIF2α-GTP is high. Ribosomes (hexagon and pentagon indicating 40S and 60S, respectively) bind the 5'-end of PKD2 mRNA and start the translation of the uORF. After the uORF translation is complete ribosomes dissociate from the PKD2 mRNA, resulting in low translation of the PKD2 ORF. During ER stress, PERK is activated by autophosphorylation, which then phosphorylates eIF2α, thereby increasing P-eIF2α and reducing eIF2α-GTP level, which allows ribosomes bypassing the inhibitory uORF and translating PKD2 ORF.

PKD2 is mainly localized on the ER membrane but is also present on the plasma and primary cilia membranes. Our data demonstrated that increased PKD2 during ER stress still predominantly localizes on the ER, which is consistent with the finding that increased PKD2 following renal ischemia is mainly ER resident [20]. We previously showed that prolonged ER stress induced by treatment of Tm (for 8 hr or more), a glycosylation inhibitor, promotes PKD2 degradation through ERAD pathway [19], consistent with our current data (Fig. 2-1C). This is presumably due to deglycosylation of PKD2 induced by Tm. Interestingly, with shorter treatment (1-6 hr) Tm exhibited up-regulation of PKD2 (Fig. 2-1C), suggesting that PKD2 degradation is less significant under this condition. In contrast, PKD2 continued to augment by Tg treatment for 24 hr (Fig. 2-1D). This is presumably because the main action of Tg is to deplete ER luminal Ca^{2+} through inhibiting the ER sarco/endoplasmic reticulum Ca^{2+} ATPase (SERCA) activity.

During ER stress conditions, global translation is rapidly repressed through phosphorylation of eIF2α in response to an accumulation of misfolded proteins in the ER, which prevents further overload [27,28]. At the same time, elevated P-eIF2α allows preferential translation of a selective panel of cellular genes that possess one or more uORFs located in their 5'UTR, including ATF4, CHOP, and Gadd34 [30,46,47]. The rapid induction of these factors is essential for cell survival because it allows them to execute protective processes as part of UPR. Thus, our current study allowed adding PKD2 as a novel member to this panel. However, it is worth to mention that ATF4, CHOP and Gadd34 are both translationally and transcriptionally up-regulated during ER stress [48-50], which would allow them to have more pronounced increases, which is in contrast to PKD2 that is only subjected to translational up-regulation (Fig. 2-1). In fact, PKD2 exhibited about 80% increase during ER stress (Fig. 2-1A and B) while ATF4 and

CHOP increased 4 folds under comparable conditions [51,52]. However, too much changes in PKD2 may be harmful to cells, as indicated by the fact that both PKD2 KO and transgenic mice develop renal cysts and are associated with over-proliferation and apoptosis [2,6].

How ER stress and UPR are implicated in human diseases has become an emerging area of research. In fact, although ER stress and UPR are involved in a number of human diseases, including Parkinson's and Alzheimer's diseases, inflammation, cancer and diseases in heart, kidney, liver, lung and pancreas [22-24,53], the underlying mechanisms have been poorly understood. Most reports have remained on the descriptive level. Eg, ER stress and several UPR factors such as PERK, activating transcription factor 6 and inositol-requiring protein-1are induced in brain and heart ischemia, leading to CHOP-dependent neuron apoptosis and cardiomyocyte degeneration [26]. Protein turnover rates are high in kidney. In fact, fractional daily protein synthesis rate in human kidney is 42% per day, compared to only 12% and 1.5% per day in an intestinal tissue and skeletal muscle, respectively [22], suggesting that renal ER is more likely to face protein misfolding or ER stress. Indeed, ER stress is involved in several renal diseases, such as membranous nephropathy, glomerular disease, and tubular disease induced by ischemic injury, heavy metal or other agents [22,24-26]. ER stress markers were found to be at high expression levels in some glomerulopathies, proteinuria, and diabetic nephropathy. Some pathogenic mutations such as those in nephrin and podocin, lead to misfolding and retention in the ER, which may result in ER stress, UPR and/or ERAD [22,24]. The implication of UPR in ADPKD is supported by our previous reports that prolonged ER stress induced by Tm promotes PKD2 degradation and that PKD2 up-regulates PERK-dependent eIF2α phosphorylation [14,19,23].

I/R causes several cellular stresses such as oxidative stress, ER stress and amino acid depletion. For example, renal I/R induces ER stress that activates PERK, which significantly

increases P-eIF2α in tubular epithelial cells in both cortex and medulla [54]. PKD2 expression is also significantly up-regulated in adult rat kidney after I/R [20]. This suggests that PKD2 has important roles in the processes against cellular stresses. Interestingly, *PKD2*$^{+/-}$ mouse kidneys have higher tubular and interstitial proliferative responses following injury compared with WT kidneys [55], suggesting that PKD2 dosage affects cellular repair responses. However, in addition to PKD2 protein expression, I/R causes an increase in the PKD2 mRNA level as well [55], indicating the presence of another factor or pathway that is activated under I/R to regulate PKD2 mRNA.

In ADPKD, heterozygous loss-of-function mutations in PKD2 cause cyst formation accompanied by over-proliferation, de-differentiation and apoptosis [56]. Our previous study revealed that PKD2 up-regulates P-eIF2α through enhancing the efficiency of eIF2α kinase PERK, thereby repressing cell proliferation and protein synthesis [14]. On the other hand, our current study showed that elevated P-eIF2α induced by cellular stresses increases PKD2 expression, indicating that PKD2 and P-eIF2α may form a positive feedback loop and reach equilibrium, which may be important for jointly regulating cell proliferation and maintaining cell homeostasis.

In summary, our present study found that PKD2 mRNA is a new member of uORF-possessing genes encoding proteins that are translationally up-regulated by P-eIF2α and cellular stresses. Because dosage matters this novel PKD2 regulation provides new sights into the mechanism of ADPKD cystogenesis and may allow discovering new therapeutic targets. In particular, salubrinal has been used to mice in previous studies and because it up-regulates PKD2 level it may be a potential therapeutic reagent through compensating for the PKD2 deficiency in PKD2+/- patients. And the fact that salubrinal acts on downstream of ER stress may mean better

specificity and less side effects than those that cause cellular stresses. Future studies using *in vivo* models such as zebrafish and mice with salubrinal injection and PKD2/PERK double heterozygous mice would provide further insights into the cross-talk between PKD2 and eIF2α pathways.

2.6 REFERENCES

1. Harris, P. C. What is the role of somatic mutation in autosomal dominant polycystic kidney disease? *J. Am. Soc. Nephrol.* **21**, 1073-1076 (2010).

2. Wu, G. *et al.* Somatic inactivation of Pkd2 results in polycystic kidney disease. *Cell* **93**, 177-188 (1998).

3. Tran, U. *et al.* The RNA-binding protein bicaudal C regulates polycystin 2 in the kidney by antagonizing miR-17 activity. *Development* **137**, 1107-1116 (2010).

4. Obara, T. *et al.* Polycystin-2 immunolocalization and function in zebrafish. *J. Am. Soc. Nephrol.* **17**, 2706-2718 (2006).

5. Lu, W. *et al.* Perinatal lethality with kidney and pancreas defects in mice with a targetted Pkd1 mutation. *Nat. Genet.* **17**, 179-181 (1997).

6. Park, E. Y. *et al.* Cyst formation in kidney via B-Raf signaling in the PKD2 transgenic mice. *J. Biol. Chem.* **284**, 7214-7222 (2009).

7. Kurbegovic, A. *et al.* Pkd1 transgenic mice: adult model of polycystic kidney disease with extrarenal and renal phenotypes. *Hum. Mol. Genet.* **19**, 1174-1189 (2010).

8. Cai, Y. *et al.* Identification and characterization of polycystin-2, the PKD2 gene product. *J. Biol. Chem.* **274**, 28557-28565 (1999).

9. Nauli, S. M. *et al.* Polycystins 1 and 2 mediate mechanosensation in the primary cilium of kidney cells. *Nat. Genet.* **33**, 129-137 (2003).

10. Chapin, H. C. & Caplan, M. J. The cell biology of polycystic kidney disease. *J. Cell Biol.* **191**, 701-710 (2010).

11. Serra, A. L. *et al.* Sirolimus and kidney growth in autosomal dominant polycystic kidney disease. *N. Engl. J Med.* **363**, 820-829 (2010).

12. Walz, G. *et al.* Everolimus in patients with autosomal dominant polycystic kidney disease. *N. Engl. J Med.* **363**, 830-840 (2010).

13. Torres, V. E. *et al.* Tolvaptan in patients with autosomal dominant polycystic kidney disease. *N. Engl. J Med.* **367**, 2407-2418 (2012).

14. Liang, G. *et al.* Polycystin-2 down-regulates cell proliferation via promoting PERK-dependent phosphorylation of eIF2alpha. *Hum. Mol. Genet.* **17**, 3254-3262 (2008).

15. Grimm, D. H. *et al.* Polycystin-2 regulates proliferation and branching morphogenesis in kidney epithelial cells. *J. Biol. Chem.* **281**, 137-144 (2006).

16. Wegierski, T. *et al.* TRPP2 channels regulate apoptosis through the Ca2+ concentration in the endoplasmic reticulum. *EMBO J.* **28**, 490-499 (2009).

17. Rutkowski, D. T. & Kaufman, R. J. That which does not kill me makes me stronger: adapting to chronic ER stress. *Trends Biochem. Sci.* **32**, 469-476 (2007).

18. Ron, D. & Walter, P. Signal integration in the endoplasmic reticulum unfolded protein response. *Nat. Rev. Mol. Cell Biol.* **8**, 519-529 (2007).

19. Liang, G. *et al.* Polycystin-2 is regulated by endoplasmic reticulum-associated degradation. *Hum. Mol. Genet.* **17**, 1109-1119 (2008).

20. Zhao, Y., Haylor, J. L. & Ong, A. C. Polycystin-2 expression is increased following experimental ischaemic renal injury. *Nephrol. Dial. Transplant.* **17**, 2138-2144 (2002).

21. Matsui, Y. *et al.* Molecular mechanisms and physiological significance of autophagy during myocardial ischemia and reperfusion. *Autophagy.* **4**, 409-415 (2008).

22. Dickhout, J. G. & Krepinsky, J. C. Endoplasmic reticulum stress and renal disease. *Antioxid. Redox. Signal.* **11**, 2341-2352 (2009).

23. Dickhout, J. G., Carlisle, R. E. & Austin, R. C. Interrelationship between cardiac hypertrophy, heart failure, and chronic kidney disease: endoplasmic reticulum stress as a mediator of pathogenesis. *Circ. Res.* **108**, 629-642 (2011).

24. Cybulsky, A. V. Endoplasmic reticulum stress in proteinuric kidney disease. *Kidney Int.* **77**, 187-193 (2010).

25. Inagi, R. Endoplasmic reticulum stress in the kidney as a novel mediator of kidney injury. *Nephron Exp. Nephrol.* **112**, e1-e9 (2009).

26. Kitamura, M. Endoplasmic reticulum stress and unfolded protein response in renal pathophysiology: Janus faces. *Am. J Physiol Renal Physiol.* **295**, F323-F334 (2008).

27. Sonenberg, N. & Hinnebusch, A. G. Regulation of translation initiation in eukaryotes: mechanisms and biological targets. *Cell* **136**, 731-745 (2009).

28. Wek, R. C., Jiang, H. Y. & Anthony, T. G. Coping with stress: eIF2 kinases and translational control. *Biochem. Soc. Trans.* **34**, 7-11 (2006).

29. Harding, H. P. *et al.* An integrated stress response regulates amino acid metabolism and resistance to oxidative stress. *Mol. Cell* **11**, 619-633 (2003).

30. Vattem, K. M. & Wek, R. C. Reinitiation involving upstream ORFs regulates ATF4 mRNA translation in mammalian cells. *Proc. Natl. Acad. Sci. U. S. A* **101**, 11269-11274 (2004).

31. Hamanaka, R. B., Bennett, B. S., Cullinan, S. B. & Diehl, J. A. PERK and GCN2 contribute to eIF2alpha phosphorylation and cell cycle arrest after activation of the unfolded protein response pathway. *Mol. Biol. Cell* **16**, 5493-5501 (2005).

32. Kim, I. *et al.* Conditional mutation of Pkd2 causes cystogenesis and upregulates beta-catenin. *J. Am. Soc. Nephrol.* **20**, 2556-2569 (2009).

33. Wu, Y. *et al.* Kinesin-2 mediates physical and functional interactions between polycystin-2 and fibrocystin. *Hum. Mol. Genet.* **15**, 3280-3292 (2006).

34. Brewer, J. W. & Diehl, J. A. PERK mediates cell-cycle exit during the mammalian unfolded protein response. *Proc. Natl. Acad. Sci. U. S. A* **97**, 12625-12630 (2000).

35. Harding, H. P., Zhang, Y. & Ron, D. Protein translation and folding are coupled by an endoplasmic-reticulum-resident kinase. *Nature* **397**, 271-274 (1999).

36. Novoa, I., Zeng, H., Harding, H. P. & Ron, D. Feedback inhibition of the unfolded protein response by GADD34-mediated dephosphorylation of eIF2alpha. *J. Cell Biol.* **153**, 1011-1022 (2001).

37. Sammarco, M. C. & Grabczyk, E. A series of bidirectional tetracycline-inducible promoters provides coordinated protein expression. *Anal. Biochem.* **346**, 210-216 (2005).

38. Friedlander, R., Jarosch, E., Urban, J., Volkwein, C. & Sommer, T. A regulatory link between ER-associated protein degradation and the unfolded-protein response. *Nat. Cell Biol.* **2**, 379-384 (2000).

39. Lass, A. *et al.* A novel function of VCP (valosin-containing protein; p97) in the control of N-glycosylation of proteins in the endoplasmic reticulum. *Arch. Biochem. Biophys.* **462**, 62-73 (2007).

40. Travers, K. J. *et al.* Functional and genomic analyses reveal an essential coordination between the unfolded protein response and ER-associated degradation. *Cell* **101**, 249-258 (2000).

41. Tian, Y. *et al.* TAZ promotes PC2 degradation through a SCFbeta-Trcp E3 ligase complex. *Mol. Cell Biol.* **27**, 6383-6395 (2007).

42. Marciniak, S. J., Garcia-Bonilla, L., Hu, J., Harding, H. P. & Ron, D. Activation-dependent substrate recruitment by the eukaryotic translation initiation factor 2 kinase PERK. *J. Cell Biol.* **172**, 201-209 (2006).

43. McEwen, E. *et al.* Heme-regulated inhibitor kinase-mediated phosphorylation of eukaryotic translation initiation factor 2 inhibits translation, induces stress granule formation, and mediates survival upon arsenite exposure. *J. Biol. Chem.* **280**, 16925-16933 (2005).

44. Zhang, F. *et al.* Binding of double-stranded RNA to protein kinase PKR is required for dimerization and promotes critical autophosphorylation events in the activation loop. *J. Biol. Chem.* **276**, 24946-24958 (2001).

45. Boyce, M. *et al.* A selective inhibitor of eIF2alpha dephosphorylation protects cells from ER stress. *Science* **307**, 935-939 (2005).

46. Palam, L. R., Baird, T. D. & Wek, R. C. Phosphorylation of eIF2 facilitates ribosomal bypass of an inhibitory upstream ORF to enhance CHOP translation. *J. Biol. Chem.* **286**, 10939-10949 (2011).

47. Lee, Y. Y., Cevallos, R. C. & Jan, E. An upstream open reading frame regulates translation of GADD34 during cellular stresses that induce eIF2alpha phosphorylation. *J. Biol. Chem.* **284**, 6661-6673 (2009).

48. Ma, Y., Brewer, J. W., Diehl, J. A. & Hendershot, L. M. Two distinct stress signaling pathways converge upon the CHOP promoter during the mammalian unfolded protein response. *J. Mol. Biol.* **318**, 1351-1365 (2002).

49. Ma, Y. & Hendershot, L. M. Delineation of a negative feedback regulatory loop that controls protein translation during endoplasmic reticulum stress. *J. Biol. Chem.* **278**, 34864-34873 (2003).

50. Dey, S. *et al.* Both transcriptional regulation and translational control of ATF4 are central to the integrated stress response. *J. Biol. Chem.* **285**, 33165-33174 (2010).

51. Ghosh, H. S., Reizis, B. & Robbins, P. D. SIRT1 associates with eIF2-alpha and regulates the cellular stress response. *Sci. Rep.* **1**, 150 (2011).

52. Saito, A. *et al.* Endoplasmic reticulum stress response mediated by the PERK-eIF2(alpha)-ATF4 pathway is involved in osteoblast differentiation induced by BMP2. *J. Biol. Chem.* **286**, 4809-4818 (2011).

53. Wang, S. & Kaufman, R. J. The impact of the unfolded protein response on human disease. *J Cell Biol.* **197**, 857-867 (2012).

54. Montie, H. L., Kayali, F., Haezebrouck, A. J., Rossi, N. F. & Degracia, D. J. Renal ischemia and reperfusion activates the eIF 2 alpha kinase PERK. *Biochim. Biophys. Acta* **1741**, 314-324 (2005).

55. Prasad, S., McDaid, J. P., Tam, F. W., Haylor, J. L. & Ong, A. C. Pkd2 dosage influences cellular repair responses following ischemia-reperfusion injury. *Am. J. Pathol.* **175**, 1493-1503 (2009).

56. Harris, P. C. What is the role of somatic mutation in autosomal dominant polycystic kidney disease? *J. Am. Soc. Nephrol.* **21**, 1073-1076 (2010).

CHAPTER 3

RESULTS #2

Far upstream element-binding protein 1 binds the 3' untranslated region of PKD2 and suppresses its translation

3.1 ABSTRACT

ADPKD pathogenesis can be recapitulated in animal models by gene mutations or dosage alterations in *PKD1* or *PKD2*, demonstrating that too much and too little PKD1/PKD2 are both pathogenic. The function of cellular proteins is determined by their total expression, single-molecule activity and subcellular localization. Mutations may alter all the three parameters while dosage in general merely refers to expression. Dosage manipulation has become an appealing approach for compensating loss- or gain-of-function due to gene mutations are difficult to correct. In this study, using cultured mammalian cells and dual-luciferase assays we first found that the 3'UTR of PKD2 mRNA displays an inhibitory effect on luciferase protein expression and then identified an inhibitory fragment called 3FI (nt 691-1044) that reduced luciferase and PKD2 expression. Using biotin-labelled 3FI as bait and by pull-down and mass spectrometry, we identified a 3FI-binding protein called far upstream element-binding protein-1 (FUBP1). We then demonstrated the inhibitory effect of FUBP1 on PKD2 protein but not mRNA expression. We next employed embryonic zebrafish and found that FUBP1 knockdown by morpholino injection increases PKD2 expression and alleviates fish tail curling caused by PKD2 morpholino knockdown. In addition, we found that FUBP1 over-expression by mRNA injection significantly increases pronephric cyst occurrence and tail curling in zebrafish embryos. Further, we showed FUBP1 directly binds with eIF4E-binding protein-1 (4EBP1), indicating its link to the translation initiation complex. In summary, the present study showed that FUBP1 binds 3FI to inhibit PKD2 translation, through which PKD2-knockdown associated zebrafish disease phenotypes are regulated by FUBP1.

3.2 INTRODUCTION

Human autosomal dominant polycystic kidney disease (ADPKD) is associated with renal and hepatic cysts and, to less extents, pancreatic cysts and vascular defects [1,2]. In humans, ADPKD is due to mutations in the *PKD1* or *PKD2* gene which encodes membrane receptor and ion channel proteins PKD1 and PKD2, respectively. In animal models including mouse, rat and zebrafish, ADPKD can be recapitulated at least in part by loss- or gain-of-function of PKD1 or PKD2 [3-8]. Therefore, their protein expression, membrane localization and function have to be narrowly regulated under normal physiological conditions.

PKD2, also called polycystin-2 or TRPP2 (transient receptor potential polycystin-2), is a 968 amino-acid (aa) integral membrane protein that acts as a cation channel permeable to Ca^{2+}, Na^{+} and K^{+} [9]. PKD2 is expressed in numerous tissues, including kidney, liver, pancreas, lung, heart, brain, intestine, and reproductive organs. PKD2 expression/function is regulated by a number of binding partners such as PKD1, TRPC1, α-actinin, mDia1, Id2, IP3R and EGFR via protein-protein interaction [10-16]. PKD2 expression can also be regulated through its 3' and 5' untranslated regions (UTRs). RNA-binding protein bicaudal C (Bicc1) disrupts the translational control of PKD2 by microRNA miR-17 through competing for the same binding site in PKD2 3'UTR, and lack or insufficiency of Bicc1 in mouse, zebrafish and *Xenopus laevis* results in renal cysts and other defects through reduced PKD2 dosage [7,17]. Through the 5' upstream open reading frame (uORF) of PKD2, cellular stress conditions and phosphorylated eIF2α up-regulate PKD2 translation [18] while they inhibit the global protein translation.

Regulation through UTRs has been much less known compared with that through the protein-protein interaction. 3'UTR-mediated regulation is usually through binding of a 3'UTR-binding protein that affects RNA stability or regulates protein translation through interacting

with the translation machinery that is in contact with the 5'UTR [19] and may also be proximate to 3'UTR through the formation of a 'closed-loop' or 'circular' mRNA structure [20,21]. Transcript circularization can occur by forming an eIF4G-poly(A)-tail-binding protein complex that promotes recycling of 40S ribosome from 3'UTR to the 5' terminus [22]. Alternatively, it can occur through interaction of 3'UTR-binding proteins with specific initiation factors thereby regulating protein translation [23,24]. In either scenario, disruption of the 5'-3' interaction would affect protein translation.

In the present study, we first identified a PKD2 3'UTR fragment and its binding protein called far upstream binding protein 1 (FUBP1) that together mediate down-regulation of PKD2 translation in cultured cells. We then used zebrafish to examine the effects of FUBP1 morpholino oligonucleotide (MO) knockdown (KD) and over-expression on PKD2 translation, PKD2-dependent tail curling and pronephric cyst formation. Finally, we performed co-immunoprecipitation (co-IP) and GST pull-down assays to reveal physical link of FUBP1 to eukaryotic initiation factor-4E (eIF4E)-binding protein-1 (4EBP1).

3.3 METHODS

Plasmid constructs, cell culture and gene transfection

Human PKD2 mRNA 3'UTR composed of 2087 nt was amplified from HeLa cells with the following primers: forward: 5'-GTCGGGCCCTATGTGTGTTTCAGTATGTG-3'; reverse: 5'-CGCCGTTTAAACTTTCTGCTACTATATCAAG-3', and subcloned into luciferase vector BI16, [25] a kind gift of Dr. Ed Grabczyk (Louisiana State University), at the ApaI and PmeI restriction sites. Fragments of human PKD2 mRNA 3'UTR were also cloned into BI16 at the same sites. Human FUBP1 coding sequence was amplified from plasmid pOTB7-FUBP1 purchased from Open Biosystems (Thermo Scientific, Waltham, MA) and inserted into pcDNA3.1(+). Flag tag was inserted to the 5' of the FUBP1 coding region. All mutations were made with the QuikChange Lighting Site-Directed Mutagenesis kit (Agilent Technologies, La Jolla, CA) and confirmed by sequencing. HeLa and HEK cells were cultured in Dulbecco's modified Eagle's medium supplemented with 10% fetal bovine serum and 1% penicillin/streptomycin (Sigma, St. Louis, MO). Cells of less than 25 passages were cultured to full confluence before collection. Transient transfection was performed on cells cultured to 70%-90% confluence using Lipofectamine 2000 (Invitrogen, Carlsbad, CA) according to the manufacturer's instruction.

Antibodies

Rabbit antibodies against PKD2 (H-280) and FLAG (D-8), goat antibody against FUBP2 (D-12), and mouse antibodies against firefly luciferase (Luci 21 1-107), β-actin (C-4) GFP (B-2), GST (B-14) and 4EBP1 (P-1) were purchased from Santa Cruz Biotechnology (Santa Cruz, CA). Mouse antibody against renilla luciferase was purchased from Chemicon International

(Temecula, CA). Goat antibody against PKD2 and Rabbit antibody against FUBP1 were from Aviva System Biology (San Diego, CA). Secondary antibodies were purchased from GE Healthcare (Baie d'Urfe, QC, Canada).

Knockdown by siRNA

Knockdown of human FUBP1 by siRNA was performed using oligonucleotides at a final concentration of 20 nM with transfection reagent Lipofectamine 2000 according to the manufacturer's instruction. siRNA oligonucleotides were purchased from Santa Cruz Biotechnology (Cat#: sc-43760) and control siRNA from Gene Pharma (Shanghai, China). The efficiency of the siRNA KD was assessed by Western blotting (WB).

Zebrafish experiments

Wild-type zebrafish AB strain was maintained and staged as previously described [26,27]. Embryos were kept in the E3 solution. A translation-blocking antisense MO (Gene Tools LLC, Philomath, OR) was injected at the one-cell stage within 1 hpf, as described [28], for zebrafish PKD2 KD. A translation-blocking *fubp1* MO (Gene Tools LLC) was also used. The MO sequences were as follow: *pkd2*, 5'-AGGACGAACGCGACTGGAGCTCATC-3'; *fubp1*, 5'-GGCCATGTCTGCACGAACAGTCTTC-3'; *gli2* (a antisense mismatch morpholino, negative control), 5'-CCTCTTACCTCAGTTACAATTTATA-3' [29]. Capped human *fubp1* mRNA was synthesized using the mMessage mMachine T7 kit (Ambion, Austin, TX) and injected into fertilized embryos (at 200 pg each). Embryos at 3 dpf were fixed in 1.5% glutaraldehyde, 1% paraformaldehyde, 70 mM $NaPO_4$ pH 7.2, 3% sucrose overnight at 4 °C. After being washed in PBS and taken through an ethanol dehydration series, they were embedded in glycolmethacrylate

(JB-4; Polyscience, Warrington, PA) according to the manufacturer's instructions and sectioned at 4 μm. Slides were stained with Methylene Blue and Azure II, [30] mounted, and examined under a microscope. The present study was approved by the Ethical Committee for Animal Experiments of the University of Alberta, and was carried out in accordance with the Guidelines for Research with Experimental Animals of the University of Alberta and the Guide for the Care and Use of Laboratory Animals (NIH Guide) revised in 1996.

RT (reverse transcription)-PCR

Total cellular RNA was prepared using TRIzol reagent (Invitrogen), according to the manufacturer's manual. Contaminating DNA was digested with RNase-free DNase (Promega, Madison, WI). Single-strand cDNA synthesis was carried out using Superscript III reverse transcriptase (Invitrogen), according to the manufacturer's instruction. End-point PCR was performed using 28-cycle protocol with Taq DNA polymerase (Invitrogen). The olgonucleotide primers for each gene were as follows: *β-actin*, sense 5'- CCTGGCACCCAGCACAAT-3' and antisense 5'- GGGCCGGACTCGTCATACT-3'; *firefly* luciferase, sense 5'- CGTTCGTCACATCTCATCTACCTCC-3' and antisense 5'- GCAGAGCGACACCTTTAGGCAGACC-3'; *renilla* luciferase, sense 5'- CATTCAAGGAGAAGGGCGAGGTTAG and antisense 5'- TGTAGTTGCGGACAATCTGGACGAC-3'; *pkd2*, sense 5'- GTATGACGGCTCACGCCTGTAATCC-3' and antisense 5'- AGAGATGGAGTTTCGCCACATTGCC-3'; *fubp1*, sense 5'- CATAGAAGAAAAGATTGGTGGC-3' and antisense 5'- AGGATTATAAGGTGCAGGGTTG-3'. Real-time PCR was performed using a 7900HT Fast Real-time PCR System (Applied

Biosystems, Carlsbad, CA) with the same primers. Fast SYBR Green Master Mix (Invitrogen) was used. 7900HT Fast Real-Time PCR System 2.4.1 software was used to perform quantification and to generate Ct values.

Biotin-RNA pull-down

Templates for *in vitro* synthesis of biotinylated RNA were generated by PCR from the BI16 vector with or without human PKD2 mRNA 3'UTR fragments. Forward and reverse primers are as follows: forward, 5'-AAATTAATACGACTCACTATAGGGACGAGCAGTAATTCTAGAGG-3' (underlined is the T7 promoter sequence), reverse, 5'- GGGCAAACAACAGATGGCTGGCAAC-3'. Biotinylated RNA was synthesized using the mMessage mMachine T7 kit (Ambion, Austin, TX) in the presence of ^{14}Biotin-UTP (Roche, Basel, Switzerland) and purified using phenol:chlorophorm extraction and MegaClean columns (Ambion). Biotin-RNA pull-down assays were carried out as described previously [31]. Briefly, the biotinylated RNA was bound to streptavidin-coated Dynabeads (Invitrogen) according to the manufacturer's instruction. The cytoplasmic extracts of HeLa cells were precleared by incubation with RNA-affinity resin containing a control fragment. The unbound fraction was incubated with RNA-affinity resin containing human PKD2 mRNA 3'UTR fragments in the binding buffer (40 mM KCl, 1.5 mM MgCl2, 0.2 mM EDTA, 1 mM DTT, 6% glycerol, 2 μg/μl heparin, 20 mM HEPES, pH8.0) supplemented with 15μg/ml yeast tRNA (Sigma) and 200 U/ml RNaseOUT (Invitrogen). After 2 hours (hr) of incubation at 4°C, the unbound proteins were removed and after extensive washes with the binding buffer, the proteins were eluted by boiling in Laemmli buffer and resolved on SDS-PAGE. Protein bands were cut for mass-spectrometric analysis (University of Alberta, Edmonton, AB).

RNA-protein immunoprecipitation (RIP)

RIP assay was carried out as previously described [32]. Briefly, HeLa cells were transfected with pCGNM2 harbouring human HA-FUBP1 (a kind gift of Dr. David Levens, National Institutes of Health). 48 hr after transfection, cells were collected using RIP buffer (150 mM KCl, 25mM Tris pH7.4, 5mM EDTA, 0.5 mM DTT, 0.5% NP-40, 100 U/ml RNAase inhibitor SUPERase•in ™ (Invitrogen), proteinase inhibitor mixture), and cell debris pelleted by centrifugation at 13,000 RPM for 10 min. HA tag Antibody (Santa Cruz, Cat# sc-805) or control IgG (Abcam, cat# ab27478) was added to the supernatant and incubated for 4 hr at 4 °C with gentle rotation. 50 µl protein G-Sepharose beads (GE Healthcare) were then added and incubated for 2 hr at 4 °C with gentle rotation. Beads were pelleted at 2,500 RPM for 30 s and washed three times with RIP buffer, followed by one wash in PBS. Co-precipitated RNAs were then isolated with Trizol and RT-PCR assays were performed with following primers: *pkd2*, sense 5'-GTATGACGGCTCACGCCTGTAATCC-3' and antisense 5'-AGAGATGGAGTTTCGCCACATTGCC-3'; *β-actin*, sense 5'-CCTGGCACCCAGCACAAT-3' and antisense 5'-GGGCCGGACTCGTCATACT-3'. Protein isolated by the beads was detected by WB.

Dual luciferase

HeLa and HEK cells were cultured and transfection was performed as described above with plasmids BI16 with or without a human PKD2 mRNA 3'UTR fragment. 12 hr after transfection, cells were collected and dual luciferase assays were carried out with Dual-Luciferase® Reporter Assay System (Promega, Madison, WI) according to the instruction.

Relative luciferase activity was assessed as the ratio of renilla to firefly luciferase units (relative light units).

Co-immunoprecipitation (Co-IP)

HEK or HeLa cell monolayer in 100-mm dishes was washed twice with PBS and solubilised in ice-cold CellLytic-M lysis buffer (Sigma) supplemented with proteinase inhibitor mixture. Supernatants were collected following centrifugation at 16,000 × g for 15 min. Equal amounts of total proteins from postnuclear supernatants were pre-cleared for 1 hour (hr) with protein G-Sepharose (GE Healthcare), and then incubated for 4 hr at 4^{o}C with the antibody against FUBP1. After the addition of 100 µl of 50% protein G-Sepharose, the mixture was incubated overnight with gentle shaking at 4^{o}C. The immune complexes absorbed to protein G-Sepharose were washed five times with Nonidet P-40 lysis buffer (50 mM Tris, pH 7.5, 150 mM NaCl, 1% Nonidet P-40) with proteinase inhibitor and eluted by SDS loading buffer. Precipitated proteins were analyzed by WB using the antibodies against FUBP1 and 4EBP1.

GST-pull down

2 µg purified GFP tagged human 4EBP1 from *E. coli* was incubated with 2 µg purified GST tagged human FUBP1 fragment from *E. coli* in the binding buffer (50mM Tris, pH 7.5, 150mM NaCl, 1mM $CaCl_2$). The mixture was incubated at room temperature for 1 hr with gentle shaking, followed by another 1 hr of incubation after addition of 100 µl 50% glutathione-agarose beads (GE Healthcare). The beads were then washed several times with 140 mM NaCl, 10mM Na_2HPO_4, 1.8 mM KH_2PO_4, pH 7.5, and the remaining proteins were eluted using 1 × SDS

loading buffer and resolved by SDS-PAGE and transferred to a nitrocellulose membrane (Bio-Rad, Hercules, CA). The membrane were then immunoblotted with GFP and GST antibodies.

Data analysis

Data were analyzed and plotted using Sigmaplot 12 (Systat Software, San Jose, CA), and expressed as mean ± SEM (N), where SEM represents the standard error of the mean and N indicates the number of experimental repeats. Paired or unpaired Student t-tests were used to compare two sets of data. A probability value (P) of less than 0.05, 0.01 and 0.001 was considered statistically significant and indicated by "*", "**" and "***", respectively.

3.4 RESULTS

Identification of PKD2 3'UTR fragments that regulate its protein translation

We previously reported that PKD2 5'UTR mediates the translational up-regulation of PKD2 under cellular stress conditions[18]. In an effort to determine whether the 2087-nucleotides (nt) PKD2 3'UTR regulates its protein expression we performed dual-luciferase assays with vector BI16[25] that we utilized recently [18]. BI16 contains a bidirectional promoter that drives the transcription of the renilla and internal control firefly luciferases. We ligated PKD2 5'UTR/3'UTR into up-/downstream of the renilla luciferase gene to form plasmids BI16-3'UTR, 5'UTR-BI16 and 5'UTR-BI16-3'UTR, and found that the luciferase activity in HeLa cells transfected with BI16-3'UTR is much lower than that with control plasmid BI16 (Fig. 3-1A). A similar inhibitory effect of 3'UTR was found in the presence of 5'UTR (by comparing between 5'UTR-BI16-3'UTR and 5'UTR-BI16). Of note, 5'UTR also exhibited an inhibitory effect on the luciferase activity, in agreement with our previous report [18]. To determine whether 3'UTR affected PKD2 mRNA stability we performed end-point and real-time RT-PCR assays and found that the PKD2 mRNA level is not significantly altered by 3'UTR or 5'UTR (Fig. 3-1B), suggesting that 3'UTR represses the protein translation of luciferase.

We next wanted to narrow down and identify a 3'UTR fragment that mediates the inhibition. For this we first divided 3'UTR into two fragments, nt 1-1044 and nt 1025-2087 (with 20-nt overlap), for the luciferase assays and found that the first half of 3'UTR exhibits an inhibitory effect while the second half has a stimulatory effect (Fig. 3-1C). Because the first fragment contains a binding site (nt 118–145) for microRNA miR-17 and Bicc1 we wanted to know whether the observed inhibition relates to miR-17 and Bicc1. For this we made BI16 constructs with nt 118–145 deletion from 3'UTR and nt 1-1044, and found that the deletion has a

minimal or no effect on the luciferase activity (Fig. 3-1D), suggesting that native miR-17 and Bicc1 do not play a significant role under our conditions, although over-expressed miR-17 was reported to exhibit a modest inhibitory effect [33].

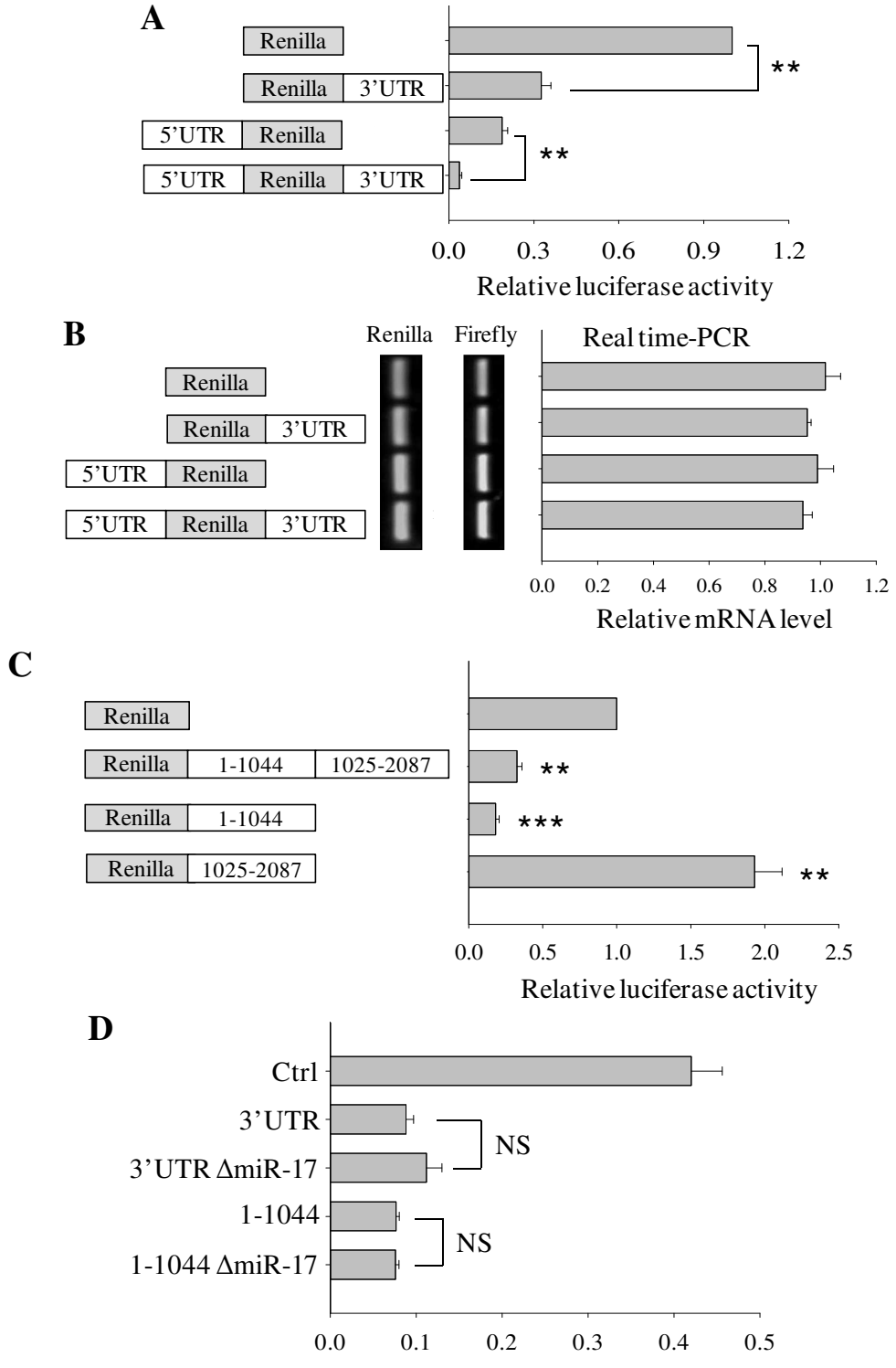

Fig. 3-1. Effects of human PKD2 3'UTR and 5'UTR on luciferase activity in HeLa cells. Statistical data on the bar graphs are mean and SEM values from three independent experiments. (**A**) Effects of 3'UTR on the relative luciferase activity revealed by dual-luciferase assays in the presence or absence of 5'UTR. "**" indicates $P < 0.01$. (**B**) Effects of 3'UTR on the mRNA level revealed by real-time PCR assays in the presence or absence of 5'UTR. Middle panels are representative data. (**C**) Effects of 3'UTR fragments nt 1-1044 and nt 1025-2087 on the relative luciferase activity revealed by dual-luciferase assays in the absence of 5'UTR. "**" and "***" indicates $P < 0.01$ and $P < 0.001$, respectively. (**D**) Effects of the binding domain (nt 118–145) for microRNA miR-17 in 3'UTR on the luciferase activity in the presence of 5'UTR. 3'UTRΔmiR-17 and nt 1–1044ΔmiR-17 respectively indicate 3'UTR and nt 1–1044 with deletion of miR-17-binding domain, nt 118–145. "Ctrl" indicates the absence of any 3'UTR fragment, but with the presence of 5'UTR. NS, not significant.

We next further divided nt 1-1044 and nt 1025-2087 into overlapping fragments and identified that nt 1-1044 and nt 691-1044 mediate inhibition while nt 1025-1129 mediates stimulation (Fig. 3-2). Of note, the nt 691-1044 fragment had slightly less inhibitory effect on luciferase expression than nt 1-1044 (Fig. 3-2A), with a unclear underlying reason. It is possible that nt 1-1044 has a more favorable conformation than nt 691-1044 in terms of interacting with the to-be-identified inhibitory binding partner. Because shorter fragments of nt 691-1044 and nt 1025-1129 substantially reduced their inhibitory and stimulatory effects, respectively (Fig. 3-2C and D) we called nt 691-1044 a 3' fragment inhibitory (3FI) and nt 1025-1129 a 3' fragment stimulatory (3FS). Of note, we selected nt 691-1044, but not nt 1-1044, because the former is much shorter and thus would be better for identifying specific binding partners. The inhibitory effect of 3FI on the translation was supported by data obtained using mutant 3'UTR with 3FI deletion (Fig. 3-3A and B). Of note, 3FI is AU-rich (68%) and has no overlap with the binding site for miR-17 and Bicc1[7]. We also performed WB assays to verify the effects of 3FI and 3FS by directly detecting the protein level of renilla luciferase. We indeed found that the renilla luciferase in HeLa and human embryonic kidney 293T (HEK) cells is regulated by 3FI and 3FS

in similar ways as by the luciferase assays (Fig. 3-3C). In addition, by replacing the coding sequence of renilla luciferase in the plasmid by that of Flag-tagged PKD2 we found that 3FI and 3FS reduces and enhances Flag-PKD2 protein expression, respectively, in both HeLa and HEK cells (Fig. 3-3D), which further confirmed the regulatory effects of 3FI and 3FS on protein translation.

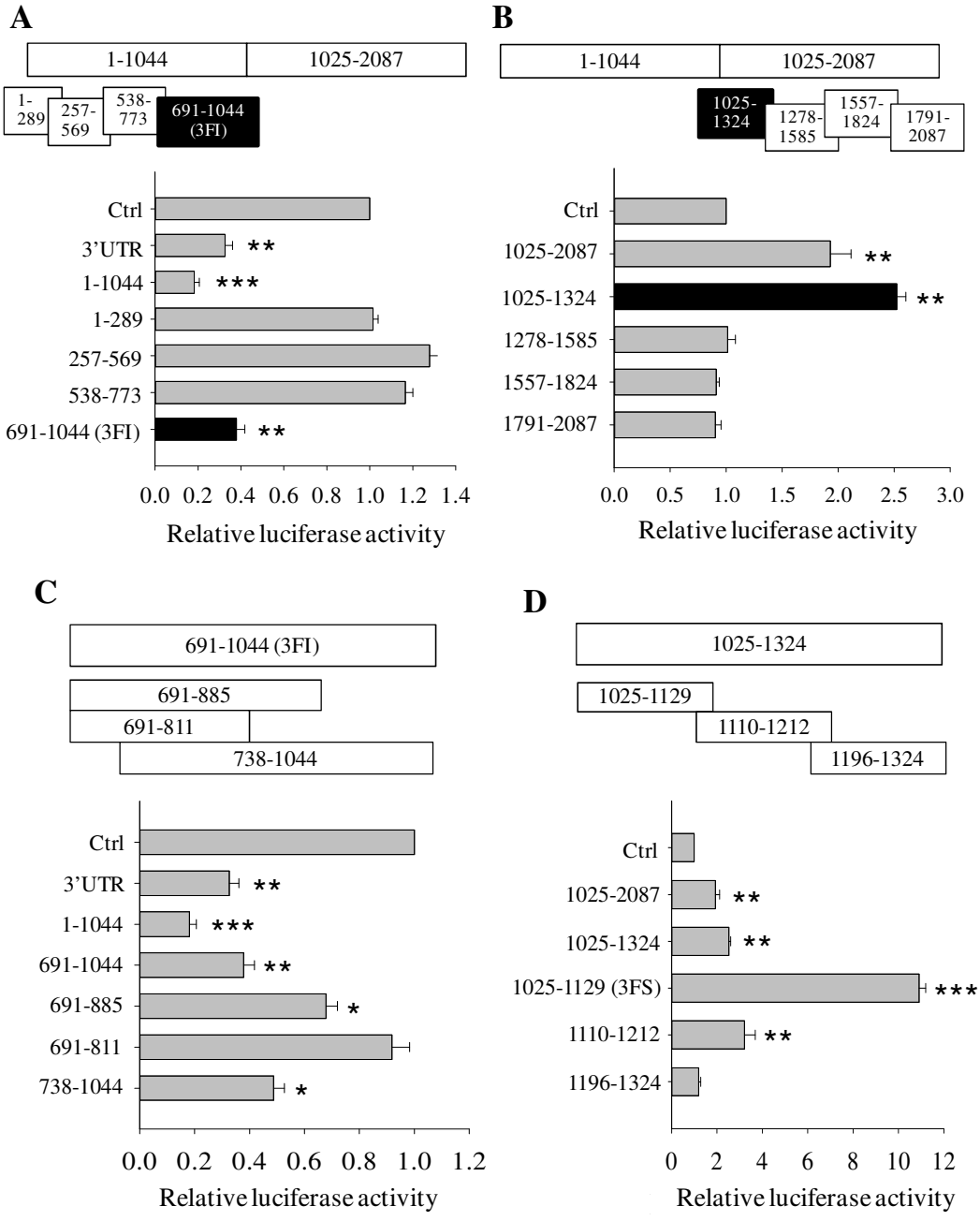

Fig. 3-2. Effects of 3'UTR fragments on luciferase activity in HeLa cells. Experimental conditions were similar to those in Fig. 3-1. Statistical data on the bar graphs are mean and SEM values from three independent experiments. "Ctrl" indicates the absence of any PKD2 3'UTR fragment or 5'UTR in the BI16 plasmid. (**A**) Effects of fragments, including 3FI, within nt 1-1044, as indicated. (**B**) Effects of fragments within nt 1025-2087, as indicated. (**C**) Effects of fragments within 3FI, as indicated. (**D**) Effects of fragments within nt 1025-1324, as indicated.

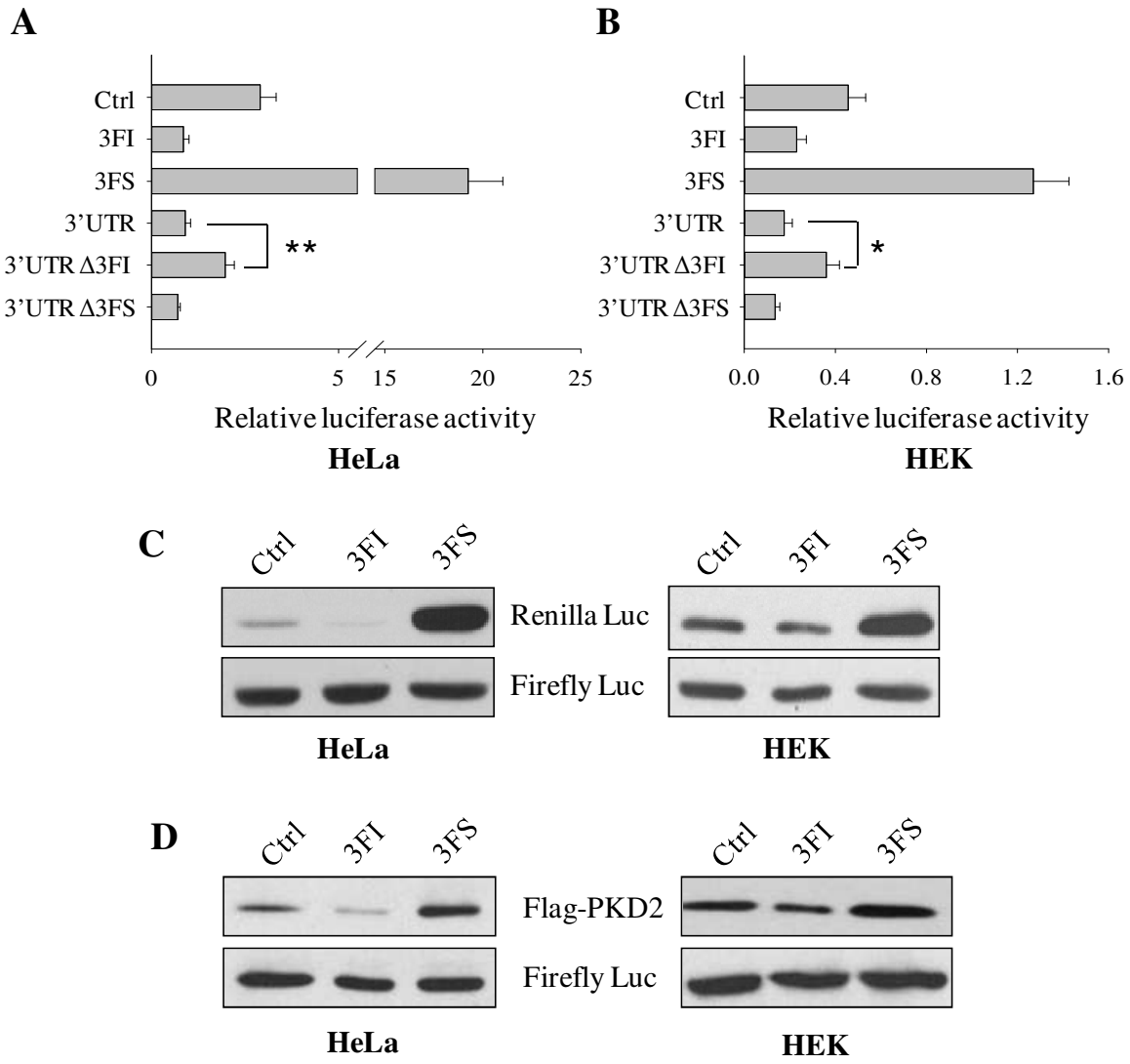

Fig. 3-3. Effects of 3FI and 3FS on luciferase activity and protein expression of luciferase and PKD2 in HeLa and HEK cells. Statistical data on the bar graphs are mean and SEM values from three independent experiments. "Ctrl" indicates the absence of any PKD2 3'UTR fragment or 5'UTR in the BI16 plasmid. (**A**) Effect of 3FI (3'UTRΔ3FI) or 3FS (3'UTRΔ3FS) deletion from 3'UTR on luciferase activity in HeLa cells. "**" indicates $P < 0.01$. (**B**) Effect of 3FI or 3FS deletion from 3'UTR on luciferase activity in HEK cells. "*" indicates $P < 0.05$. (**C**) Representative WB data showing the effects of 3FI and 3FS on the expression of renilla

luciferase protein in HeLa and HEK cells, as indicated. Firefly luciferase blots serve as an internal control. Experiments were repeated three times. (**D**) Representative WB data showing the effects of 3FI and 3FS on the expression of Flag-PKD2 in HeLa and HEK cells, as indicated. Firefly luciferase blots serve as an internal control. Experiments were repeated three times.

Identification of 3FI-binding partner FUBP1 that suppresses PKD2 protein translation

We next wanted to focus on 3FI by examining how it down-regulates PKD2 translation. We reasoned that there may be a RNA-binding protein that interacts with 3FI and mediates the inhibitory effect on the translation. For this we used PCR products from BI16-3FI and BI16 (Ctrl) as template (see Methods part) for *in vitro* transcription using biotin-labelled UTP to obtain biotinylated 3FI- or Ctrl RNA fragments that were incubated with HeLa cell lysates, followed by pull-down using streptavidin beads. Proteins in the precipitated lysates were separated by SDS-PAGE for mass spectrometry analysis of bands present in the 3FI, but not the control, lane, which identified FUBP1, FUBP2 and eIF4G as 3FI-interacting partners (see Supplementary Table 1 for a full list of the identified partners). FUBP1 and -2 are DNA-/RNA-binding proteins that regulate transcription, translation or mRNA stability of target genes, while eIF4G is a ribosomal protein and a key factor of the translation initiation complex.

We then wondered whether FUBP1 and -2 actually down-regulates PKD2 expression. For this we performed WB assays in HeLa cells and found that over-expression of FUBP1, but not of FUBP2, indeed reduces the PKD2 protein level to 45 ± 5% ($N = 3$, $p = 0.004$) (Fig. 3-4A). On the other hand, FUBP1 had no effect on the PKD2 mRNA level. We also found that over-expression of nuclear fragile X mental retardation-interacting protein 2, another RNA-binding protein identified as a 3FI partner (Supplementary Table 1), has no effect on PKD2 expression (data no shown). To verify the specificity, we also employed FUBP1 KD by siRNA and found

that FUBP1 KD in HEK cells leads to an increase of 80 ± 11% (N = 3, p = 0.005) in the PKD2 protein level while having no

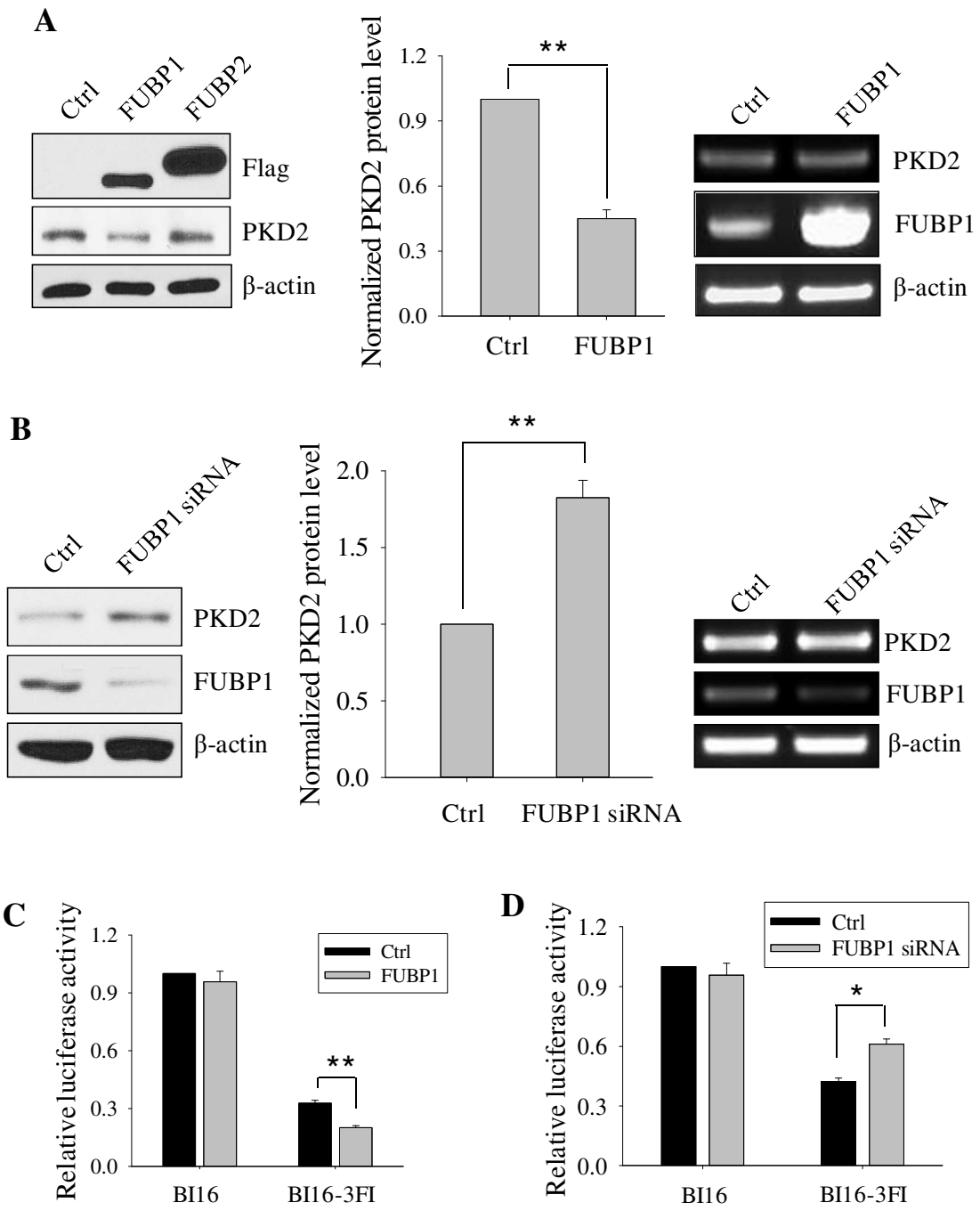

Fig. 3-4. Effect of FUBP1 on PKD2 protein and mRNA levels. (**A**) Effect of FUBP1 over-expression on PKD2 in HeLa cells. *Left*, representative WB data. *Centre*, quantified WB data averaged from N = 3 independent experiments. "**" indicates P < 0.01. *Right*, representative data showing PKD2 mRNA expression by RT-PCR. (**B**) Effect of FUBP1 siRNA KD on PKD2

in HEK cells. Experimental conditions were similar to those in panel A. Bar graphs showing data averaged from N = 3 independent experiments. "**" indicates P < 0.01. (**C**) Effect of FUBP1 over-expression on activity of luciferase without (BI16) or with 3FI (BI16-3FI) as 3'UTR in HeLa cells. Data were obtained from N = 3 independent experiments. (**D**) Effect of FUBP1 siRNA KD on activity of luciferase without (BI16) or with 3FI (BI16-3FI) as 3'UTR in HEK cells. Data were obtained from N = 3 independent experiments.

significant effect on the PKD2 mRNA level (Fig. 3-4B). In order to see whether translational inhibition by FUBP1 is mediated through 3FI, we co-transfected FUBP1 expressing plasmid and luciferase plasmid BI16 without or with 3FI into HeLa cells and found that FUBP1 over-expression significantly reduced luciferase expression in the presence of 3FI while had no effect in the absence of 3FI (Fig. 3-4C). Consistently, FUBP1 KD by siRNA increased luciferase expression in the presence of 3FI while had no effect in the absence of 3FI in HEK cells (Fig. 3-4D). FUBP1 was previously reported to bind AU-rich regions of RNAs through a signature sequence of AUUUA [34]. Indeed, human 3FI contains 68% AU and 3FI from different species all contain one to three AUUUA sequences (Fig. 3-S1). These results together showed a specific effect of FUBP1 on PKD2 translation but not on its mRNA stability, and suggest that FUBP1 may have mediated, at least in part, our observed inhibitory effect of 3FI.

Because FUBP1 was identified *in vitro* using biotin-RNA pull-down assays with fragment 3FI, it remains to be determined whether FUBP1 is able to bind native 3FI inside the cell in which full length PKD2 3'UTR has its distinct conformation. For this purpose we performed RIP assays by transfecting HeLa cells with HA-FUBP1 or empty vector (control) and then precipitating HA-FUBP1 whole cell extracts using HA antibody (Fig. 3-5A). After total RNAs were isolated from HA-FUBP1 immunoprecipitates, PKD2 mRNA was indeed detected by RT-

PCR while no PKD2 mRNA was detected in control groups (Fig. 3-5B), indicating that FUBP1 binds the endogenous PKD2 mRNA.

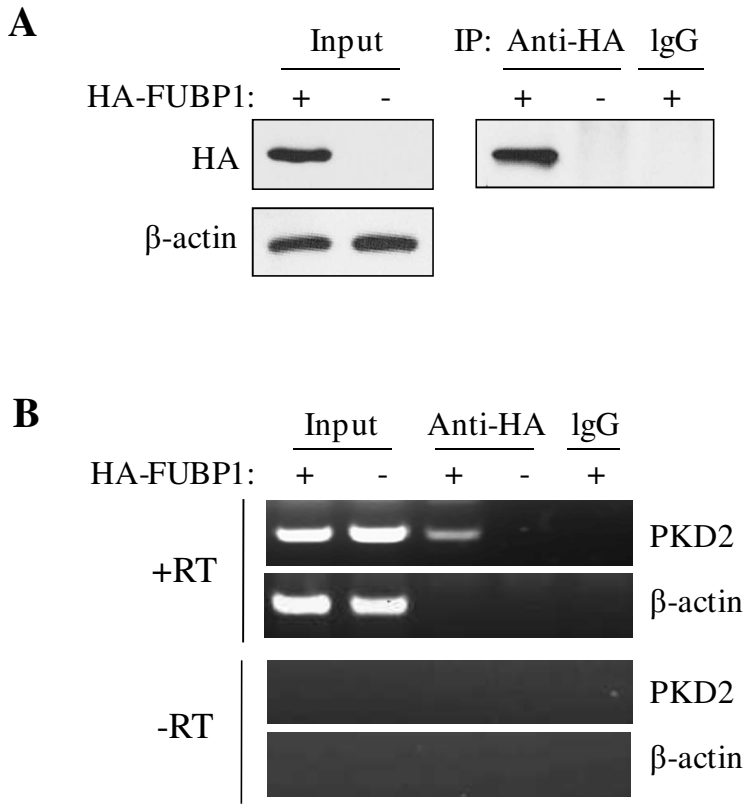

Fig. 3-5. Interaction between FUBP1 and native PKD2 mRNA. HeLa cells were transfected with HA-FUBP1 or empty vector. 48 hr after transfection, cell lysates were immunoprecipitated with HA antibody or non-immune rabbit IgG (control). (**A**) WB analysis of cell lysates (Inputs) and immunoprecipitates with antibodies indicated. (**B**) RT-PCR analysis of RNAs isolated from immunoprecipitates. +RT and –RT represent RT reactions carried out in the presence and absence of reverse transcriptase, respectively.

Effects of FUBP1 on PKD2 expression and disease phenotypes in zebrafish

Although zebrafish PKD2 mRNA 3'UTR (201-nt) is much shorter than that of human (2087-nt), the corresponding 3FI is also AU-rich (66%) and contains one AUUUA sequence (Fig. 3-S1). On the other hand, zebrafish FUBP1 shares 68% amino acid sequence identity with human FUBP1. We next employed *in vivo* larval zebrafish to study regulation of PKD2

expression and associated disease phenotypes by FUBP1. For this, we injected commercially acquired MO antisense oligonucleotide against PKD2 or FUBP1, control MO (Gene Tools), or water into 1- to 4-cell zebrafish embryos within 1 hour post-fertilization (hpf), using a Picospritzer III pressure injector (Parker Hannifin). PKD2 MO was used as previously reported [28]. Two days after injection, we manually de-chorionated embryos and found that fish with PKD2 MO injection, but not those with control MO injection, display curled tails (Fig. 3-6A) and pronephric cysts, consistent with previously published results that the presence of the two phenotypes are significantly correlated to each other [35,36]. Additionally, tail curling angle strongly correlates with PKD2 dosage (Fig. 3-6D). We thus decided to use 'tail curling' as a valid readout to examine the functional implications of regulation of PKD2 expression by FUBP1. While FUBP1 MO injection alone did not lead to tail curling, fish with co-injection of FUBP1 and PKD2 MOs showed substantially reduced tail curling, as compared with PKD2 MO injection alone, indicating that FUBP1 KD rescues the phenotype caused by PKD2 KD. After 2 dpf, tail curling gradually increased in fish with PKD2 MO injection alone while in fish with FUBP1 MO co-injection tail curling gradually decreased (Fig. 3-6A and C). On average, the angle of tail curling with PKD2 KD alone increased from 154 ± 23 degree at 2 dpf to 224 ± 32 degree at 5 dpf (N = 55), showing increased severity with time, while that with PKD2+FUBP1 MO co-injection decreased from 58 ± 11 degree at 2 dpf to 18 ± 8 degree at 5 dpf (N = 43), indicating an increasing rescuing effect with time.

We next examined PKD2 and FUBP1 expression in these fish by WB, using antibodies against zebrafish PKD2 and FUBP1. We found that MO injection effectively reduces PKD2 or FUBP1 expression, and that PKD2 expression increases in fish with FUBP1 MO injection (Fig. 3-6B), in agreement with our *in vitro* data (Fig. 3-3 and 4). These data indicate that reduced

PKD2 dosage in larval zebrafish results in tail curling that is rescued or alleviated by FUBP1 KD through up-regulating PKD2 expression. Consistently, we found that combined injection of *in vitro* transcribed

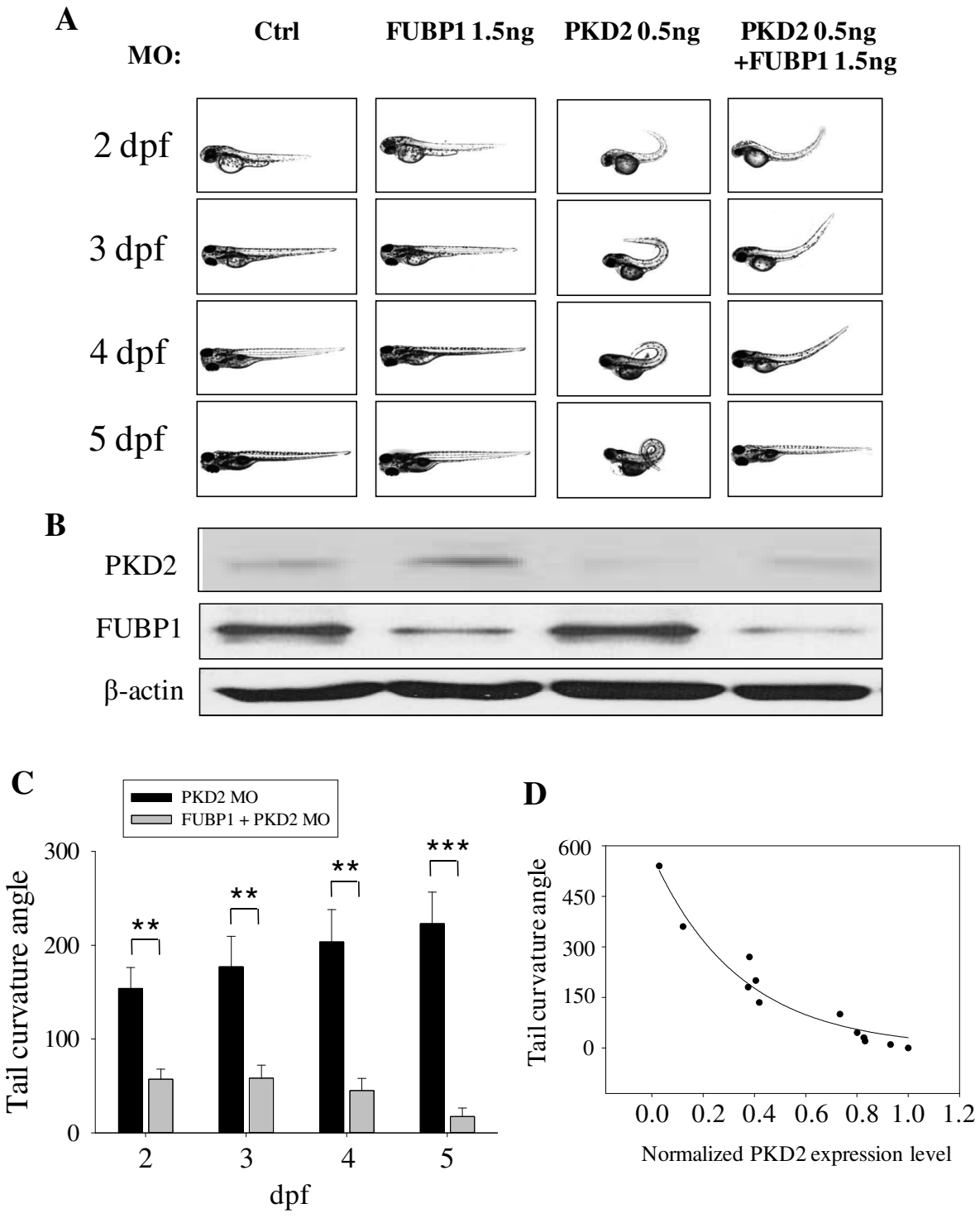

Fig. 3-6. Effect of FUBP1 KD on PKD2 expression and tail curling in embryonic zebrafish. (**A**) Representative pictures of 2-5 dpf zebrafish. Embryos were injected with MO(s) of PKD2 (0.5 ng), PKD2+FUBP1 (0.5+1.5 ng), FUBP1 (1.5 ng), or Ctrl (2 ng), within 1 hpf. (**B**) Representative WB data from 5-dpf larvae obtained using PKD2 and FUBP1 antibodies (Cat#: OAEB01480 and ARP37732_T100, Aviva System Biology). (**C**) Averaged tail curling angle for PKD2 (N = 55) and PKD2+FUBP1 (N = 43) MO injections. The angles for FUBP1 (N = 76) and Ctrl (N = 60) MOs were both zero and thus not plotted here. (**D**) Tail curling angle plotted against PKD2 dosage from 12 individual fish, showing different tail angle with PKD2 MO injection, of 5 dpf. PKD2 WB bands were quantified and divided by the corresponding β-actin bands using ImageJ and normalized to the fish showing no tail curvature. The curve is an empirical exponential decay fit that generated a correlation coefficient of R = 0.93.

human FUBP1 mRNA and PKD2 MO, but not single injection of any of the two, results in fish tail curling (Fig. 3-7A and B), presumably due to reduction in the PKD2 expression to below a threshold value by the co-injection. Further, we wanted to determine whether FUBP1 also regulates PKD2 knockdown-associated pronephric cyst formation. For this we employed FUBP1 over-expression through mRNA injection and found that FUBP1 mRNA injection significantly increases the occurrence rate of pronephric cysts induced by PKD2 MO knockdown in zebrafish (Fig. 3-7C-E). Thus, our data together demonstrated that FUBP1 regulates PKD2-associated disease phenotypes (tail curling and pronephric cyst) in larval zebrafish, presumably through regulating PKD2 protein dosage.

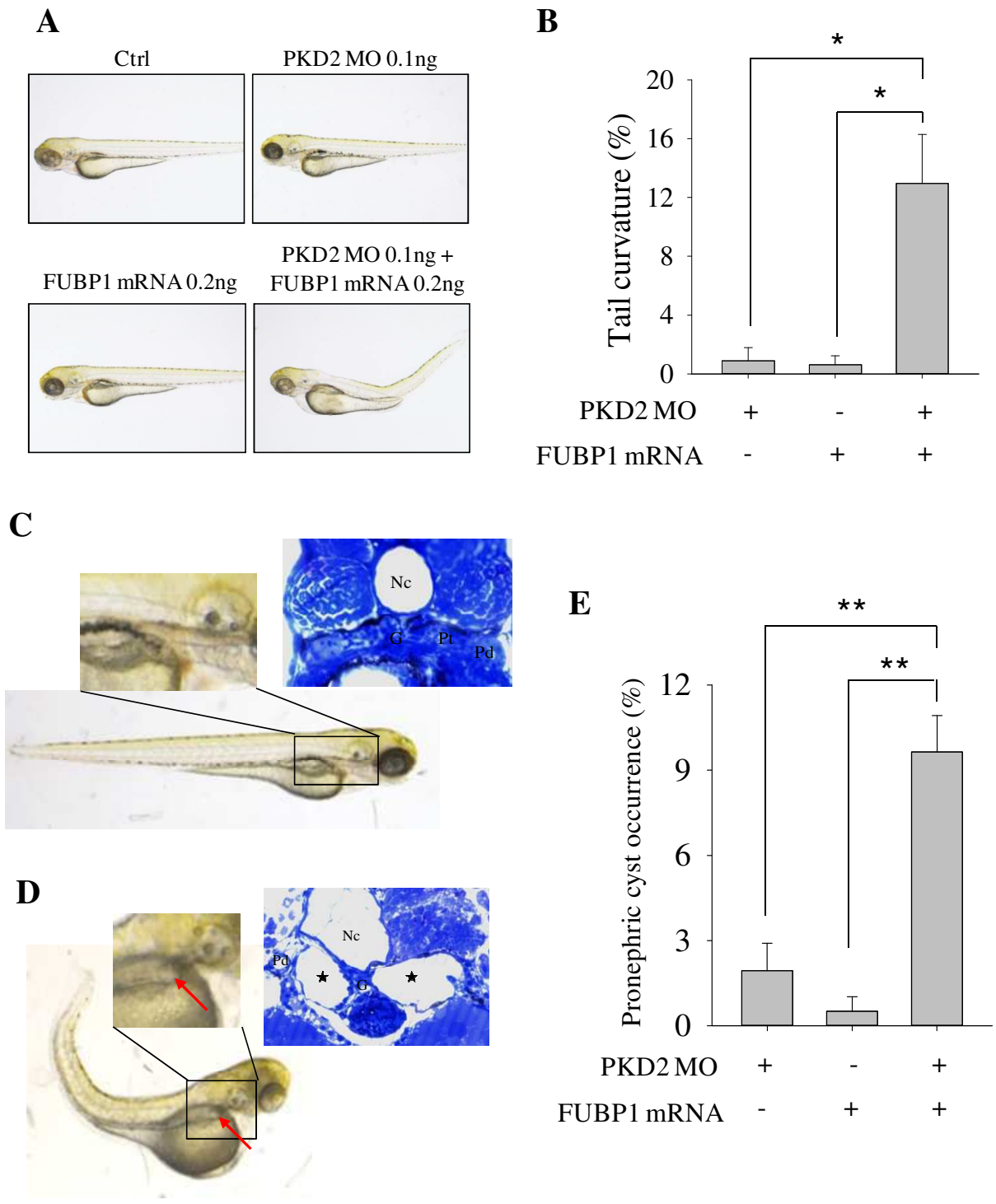

Fig. 3-7. Effect of FUBP1 over-expression on tail curling and pronephric cystogenesis of larval zebrafish. (**A**) Representative pictures showing tails of 3 dpf zebrafish with injection of PKD2 MO, FUBP1 mRNA, or water (Ctrl) within 1 hpf. (**B**) Average percentages of fish having a curled tail under different conditions: PKD2 MO injection alone (N = 112), FUBP1 mRNA injection alone (N = 152), and co-injection (N = 95). (**C**) Control (water-injected) larva with

histologically normal glomerulus and adjacent tubules at 3 dpf. G, glomerulus; Pt/Pd, pronephric tubule/duct; Nc, notochord. (**D**) PKD2 MO-injected larva (3 dpf) showing curly tail and pronephric cyst formation (arrows), which is confirmed by a histological section that also displayed dilated pronephric tubules (★). (**E**) Average percentages of fish exhibiting pronephric cysts under different conditions: PKD2 MO (0.15 ng) injection alone (N = 257), FUBP1 mRNA (200 pg) injection alone (N = 157), and co-injection (N = 248). "**", $P < 0.01$.

Interaction between FUBP1 and translation regulator 4EBP1

We next investigated whether there are molecular links of 3FI and FUBP1 to the translation initiation, which may be the basis for the down-regulation of PKD2 translation by 3FI and FUBP1. It is well known that 4EBP1 binds to eIF4E to disrupt the eIF4E-eIF4G initiation complex thereby reducing the translation initiation activity. Some better understood examples of RNA-binding proteins conform to a generic model in which 3'UTR-specific binding protein, which is often (but not always) a member of the PUF family, reduces initiation complex eIF4E-eIF4G formation through interacting with 4EBPs [19,37]. We thus first examined by co-IP assays to see whether FUBP1 interacts with 4EBP1. In both HEK and HeLa cells, we found that FUBP1 indeed precipitates 4EBP1 (Fig. 3-8A), indicating that they are in the same protein complex in these cells. To determine whether they associate with each other directly, we performed GST pull down assays. For this purpose, we divided human FUBP1 into three over-lapping fragments, the N-terminus (NT, aa 1-112), central domain (CD, aa 100-447) and C-terminus (CT, aa 442-644), and purified them from *E coli*. We found that the central domain, but not the two other fragments, is able to precipitate 4EBP1 protein purified from *E coli*. (Fig. 3-8B). Further, we found that addition of 3FI RNA, but not a control RNA fragment, significantly increases the binding between the FUBP1 CD and purified 4EBP1 (Fig. 3-8C). Interestingly, FUBP1 CD was found to have 4 KH domains for DNA and RNA binding. These data suggest that the inhibitory

effect of 3FI and FUBP1 on PKD2 translation is mediated by the FUBP1-4EBP1 binding strength. In summary, these experiments together demonstrated that FUBP1 is indeed physical linked to 4EBP1 that is a regulator of translation initiation.

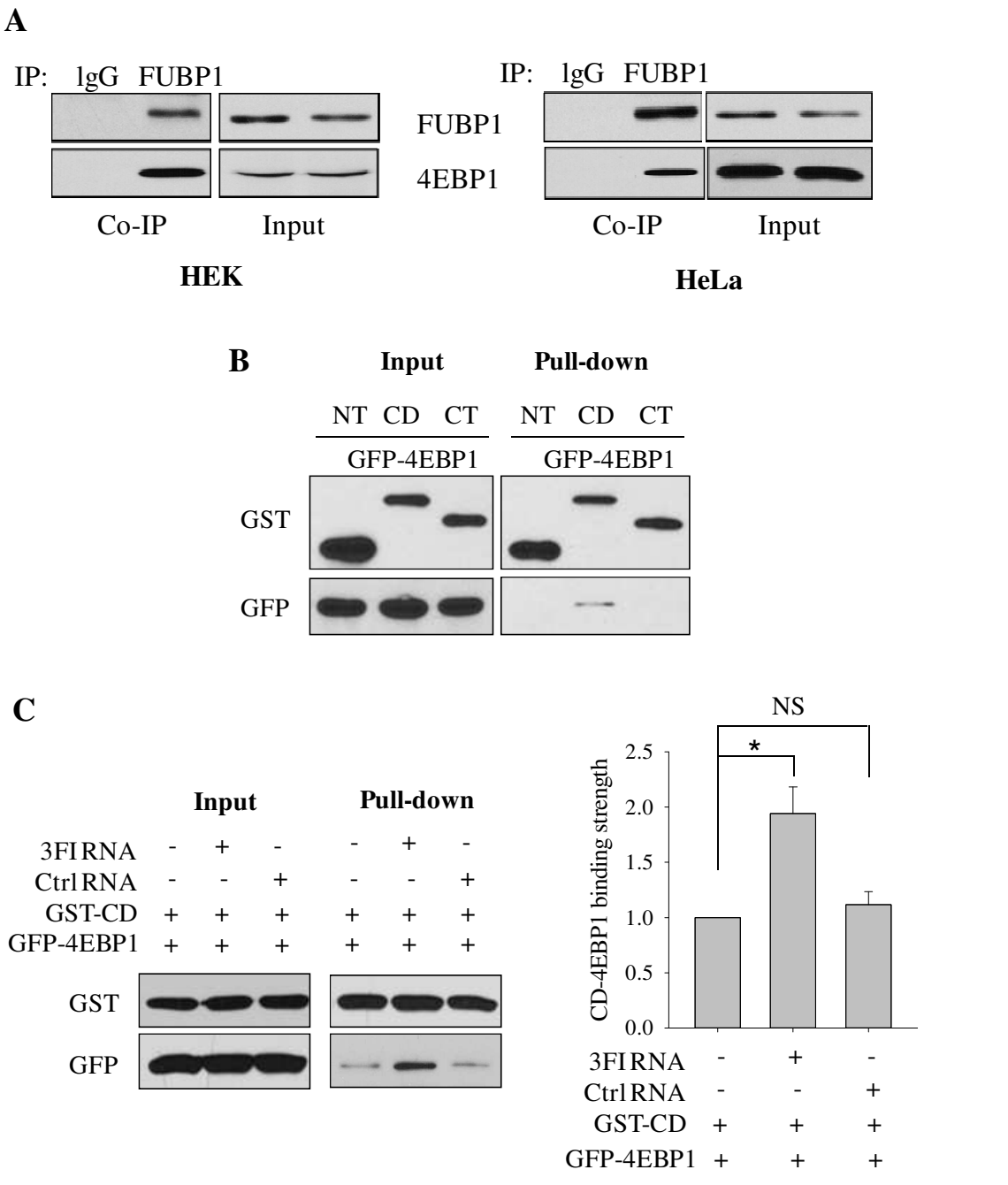

Fig. 3-8. Interaction between FUBP1 and 4EBP1, and effect of 3FI. (**A**) Co-IP experiments using native HEK and HeLa cells. FUBP1 antibody (ARP37732_T100, Aviva System Biology)

was used for precipitation and 4EBP1 antibody (P-1, Santa Cruz Biotechnology) for immunoblotting. (**B**) GST pull-down experiments using purified GST-tagged human N-terminus (NT, aa 1-112), central domain (CD, aa 100-447) and C-terminus (CT, aa 442-644) peptides and GFP-tagged human 4EBP1 protein from *E. coli*. (**C**) Effect of 3FI on *in vitro* binding between purified GST-CD and GFP-4EBP1. *Left*, representative WB data. The reaction system containing purified GST-CD and GFP-4EBP1 was supplemented with 3FI RNA, an unrelated RNA (Ctrl RNA), or none. GST pull-down assays were then performed, with GST and GFP antibodies for immunoblotting. *Right*, quantified and normalized WB data averaged from three independent experiments. "*", P = 0.03.

3.5 DISCUSSION

We previously reported that PKD2 is translationally up-regulated under cellular stress conditions and that this regulation is related to the presence of a conserved short upstream open reading frame fragment in the PKD2 mRNA 5'UTR [18]. In the current study, we studied roles of PKD2 mRNA 3'UTR in the regulation of PKD2 protein level. By dual-luciferase assays and RT-PCR, we have first shown that human PKD2 3'UTR represses the protein translation of luciferase. We have then identified the inhibitory nucleotide fragment 3FI (nt 691-1044) and, by biotin-labelled RNA pull-down assays, its binding protein FUBP1. We have shown that FUBP1 does exhibit an inhibitory effect on PKD2 translation, but not transcription, in cultured cells. Finally, we have shown that in embryonic zebrafish FUBP1 regulates the severity of tail curling and pronephric cystogenesis due to PKD2 MO knockdown, presumably through regulating PKD2 expression in a similar way as in cultured cells.

A “two hit” model was firstly proposed in 1992 to illustrate a possible mechanism underlying the cystogenesis of ADPKD [38]. This hypothesis suggested that the occurrence of a somatic mutation in the remaining normal allele of some cells initiated cyst formation in the affected cells. In other words, ADPKD is recessive at the cellular level. This model received strong support from the identification of somatic mutations that inactivated the normal alleles in 20-43% of the analyzed *PKD1* or *PKD2* renal cysts [39-42]. However, no somatic mutation in the normal allele was found in the remaining cysts. Over the past decades, increasing evidence has been in support of a "dosage" model that renal cystogenesis can be initiated when the wild-type PKD1 or PKD2 protein level is reduced to a threshold level, in the absence of a somatic mutation [43-45]. Therefore, it became important to elucidate how PKD1 and PKD2 protein expression is regulated, which may lead to identification of new therapeutic targets, especially when the

outcomes of the clinic trials were rather negative. FUBP1 identified in the present study represents a novel translational regulator of PKD2 and indeed regulated PKD2-associated zebrafish tail curvature and pronephric cystogenesis, which can be accounted for by changes in the PKD2 protein dosage.

The fact that both loss- and gain-of-function of PKD2 are pathogenic indicates that PKD2 protein level must be strictly regulated within a narrow range [3,6]. Consistent with this, it was known that PKD2 protein expression is developmentally regulated [46]. Generally the protein level is regulated transcriptionally or translationally. By computational analyses, putative binding sites for transcription factors E2F, EGRF, ETS, SP1 and ZBP-89 were identified in the promoter region of both human and mouse PKD2 [47]. However, little experimental data have so far been available regarding transcription factors that regulate PKD2 transcription, suggesting the possibility that translational regulation of PKD2 plays important roles. Indeed a short upstream open reading frame in PKD2 mRNA 5'UTR was reported to be implicated in the translational up-regulation of PKD2 by cellular stresses [18]. It was also found that microRNA-17 post-transcriptionally down-regulates PKD2 expression by binding to its mRNA 3'UTR thereby promoting cell proliferation [33]. Further, it was reported that the RNA-binding protein bicaudal C up-regulates PKD2 expression by antagonizing the repressive activity of miR-17 through competitively binding to the same site on the PKD2 mRNA 3'UTR.[7] Of note, our identified 3FI and 3FS from the current study do not overlap with the miR-17 binding site. These together show that 3'UTR possesses multiple elements important for complex regulation of PKD2 protein level. FUBP1 was first identified as a single-strand DNA-binding protein that up-regulates the transcription of proto-oncogen *c-Myc* through binding to the far upstream element (FUSE) in the promoter region 1.5 kb upstream of the transcription start site [48]. It promotes cell proliferation,

survival and metastasis through up-regulating *c-Myc* and plays important roles in organ development such as lung, brain and neural network [34,49,50]. In contrast, FUBP1 was known to transcriptionally down-regulate the expression of TNFα [51]. Interestingly, c-Myc is elevated in cystic tissues of various PKD models and TNFα is elevated in PKD2$^{+/-}$ mice [52-54]. Moreover, c-Myc transgenic mice and *in vitro* application of TNFα to kidney in culture developed cysts [52,53]. Thus, although FUBP1 altered the expression of three cystogenic proteins PKD2 (down), TNFα (down) and c-Myc (up) whether and how FUBP1 is implicated in cystogenesis remains to be determined.

Although FUBP1 was originally identified as a transcription factor (of c-Myc), recent reports demonstrated that FUBP1 also functions as a RNA-binding protein for translational regulation of its bound genes, including GAP43, p21, Cox-2 and NPM [55-58]. Similar to bicaudal C that contains three RNA-binding KH domains and binds to the 3'UTR of PKD2, FUBP1 has four KH domains. Sequence analysis found that FUBP1 binds to AU-rich regions in mRNA 3'UTR, which is supported by the fact that the FUBP1-binding 3FI contains 68% AU. FUBP1 is present in multiple tissues including kidney, liver, pancreas, thymus, ovary and skin [59,60]. In kidney FUBP1 is expressed at various locations, including podocytes, proximal and distal tubules (Fig. 3-S2), and developmentally decreases [59,60] while the PKD2 protein level increases in the kidney during development [46], consistent with down-regulation of PKD2 translation by FUBP1.

As a transcription regulator, FUBP1was reported to be primarily localized in the nucleus [61-63]. However, to function as a translational regulator, FUBP1 is also required to be located in the cytoplasm. It was known that under normal physiological conditions, FUBP1 primarily localizes in the nucleus, and that under stress conditions such as in the presence of heat shock, viral

infection and oxidative stress FUBP1 either stops entering the nucleus or translocates from the nucleus to the cytoplasm, resulting in cytoplasmic accumulation [34]. Interestingly, TGF-β1, which is up-regulated in ADPKD, was also reported to induce translocation of FUBP1 from the nucleus to the cytoplasm [64].

The presence of physical interaction between FUBP1 and eIF4E binding protein 4EBP1 suggests the complex 3FI-FUBP1 located at the 3'UTR of PKD2 mRNA is indeed connected, via 4EBP1, to the initiation complex located at the 5'UTR of PKD2 mRNA. Thus, our study may have identified a novel example in support of a 'closed-loop' or 'circular' model of mRNAs. However, it remains to be determined in the future as to whether 3FI and FUBP1 enhances the 4EBP1-eIF4E binding thereby reducing the eIF4E-eIF4G binding in the proximity of PKD2 5'UTR.

In summary, our present study found that FUBP1 binds with the AU-rich 3FI in the PKD2 mRNA 3'UTR and negatively regulates PKD2 protein translation in cultured cell lines. In embryonic zebrafish, decreased FUBP1 by MO injection and increased FUBP1 by mRNA injection alleviates and aggravates, respectively, the tail curling and/or pronephric cyst occurrence due to reduced PKD2 level by MO injection, presumably through affecting PKD2 dosage. In fact, for human patients whose PKD2 mutant(s) remains partially functional, a peptide (of FUBP1), RNA fragment (of human PKD2 3FI), or chemical that disrupts the FUBP1-3'UTR binding may be a potential drug candidate, because it would abolish (or significantly reduce) the down-regulation of PKD2 translation by FUBP1, thereby increasing PKD2 dosage and compensating for partial loss of PKD2 function. Our study thus unveiled a novel mechanism of dosage regulation that is important for ADPKD pathogenesis and may allow discovering new therapeutic targets with future studies.

3.6 REFERENCES

1. Qian, F. & Noben-Trauth, K. Cellular and molecular function of mucolipins (TRPML) and polycystin 2 (TRPP2). *Pflugers Arch.* **451**, 277-285 (2005).

2. Bichet, D., Peters, D., Patel, A. J., Delmas, P. & Honore, E. Cardiovascular polycystins: insights from autosomal dominant polycystic kidney disease and transgenic animal models. *Trends Cardiovasc. Med.* **16**, 292-298 (2006).

3. Wu, G. *et al.* Somatic inactivation of Pkd2 results in polycystic kidney disease. *Cell* **93**, 177-188 (1998).

4. Lu, W. *et al.* Perinatal lethality with kidney and pancreas defects in mice with a targetted Pkd1 mutation. *Nat. Genet.* **17**, 179-181 (1997).

5. Kurbegovic, A. *et al.* Pkd1 transgenic mice: adult model of polycystic kidney disease with extrarenal and renal phenotypes. *Hum. Mol. Genet.* **19**, 1174-1189 (2010).

6. Park, E. Y. *et al.* Cyst formation in kidney via B-Raf signaling in the PKD2 transgenic mice. *J. Biol. Chem.* **284**, 7214-7222 (2009).

7. Tran, U. *et al.* The RNA-binding protein bicaudal C regulates polycystin 2 in the kidney by antagonizing miR-17 activity. *Development.* **137**, 1107-1116 (2010).

8. Dutcher, S. K. & Lin, H. Tying TAZ and Nek1 into polycystic kidney disease through polycystin 2 levels. *J. Am. Soc. Nephrol.* **22**, 791-793 (2011).

9. Gonzalez-Perret, S. *et al.* Polycystin-2, the protein mutated in autosomal dominant polycystic kidney disease (ADPKD), is a Ca2+-permeable nonselective cation channel. *Proc. Natl. Acad. Sci. U. S. A* **98**, 1182-1187 (2001).

10. Li, Q. *et al.* Alpha-actinin associates with polycystin-2 and regulates its channel activity. *Hum. Mol. Genet.* **14**, 1587-1603 (2005).

11. Li, X. *et al.* Polycystin-1 and polycystin-2 regulate the cell cycle through the helix-loop-helix inhibitor Id2. *Nat. Cell Biol.* **7**, 1202-1212 (2005).

12. Li, Y., Wright, J. M., Qian, F., Germino, G. G. & Guggino, W. B. Polycystin 2 interacts with type I inositol 1,4,5-trisphosphate receptor to modulate intracellular Ca2+ signaling. *J. Biol. Chem.* **280**, 41298-41306 (2005).

13. Ma, R. *et al.* PKD2 functions as an epidermal growth factor-activated plasma membrane channel. *Mol. Cell Biol.* **25**, 8285-8298 (2005).

14. Rundle, D. R., Gorbsky, G. & Tsiokas, L. PKD2 interacts and co-localizes with mDia1 to mitotic spindles of dividing cells: Role of mDia1 in PKD2 localization to mitotic spindles. *J. Biol. Chem.* **279**, 29728-29739 (2004).

15. Tsiokas, L., Kim, E., Arnould, T., Sukhatme, V. P. & Walz, G. Homo- and heterodimeric interactions between the gene products of PKD1 and PKD2. *Proc. Natl. Acad. Sci. U. S. A* **94**, 6965-6970 (1997).

16. Tsiokas, L. *et al.* Specific association of the gene product of PKD2 with the TRPC1 channel. *Proc. Natl. Acad. Sci. U. S. A* **96**, 3934-3939 (1999).

17. Bouvrette, D. J., Sittaramane, V., Heidel, J. R., Chandrasekhar, A. & Bryda, E. C. Knockdown of bicaudal C in zebrafish (Danio rerio) causes cystic kidneys: a nonmammalian model of polycystic kidney disease. *Comp Med.* **60**, 96-106 (2010).

18. Yang, J. *et al.* Translational up-regulation of polycystic kidney disease protein PKD2 by endoplasmic reticulum stress. *FASEB J.* **27**, 4998-5009 (2013).

19. Jackson, R. J., Hellen, C. U. & Pestova, T. V. The mechanism of eukaryotic translation initiation and principles of its regulation. *Nat. Rev. Mol. Cell Biol.* **11**, 113-127 (2010).

20. Gallie, D. R. A tale of two termini: a functional interaction between the termini of an mRNA is a prerequisite for efficient translation initiation. *Gene.* **216**, 1-11 (1998).

21. Varani, G. Delivering messages from the 3' end. *Proc. Natl. Acad. Sci. U. S. A.* **98**, 4288-4289 (2001).

22. Gingras, A. C., Raught, B. & Sonenberg, N. eIF4 initiation factors: effectors of mRNA recruitment to ribosomes and regulators of translation. *Annu. Rev. Biochem.* **68:913-63.**, 913-963 (1999).

23. Ostareck, D. H., Ostareck-Lederer, A., Shatsky, I. N. & Hentze, M. W. Lipoxygenase mRNA silencing in erythroid differentiation: The 3'UTR regulatory complex controls 60S ribosomal subunit joining. *Cell.* **104**, 281-290 (2001).

24. Mazumder, B., Seshadri, V., Imataka, H., Sonenberg, N. & Fox, P. L. Translational silencing of ceruloplasmin requires the essential elements of mRNA circularization: poly(A) tail, poly(A)-binding protein, and eukaryotic translation initiation factor 4G. *Mol. Cell Biol.* **21**, 6440-6449 (2001).

25. Sammarco, M. C. & Grabczyk, E. A series of bidirectional tetracycline-inducible promoters provides coordinated protein expression. *Anal. Biochem.* **346**, 210-216 (2005).

26. Roy, B., Ferdous, J. & Ali, D. W. NMDA receptors on zebrafish Mauthner cells require CaMKII-alpha for normal development. *Dev. Neurobiol.* **75**, 145-162 (2015).

27. Brewster, D. L. & Ali, D. W. Expression of the voltage-gated potassium channel subunit Kv1.1 in embryonic zebrafish Mauthner cells. *Neurosci. Lett.* **539:54-9. doi: 10.1016/j.neulet.2013.01.042. Epub@2013 Feb 4.**, 54-59 (2013).

28. Sun, Z. *et al.* A genetic screen in zebrafish identifies cilia genes as a principal cause of cystic kidney. *Development* **131**, 4085-4093 (2004).

29. Karlstrom, R. O. *et al.* Genetic analysis of zebrafish gli1 and gli2 reveals divergent requirements for gli genes in vertebrate development. *Development.* **130**, 1549-1564 (2003).

30. Drummond, I. A. *et al.* Early development of the zebrafish pronephros and analysis of mutations affecting pronephric function. *Development.* **125**, 4655-4667 (1998).

31. Takagi, M., Absalon, M. J., McLure, K. G. & Kastan, M. B. Regulation of p53 translation and induction after DNA damage by ribosomal protein L26 and nucleolin. *Cell.* **123**, 49-63 (2005).

32. Rinn, J. L. *et al.* Functional demarcation of active and silent chromatin domains in human HOX loci by noncoding RNAs. *Cell.* **129**, 1311-1323 (2007).

33. Sun, H. *et al.* MicroRNA-17 post-transcriptionally regulates polycystic kidney disease-2 gene and promotes cell proliferation. *Mol. Biol. Rep.* **37**, 2951-2958 (2010).

34. Zhang, J. & Chen, Q. M. Far upstream element binding protein 1: a commander of transcription, translation and beyond. *Oncogene.* **32**, 2907-2916 (2013).

35. Giamarchi, A. *et al.* A polycystin-2 (TRPP2) dimerization domain essential for the function of heteromeric polycystin complexes. *EMBO J.* **29**, 1176-1191 (2010).

36. Feng, S. *et al.* Identification and functional characterization of an N-terminal oligomerization domain for polycystin-2. *J. Biol. Chem.* **283**, 28471-28479 (2008).

37. Kong, J. & Lasko, P. Translational control in cellular and developmental processes. *Nat. Rev. Genet.* **13**, 383-394 (2012).

38. Reeders, S. T. Multilocus polycystic disease. *Nat. Genet.* **1**, 235-237 (1992).

39. Cornec-Le, G. E., Audrezet, M. P., Meur, Y. L., Chen, J. M. & Ferec, C. Genetics and pathogenesis of autosomal dominant polycystic kidney disease: 20 years on. *Hum. Mutat.* **35**, 1393-1406 (2014).

40. Pei, Y. *et al.* Somatic PKD2 mutations in individual kidney and liver cysts support a "two-hit" model of cystogenesis in type 2 autosomal dominant polycystic kidney disease. *J. Am. Soc. Nephrol.* **10**, 1524-1529 (1999).

41. Koptides, M., Hadjimichael, C., Koupepidou, P., Pierides, A. & Constantinou, D. C. Germinal and somatic mutations in the PKD2 gene of renal cysts in autosomal dominant polycystic kidney disease. *Hum. Mol. Genet.* **8**, 509-513 (1999).

42. Brasier, J. L. & Henske, E. P. Loss of the polycystic kidney disease (PKD1) region of chromosome 16p13 in renal cyst cells supports a loss-of-function model for cyst pathogenesis. *J. Clin. Invest.* **99**, 194-199 (1997).

43. Lantinga-van, L., I *et al.* Lowering of Pkd1 expression is sufficient to cause polycystic kidney disease. *Hum. Mol. Genet.* **13**, 3069-3077 (2004).

44. Kim, I. *et al.* Polycystin-2 expression is regulated by a PC2-binding domain in the intracellular portion of fibrocystin. *J. Biol. Chem.* **283**, 31559-31566 (2008).

45. Jiang, S. T. *et al.* Defining a link with autosomal-dominant polycystic kidney disease in mice with congenitally low expression of Pkd1. *Am. J. Pathol.* **168**, 205-220 (2006).

46. Markowitz, G. S. *et al.* Polycystin-2 expression is developmentally regulated. *Am. J. Physiol* **277**, F17-F25 (1999).

47. Lantinga-van, L., I *et al.* Common regulatory elements in the polycystic kidney disease 1 and 2 promoter regions. *Eur. J. Hum. Genet.* **13**, 649-659 (2005).

48. Duncan, R. *et al.* A sequence-specific, single-strand binding protein activates the far upstream element of c-myc and defines a new DNA-binding motif. *Genes Dev.* **8**, 465-480 (1994).

49. Kim, M. J. *et al.* Downregulation of FUSE-binding protein and c-myc by tRNA synthetase cofactor p38 is required for lung cell differentiation. *Nat. Genet.* **34**, 330-336 (2003).

50. Irwin, N., Baekelandt, V., Goritchenko, L. & Benowitz, L. I. Identification of two proteins that bind to a pyrimidine-rich sequence in the 3'-untranslated region of GAP-43 mRNA. *Nucleic Acids Res.* **25**, 1281-1288 (1997).

51. Rabenhorst, U. *et al.* Overexpression of the far upstream element binding protein 1 in hepatocellular carcinoma is required for tumor growth. *Hepatology.* **50**, 1121-1129 (2009).

52. Li, X. *et al.* A tumor necrosis factor-alpha-mediated pathway promoting autosomal dominant polycystic kidney disease. *Nat. Med.* **14**, 863-868 (2008).

53. Lanoix, J., D'Agati, V., Szabolcs, M. & Trudel, M. Dysregulation of cellular proliferation and apoptosis mediates human autosomal dominant polycystic kidney disease (ADPKD). *Oncogene* **13**, 1153-1160 (1996).

54. Ricker, J. L., Mata, J. E., Iversen, P. L. & Gattone, V. H. c-myc antisense oligonucleotide treatment ameliorates murine ARPKD. *Kidney Int.* **61**, S125-S131 (2002).

55. Kusik, B. W., Hammond, D. R. & Udvadia, A. J. Transcriptional regulatory regions of gap43 needed in developing and regenerating retinal ganglion cells. *Dev. Dyn.* **239**, 482-495 (2010).

56. Wang, W. *et al.* HuR regulates p21 mRNA stabilization by UV light. *Mol. Cell Biol.* **20**, 760-769 (2000).

57. Dean, J. L., Sully, G., Clark, A. R. & Saklatvala, J. The involvement of AU-rich element-binding proteins in p38 mitogen-activated protein kinase pathway-mediated mRNA stabilisation. *Cell Signal.* **16**, 1113-1121 (2004).

58. Olanich, M. E., Moss, B. L., Piwnica-Worms, D., Townsend, R. R. & Weber, J. D. Identification of FUSE-binding protein 1 as a regulatory mRNA-binding protein that represses nucleophosmin translation. *Oncogene.* **30**, 77-86 (2011).

59. Weber, A. *et al.* The FUSE binding proteins FBP1 and FBP3 are potential c-myc regulators in renal, but not in prostate and bladder cancer. *BMC. Cancer.* **8:369. doi: 10.1186/1471-2407-8-369.**, 369-8 (2008).

60. Lu, J. Y. & Schneider, R. J. Tissue distribution of AU-rich mRNA-binding proteins involved in regulation of mRNA decay. *J. Biol. Chem.* **279**, 12974-12979 (2004).

61. Jang, M. *et al.* Far upstream element-binding protein-1, a novel caspase substrate, acts as a cross-talker between apoptosis and the c-myc oncogene. *Oncogene.* **28**, 1529-1536 (2009).

62. Liu, J. *et al.* JTV1 co-activates FBP to induce USP29 transcription and stabilize p53 in response to oxidative stress. *EMBO J.* **30**, 846-858 (2011).

63. Bazar, L., Harris, V., Sunitha, I., Hartmann, D. & Avigan, M. A transactivator of c-myc is coordinately regulated with the proto-oncogene during cellular growth. *Oncogene.* **10**, 2229-2238 (1995).

64. Milosevic, J., Bulau, P., Mortz, E. & Eickelberg, O. Subcellular fractionation of TGF-beta1-stimulated lung epithelial cells: a novel proteomic approach for identifying signaling intermediates. *Proteomics.* **9**, 1230-1240 (2009).

Supplementary Table S1. List of identified 3FI-binding partner proteins and their basic characteristics

Accession	Description	Score	Coverage	# Proteins	# Unique Peptides	# Peptides	# PSMs	Molecular Function	Cellular Component	Biological Process	# AAs	MW [kDa]	calc. pI
Q96AE4	Far upstream element-binding protein 1 OS=Homo sapiens GN=FUBP1 PE=1 SV=2 - [FUBP1_HUMAN]	166.56	42.33	1	24	24	53	DNA binding; RNA binding	cytoplasm; cytosol; nucleus; organelle lumen	metabolic process; regulation of biological process; transport	644	70.9	7.30
Q01813	6-phosphofructokinase type C OS=Homo sapiens GN=PFKP PE=1 SV=2 - [K6PP_HUMAN]	96.18	30.74	1	18	19	30	catalytic activity; metal ion binding; nucleotide binding	cytoplasm; cytosol	metabolic process	784	85.5	7.55
P04264	Keratin, type II cytoskeletal 1 OS=Homo sapiens GN=KRT1 PE=1 SV=6 - [K2C1_HUMAN]	39.28	13.51	1	8	10	13	catalytic/motor/receptor/structural molecule/transporter activity; protein binding	cytoskeleton; membrane	coagulation; defense response; development; metabolic process; regulation of biological process; response to stimulus; transport	644	66.0	8.12
Q7Z417	Nuclear fragile X mental retardation-interacting protein 2 OS=Homo sapiens GN=NUFIP2 PE=1 SV=1 - [NUFP2_HUMAN]	37.70	21.87	1	10	10	12	protein binding; RNA binding	cytoplasm; nucleus; ribosome		695	76.1	8.70
P46060	Ran GTPase-activating protein 1 OS=Homo sapiens GN=RANGAP1 PE=1 SV=1 - [RAGP1_HUMAN]	36.64	23.51	1	11	11	13	enzyme regulator activity; protein binding	chromosome; cytoplasm; cytoskeleton; cytosol; membrane; nucleus	cell communication; cell organization and biogenesis; metabolic process; regulation of biological process; response to stimulus; transport	587	63.5	4.68
P54886	Delta-1-pyrroline-5-carboxylate synthase OS=Homo sapiens GN=ALDH18A1 PE=1 SV=2 - [P5CS_HUMAN]	36.30	14.59	1	9	9	12	catalytic activity; nucleotide binding	cytoplasm; membrane; mitochondrion	metabolic process	795	87.2	7.12

P08237	6-phosphofructokinase, muscle type OS=Homo sapiens GN=PFKM PE=1 SV=2 - [K6PF_HUMAN]	30.60	17.69	1	9	10	12	catalytic activity; metal ion binding; nucleotide binding; protein binding	cytoplasm; cytosol; membrane	cell organization and biogenesis; cellular homeostasis; metabolic process	780	85.1	7.99
Q99567	Nuclear pore complex protein Nup88 OS=Homo sapiens GN=NUP88 PE=1 SV=2 - [NUP88_HUMAN]	29.97	19.70	1	9	9	9	transporter activity	cytoplasm; cytosol; membrane; nucleus; organelle lumen	cell communication; metabolic process; regulation of biological process; response to stimulus; transport	741	83.5	5.69
Q92945	Far upstream element-binding protein 2 OS=Homo sapiens GN=KHSRP PE=1 SV=4 - [FUBP2_HUMAN]	25.56	20.33	1	9	9	10	DNA binding; RNA binding	cytoplasm; cytosol; nucleus; organelle lumen	metabolic process; regulation of biological process; transport	711	73.1	5.70
P13645	Keratin, type I cytoskeletal 10 OS=Homo sapiens GN=KRT10 PE=1 SV=6 - [K1C10_HUMAN]	24.43	20.21	1	9	9	9	structural molecule activity	cytoplasm; cytoskeleton	cell differentiation; development; response to stimulus	584	58.8	5.21
C9JJE2	Splicing factor 1 OS=Homo sapiens GN=SF1 PE=4 SV=2 - [C9JJE2_HUMAN]	22.98	12.89	2	5	5	8	metal ion binding; RNA binding	nucleus; organelle lumen		613	65.3	8.38
B4E2Z3	4F2 cell-surface antigen heavy chain OS=Homo sapiens GN=SLC3A2 PE=2 SV=1 - [B4E2Z3_HUMAN]	22.63	22.11	3	8	8	8	catalytic activity		metabolic process	511	55.9	5.17
P14923	Junction plakoglobin OS=Homo sapiens GN=JUP PE=1 SV=3 - [PLAK_HUMAN]	19.64	12.08	1	7	7	7	protein binding; structural molecule activity	cytoplasm; cytoskeleton; cytosol; membrane; nucleus; organelle lumen	cell communication; cell differentiation; cell organization and biogenesis; cellular component movement; development; metabolic process; regulation of biological process; reproduction; response to stimulus; transport	745	81.7	6.14
P35908	Keratin, type II cytoskeletal 2 epidermal OS=Homo sapiens GN=KRT2 PE=1 SV=2 - [K22E_HUMAN]	18.56	8.61	1	3	5	6	structural molecule activity	cytoplasm; cytoskeleton; Golgi	cell differentiation; cell proliferation; cellular component movement; development	639	65.4	8.00

P35527	Keratin, type I cytoskeletal 9 OS=Homo sapiens GN=KRT9 PE=1 SV=3 - [K1C9_HUMAN]	15.00	12.36	1	6	6	6	structural molecule activity	cytoplasm; cytoskeleton	cell organization and biogenesis; development; reproduction	623	62.0	5.24
F5H365	Protein transport protein Sec23A OS=Homo sapiens GN=SEC23A PE=4 SV=1 - [F5H365_HUMAN]	12.85	7.88	2	4	4	4	metal ion binding	cytoplasm; membrane	transport	736	82.9	7.46
O95202	LETM1 and EF-hand domain-containing protein 1, mitochondrial OS=Homo sapiens GN=LETM1 PE=1 SV=1 - [LETM1_HUMAN]	12.58	7.85	1	5	5	5	metal ion binding; protein binding	cytoplasm; membrane; mitochondrion	cell organization and biogenesis	739	83.3	6.70
O43390	Heterogeneous nuclear ribonucleoprotein R OS=Homo sapiens GN=HNRNPR PE=1 SV=1 - [HNRPR_HUMAN]	11.92	9.64	1	4	4	4	nucleotide binding; protein binding; RNA binding	cytoplasm; nucleus; organelle lumen; spliceosomal complex	metabolic process	633	70.9	8.13
Q9UHD2	Serine/threonine-protein kinase TBK1 OS=Homo sapiens GN=TBK1 PE=1 SV=1 - [TBK1_HUMAN]	10.26	8.09	1	4	4	4	catalytic activity; nucleotide binding; protein binding	cytoplasm; cytosol; endosome; membrane	cell communication; defense response; metabolic process; regulation of biological process; reproduction; response to stimulus	729	83.6	6.79
Q9H9E3	Conserved oligomeric Golgi complex subunit 4 OS=Homo sapiens GN=COG4 PE=1 SV=3 - [COG4_HUMAN]	9.89	7.39	1	4	4	4	protein binding	cytoplasm; Golgi; membrane	cell organization and biogenesis; transport	785	89.0	5.19
Q6PJG6	BRCA1-associated ATM activator 1 OS=Homo sapiens GN=BRAT1 PE=1 SV=2 - [BRAT1_HUMAN]	8.77	4.26	1	3	3	3	protein binding	nucleus	response to stimulus	821	88.1	5.27
Q8N1F7	Nuclear pore complex protein Nup93 OS=Homo sapiens GN=NUP93 PE=1 SV=2 - [NUP93_HUMAN]	8.39	5.13	1	3	3	3		membrane; nucleus	cell communication; metabolic process; regulation of biological process; response to stimulus; transport	819	93.4	5.72

Q8IY67	Ribonucleoprotein PTB-binding 1 OS=Homo sapiens GN=RAVER1 PE=1 SV=1 - [RAVR1_HUMAN]	7.24	6.60	2	2	2	2	nucleotide binding; RNA binding	cytoplasm; nucleus		606	63.8	8.48
Q96T51	RUN and FYVE domain-containing protein 1 OS=Homo sapiens GN=RUFY1 PE=1 SV=2 - [RUFY1_HUMAN]	6.26	4.52	1	3	3	3	metal ion binding; protein binding	cytoplasm; endosome; membrane	transport	708	79.8	5.74
F5H6Z6	Transcription factor 12 OS=Homo sapiens GN=TCF12 PE=4 SV=1 - [F5H6Z6_HUMAN]	5.92	5.14	2	2	2	2				681	72.5	7.64
Q86U12	Full-length cDNA clone CS0CAP007YF18 of Thymus of Homo sapiens (human) OS=Homo sapiens GN=HSP90AA1 PE=2 SV=1 - [Q86U12_HUMAN]	5.63	5.57	3	2	2	2	nucleotide binding; protein binding		metabolic process; response to stimulus	413	49.3	5.41
Q9H6T0	Epithelial splicing regulatory protein 2 OS=Homo sapiens GN=ESRP2 PE=1 SV=1 - [ESRP2_HUMAN]	4.45	3.16	1	2	2	2	nucleotide binding; RNA binding	nucleus	metabolic process; regulation of biological process	727	78.4	6.71

Q92616	Translational activator GCN1 OS=Homo sapiens GN=GCN1L1 PE=1 SV=6 - [GCN1L_HUMAN]	67.93	12.21	1	22	22	24	protein binding; RNA binding	cytoplasm; ribosome	metabolic process; regulation of biological process	2671	292.6	7.47
P35658	Nuclear pore complex protein Nup214 OS=Homo sapiens GN=NUP214 PE=1 SV=2 - [NU214_HUMAN]	49.71	13.49	1	17	17	18	protein binding; transporter activity	cytoplasm; cytosol; membrane; nucleus; organelle lumen	cell communication; metabolic process; regulation of biological process; response to stimulus; transport	2090	213.5	7.47

A5YKK6	CCR4-NOT transcription complex subunit 1 OS=Homo sapiens GN=CNOT1 PE=1 SV=2 - [CNOT1_HUMAN]	46.07	8.75	1	17	17	17	protein binding	cytoplasm; cytosol; membrane	metabolic process; regulation of biological process	2376	266.8	7.11
P04264	Keratin, type II cytoskeletal 1 OS=Homo sapiens GN=KRT1 PE=1 SV=6 - [K2C1_HUMAN]	43.65	19.57	1	10	11	14	catalytic activity; motor activity; protein binding; receptor activity; structural molecule activity; transporter activity	cytoskeleton; membrane	coagulation; defense response; development; metabolic process; regulation of biological process; response to stimulus; transport	644	66.0	8.12
Q92538	Golgi-specific brefeldin A-resistance guanine nucleotide exchange factor 1 OS=Homo sapiens GN=GBF1 PE=1 SV=2 - [GBF1_HUMAN]	28.02	7.80	1	10	10	10	enzyme regulator activity	cytoplasm; Golgi; membrane	cell communication; cell organization and biogenesis; regulation of biological process; response to stimulus; transport	1859	206.3	5.73
P13645	Keratin, type I cytoskeletal 10 OS=Homo sapiens GN=KRT10 PE=1 SV=6 - [K1C10_HUMAN]	25.99	19.01	1	8	8	9	structural molecule activity	cytoplasm; cytoskeleton	cell differentiation; development; response to stimulus	584	58.8	5.21
F8VPD4	Dihydroorotase OS=Homo sapiens GN=CAD PE=3 SV=1 - [F8VPD4_HUMAN]	24.07	5.64	2	9	9	9	catalytic activity; metal ion binding; nucleotide binding		metabolic process	2162	235.9	6.55
G5E9S1	Eukaryotic translation initiation factor 4 gamma 1 OS=Homo sapiens GN=EIF4G1 PE=4 SV=1 - [G5E9S1_HUMAN]	23.83	8.76	6	8	8	8	DNA binding; enzyme regulator activity; protein binding; RNA binding	cytoplasm	metabolic process; regulation of biological process	1404	154.8	5.16
P35908	Keratin, type II cytoskeletal 2 epidermal OS=Homo sapiens GN=KRT2 PE=1 SV=2 - [K22E_HUMAN]	17.04	7.82	1	3	4	5	structural molecule activity	cytoplasm; cytoskeleton; Golgi	cell differentiation; cell proliferation; cellular component movement; development	639	65.4	8.00
C9JCN0	Myoferlin OS=Homo sapiens GN=MYOF PE=4 SV=2 - [C9JCN0_HUMAN]	11.59	3.02	3	5	5	5	protein binding	membrane		2051	233.3	6.04

Q14160	Protein scribble homolog OS=Homo sapiens GN=SCRIB PE=1 SV=4 - [SCRIB_HUMAN]	11.59	4.97	1	4	4	4	protein binding	cytoplasm; membrane	cell death; cell differentiation; cell proliferation; cellular component movement; development; metabolic process; regulation of biological process; reproduction; response to stimulus	1630	174.8	5.07

Definitions

Accession:	The unique protein assention number for the identification.
Description:	Protein Name
Score:	Sequest Score
Coverage:	Percent coverage of the protein observed.
# Proteins:	Number of proteins matching the peptides identified. These are typically isoforms etc. which are difficult to differentiate.
# Unique Peptides:	Unique peptides identified which only occur in the protein identified.
# Peptides:	All unique peptide plus peptides that may be common between two or more proteins.
# PSMs:	Peptide Spectral Matches. PSMs are roughly proportional to protein abundance. PSMs for the same protein in different samples can be used to compare changes in relative abundance.
Molecular Function:	From literature
Cellular Component:	From literature
Biological Process:	From literature
# Aas:	Number of amino acids in the intact protein (theoretical)
MW [kDa]:	Molecular Weight of the intact protein (theoretical)
calc. pI:	Calculated PI of the intact protein (theoretical)

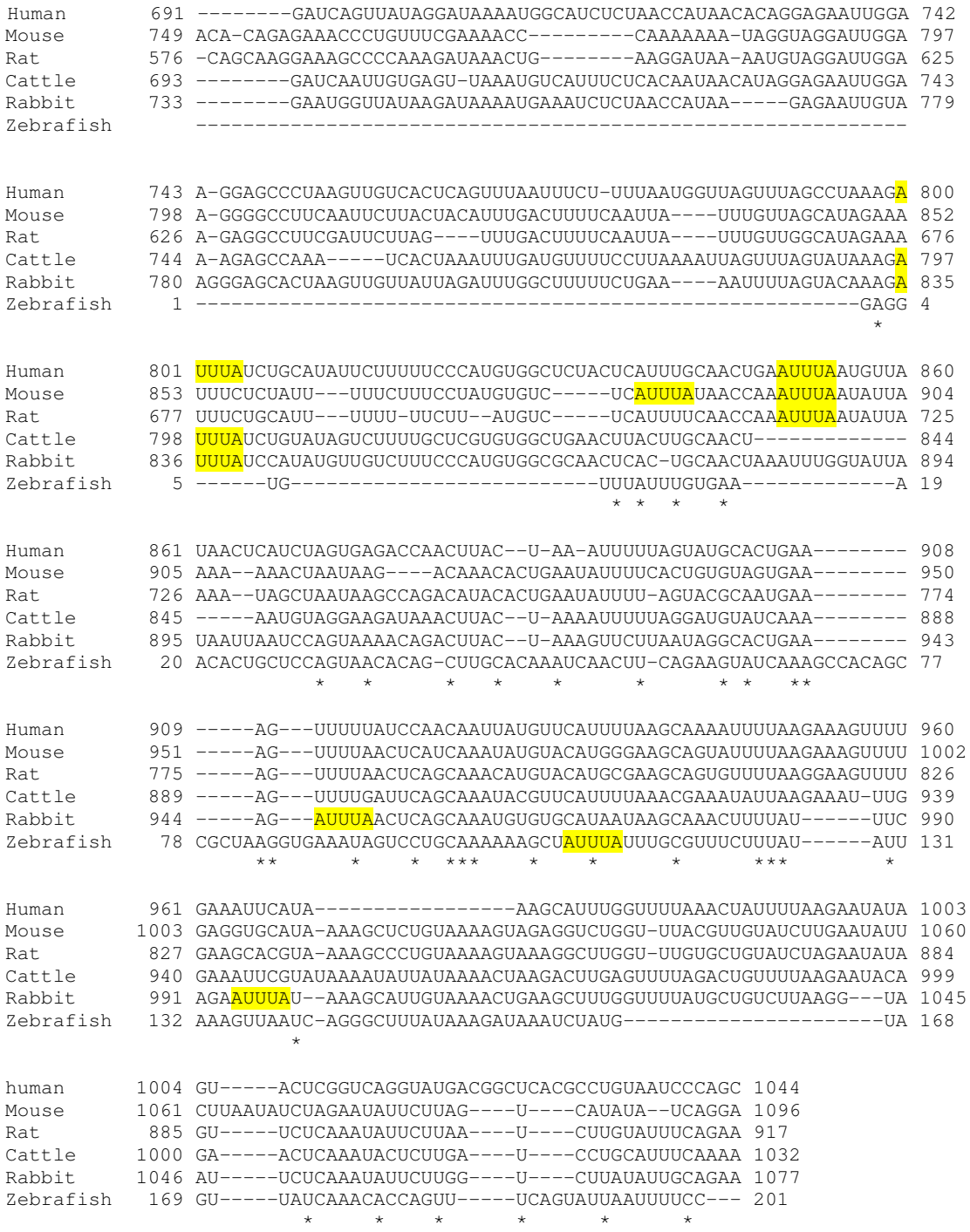

Fig. 3-S1. Sequence alignment of PKD2 mRNA 3FI from indicated species. National Center for Biotechnology Information accession number for sequences used here are NM_000297.3 (Human), NM_008861.3 (Mouse), NM_001191934.1 (Rat), NM_001046312.1 (Cattle), XM_002717010.2 (Rabbit), and NM_001002310.1 (Zebrafish). Identical residues among the species are indicated by "*" and AUUUA signature sequences were highlighted with yellow. 3FI AU contents for different species are as follows: Human, 67.5% AU with two AUUUA sequences; Mouse, 70.4% AU with two AUUUA sequences; Rat, 67.8% AU with one AUUUA

sequence; Cattle, 72.6% AU with one AUUUA sequence; Rabbit, 70% AU with three AUUUA sequences; Zebrafish, 66.2% AU with one AUUUA sequence.

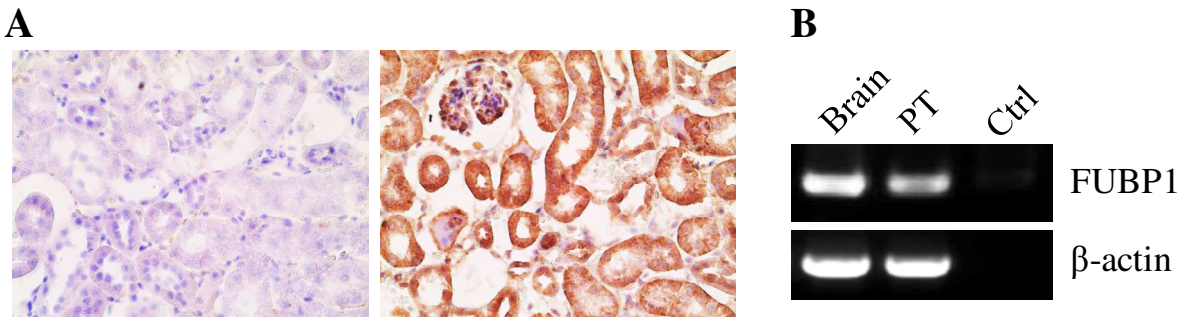

Fig. 3-S2. Expression of FUBP1 in mouse normal kidney. (**A**) immunohistochemisty shows expression of FUBP1 protein in both proximal tubules and distal tubules. *Left panel*, Ctrl; *Right panel*, FUBP1 staining with antibody from AVIVA SYSTEMS BIOLOGY (#ARP35704_P050). (**B**) RT-PCR shows expression of FUBP1 mRNA in PT (proximal tubules). The whole brain tissue was used as a positive control and "Ctrl" represents PT without reverse transcription. The FUBP1 primers used in the PCR are the same with ones in Zhang et al, *Onkologie*, 36(11): 650-5, 2013. Two round of PCR with each 25 cycles were performed for FUBP1 detection.

CHAPTER 4

RESULTS #3

A novel PKD2L1 C-terminal domain critical for trimerization and channel function

4.1 ABSTRACT

As a transient receptor potential (TRP) superfamily member, polycystic kidney disease 2-like-1 (PKD2L1) is also called TRPP3 and has similar membrane topology as voltage-gated cation channels. PKD2L1 is involved in hedgehog signaling, intestinal development, and sour tasting. PKD2L1 and PKD1L3 form heterotetramers with 3:1 stoichmiometry. C-terminal coiled-coil-2 (CC2) domain (G699-W743) of PKD2L1 was reported to be important for its trimerization but independent studies showed that CC2 does not affect PKD2L1 channel function. It thus remains unclear how PKD2L1 proteins oligomerize into a functional channel. By SDS-PAGE, blue native PAGE and mutagenesis we here identified a novel C-terminal domain called C1 (K575-T622) involved in stronger homotrimerization than the non-overlapping CC2, and found that the PKD2L1 N-terminus is critical for dimerization. By electrophysiology and *Xenopus* oocyte expression, we found that C1, but not CC2, is critical for PKD2L1 channel function. Our co-immunoprecipitation and dynamic light scattering experiments further supported involvement of C1 in trimerization. Further, C1 acted as a blocking peptide that inhibits PKD2L1 trimerization and PKD2L1 and PKD2L1/PKD1L3 channel function. Thus, our study identified C1 as the first PKD2L1 domain essential for both PKD2L1 trimerization and channel function, and suggest that PKD2L1 and PKD2L1/PKD1L3 channels share the PKD2L1 trimerization process.

4.2 INTRODUCTION

Eight members in the polycystic kidney disease (PKD) family of proteins have so far been identified: PKD1,-1L1, -1L2, -1L3, -REJ; PKD2, -2L1 and -2L2. Among them, only PKD1 and PKD2 are mutated in autosomal dominant PKD (ADPKD) [1,2]. PKD2, -2L1 and -2L2 form the transient receptor potential (TRP) polycystin (TRPP) subfamily and are called TRPP2, -3 and -5, respectively. Members of the TRP superfamily are cation channels and play critical roles in sensory physiology [3,4]. PKD2L1 and PKD2 share 50% sequence identity and 71% similarity and are predicted to have a similar membrane architecture: six transmembrane (TM) segments flanked by the intracellular amino- (N-) terminus (NT, M1-Y96) and carboxyl- (C-) terminus (CT, E566-S805), with a pore loop between TM5 and TM6. Sharing these topological features with other TRP members TRPP channels are presumably organized as homotetramers [5-7]. When over-expressed in *Xenopus* oocytes alone, PKD2L1 channel was found to traffic to the plasma membrane and be activated by Ca^{2+} and permeable to Ca^{2+} [8,9]. PKD2L1 also acts as a Ca^{2+} channel on the mammalian cell surface membrane and primary cilia where it regulates Ca^{2+} concentration and Ca^{2+}-dependent hedgehog signaling [10,11]. The same studies found that PKD2L1 knockout (KO) mice exhibit defective intestinal development. When over-expressed in human embryonic kidney (HEK) cells PKD2L1 is regulated by extracellular pH and cell swelling [12]. In addition, PKD2L1 is expressed in bipolar neurons in the tongue taste buds and neurons surrounding the central canal of spinal cord where it responds to a decrease in extracellular pH [13]. In fact, the same study found that genetic ablation of cells expressing PKD2L1 eliminates gustatory nerve response to sour stimuli in mice. The involvement of PKD2L1 in sour tasting was later confirmed using KO mouse models [14].

There are theoretically 15 possible ways of complexing between a PKD1 and PKD2 homologue, which may nicely respond to various tissue-specific needs of sensory functions and regulations. Eg, the PKD2/PKD1 and PKD2L1/PKD1L3 channel complexes were reported to sense fluid flow and acid, in primary cilia and surface membrane, respectively [15,16]. PKD1 and PKD2L1 were also reported to form a channel complex when co-expressed in HEK cells, but the physiological role has remained unknown [17]. At least when co-expressed in HEK cells, PKD2L1 also interacts with PKD1L3 such that both efficiently traffic to the surface membrane where they act as an extracellular acid-induced off-response cation channel, ie, activation occurred only after low extracellular pH was removed [15,18]. Further, they are co-expressed in mouse circumvallate and foliate papillae although only PKD2L1 is found in other taste bud areas, including fungiform and palate taste buds [15,18]. These *in vitro* and *in vivo* data suggest that PKD2L1 and PKD1L3 are synergistically involved in acid sensing pathways. However, unlike PKD2L1 KO mice, PKD1L3 KO mice were not found to have defects in sour tasting [19], arguing against the assumption that they are in the same pathway in the tongue. In primary cilia PKD2L1 and PKD1L1 form a Ca^{2+} channel that regulates the ciliary Ca^{2+} concentration and Ca^{2+}-dependent hedgehog signaling pathway, which seems to be developmentally important [10,11]. In these studies, PKD1L1 was found to regulate the single-channel conductance of PKD2L1. However, it remains to be determined whether PKD1L1 KO mice also display similar developmental defects as those observed in PKD2L1 KO mice. Optimistically, more diverse functions and regulations associated with pairs of PKD proteins will be discovered in near future.

How does a PKD2 homologue complex with a PKD1 homologue? Studies using mammalian cell and *Xenopus* oocyte expression showed that both the PKD2/PKD1 and PKD2L1/PKD1L3 complexes form heterotetramers with 3:1 stoichiometry, ie, one PKD2 (or

PKD2L1) trimer paired with one PKD1 (or PKD1L3) monomer [20,21]. Although no corresponding information for PKD2L1/PKD1 and PKD2L1/PKD1L1 is available it is reasonable to speculate that they are also organized with the same stoichiometry. The PKD2L1 C-terminal coiled-coil 2 domain (CC2, G699-W743) was found to homotrimerize *in vitro* and be important for PKD2L1 homomeric assembly and PKD2L1/PKD1L3 surface expression in *Xenopus* oocytes [21-23]. However, a previous study found that PKD2L1 truncation mutants lacking CC2 possess similar Ca^{2+}-activated channel function as wild-type (WT) PKD2L1 and that PKD2L1 and PKD1L3 interact with each other through their TMs, which is required for PKD2L1/PKD1L3 surface expression in HEK cells [24]. This study also showed that cells still respond to 25 mM citric acid solution when co-expressed full-length PKD1L3 with PKD2L1 truncation mutant lacking either CC2 (PKD2L1ΔCC, M1-E653) or both CC2 and the EF-hand domain (PKD2L1ΔEF-CC, M1-F621), but little response was observed with PKD2L1 truncation mutant lacking the entire C-terminus (PKD2L1ΔCT, M1-I560), despite robust cell surface expression. This suggests the importance of a domain within I560-F621 for channel function [25].

Based on the tetrameric assembly of PKD2 [26,27] and other TRP channels [5-7] it is likely that PKD2L1 also possesses tetrameric organization. It may be speculated that a TRP homotetrameric channel is formed through dimerization of two homodimers. If such speculation would be true for PKD2L1, then it should possess two distinct domains, for dimerization of two monomers and of two homodimers, respectively, and these domains should also be distinct from a trimerization domain, eg, CC2. Unfortunately, it has so far remained unknown as to which PKD2L1 domains are critical for both its homomerization and channel function. In the present study, through the use of mutagenesis, non-reducing SDS-PAGE, blue native PAGE (BN-PAGE) and electrophysiology, among others, we discovered that a novel C-terminal domain called C1

(K575-T622) is essential for both homotrimerization and channel function, challenging the speculation that a functional homotetrameric TRP channel is formed through two consecutive steps of homodimerization.

4.3 METHODS

Plasmids construction

Human full-length PKD2L1 cDNA was amplified from pCHGF [9] by PCR and subcloned into pcDNA3.1(+) and pEGFP-C2 for mammalian cell expression. Flag tag was inserted 5' of the PKD2L1 coding region in pcDNA3.1 (+). Mouse PKD1L3 plasmid was a kind gift of Dr. H. Matsunami from Duke University. All mutations were made with QuikChange Lightning Site-Directed Mutagenesis kit (Agilent Technologies, La Jolla, CA) and confirmed by sequencing.

Cell culture and transfection

HeLa and HEK cells were cultured in Dulbecco's modified Eagle's medium supplemented with 10% fetal bovine serum (FBS) and 1% penicillin/streptomycin (Sigma, St. Louis, MO). Cells of less than 25 passages were cultured to full confluence before collection. Transient transfection was performed on cells cultured to 70%-90% confluence using Lipofectamine 2000 (Invitrogen, Carlsbad, CA) according to the manufacturer's instruction.

Westing blot (WB)

Protein samples were separated on 8% SDS-PAGE gels. For the non-reducing SDS-PAGE, samples were mixed with SDS loading buffer without reducing reagents and kept on ice for 5 minutes (min) prior to electrophoresis. For the reducing SDS-PAGE, samples were mixed with loading buffer supplemented with 0.5 M DTT or 5% 2-mercaptoethanol (2-ME), and subject to heating at 65^{o}C for 5 min. 30 μg of total protein was loaded per lane. Flag and GFP (B-2) antibodies were purchased from Santa Cruz Biotechnology (Santa Cruz, CA). PKD2L1 antibody (H00009033) was purchased from Abnova (Taipei, Taiwan) for tissue detection. Rabbit antibody

against PKD2L1 (PR71) was custom made and used previously [28]. Secondary antibodies were purchased from GE Healthcare (Baie d'Urfe, QC, Canada). Band intensity was analyzed with the software ImageJ (NIH, Bethesda, MD).

Blue native-PAGE (BN-PAGE)

HeLa cell lysates for BN-PAGE were prepared with NativePAGE Sample Prep Kit (Invitrogen) according to the manufacturer's protocol. Coomassie blue G-250 was added to supernatants at 8:1 detergent:G-250 ratio. Protein complexes were separated at 150 V for 90 min using NativePAGE Novex 3-12% BisTris gels (Invitrogen). For immunoblotting, gel was incubated in 20 mM Tris-HCl (pH 8.3), 0.15 M glycine, and 0.02% SDS for 5 min at room temperature. Proteins were then transferred to polyvinylidene difluoride membranes (at 150 mA for 90 min and 4˚C). Membranes were blocked with 3% skimmed milk in PBS buffer with 0.1% tween-20 for 40 min at room temperature and then incubated with antibodies.

Dot blot

Lysates of *Xenopus* oocytes were spotted onto a nitrocellulose membrane and then let the membrane dry. Glutaraldehyde fixation was applied as previously described [29] to enhance the retention of short peptides on the membrane. Briefly, membrane was immersed in PBS containing 0.5% (v/v) glutaraldehyde for 5 min and moved to a fresh PBS/glutaraldehyde solution for 10 min, followed by placement in PBS containing 50 mM glycine to stop cross-linking reaction. Membrane was then washed once with PBS buffer and subjected to normal WB procedure.

Immunofluorescence

Xenopus oocytes were washed in PBS, fixed in 3% paraformaldehyde for 15 min, washed 3 times in PBS plus 50 mM NH_4Cl, and then permeabilized with 0.1% Triton X-100 for 4 min. Oocytes were then washed 3 times in PBS for 5 min each time, blocked in 3% skim milk in PBS for 30 min, and then incubated overnight with the rabbit anti-PKD2L1 polyclonal antibody (cat# PAB5914, Abnova). This was followed by 3 times 10-min washes in PBS. Oocytes were then incubated with a secondary AlexaFluor 488-conjugated donkey anti-rabbit antibody (Jackson ImmunoResearch Laboratories, West Grove, PA) for 30 min, followed by 3-time washes in PBS and mounting in Vectashield (Vector Labs, Burlington, ON). The slides were examined on an AIVI spinning disc confocal microscopy (Cell Imaging Facility, Faculty of Medicine and Dentistry, University of Alberta). Plasma membrane intensity of WT or mutant PKD2L1 was assessed by quantifying the plasma membrane immunofluorescence using Volocity 6.2 (Perkin Elmer, Waltham, MA). Background fluorescence was subtracted and data were normalized to the average PKD2L1 WT intensity.

Co-immunoprecipitation (Co-IP)

Co-IP was performed using lysates of HeLa cells over-expressing GFP-PKD2L1 and Flag-tagged mutant PKD2L1 constructs. HeLa cell monolayer in 100-mm dishes was washed twice with PBS and solubilized in ice-cold CellLytic-M lysis buffer supplemented with proteinase inhibitor mixture (Sigma). Supernatants were collected following centrifugation at 16,000 × *g* for 15 min. Equal amounts of total proteins from postnuclear supernatants were pre-cleared for 1 hour (hr) with protein G-Sepharose (GE Healthcare), and then incubated for 4 hr at 4^{o}C with the

antibody against GFP. After the addition of 100 µl of 50% protein G-Sepharose, the mixture was incubated overnight with gentle shaking at 4°C. The immune complexes absorbed to protein G-Sepharose were washed five times with Nonidet P-40 lysis buffer (50 mM Tris, pH 7.5, 150 mM NaCl, 1% Nonidet P-40) with proteinase inhibitor and eluted by SDS loading buffer. Precipitated proteins were analyzed by WB using the antibodies against Flag or GFP.

Protein expression in and purification from *E. coli*

DNA fragment encoding C1 was inserted into pET28a(+) that contains upstream GFP gene. BL21 (DE3) strain (Novagen, Darmstadt, Germany) was used for expression. Following growth at 37˚C to an optical density (OD) of 0.6, cultures were cooled to 30˚C, induced with 1 mM isopropyl β-D-thiogalactoside and incubated for 6 hr. Cell lysates from 50 mL culture were prepared with CellLytic-B lysis buffer (Sigma) according to the manufacturer's instruction. Proteins were pulled down with Ni-NTA resin (Qiagen, Venlo, Netherlands) and eluted from beads with 250 mM imidazole by following the manufacturer's manual.

Preparation of mRNAs and microinjection into oocytes

Capped mRNAs of WT or mutant PKD2L1 were synthesized by *in vitro* transcription from a linearized template in the pCHGF vector using the mMESSAGE mMACHINE1 kit (Ambion, Austin, TX). Stage V-VI oocytes were isolated from *Xenopus laevis*. Defolliculation of oocytes was performed through incubation in Ca^{2+}-free Barth's solution [24] containing collagenase (2 mg/ml) at RT for 2-2.5 hr. Oocytes were then incubated at 18˚C in the Barth's solution for at least 3 hr before injection of 50 nl RNase-free water containing 50 ng mRNAs. An equal volume of water was injected into each control oocyte. The present study was approved by the Ethical

Committee for Animal Experiments of the University of Alberta, and was carried out in accordance with the Guidelines for Research with Experimental Animals of the University of Alberta and the Guide for the Care and Use of Laboratory Animals (NIH Guide) revised in 1996. Injected oocytes were incubated at 16-18˚C in the Barth's solution supplemented with antibiotics for 2-4 days prior to experiments.

Two-microelectrode voltage clamp

Two-microelectrode voltage clamp experiments were performed as described before [9]. Briefly, the two electrodes (Capillary pipettes, Warner Instruments, Hamden, CT) impaling oocytes were filled with 3 M KCl to form a tip resistance of 0.3-2 MΩ. The standard extracellular solution (pH 7.5) containing 100 mM NaCl, 2 mM KCl, 1 mM $MgCl_2$ and 10 mM HEPES was used. The solution containing extracellular Ca^{2+} was prepared from the standard solution with the addition of $CaCl_2$ to a final concentration of 5 mM. Duration of application of Ca^{2+} medium was indicated in time course recordings. Oocyte whole-cell currents were recorded using a Geneclamp 500B amplifier and Digidata 1322A AD/DA converter (Molecular Devices, Union City, CA). The pClamp 9 software (Axon Instruments, Union City, CA) was applied for data acquisition and analysis. Currents and voltages were digitally recorded at 200 μs/sample and filtered at 2 kHz through a Bessel filter. SigmaPlot 12 (Systat Software, San Jose, CA) was used for data fitting and plotting.

Dynamic light scattering (DLS)

DLS experiments were performed using a Malvern Zetasizer Nano ZS instrument (Malvern, Worcestershire, UK) at 25˚C, as described previously [30]. Freshly purified PKD2L1 CT and

deletion mutants from *E. coli* in a solution containing 50 mM NaH_2PO4, 300 mM NaCl and 250 mM imidazole, pH 8.0 were passed through a 0.22 μm filter to remove large particles or aggregates and diluted to 0.4 mg/ml before measurements. Correlation data obtained with DynaLS software (Malvern) were fitted using SigmaPlot 12 (Systat Software) to derive the average apparent hydrodynamic diameter.

Statistic analysis

Data were analyzed and plotted using SigmaPlot 12 (Systat Software), and expressed as mean ± SEM (N), where SEM stands for the standard error of the mean and N indicates the number of experimental repeats. Paired or unpaired Student t-test was used to compare two sets of data. A probability value (P) of less than 0.05, 0.01 and 0.001 was considered statistically significant and indicated by "*", "**" and "***", respectively.

4.4 RESULTS

Oligomeric state of PKD2L1 in mouse tissues and human cells

Previous studies on PKD2L1 oligomerization were limited to *in vitro* conditions, including trimerization of its purified C-terminus or of the full-length protein over-expressed in *Xenopus* oocytes [21-23]. In order to determine the oligomeric states of PKD2L1 under more *in vivo* and physiological conditions, we performed Western Blot (WB) experiments using mouse tissues under the non-reducing and reducing conditions (see EXPERIMENTAL PROCEDURES). We found that in the kidney, testis and brain under the non-reducing condition, endogenous PKD2L1 displays similar oligomeric patterns from which the band sizes suggest the presence of either PKD2L1 homodimers, -trimers and –tetramers, or its heteromerization with endogenous interacting partner proteins (Fig. 4-1A). These oligomer bands disappeared in the presence of the reducing condition. To provide further documentations regarding whether these bands correspond to PKD2L1 homo- or heterooligomers we over-expressed human PKD2L1 in HEK (HEK293T) and HeLa cells in which partners of PKD2L1 were assumed to have little influence due to their absence or relatively low expression levels. In both HEK and HeLa cells under the non-reducing condition, we still detected four bands (Fig. 4-1B and C) that were comparable to the patterns obtained using mouse tissues. We thus tentatively assigned them as monomer, dimer, trimer and tetramer. Interestingly, under the reducing condition, a significant portion of trimers remained while all tetramers and the majority of dimers were absent. These data indicated that the oligomerization strength follows an order of trimer >> dimer > tetramer, consistent with a previous finding that the PKD2L1 CT forms very stable trimers *in vitro* [22,23].

Because oligomerization may occur through a disulfide bond between two cysteine residues during lysate preparations or SDS-PAGE under denaturing conditions, and there are

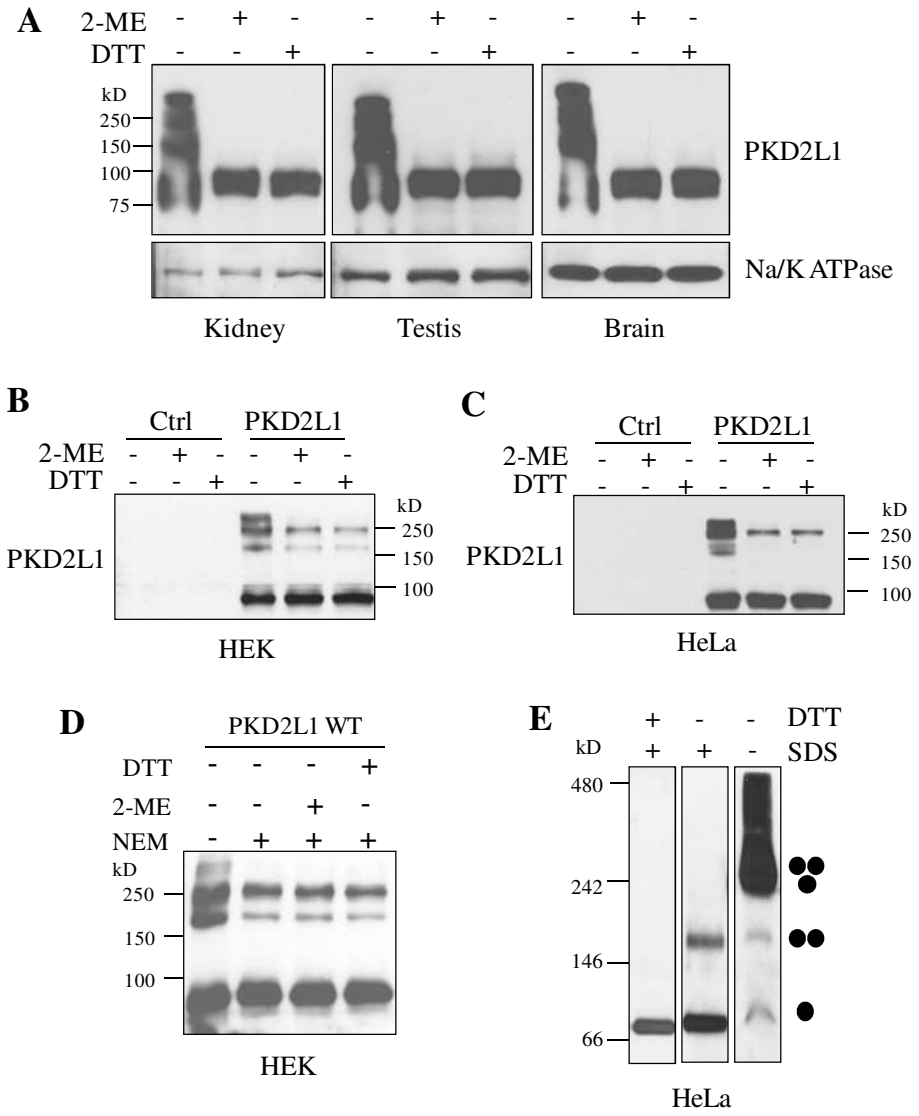

Fig. 4-1. Oligomers of PKD2L1 in mouse tissues and human cell lines. (**A**) Detection of PKD2L1 in mouse kidney, testis, and brain tissues by WB. Samples were prepared with SDS loading buffer under the non-reducing and reducing (supplemented with 5% 2-ME or 0.5 M DTT) conditions. PKD2L1 was detected with an antibody from Abnova. Na/K ATPase was used as a loading control. Detection of over-expressed human PKD2L1 in HEK (**B**) and HeLa cells (**C**). pcDNA3.1(+) containing human PKD2L1 or empty vector (Ctrl) was transfected into HEK and HeLa cells. Cell lysates were collected 48 hr after transfection. Samples for SDS-PAGE were prepared under non-reducing or reducing condition. (**D**) Detection of over-expressed human PKD2L1 in HEK cells under non-reducing and reducing conditions. Samples were prepared with or without treatment by 10 mM NEM. (**E**) WB analysis after BN-PAGE of Flag-tagged PKD2L1 in HeLa cells. Samples were prepared with or without 2.5% SDS, or with 2.5% SDS plus 0.1 M DTT. An anti-Flag antibody was used for WB detection. Putative PKD2L1 monomer, dimer and trimer are indicated.

residues under oxidative conditions account for the observed oligomers. For this we included 10

mM N-ethylmaleinide (NEM) in cell lysis buffer to inhibit disulfide bond formation by modifying free cysteine residues. We found that the amount of oligomers decreases with the NEM treatment in HEK cells but does not further decrease with additional reducing agents, indicating that the observed oligomers in Fig. 4-1B and C are partially due to disulfide bond formation during sample preparations and/or electrophoresis, and that the oligomers detected in the presence of the NEM treatment are formed through peptide-peptide interactions.

We also employed BN-PAGE to check PKD2L1 oligomeric state under the non-denaturing condition. No disulfide bonds would be formed during sample preparation and/or electrophoresis with BN-PAGE. Our data indicated that PKD2L1 is mainly present as homotrimers, and possibly also as homotetramers or hetero-oligomers with its partner proteins, while monomers and dimers are still detectable under this condition (Fig. 4-1E). Only monomers were observed in the presence of SDS and dithiothreitol (DTT), while dimers were detectable if only SDS was applied (Fig. 4-1E). Previous studies showed that peptide-peptide interaction mediated oligomers of some membrane proteins, especially multiple-transmembrane proteins, can also be detected with non-reducing SDS-PAGE under denaturing conditions [31-33] because SDS as a detergent may form micelles, similar to lipid vesicles, at certain concentrations to hold denatured oligomers by binding to hydrophobic transmembrane domains rather to disrupting them into monomers [34]. However, since there is no SDS in the gel or running buffer on BN-PAGE compared with SDS-PAGE, these oligomers/SDS micelle complexes may be dissociated once the samples are loaded into the gel. That may be the reason why no trimers were detected on BN-PAGE with SDS while trimers can still be observed on non-reducing SDS-PAGE. Taken together, our data using over-expressed PKD2L1 together with our *in vivo* data using mouse tissues strongly indicated that PKD2L1 forms homodimers, -trimers and -tetramers.

Effects of intracellular N- and C-termini of PKD2L1 on its channel function and homomerization

PKD2L1 was first found to act as a Ca^{2+}-activated non-selective cation channel when over-expressed in *Xenopus* oocytes in which PKD2L1 traffics to the plasma membrane [8,9]. Previous studies demonstrated that the PKD2L1 C-terminal domain CC2 formed a trimer *in vitro* [22,23] but truncation mutant channels T622X and V670X that do not contain CC2 are still functional [24], indicating that CC2 is not important for PKD2L1 channel function. On the other hand, mutant PKD2L1 lacking CT is still able to oligomerize [25], indicating that a domain outside CT mediates the oligomerization. In an effort to identify domain(s) that are important for both PKD2L1 homomerization and channel function we first set to examine the effects of the PKD2L1 CT and NT on its channel function. For this we over-expressed PKD2L1 truncation mutant with deletion of CT (named ΔCT) or NT (named ΔNT) in *Xenopus* oocytes, and measured Ca^{2+}-induced channel activation currents with the two-microelectrode voltage clamp. We found that both the ΔCT and ΔNT mutants are functionally dead although they continue to traffic to the plasma membrane (Fig. 4-2A-E), which is consistent with previous findings that PKD1L3/PKD2L1 ΔCT or PKD1L3/PKD2L1 ΔNT complex shows no response to 25 mM citric acid [25].

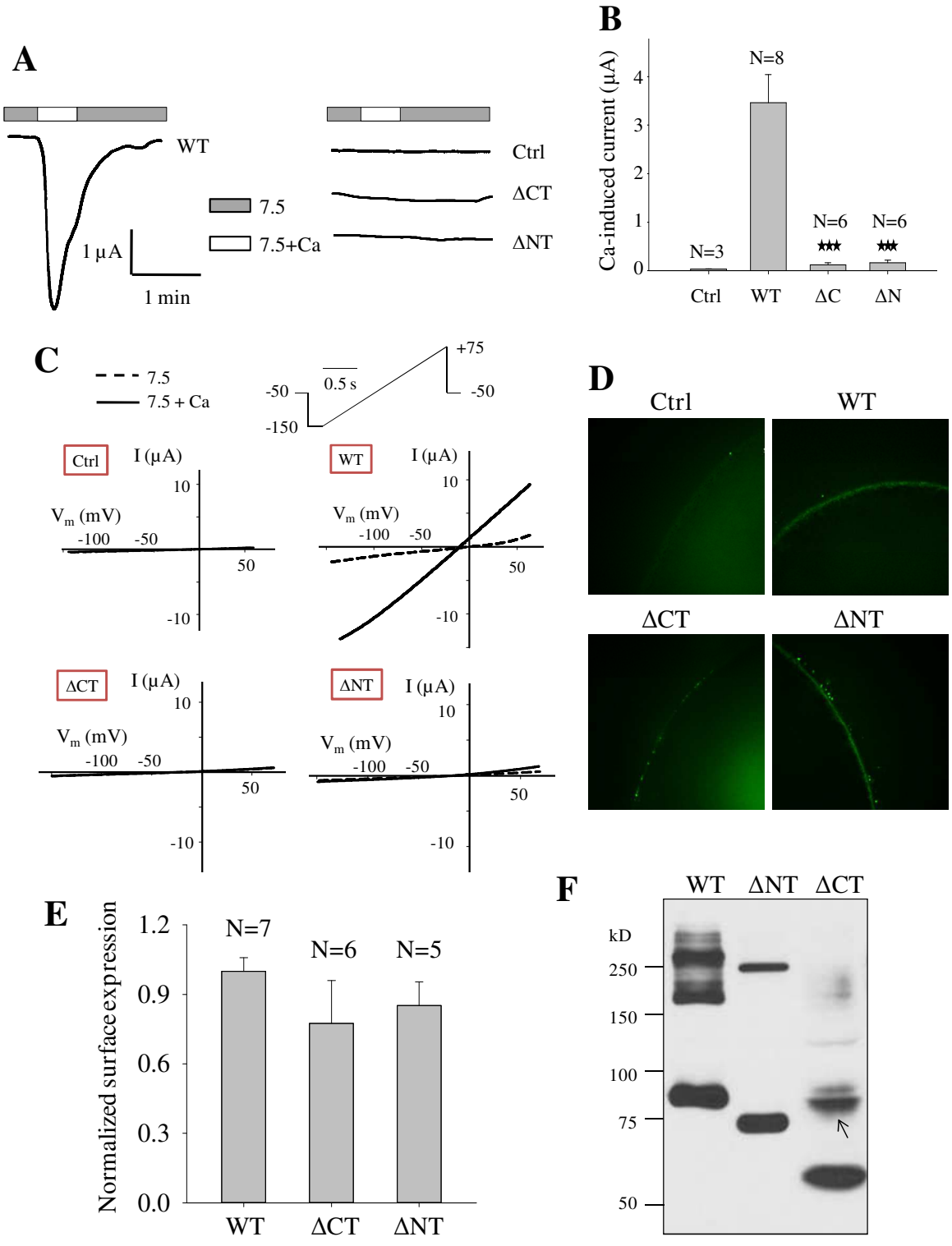

Fig. 4-2. Roles of the human PKD2L1 N- and C-termini in its channel activity and oligomerization. (**A**) Representative whole-cell current tracings obtained from using *Xenopus* oocytes expressing PKD2L1 WT, mutant ΔCT (deletion of E566-S805) or ΔNT (deletion of M1-Y96) using the two-microelectrode voltage clamp technique. Oocytes were voltage clamped at -

50 mV. Data from a water-injected oocyte served as a negative control (Ctrl). Currents were measured using standard extracellular solution (pH 7.5) (7.5) or standard extracellular solution containing 5 mM $CaCl_2$ (7.5+Ca). (**B**) Averaged currents obtained from oocytes expressing PKD2L1 WT, ΔCT, ΔNT or water (Ctrl). Currents were averaged from different numbers of oocytes, as indicated. '***' indicates $p \leq 0.001$ when compared with the WT data. (**C**) Representative current–voltage relationship curves obtained using a voltage ramp protocol, as indicated, before (7.5) and after (7.5+Ca) addition of 5 mM $CaCl_2$. (**D**) Representative immunofluorescence data showing the plasma membrane expression of PKD2L1 WT, ΔCT and ΔNT in oocytes. (**E**) Averaged and normalized surface expression of PKD2L1 WT, ΔCT and ΔNT in oocytes. Surface expressions were averaged from indicated numbers of oocytes and normalized to that of PKD2L1 WT. (**F**) WB detection of Flag-tagged human PKD2L1 WT, ΔNT and ΔCT over-expressed in HeLa cells under the non-reducing condition. A band (indicated by an arrow) that is unlikely a dimer based on its size remained unaccounted for was detected with the CT deletion.

We next wanted to determine whether NT is important for oligomerization using HeLa cells. Absence of NT in mutant ΔNT abolished the oligomers except trimers with both SDS-PAGE (Fig. 4-2F) and BN-PAGE (Fig. 4-3B), suggesting that NT mediates homodimerization. Interestingly, deletion of CT resulted in loss of all trimers and most of dimers (Fig. 4-2F), suggesting the possibility that the dimerization is dependent, at least in part, on trimerization. Because we showed that part of dimmers were due to disulfide bonds formation during lysate preparations or SDS-PAGE under denaturing conditions (Fig. 4-1D), and there are four cysteine residues in NT, we wondered whether disulfide bonds formed by these residues under oxidative conditions account for the observed dimerization. For this we mutated one or more of these cysteine residues to alanine and found that mutation C38A, but not any of the other three mutations (C60A, C70A and C74A), substantially reduces the dimer band (Fig. 4-3A). Further, inclusion of NEM in cell lysis buffer exhibited a similar effect (Fig. 4-3A), which was confirmed with BN-PAGE (Fig. 4-3B). These data together showed that part of the dimer band observed under SDS-PAGE attributes to the disulfide bond formed between two C38 residues during the

denaturing step and indicated that the rest of the dimer band is due to specific dimerization of NT *in vivo*.

To gain insights into domains responsible for trimerization without 'contamination' of di- and tetramerization we thus utilized the Flag-tagged ΔNT mutant to construct plasmids with deletion of C-terminal fragments. We found that while the mutant with T622X truncation from ΔNT (named ΔNT/T622X) still forms trimers, the mutant with the entire CT deleted from ΔNT (named ΔNT/ΔCT) has no trimer (Fig. 4-3D). Since no cysteine residue is present in the CT, the observed trimer band likely corresponds to the specific trimierzation of PKD2L1 *in vivo*. Because domain CC2 is absent in these mutants, and ΔCT and T622X are dead (Fig. 4-2B) and functional [24] mutants, respectively, our data indicated that the C-terminal fragment E566-T622 contains a novel domain that is critical for both PKD2L1 trimerization and channel function.

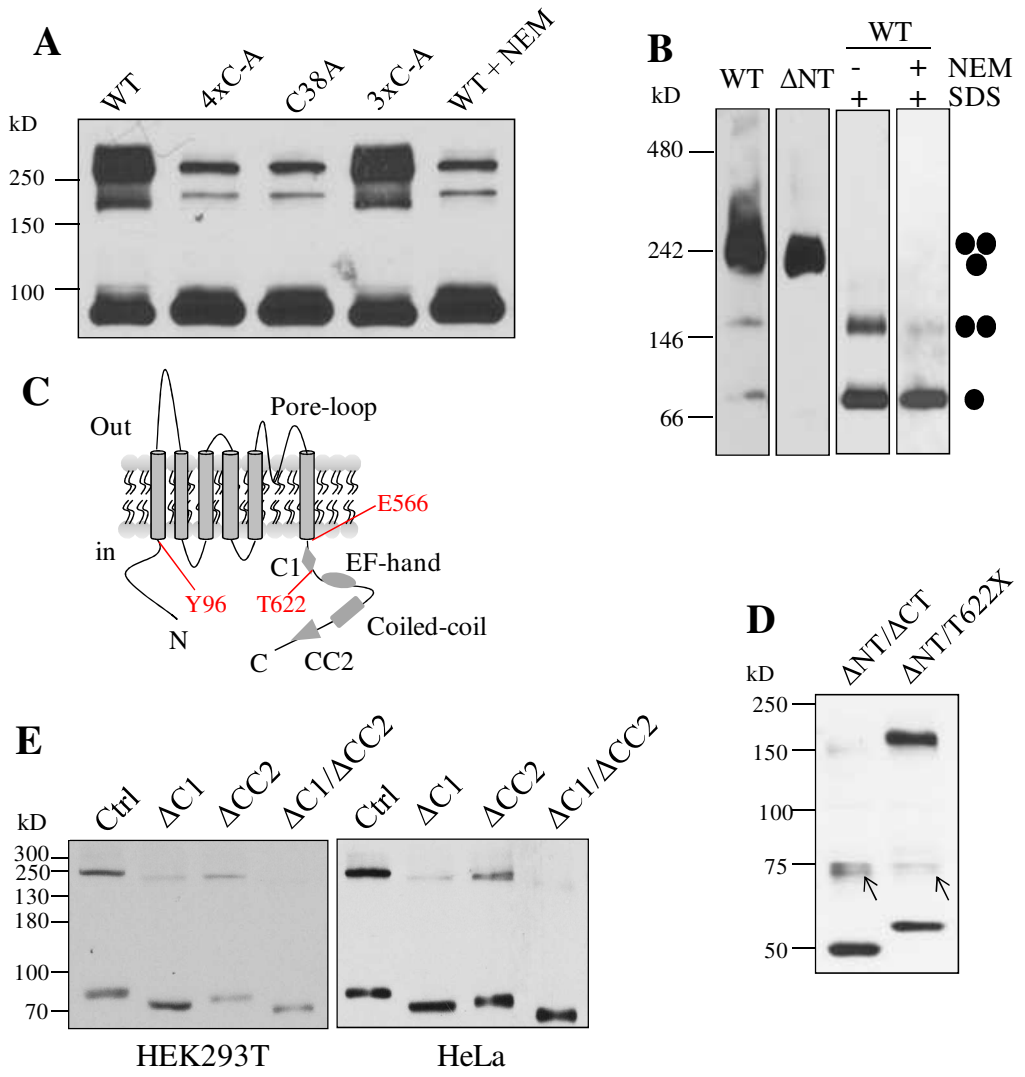

F

```
Human      575 KDELQLSDLLKQGYNKTLLRLRLRKERVSDVQKVLQGGEQEIQFEDFT 622
Mouse      575 KDQLQLSDFLKQSYNKTLLRLRLRKERVSDVQKVLKGGEPEIQFEDFT 622
Chicken    595 KDELQLSDILKQSYNRTLMRLKLKKEQISDVQKALQNGTKELGFEDFK 643
Dog        893 KDELQLSDLLKQGYNKTLLRLRLRKERVSDVQKVLQGGEQEIQFEDFT 940
Cattle     575 KDELQLSDLLRQGYNKTLRRLHLRKEQVSDVQKVLQAGEQEIQFEDFT 622
Chimpanzee 575 KDELQLSDLLRQGYNKTLLRLRLRKERVSDVQKVLQGGEQEIQFEDFT 622
```

Fig. 4-3. Identification of domain C1 of PKD2L1 critical for its trimerization. (**A**) WB detection of over-expressed Flag-tagged PKD2L1 WT, without or with 10 mM NEM treatment, or mutants 4xC-A (quadruple C38A, C60A, C70A and C74A mutations), C38A and 3xC-A (triple C60A, C70A and C74A mutations) under non-reducing condition. (**B**) WB analysis after BN-PAGE of Flag-tagged PKD2L1 WT and ΔNT over-expressed in HeLa cells. WT samples were prepared with or without 2.5% SDS, or with 2.5% SDS plus 10 mM NEM. Putative

PKD2L1 monomer, dimer and trimer are indicated. (**C**) Schematic illustration of PKD2L1 membrane topology. TMs, pore-loop, C1, CC2, EF-hand, coil-coiled domains, and positions of residues Y96, E566 and T622 are indicated. (**D**) WB detection of Flag-tagged PKD2L1 mutants ΔNT/ΔCT (M1-Y96 and E566-S805 double deletion) and ΔNT/T622X (M1-Y96 and T622-S805 double deletion) over-expressed in HeLa cells under the non-reducing condition. Two unknown bands similar to one in panel C remained unaccounted for. (**E**) WB detection of over-expressed Flag-tagged PKD2L1 mutants in HEK or HeLa cells. All constructs were made from ΔNT. These included Ctrl (ΔNT), ΔC1 (C1, K575-T622, deletion from ΔNT), ΔCC2 (CC2, G699-W743, deletion from ΔNT), or ΔC1/ΔCC2 (C1 and CC2 double deletion from ΔN). (**F**) Amino acid sequence alignment of human PKD2L1 C1 from indicated species. National Center for Biotechnology Information accession number for sequences used here are NP_057196 (human), NP_852087 (mouse), XP_426509 (chicken), XP_005637930 (dog), XP_002698535 (cattle), and XP_001168415 (chimpanzee). Identical residues among the species are indicated by black bold letters.

Identification of a C-terminal domain critical for both PKD2L1 homotrimerization and channel function

For WT or a mutant PKD2L1 channel to be functional it is necessary that they are in a correct oligomeric state. In an effort to identify a PKD2L1 domain that is essential for both trimerization and channel function we first made two deletion mutants with C1 or CC2 deleted from truncation mutant Flag-ΔNT (see Fig. 4-3A for a schematic illustration of the C1 and CC2 positions in CT), and performed WB experiments under the non-reducing condition. We found that while CC2 deletion significantly reduces the trimerization C1 deletion has more substantial effect (Fig. 4-3E). Consistently, double deletion of C1 and CC2 completely abolished the trimer band. These data indicated that there exist two domains, C1 and CC2 [22,23] in CT , that are essential for trimerization. Human PKD2L1 C1 is a 48-amino-acid peptide containing 16 highly hydrophobic residues and 7 and 8 negatively and positively charged residues, respectively. Sequence alignment showed that C1 is the most conserved part in CT and shares overall 62.5% identity among different species (Fig. 4-3F), suggesting its importance in the PKD2L1 assembly

and/or function. We next performed electrophysiology experiments using various C-terminal deletion and truncation mutations from WT PKD2L1. We found that any domain after T622 is not important for the channel function, as supported by functional mutant V670X and T622X channels. In contrast, truncation mutant S581X and the mutant with C1 deletion did not exhibit channel function (Fig. 4-4A-C). Our immunofluorescence data indicated that all these mutants target to the plasma membrane (Fig. 4-4D and E). These data together demonstrated that C1, but not CC2, is critical for PKD2L1 channel function. Thus, we have discovered for the first time a domain in PKD2L1, C1, that is essential for both homotrimerization and channel function. Interestingly, Ishimaru et al also found that PKD1L3/PKD2L1 M1-F621 responds to citric acid while PKD1L3/PKD2L1 M1-I560 shows no response, suggesting that domain C1 is also important for PKD1L3/PKD2L1 complex off-response channel function [25].

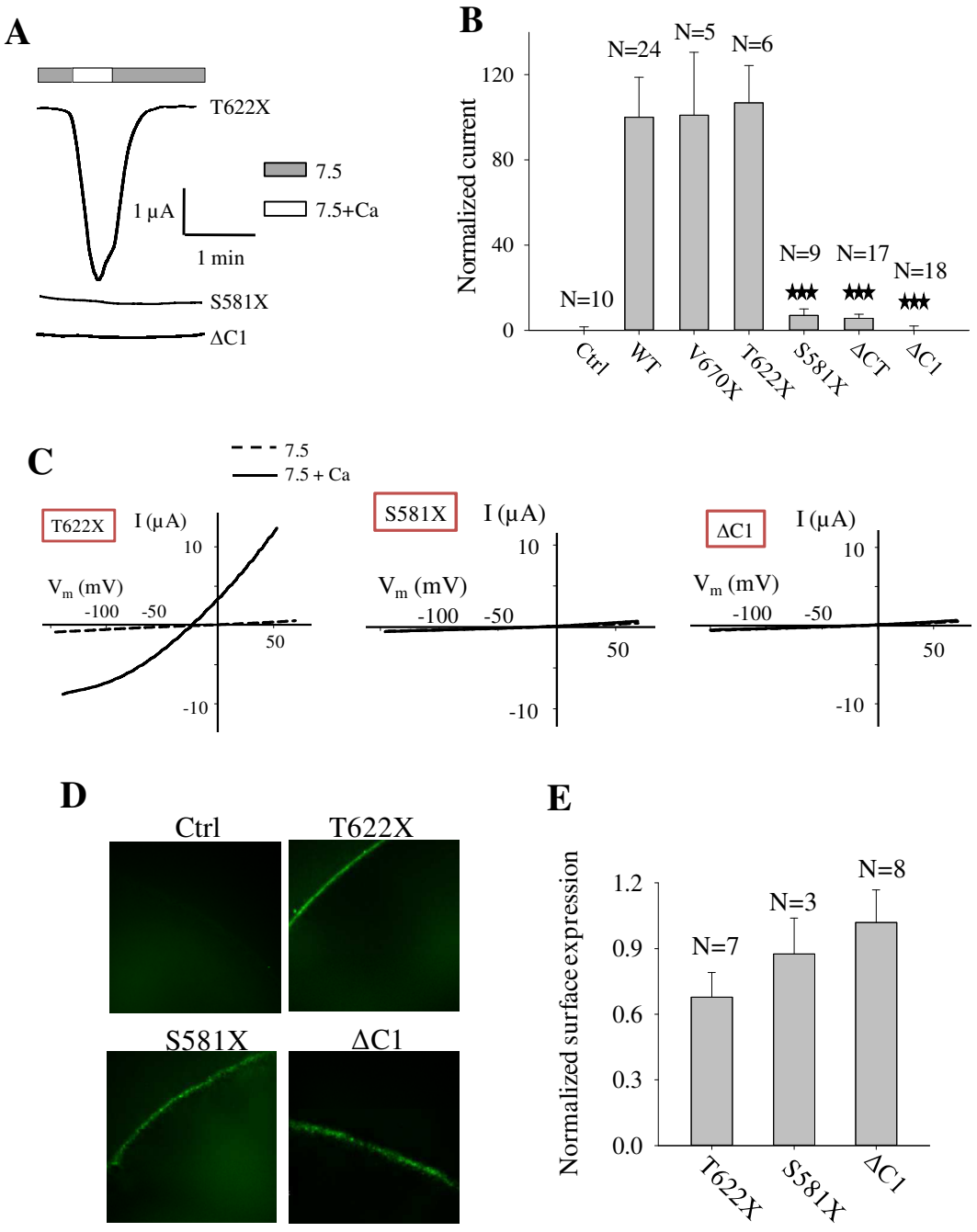

Fig. 4-4. Identification of domain C1 of PKD2L1 critical for its channel function. (A) Representative whole-cell current tracings obtained from *Xenopus* oocytes expressing PKD2L1 truncation mutant T622X, S581X, or deletion mutant ΔC1 (C1 deletion from PKD2L1 WT) using the two-microelectrode voltage clamp technique under similar experimental conditions as those for Fig. 4-2. (**B**) Averaged currents obtained from oocytes expressing PKD2L1 WT or truncation/deletion mutants, as indicated. Currents at -50 mV were averaged from indicated numbers of oocytes and normalized to that of PKD2L1 WT. Water-injected oocytes were used as control (Ctrl). '***' indicates $P \leq 0.001$ when comparing with "WT". (**C**) Representative current–

voltage relationship curves obtained using a voltage ramp protocol, as indicated in Fig. 4-2C, before (7.5) and after (7.5+Ca) addition of 5 mM $CaCl_2$. (**D**) Representative immunofluorescence data showing the plasma membrane expression of mutants T622X, S581X and ΔC1 expressed in oocytes, or those injected with water (Ctrl). (**E**) Surface membrane expression of mutants T622X, S581X and ΔC1 were averaged from the indicated numbers of oocytes and normalized to that of PKD2L1 WT.

Further characterization of C1-involved trimerization

To provide further documentations on the involvement of C1 in trimerization we first employed co-immunoprecipitation (co-IP) assays to determine the effect of C1 on the interaction between two differently tagged WT or mutant PKD2L1 proteins. To enhance the co-expression efficiency, we transfected HeLa cells with GFP-WT first and 12 hr later with Flag-T622X or -K575X. We collected cell lysates 30 hr after the second transfection. We found that the strength of the interaction of WT with K575X (that lacks C1), assessed by the immunoblotting band after normalization by input bands, is 36.5 ± 6.8% (N = 3, P < 0.001, by paired t-test) less than the interaction with T622X (Fig. 4-5A and B). We believe that the interaction between WT PKD2L1 and K575X is largely mediated through their N-terminus. In summary, our further *in vitro* data were in support of the involvement of C1 in trimerization.

Further, we employed Dynamic light scattering (DLS) to examine the role of C1 in the trimerization of purified CT in solution. DLS assesses a protein's apparent hydrodynamic diameter (D_H) as being the size of a hypothetical hard sphere that diffuses in the same fashion as the hydrated protein being measured. We expressed and purified CT and its deletion mutants CT-ΔC1 (with C1 deletion) and CT-Δdouble (with both C1 and CC2 deletions) from *E. coli* (Fig. 4-5C). We found that the D_H of CT measured by DLS is 8.88 ± 0.26 nm (N = 6), which is significantly reduced to 5.80 ± 0.17 nm (N = 5, P < 0.001) and 5.49 ± 0.05 nm (N = 5, P < 0.001)

for C1 and double deletions, respectively (Fig. 4-5D). Using the Mark-Houwink-Sakurada equation, molecular weight = $a(D_H)^b$, where parameters a and b were found to be 0.41 ± 0.05 and 2.48 ± 0.04, respectively, for proteins in the range of 17 - 440 kD [35], the corresponding molecular weights deduced from these D_H values are 93 ± 6 kD, 32 ± 2 kD and 28 ± 1 kD, for CT, CT-ΔC1 and CT-Δdouble, respectively, indicating a predominant trimeric structure for CT and monomeric structures for the two deletion mutants under this experimental condition. These data indicated that C1 deletion significantly breaks down trimerization of CT, in support of the importance of C1 for oligomerization.

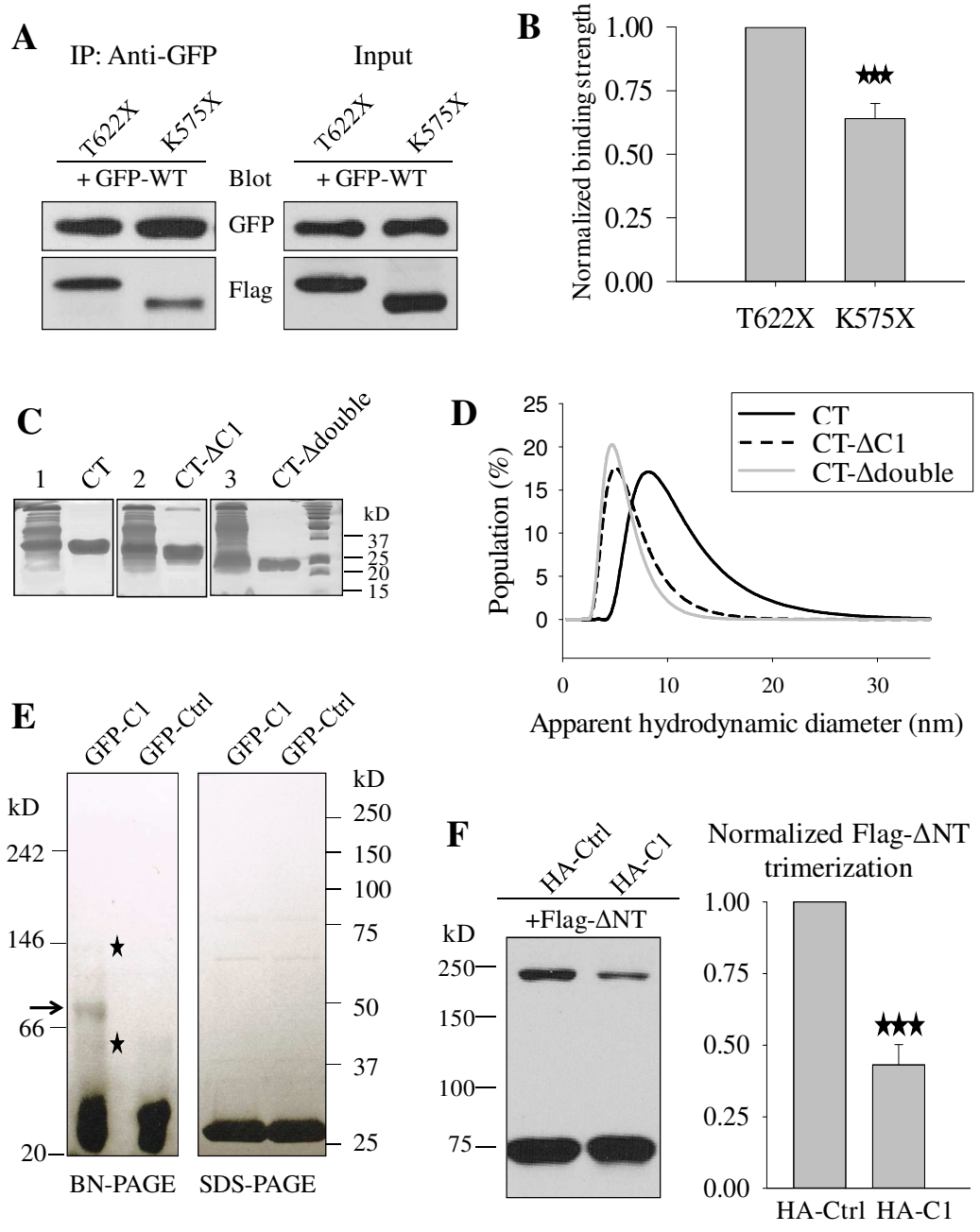

Fig. 4-5. Further evidences for C1 involvement in trimerization. (**A**) Effect of C1 on the interaction between two PKD2L1 proteins assessed by co-IP. Left panel: representative data showing the interaction of GFP-PKD2L1 (GFP-WT) with Flag-T622X or Flag-K575X in HeLa cells. GFP-WT was first transfected, followed by transfection of T622X and K575X 12 hr later. Right panel: representative input data by WB showing the expression of WT, T622X and K575X. (**B**) Data from experiments in panel A were quantified, averaged, normalized, and then compared by paired t-test (***$P \leq 0.001$, $N = 3$). (**C**) Coomassie blue staining of purified PKD2L1 C-terminus (CT, E566-S805), CT-ΔC1 (C1 deletion from CT), and CT-Δdouble (C1 and CC2 double deletion from CT) from *E. coli*. Date using crude lysates are shown on their left (lanes 1, 2 and 3). (**D**) Analysis of size distribution of purified CT, CT-ΔC1, and CT-Δdouble

fragments by dynamic light scattering experiments. (**E**) Coomassie blue staining analysis of BN-PAGE or SDS-PAGE of purified protein GFP-C1 or GFP-Ctrl (human 4EBP1 M1-T50 fragment). Putative GFP-C1 trimer is indicated by an arrow on BN-PAGE. The faint bands below and above the putative trimer are indicated with stars. (**F**) Left panel: WB detection of over-expressed Flag-ΔNT with co-expression of HA-tagged blocking peptide C1 (HA-C1) or control peptide T622-E675 (HA-Ctrl) in HeLa cells under the non-reducing condition. 200 ng Flag-ΔNT plasmid and 1000 ng HA-C1 or HA-Ctrl plasmid were used in the co-transfection. Right panel: trimer bands were quantified, averaged, normalized, and compared by paired t-test (***$P \leq 0.001$, $N = 3$).

Next, we examined whether peptide C1 is sufficient to form trimers by itself. For this we first expressed in and purified C1 from *E. coli*. Because C1 was not expressed alone, presumably due to its small size and/or instability we utilized fusion protein GFP-C1 for *E. coli* expression. As a negative control, we expressed and purified GFP protein fused with human 4EBP1 fragment (M1-T50) (GFP-Ctrl) of a similar size. We then carried out BN-PAGE experiments which indeed revealed the presence of a trimer band for GFP-C1 but not for GFP-Ctrl (Fig. 4-5E). Of note, the trimer band was relatively weak, which may be due to the added coomassie blue G-250 that gave negative changes to C1 and reduced its trimerization during sample preparation for BN-PAGE. As a comparison and control, we carried out SDS-PAGE analysis as well and found no trimer band for C1 under this condition (Fig. 4-5E). Therefore, our data showed that purified C1 itself forms trimers. We also noted visible weak bands below and above the trimer band, which may represent a dimer due to the well-known weak dimerization of GFP and a hexamer due to GFP dimerization plus C1 trimerization, respectively.

Role of C1 as a blocking peptide

We reasoned that C1 may disrupt the oligomerization of full-length PKD2L1 through competitive binding, thereby inhibiting channel function. To test this, we applied a similar blocking peptide strategy that we described previously [9]. We first co-transfected PKD2L1 ΔNT

with HA-tagged C1 or control plasmid encoding HA-T622-E657 (negative Ctrl) that has no overlap with C1 or CC2. Indeed, we found that co-expression of C1 decreases ΔNT trimerization to 42.7 ± 7.5% (N = 3, P < 0.001, by paired t-test) (Fig. 4-5F). Next, using oocyte expression and electrophysiology, we found that expression of C1 substantially inhibits the channel function of PKD2L1 alone and complex PKD2L1/PKD1L3 (Fig. 4-6A, B and D). Our WB assays using similarly prepared oocytes showed that C1 expression significantly reduces the formation of PKD2L1 oligomers but not monomers, regardless whether PKD1L3 was co-expression or not (Fig. 4-6C). Of note, due to its small size of only about 5 kD, we carried out dot blot assays and confirmed its expression (Fig. 4-6C). Our immunofluorescence data indicated that over-expression of C1 reduces PKD2L1 surface expression (Fig. 4-6E and F), which may be the reason why reduction in the trimer band did not result in an increase in the monomer band in our WB experiments (Fig. 4-6C).

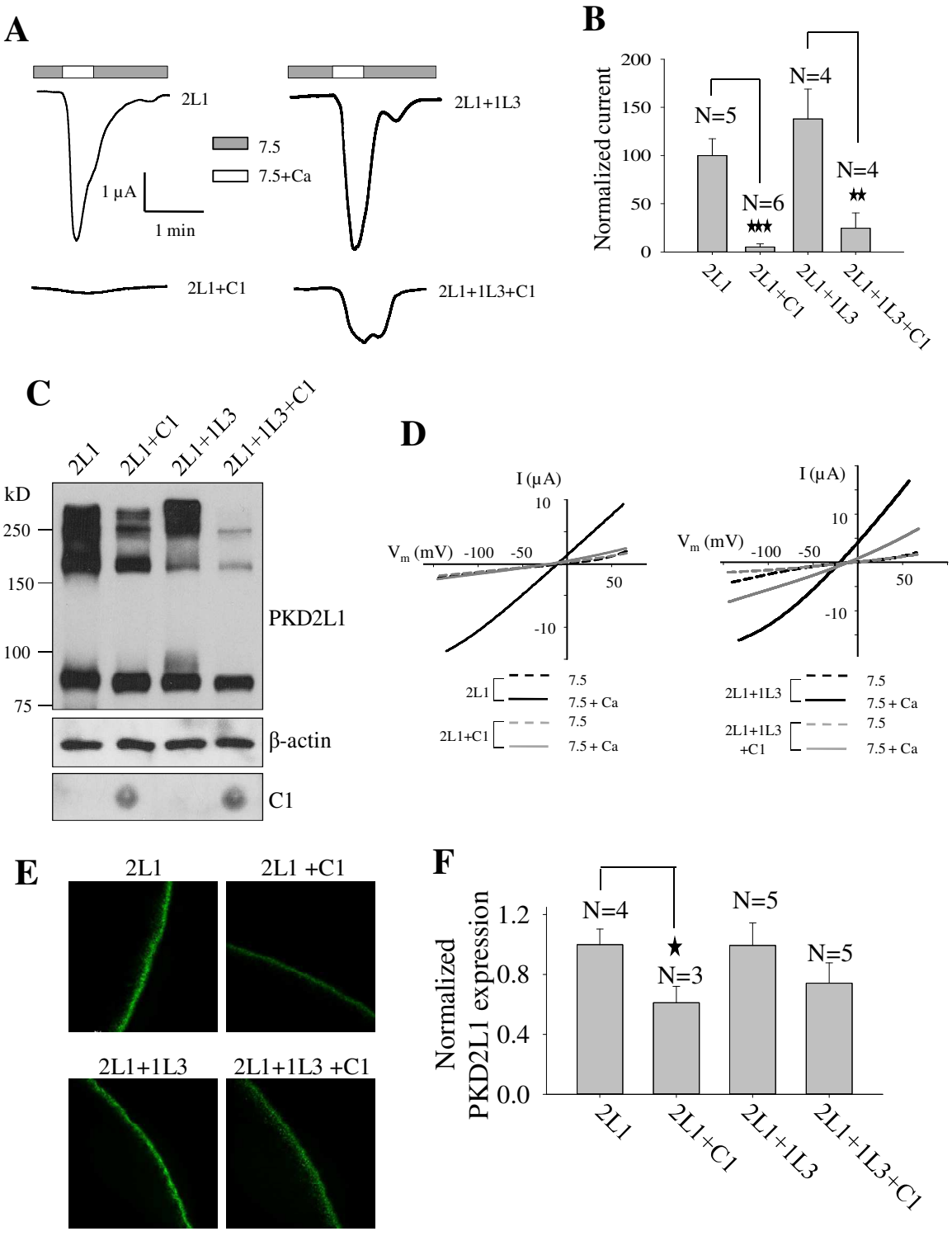

Fig. 4-6. Effect of C1 on PKD2L1 trimerization and function. (**A**) Representative whole-cell current tracings from *Xenopus* oocytes expressing PKD2L1 (2L1) or PKD2L1/PKD1L3 (2L1+1L3), with or without C1 using the two-microelectrode voltage clamp technique under similar conditions as for Fig. 4-2. (**B**) Averaged currents elicited by extracellular 5 mM Ca^{2+}

from oocytes expressing 2L1 or 2L1+1L3, with or without C1, and voltage clamped at -50 mV. Currents were averaged from different numbers of oocytes, as indicated, and normalized to that of WT PKD2L1 alone. (**C**) WB detection of PKD2L1 expression or dot blot detection of C1 expression in oocytes. (**D**) Representative current–voltage relationship curves obtained using a voltage ramp protocol, as indicated in Fig. 4-2C, before (7.5) and after (7.5+Ca) addition of 5 mM $CaCl_2$. (**E**) Representative immunofluorescence data showing the oocyte plasma membrane expression of 2L1 and 2L1+1L3, with or without C1. (**F**) Surface expression was quantified and averaged from the indicated numbers of oocytes, and normalized to that of 2L1.

4.5 DISCUSSION

Because the function of an ion channel presumably relies on its intact oligomeric state deletion of or alterations in an oligomerization domain would substantially affect the channel architecture and consequently channel activity. Up to now it has remained unknown as to which domains of PKD2L1 that are important for both oligomerization and function. Previous studies identified CC2 as a trimeric domain in CT that is important for the surface membrane expression of PKD2L1 and complex PKD2L1/PKD1L3 [21-23]. However, using the *Xenopus* oocyte expression system, it was previously shown that PKD2L1 with truncation either before or after the CC2 domain does not significantly affect the channel function [24], which is also confirmed by the current study (Fig. 4-4B), indicating that CC2 is not required for PKD2L1 channel function. The reported 3:1 oligomeric assembly for PKD2L1/PKD1L3 channel complex and our current *in vivo* data from mouse tissues showing the presence of trimeric assembly indicate the presence of a yet to-be-identified domain(s) important for a functional PKD2L1 trimeric state. Indeed, our current studies using a combination of *in vitro* expression in mammalian cells and *Xenopus* oocytes, electrophysiology, mutagenesis, protein-protein interaction, and dynamic light scattering identified the C-terminal C1 domain that is the most conserved in CT and critical for both PKD2L1 trimerization and channel function.

Our non-reducing SDS-PAGE with mouse tissues showed the same oligomers pattern in kidney, testis and brain and these oligomers were reduced to monomer with reducing agents (Fig. 4-1A), so it may be assumed that all PKD2L1 oligomers in the tissues are generated through cysteine-cysteine disulfide bonds since reducing agents are expected to only disrupt oligomerization mediated by disulfide bonds. However, for some unknown reasons, reducing agents may also disrupt oligomerization mediated by peptide-peptide interactions, at least for

some multiple-transmembrane proteins. For example, Feng et al showed that dimers of PKD2 truncation mutant PKD2-L703X detected with non-reducing SDS-PAGE disappeared by the addition of reducing agents and that these dimers are indeed formed by an peptide-peptide interaction in the N-terminus of PKD2 [26]. Further, oligomers formed through peptide-peptide interactions under non-reducing SDS-PAGE may be more vulnerably disrupted by reducing agents in tissue lysates than in cell line lysates by unclear reasons. For example, almost all PKD2 oligomers were reduced into monomers with addition of reducing agents in human kidney tissues, but the effect of reducing agents were only moderate in cell lines [36]. In the case of PKD2L1, previous studies by other groups have reported the presence of PKD2L1 homooligomers through its C-terminal peptide-peptide interactions, eg, through CC2 trimerization [21] and PKD2L1/PKD1L3 heterooligomerization at 3:1 stoichiometry through peptide-peptide interaction [25]. Together with our current data on its C-terminal C1 trimerization, we think that part of PKD2L1 oligomers detected with non-reducing SDS-PAGE using tissue lysates should be mediated by peptide-peptide interactions, possibly the C1-C1 interaction, and reduced to monomers by reducing agents.

TRPC, TRPM and TRPN channels were found to contain a conservative intracellular TRP domain downstream of TM6, which is similarly located as C1. This TRP domain was proposed to participate in subunit assembly and/or allosteric modulation of channel gating [37]. Interestingly, the recently resolved TRPV1 structure showed that charged side chains within the TRP domain interact with pre-S1 helix in the N-terminus through hydrogen bonding and salt bridging [38]. It is possible that C1 shares some functional similarities and plays corresponding roles in PKD2L1. Eg, in addition to its trimerization role, it seemed to regulate PKD2L1

dimerization formed by PKD2L1 NT (see Fig. 4-2F). Future studies will need to address this by providing more direct evidence.

We wondered why PKD2L1 needs two distinct trimerization domains in CT of PKD2L1. PKD2L1 channel is activated by Ca^{2+} followed by channel inactivation, presumably through an increase in the intracellular Ca^{2+} concentration [8], but it remains unclear whether Ca^{2+} regulates PKD2L1 channel activity through direct binding. CT contains a Ca^{2+}-binding EF hand motif (E637-L665) that negatively regulates the ability of PKD2L1 channel to be activated by Ca^{2+}, suggesting that Ca^{2+} binds to this domain to prevent the channel from over-activation [24]. Direct binding of Ca^{2+} to CT was indeed reported [23] although it remains unknown whether and how this binding is relevant to channel function. At least, this same study showed that Ca^{2+} binding is not affected by mutations of 6 residues to alanine within CC2, suggesting that CC2 is not involved in Ca^{2+} binding. More importantly, our previous and current studies both demonstrated that CC2 is not important for PKD2L1 channel function. Although CC2 was found to be important for surface expression of PKD2L1 and complex PKD2L1/PKD1L3 in *Xenopus* oocytes [21] whether it promotes the trafficking to, or prevents the retrieval from, the surface membrane remains unknown. In contrast, although C1 did not seem to affect PKD2L1 surface membrane expression (Fig. 4-4E) it is critical for the channel function. It is possible that nature chooses to have two trimerization domains that together ensure proper surface membrane configuration and stability, as well as channel function.

Members of the TRP superfamily including PKD2 and PKD2L1 are assumed to assemble into homo- and/or hetero-tetramers with either a PKD1 homologue or another TRP protein, but the molecular mechanisms underlying these assemblies are still unclear. Like PKD2L1, the PKD2 C-terminus was found to form trimers [20,22]. The trimerization of the PKD2 or PKD2L1 C-

termini seems to nicely explain the tetrameric organization of the PKD2/PKD1 or PKD2L1/PKD1L3 complex with a trimer/monomer assembly [20,21]. Based on our current data we propose that a functional PKD2L1 homotetramer can be formed either through C-terminal trimerization followed by N-terminal dimerization of a fourth subunit with a subunit in the trimer or through dimerization followed by trimerization (see model in Fig. 4-7). Thus, we think that, under physiological conditions, depending on the availability of a co-localized PKD1 homologue, PKD2L1 forms homo- or heterotetramers by a shared way, namely, homotrimerization of PKD2L1 and heterodimerization of PKD2L1-PKD1 homologue (Fig. 4-7). We should however bear in mind that interaction forces involved in the organization of TMs for a pore forming architecture are important as well although they are not discussed here.

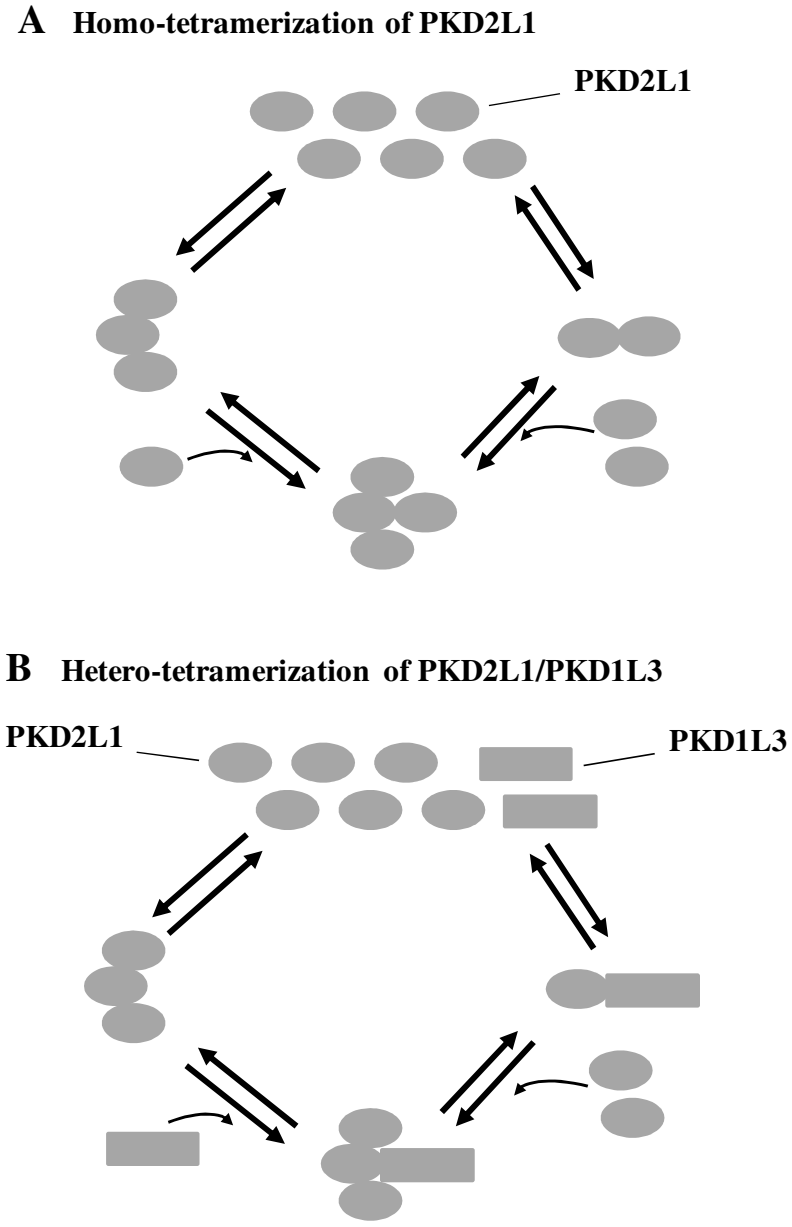

Fig. 4-7. Model illustrating how a PKD2L1 homo- or heterotetramerer can be formed. (**A**) A PKD2L1 (oval) homotetramer can be formed either through first homotrimerization followed by recruitment of a fourth subunit to the trimer by dimerization or through first homodimerization followed by recruitment of two subunits to form a trimer with a subunit in the dimer. Of notes, 1) the illustration is only to indicate trimeric and dimeric binding and does not intend to show how the pore region is organized; and 2) the drawn trimer does not intend to mean that there are two points of contact. (**B**) A PKD2L1 heterotetramer can be formed with a PKD1 homologue (square), eg, PKD1L3 or PKD1L1, through first trimerization of PKD2L1 and then recruitment of a PKD1 homologue, or reversely, through first heterodimerization between PKD2L1 and a PKD1 homologue, followed by recruitment of two PKD2L1 subunits to form a trimer with the existing PKD2L1 subunit.

It is noted that such a 3+1 assembly protocol for forming homo- and heterotetramers has been reported for other channels. Eg, the cytoplasmic C-terminal leucine zipper domain (G488-Y526) of small conductance voltage-gated Ca^{2+}-activated K^+ channel (SK_{Ca}) forms trimers, as shown by crystallographic analyses [39] while the functional full-length SK_{Ca} channel forms homotetramers [40]. Similarly, a C-terminal domain (R583-D611) of voltage-gated K^+ channel $K_v7.1$ was shown to trimerize but the full-length channel forms tetramers [41]. Under physiological conditions, cyclic-nucleotide-gated channels are more likely heterotetramers consisting of the A and B subtypes with the A-trimer:B-monomer assembly when both are present. In cells over-expressing the A subtype, homotetramers were found [42-44]. Therefore, PKD2L1 as a TRP superfamily member may possess a strategy of oligomeric assembly that is shared by other families of ion channel.

In summary, our study has found that endogenous PKD2L1 in mouse tissues exhibits oligomeric states including dimers, trimers and tetramers. We identified a novel PKD2L1 C-terminal C1 domain that is associated with stronger trimerization than the previously reported CC2 domain. Importantly, C1 represents the first oligomerization domain critical for PKD2L1 channel function. We thus propose that functional PKD2L1 channel assembly involves both trimerization and dimerization, a mechanism possibly shared by some non-TRP types of ion channel.

4.6 REFERENCES

1. Tan, Y. C., Blumenfeld, J. & Rennert, H. Autosomal dominant polycystic kidney disease: genetics, mutations and microRNAs. *Biochim. Biophys. Acta.* **1812**, 1202-1212 (2011).

2. Wilson, P. D. Polycystic kidney disease. *N. Engl. J. Med.* **350**, 151-164 (2004).

3. Montell, C. The TRP superfamily of cation channels. *Sci. STKE.* **2005**, re3 (2005).

4. Eijkelkamp, N., Quick, K. & Wood, J. N. Transient receptor potential channels and mechanosensation. *Annu. Rev. Neurosci.* **36**, 519-546 (2013).

5. Wu, L. J., Sweet, T. B. & Clapham, D. E. International Union of Basic and Clinical Pharmacology. LXXVI. Current progress in the mammalian TRP ion channel family. *Pharmacol. Rev.* **62**, 381-404 (2010).

6. Owsianik, G., D'hoedt, D., Voets, T. & Nilius, B. Structure-function relationship of the TRP channel superfamily. *Rev. Physiol Biochem. Pharmacol.* **156**, 61-90 (2006).

7. Venkatachalam, K. & Montell, C. TRP channels. *Annu. Rev. Biochem.* **76**, 387-417 (2007).

8. Chen, X. Z. *et al.* Polycystin-L is a calcium-regulated cation channel permeable to calcium ions. *Nature.* **401**, 383-386 (1999).

9. Yang, J. *et al.* Receptor for activated C kinase 1 (RACK1) inhibits function of transient receptor potential (TRP)-type channel Pkd2L1 through physical interaction. *J. Biol. Chem.* **287**, 6551-6561 (2012).

10. DeCaen, P. G., Delling, M., Vien, T. N. & Clapham, D. E. Direct recording and molecular identification of the calcium channel of primary cilia. *Nature.* **504**, 315-318 (2013).

11. Delling, M., DeCaen, P. G., Doerner, J. F., Febvay, S. & Clapham, D. E. Primary cilia are specialized calcium signalling organelles. *Nature.* **504**, 311-314 (2013).

12. Shimizu, T., Janssens, A., Voets, T. & Nilius, B. Regulation of the murine TRPP3 channel by voltage, pH, and changes in cell volume. *Pflugers Arch.* **457**, 795-807 (2009).

13. Huang, A. L. *et al.* The cells and logic for mammalian sour taste detection. *Nature.* **442**, 934-938 (2006).

14. Horio, N. *et al.* Sour taste responses in mice lacking PKD channels. *PLoS. One.* **6**, e20007 (2011).

15. Inada, H. *et al.* Off-response property of an acid-activated cation channel complex PKD1L3-PKD2L1. *EMBO Rep.* **9**, 690-697 (2008).

16. Nauli, S. M. *et al.* Polycystins 1 and 2 mediate mechanosensation in the primary cilium of kidney cells. *Nat. Genet.* **33**, 129-137 (2003).

17. Murakami, M. *et al.* Genomic organization and functional analysis of murine PKD2L1. *J. Biol. Chem.* **280**, 5626-5635 (2005).

18. Ishimaru, Y. *et al.* Transient receptor potential family members PKD1L3 and PKD2L1 form a candidate sour taste receptor. *Proc. Natl. Acad. Sci. U. S. A.* **103**, 12569-12574 (2006).

19. Nelson, T. M. *et al.* Taste function in mice with a targeted mutation of the pkd1l3 gene. *Chem. Senses.* **35**, 565-577 (2010).

20. Yu, Y. *et al.* Structural and molecular basis of the assembly of the TRPP2/PKD1 complex. *Proc. Natl. Acad. Sci. U. S. A.* **106**, 11558-11563 (2009).

21. Yu, Y. *et al.* Molecular mechanism of the assembly of an acid-sensing receptor ion channel complex. *Nat. Commun.* **3**, 1252 (2012).

22. Molland, K. L., Narayanan, A., Burgner, J. W. & Yernool, D. A. Identification of the structural motif responsible for trimeric assembly of the C-terminal regulatory domains of polycystin channels PKD2L1 and PKD2. *Biochem. J.* **429**, 171-183 (2010).

23. Molland, K. L., Paul, L. N. & Yernool, D. A. Crystal structure and characterization of coiled-coil domain of the transient receptor potential channel PKD2L1. *Biochim. Biophys. Acta.* **1824**, 413-421 (2012).

24. Li, Q., Liu, Y., Zhao, W. & Chen, X. Z. The calcium-binding EF-hand in polycystin-L is not a domain for channel activation and ensuing inactivation. *FEBS Lett.* **516**, 270-278 (2002).

25. Ishimaru, Y. *et al.* Interaction between PKD1L3 and PKD2L1 through their transmembrane domains is required for localization of PKD2L1 at taste pores in taste cells of circumvallate and foliate papillae. *FASEB J.* **24**, 4058-4067 (2010).

26. Feng, S. *et al.* Identification and functional characterization of an N-terminal oligomerization domain for polycystin-2. *J. Biol. Chem.* **283**, 28471-28479 (2008).

27. Feng, S., Rodat-Despoix, L., Delmas, P. & Ong, A. C. A single amino acid residue constitutes the third dimerization domain essential for the assembly and function of the tetrameric polycystin-2 (TRPP2) channel. *J. Biol. Chem.* **286**, 18994-19000 (2011).

28. Li, Q. *et al.* Direct binding of alpha-actinin enhances TRPP3 channel activity. *J. Neurochem.* **103**, 2391-2400 (2007).

29. Karey, K. P. & Sirbasku, D. A. Glutaraldehyde fixation increases retention of low molecular weight proteins (growth factors) transferred to nylon membranes for western blot analysis. *Anal. Biochem.* **178**, 255-259 (1989).

30. Imam, M., Singh, S., Kaushik, N. K. & Chauhan, V. S. Plasmodium falciparum merozoite surface protein 3: oligomerization, self-assembly, and heme complex formation. *J. Biol. Chem.* **289**, 3856-3868 (2014).

31. Giudici, A. M. *et al.* Detergent-labile, supramolecular assemblies of KcsA: relative abundance and interactions involved. *Biochim. Biophys. Acta.* **1828**, 193-200 (2013).

32. Raja, M. The potassium channel KcsA: a model protein in studying membrane protein oligomerization and stability of oligomeric assembly? *Arch. Biochem. Biophys.* **510**, 1-10 (2011).

33. Milligan, G. G protein-coupled receptor dimerization: function and ligand pharmacology. *Mol. Pharmacol.* **66**, 1-7 (2004).

34. Thevenin, D., Lazarova, T., Roberts, M. F. & Robinson, C. R. Oligomerization of the fifth transmembrane domain from the adenosine A2A receptor. *Protein Sci.* **14**, 2177-2186 (2005).

35. Faggiano, S., Ronda, L., Bruno, S., Jankevics, H. & Mozzarelli, A. Polymerized and polyethylene glycol-conjugated hemoglobins: a globin-based calibration curve for dynamic light scattering analysis. *Anal. Biochem.* **401**, 266-270 (2010).

36. Newby, L. J. *et al.* Identification, characterization, and localization of a novel kidney polycystin-1-polycystin-2 complex. *J. Biol. Chem.* **277**, 20763-20773 (2002).

37. Latorre, R., Zaelzer, C. & Brauchi, S. Structure-functional intimacies of transient receptor potential channels. *Q. Rev. Biophys.* **42**, 201-246 (2009).

38. Liao, M., Cao, E., Julius, D. & Cheng, Y. Structure of the TRPV1 ion channel determined by electron cryo-microscopy. *Nature.* **504**, 107-112 (2013).

39. Kim, J. Y., Kim, M. K., Kang, G. B., Park, C. S. & Eom, S. H. Crystal structure of the leucine zipper domain of small-conductance Ca2+-activated K+ (SK(Ca)) channel from Rattus norvegicus. *Proteins.* **70**, 568-571 (2008).

40. MacKinnon, R. Determination of the subunit stoichiometry of a voltage-activated potassium channel. *Nature.* **350**, 232-235 (1991).

41. Xu, Q. & Minor, D. L., Jr. Crystal structure of a trimeric form of the K(V)7.1 (KCNQ1) A-domain tail coiled-coil reveals structural plasticity and context dependent changes in a putative coiled-coil trimerization motif. *Protein Sci.* **18**, 2100-2114 (2009).

42. Matulef, K. & Zagotta, W. N. Cyclic nucleotide-gated ion channels. *Annu. Rev. Cell Dev. Biol.* **19**, 23-44 (2003).

43. Zheng, J., Trudeau, M. C. & Zagotta, W. N. Rod cyclic nucleotide-gated channels have a stoichiometry of three CNGA1 subunits and one CNGB1 subunit. *Neuron.* **36**, 891-896 (2002).

44. Zhong, H., Molday, L. L., Molday, R. S. & Yau, K. W. The heteromeric cyclic nucleotide-gated channel adopts a 3A:1B stoichiometry. *Nature.* **420**, 193-198 (2002).

CHAPTER 5

RESULTS #4

Regulation of TRPP3 channel function by N-terminal domain palmitoylation and phosphorylation

5.1 ABSTRACT

Transient receptor potential polycystin-3 (TRPP3) is a cation channel activated by calcium and proton and is involved in hedgehog signaling, intestinal development, and sour tasting. How TRPP3 channel function is regulated remains poorly understood. By N-terminal truncation mutations, electrophysiology and *Xenopus* oocytes expression, we first identified fragment D21-S42 to be functionally important. We then found that deletion mutant Δ1-36 (TRPP3 missing fragment M1-R36) has similar function as wild-type TRPP3 while Δ1-38 is functionally dead, suggesting the importance of V37 or C38. Further studies found that C38, but not V37, is functionally critical. C38 is a predicted site of palmitoylation, and indeed TRPP3 channel activity was inhibited by palmitoylation inhibitor 2-bromopalmitate and rescued by palmitoylation substrate palmitic acid. The TRPP3 N-terminus (TRPP3NT, M1-L95) localized along the plasma membrane of HEK293 cells, but stayed in the cytoplasm with 2-bromopalmitate treatment or C38A mutation, indicating that TRPP3NT anchors to the surface membrane through palmitoylation at C38. By acyl-biotin exchange assays we showed that TRPP3, but not mutant C38A, is indeed palmitoylated. On the other hand, when putative phosphorylation sites near C38 were mutated to D or E to mimic phosphorylation, only T39D and T39E reduced TRPP3 function. Further, TRPP3NT displayed double bands of which the upper band was abolished by lambda phosphatase treatment or T39A mutation. However, palmitoylation at C38 and phosphorylation at T39 independently regulated TRPP3 channel function, in contrast to previous reports about correlated palmitoylation with a proximal phosphorylation. Palmitoylation at C38 represents a novel mechanism of functional regulation for TRPP3.

5.2 INTRODUCTION

Transient receptor potential (TRP) channels are a superfamily of cation channels that play distinct sensory roles in response to a variety of extracellular stimuli, including light, sound, chemicals, temperature, and touch [1]. The TRP superfamily has been divided into eight subfamilies named after the first identified member in each subfamily: TRPC, TRPV, TRPM, TRPA, TRPN, TRPY, TRPML and TRPP. Similar to voltage-gated potassium channels, TRP channels were predicted to function as tetramers in which each subunit has six transmembrane helices (TM1-TM6), with a pore loop between TM5 and TM6, and cytosolic amino- and carboxy-termini of varying sizes [2]. This structural architecture was confirmed by recently published TRPV1, -2, -6 and TRPA1 structures [3-6].

The founding member of the TRP polycystin (TRPP) subfamily, TRPP2 (also called PKD2 or polycystin-2), was mutated in 15% autosomal dominant polycystic kidney disease (ADPKD), the most common genetic disorder of the kidney, affecting 1 in 400 to 1000 individuals worldwide [7]. The remaining ADPKD is caused by mutations in the *PKD1* gene. TRPP3, also called PKD2L1 or polycystin-L, is a homologue of TRPP2 with 50% identity in protein sequence, but is not involved in ADPKD. TRPP3 is expressed in bipolar neurons in the tongue taste buds where it presumably plays an important role in sour tasting. Genetic ablation of cells expressing TRPP3 eliminates gustatory nerve response to sour stimuli in mice [8-10]. Involvement of TRPP3 in sour tasting was later supported by the report that TRPP3 knockout mice display defective ability of tasting acid [11]. TRPP3 is expressed in neurons surrounding the central canal of spinal cord where it may be implicated in modulating pH-dependent action potential characteristics [8,12,13]. TRPP3 is also expressed in brain, kidney and heart with unknown function [14].

TRPP3 is localized on the surface membrane and/or endoplasmic reticulum (ER) membrane, in part depending on the cell type. In *Xenopus laevis* oocytes, TRPP3 targets to the plasma membrane when expressed alone and acts as Ca^{2+}-activated channel permeable to Na^{+}, K^{+} and Ca^{2+} [15,16]. In human embryonic kidney (HEK) cell lines, TRPP3 mainly targets to the ER membrane when expressed alone, but traffics to the plasma membrane when co-expressed with PKD1 or PKD1L3, a homologue of PKD1 [9,17,18] . TRPP3 and PKD1L3 together mediate pH-dependent cation conductance in a off-response manner, ie, activation occurred only after low extracellular pH was removed [9,19]. TRPP3 was also found to be expressed in primary cilium and regulate ciliary Ca^{2+} concentration and hedgehog signaling [20,21]. Although TRPP3 contains putative phosphorylation, glycosylation and palmitoylation sites, it is unclear whether and how it is regulated via post-translational modifications. Its homologue TRPP2 channel activity or trafficking was reported to be regulated by phosphorylation at C-terminal S812 by casein kinase II [22] and N-terminal S76 by glycogen synthase kinase 3 [23]. Besides, TRPP2 is also glycosylated but with unclear functional role [24].

Palmitoylation is a reversible covalent fatty-acid modification which attaches the C16 fatty acid palmitate to a cytoplasmic cysteine residue [25]. Like other lipid modifications, such as myristoylation and prenylation, palmitoylation serves to tether cytoplasmic proteins to the surface of membranes. In mammals, there are 23 palmitoyl-transferases (PATs) containing a conserved zinc binding site and DHHC (Asp-His-His-Cys) motif, thus these enzymes are often referred to as zDHHC-PATs [26,27]. The reversibility of the palmitoylation reaction provides a dynamic regulation mechanism. In transmembrane domain containing proteins, such as G protein coupled receptors, palmitoylation of the C-terminal domain has lead to the formation of a seventh intra-cellular loop linked to receptor de-sensitization [28-30]. Increasing number of ion

channel proteins have been reported to undergo palmitoylation as a way of controlling the anchorage of an intracellular domain to membranes [31]. An interplay between palmitoylation and phosphorylation has recently been recognized as a new mechanism of regulating the trafficking or function of ion channels [31]. Among them, TRPML1 has been reported to undergo palmitoylation and de-phosphorylation, following histamine stimulation of gastric acid secretion, which may underlie the mechanism of its endocytosis [32,33].

In this study, using *Xenopus laevis* oocyte expression and the two-electrode voltage clamp (TEVC) technique, we first identified the N-terminal residue C38 in human TRPP3 to be critical for its channel function. We then showed that this is mediated through palmitoylation at C38. We also identified T39 to be a functionally important phosphorylation site immediately downstream of C38. At last, we showed that palmitoylation at C38 and phosphorylation at T39 regulate TRPP3 channel function rather independently, in contrast to other ion channels that are regulated by palmitoylation and correlated phosphorylation at a proximal residue.

5.3 METHODS

Vectors, plasmids and antibodies

Human full-length TRPP3 cDNA was subcloned into vector pCHGF [34] for *Xenopus laevis* oocyte expression. Flag tag was then inserted 5' of the TRPP3 coding region for detection. cDNAs coding for the N- or C-termini of human TRPP3 and TRPP2 were subcloned into the pEGFPC2 vector for mammalian cell expression. All mutations were made with QuikChange Lighting Site Directed Mutagenesis kit (Agilent Technologies, La Jolla, CA) and confirmed by sequencing. Rabbit antibodies against FLAG (D-8), Na^+/K^+ ATPase (H-300) and mouse antibodies against β-actin (C-4) were purchased from Santa Cruz Biotechnology (Santa Cruz, CA). Mouse antibody against HA (HA.C5) was purchased from Abcam (Cambridge, MA). Secondary antibodies were purchased from GE Healthcare (Waukesha, WI).

Preparation of mRNAs and microinjection into oocytes

pCHGF plasmids containing TRPP3 WT or mutant cDNAs were linearized with *Mlu* I, followed by phenol/chloroform purification and ethanol precipitation. Linearized DNAs were then used to *in vitro* synthesize capped mRNAs using mMESSAGE mMACHINE kit (Ambion, Austin, TX). Stage V-VI oocytes were isolated from *Xenopus laevis*. Defolliculation of oocytes was performed through incubation in Ca^{2+}-free Barth's solution [35] containing collagenase (2 mg/ml) at room temperature (RT) for 1 hour (hr). Oocytes were then incubated at 18˚C in the Barth's solution for at least 3 hr before injection of 25 nl RNase-free water containing 25 ng mRNAs using picospritzer III (Parker Hannifin, Cleveland, OH). An equal volume of water was injected into each control oocyte. The present study was approved by the Ethical Committee for Animal Experiments of the University of Alberta, and was carried out in accordance with the

Guidelines for Research with Experimental Animals of the University of Alberta and the Guide for the Care and Use of Laboratory Animals (NIH Guide) revised in 1996. Injected oocytes were incubated at 18 ℃ in the Barth's solution supplemented with antibiotics for 2-4 days prior to experiments.

^{45}Ca uptake

Radiotracer uptake experiments were performed as previously described [15]. In brief, radioactive $^{45}CaCl_2$ (Amersham Biosciences, Amersham, UK) at 30 μM was added to the uptake solution (100 mM *N*-methyl-d-glucamine, 2 mM KCl, 1 mM $MgCl_2$, 10 mM HEPES, pH 7.5) plus 1 mM non-radioactive $CaCl_2$. Ten oocytes of each sample were incubated in 0.5 ml of the uptake solution for 30 min, and the incubation was terminated by washing oocytes with ice-cold NaCl-containing solution (100 mM NaCl, 2 mM KCl, 1 mM $MgCl_2$, 10 mM HEPES, pH 7.5). Individual oocytes were then dissolved in 250 μl of 10% SDS and mixed with 2.5 ml of scintillation mixture prior to scintillation counting.

Two-electrode voltage clamp

TEVC experiments were performed as described before [34]. Briefly, the two electrodes (Capillary pipettes, Warner Instruments, Hamden, CT) impaling an oocyte were filled with 3 M KCl to form a tip resistance of 0.3-2 MΩ. The standard extracellular solution containing 100 mM NaCl, 2 mM KCl, 1 mM $MgCl_2$ and 10 mM HEPES (pH 7.5) with or without 5 mM $CaCl_2$ was used. The Duration of application of Ca^{2+} solution was indicated in time course recordings. The palmitoylation inhibitor 2BP (Sigma) was made as a fresh 100 mM stock in DMSO and applied

at various concentrations from 1 μM to 50 μM overnight. Oocyte whole-cell currents were recorded using a Geneclamp 500B amplifier and Digidata 1322A AD/DA converter (Molecular Devices, Union City, CA). The pClamp 9 software (Axon Instruments, Union City, CA) was employed for data acquisition and analysis. Currents and voltages were digitally recorded at 200 μs/sample and filtered at 2 kHz through a Bessel filter. SigmaPlot 12 (Systat Software, San Jose, CA) was used for data fitting and plotting.

Oocyte immunofluorescence

Immunofluorescence assays using oocyte slices were performed as previously described [34]. Whole mount staining was performed as follows: *Xenopus* oocytes were washed in PBS, fixed in 4% paraformaldehyde for 15 min, washed 3 times in PBS plus 50 mM NH_4Cl, and then permeabilized with 0.1% Triton X-100 for 4 min. Oocytes were then blocked in PBS plus 3% skim milk for 30 min, and then incubated overnight with the rabbit anti-TRPP3 polyclonal antibody (cat# PAB5914, Abnova, Taiwan), followed by incubation with a secondary AlexaFluor 488-conjugated donkey anti-rabbit antibody (Jackson ImmunoResearch Laboratories, West Grove, PA) for 30 min. Oocytes were then mounted in Vectashield (Vector Labs, Burlington, ON) and examined on an AIVI spinning disc confocal microscopy (Cell Imaging Facility, Faculty of Medicine and Dentistry, University of Alberta).

Western blotting

Protein samples were prepared with CelLytic M lysis buffer (Sigma) from oocytes or mammalian cells according to the manufacturer's instruction. 50-80 μg total proteins were then

separated on 8% SDS-PAGE gels and transferred to nitrocellulose membranes which were then blocked for 1 hr at room temperature with 3% skim milk in PBS buffer supplemented with 1% Tween-20. This was followed by overnight incubation at 4 ℃ with diluted primary antibodies in blocking buffer according to suppliers' suggestions. Secondary horseradish peroxidase-coupled anti-mouse and anti-rabbit antibodies were purchased from GE.

Biotinylation

Xenopus oocytes were washed 3 times with PBS followed by incubation with 0.5 mg/ml sulfo-NHS-SS-Biotin (Pierce, Rockford, IL) for 30 min at RT. 1 M NH_4Cl was used to quench the non-reacted biotin. Oocytes were then washed with PBS and harvested in ice-cold CelLytic M lysis buffer (Sigma, St. Louis, MO) supplemented with proteinase inhibitor mixture (Thermo Scientific, Waltham, MA). Lysates were incubated at RT for 3 hr with gentle shaking upon addition of 100 µl of streptavidin (Pierce). The surface protein absorbed by streptavidin was resuspended in SDS and subjected to SDS-PAGE.

Mammalian cell culture, transfection and treatments

HEK293 cells were cultured in Dulbecco's modified Eagle's medium (DMEM) supplemented with 10% fetal bovine serum (FBS) and 1% penicillin/streptomycin (Sigma). Transient transfection was performed using Lipofectamine 2000 (Invitrogen, Carlsbad, CA) according to the manufacturer's instruction. The palmitoylation inhibitor 2-BP (Sigma) was made as a fresh 100 mM stock in DMSO and applied at a final concentration of 100 µM

overnight. For fatty acid starvation, cells were incubated overnight with DMEM supplemented with 10% FBS treated with 5% dextran-coated charcoal (Sigma).

Confocal imaging

Transfected HEK cells were washed in PBS and fixed in 4% paraformaldehyde for 15 min followed by permeabilization in 0.1% Triton X-100 for 15 min at RT. Cells were then blocked with 3% bovine serum albumin in PBS for 30 min. Where indicated, cells were stained with mouse antibody against Na^+/K^+ ATPase (cat# ab7671, Abcam) or rat 1:200 dilution for 1 hr at RT, followed by incubation with a secondary Cy3-conjugated goat anti-mouse antibody (Jackson ImmunoResearch Laboratories) for 30 min. Cells were then mounted in ProLong® Diamond Antifade Mountant with DAPI (Molecular Probes, Eugene, OR) and examined on an AIVI spinning disc confocal microscopy (University of Alberta).

Acyl-biotin exchange assay

Transfected or treated HEK cells were washed three times in PBS and lysed in 500 µl lysis buffer (LB, 1% IGEPAL CA-630, 50 mM Tris-HCl, pH 7.5, 150 mM NaCl, and 10% glycerol) supplemented with protease inhibitor cocktail (Thermo Scientific) and 50 mM freshly made N-ethylmaleimide (NEM, Thermo Scientific). Acyl-biotin exchange experiments were performed as previously described [36]. In brief, proteins were immunoprecipitated with rabbit anti-Flag antibody (Cat# ab1162, Abcam) and 50% slurry of protein G-coated sepharose beads (GE Healthcare). After three times wash with LB supplemented with 0.1% SDS, each sample of beads was split into two with one incubated with 500 µl LB (pH 7.2) and the other with the same

volume of LB containing 1 M HAM (Sigma) to cleave thioester bond. The samples were rotated at room temperature for 1 hr. After the beads were washed once in pH 6.2 LB, the samples were incubated with 3 μM biotin-BMCC (Thermo Scientific) in LB (pH 6.2) to label the unmasked free thiol groups of cysteine residues. The biotin-conjugated proteins were then eluted with 2X SDS loading buffer, subjected to SDS-PAGE and blotted with streptavidin-HRP antibody (Thermo Scientific) or mouse anti-Flag antibody (Cat# 8146, Cell Signaling Technology, Danvers, MA).

Statistical analysis

Data were analyzed and plotted using SigmaPlot 12 (Systat Software), and expressed as mean ± SD, where SD stands for the standard deviation. One-way ANOVA with a post-hoc test (Bonferroni adjustment) was used to compare two sets of data. A probability value (P) of less than 0.05, 0.01 and 0.001 was considered statistically significant and indicated by "*", "**" and "***", respectively.

5.4 RESULTS

Identification of TRPP3 N-terminal C38 important for its channel function

Our previous report showed importance of the N-terminus of TRPP3 (TRPP3NT, M1-L95) for its Ca^{2+}-activated channel activity when expressed in *Xenopus* oocytes [16]. Consistently, deletion of TRPP3NT abolished the off-response channel activity of the TRPP3/PKD1L3 complex expressed in HEK cells [37]. In order to determine which domain(s)/residue(s) in TRPP3NT is critical for its channel function, we first generated several truncation mutants, named Δ1-20 (with fragment M1-W20 deleted), Δ1-41, Δ1-60, Δ1-81 and Δ1-95 (Fig. 5-1A). When expressed in oocytes, Δ1-20 exhibited similar radiotracer Ca^{2+} transport activity as the wild-type (WT) TRPP3 while the other mutants did not exhibit significant activity (Fig. 5-1B). Consistently, when the whole-cell currents were measured at -50 mV using the TEVC technique, Δ1-20 and WT channels had similar channel function while the other mutants did not produce any appreciable currents (Fig. 5-1C and D). Similar results were obtained when currents were measured at other membrane potentials using a ramp protocol (Fig. 5-1E). We then performed immunofluorescence assays to examine the surface membrane localization of these mutants and found that these mutations do not significantly affect the surface membrane targeting (Fig. 5-1F). Taken together, these data demonstrate that the D21-S41 fragment is important for TRPP3 channel function.

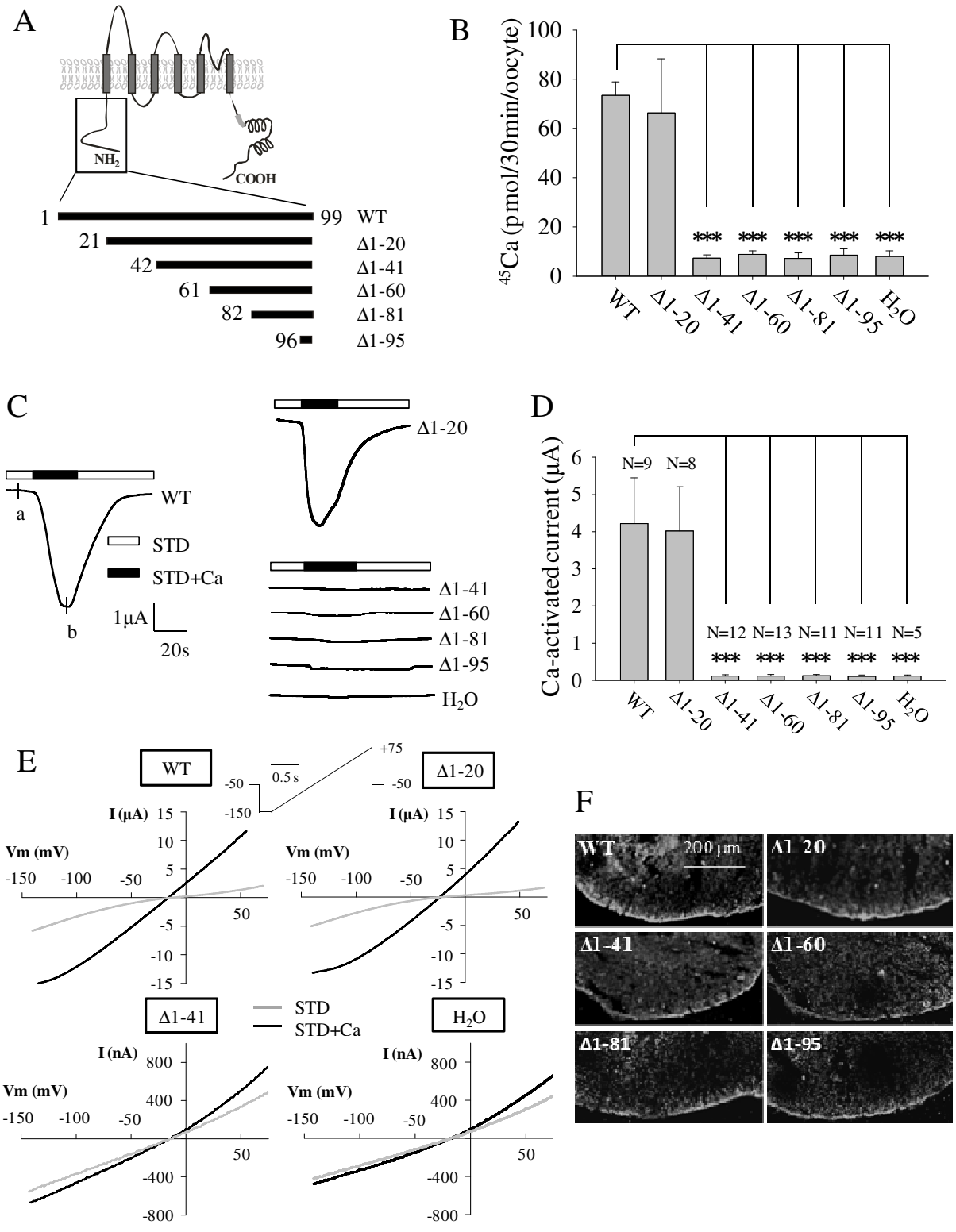

Fig. 5-1. Channel function of human TRPP3 N-terminal truncation mutants. (**A**) Putative membrane topology predicted for TRPP3 (top) and five truncated mutants with indicated positions of the starting amino-acid residue (bottom). (**B**) Radiolabeled ^{45}Ca uptake in *Xenopus*

laevis oocytes expressing TRPP3 wild-type (WT) or mutants at day 3 following RNA injection. Oocytes injected with H_2O were used as a negative control. Data were averaged from three independent experiments. '***' indicates $p < 0.001$. (**C**) Representative whole-cell current traces obtained from *Xenopus* oocytes expressing TRPP3 WT or an indicated truncation mutant, using the two-electrode voltage clamp (TEVC). Oocytes were voltage clamped at -50 mV. Data from H_2O-injected oocytes served as a negative control. Currents were measured using the standard, Na-containing extracellular solution without (STD) or with (STD+Ca) 5 mM $CaCl_2$. (**D**) Averaged Ca-activated currents obtained at -50 mV from oocytes expressing TRPP3 WT or an indicated mutant, or those injected with H_2O. Currents were averaged from three independent experiments with total numbers of tested oocytes, as indicated. '***' indicates $p < 0.001$. (**E**) Representative current-voltage relationship curves obtained using a voltage ramp protocol, as indicated, before (STD) and after (STD+Ca) addition of 5 mM $CaCl_2$ at the time point marked with 'a' and 'b', respectively, in the panel C. (**F**) Representative immunofluorescence data using oocyte slices, showing expression of TRPP3 WT and indicated truncation mutants.

We next performed further mutations truncating at various positions within D21-S41 and found that the function of Δ1-30 and Δ1-36 is similar to WT channel while mutants Δ1-38 and Δ1-40 completely lose their function with unaffected surface membrane localization (Fig. 5-2A and B), indicating that residue V37 or C38 is important for TRPP3 channel function. We then generated single point mutants V37A, C38A and double point mutant V37A/C38A and found that only C38A and V37A/C38A mutations result in substantially reduced channel activity while V37A mutation has little effect on channel activity (Fig. 5-2C-E). Biotinylation assays showed that surface membrane localization is not significantly affected by any of these mutations (Fig. 5-2F). Altogether these data demonstrate that C38, but not V37, is important for TRPP3 channel function.

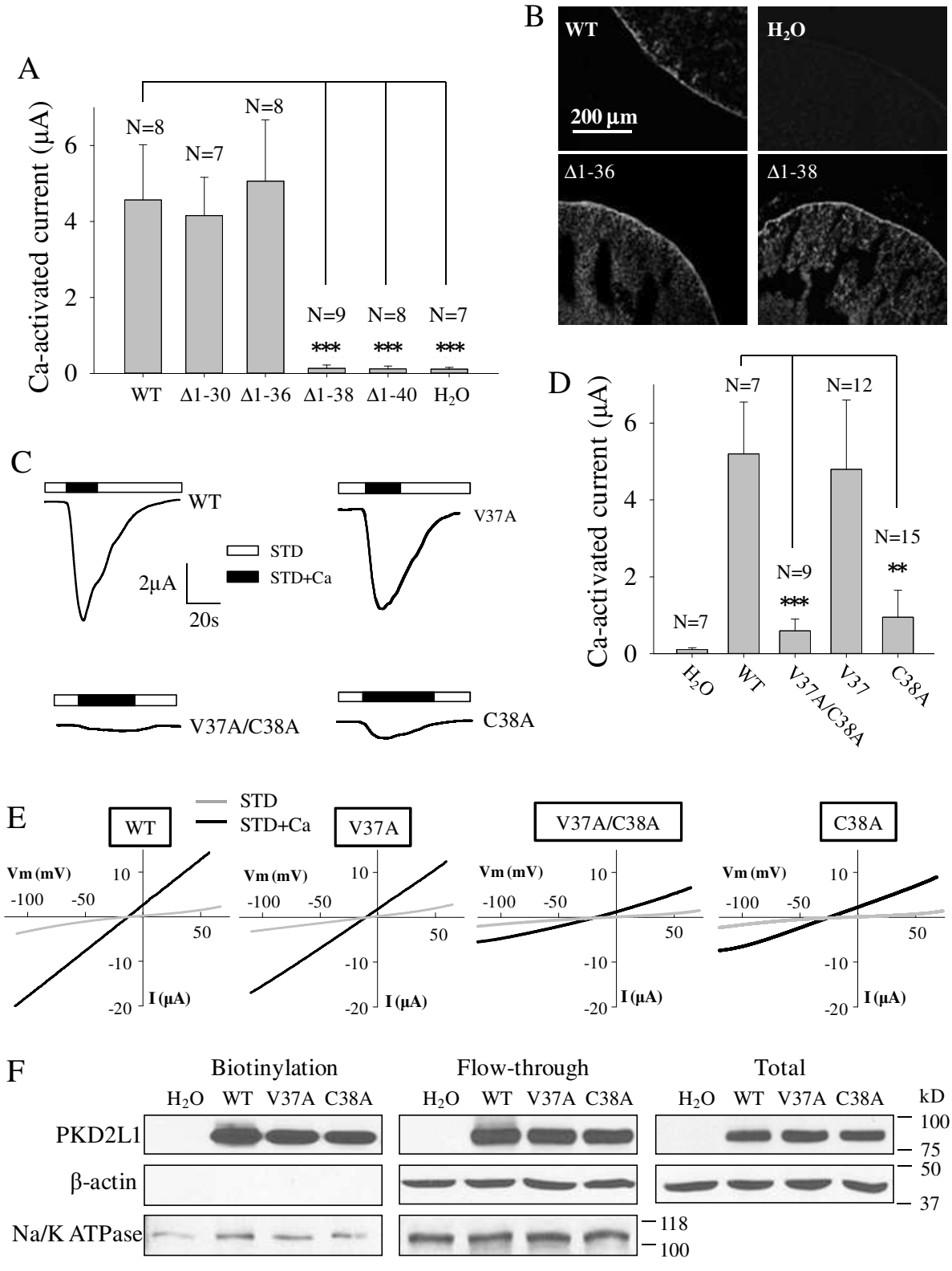

Fig. 5-2. Effects of truncation mutations within D21-S41 and point mutations V37A and C38A on TRPP3 channel function. (**A**) Averaged Ca-activated currents obtained at -50 mV

from oocytes expressing TRPP3 WT or an indicated mutant, or from control oocytes (H_2O). Currents were averaged from three independent experiments with indicated total numbers of tested oocytes. '***' indicates $p < 0.001$. (**B**) Representative immunofluorescence data using oocyte slices, showing expression of TRPP3 WT and indicated truncation mutants. H_2O-injected oocytes served as a negative control. (**C**) Representative whole-cell current traces obtained from oocytes expressing TRPP3 WT, V37A, C38A, or V37A/C38A (double V37A and C38A mutations) using the TEVC technique under similar experimental conditions as those for Fig. 5-1C. (**D**) Averaged Ca-activated currents obtained at -50 mV from oocytes expressing TRPP3 WT, V37A, C38A, or V37A/C38A. Currents were averaged from three independent experiments with indicated total numbers of tested oocytes. '**' and '***' indicates $p < 0.01$ and 0.001, respectively. (**E**) Representative current-voltage relationship curves obtained using a voltage ramp protocol, as indicated in Fig. 5-1E, before (STD) and after (STD+Ca) addition of 5 mM $CaCl_2$. (**F**) Left panel, representative data on the plasma membrane (PM) expression of TRPP3 by biotinylation. Na^+/K^+ ATPase (PM marker) and β-actin (non-PM markers) were used as controls. Centre and right panels, flow-through and total input data, respectively, from the same experiment.

Palmitoylation of TRPP3 at C38

We next examined the functional role of the other cysteine residues located outside the putative intra-membrane helices, including C69, C70, C74, C210, C223 and C512 (Fig. 5-3A). Mutations of these cysteine residues to alanine did not affect channel function (Fig. 5-3B). Thus, C38, highly conserved among various species (Fig. 5-3C), is the only functionally important cysteine residue outside the putative membrane helices. Of note, based on sequence alignment, TRPP3 C512 and its counterpart in human TRPP2, C631, are both located within the short helix of their TM5-TM6 pore loop. Interestingly, TRPP2 C631 was previously reported to be involved in disulfide bond formation and be essential for its tetrameric assembly and channel function in HEK cells [38]. Due to the presence of reducing cytosolic environments it is unlikely that C38 forms a disulfide bond with another cysteine residue from the same or a different TRPP3 monomer subunit. We thus wondered how C38 contributes to TRPP3 channel function.

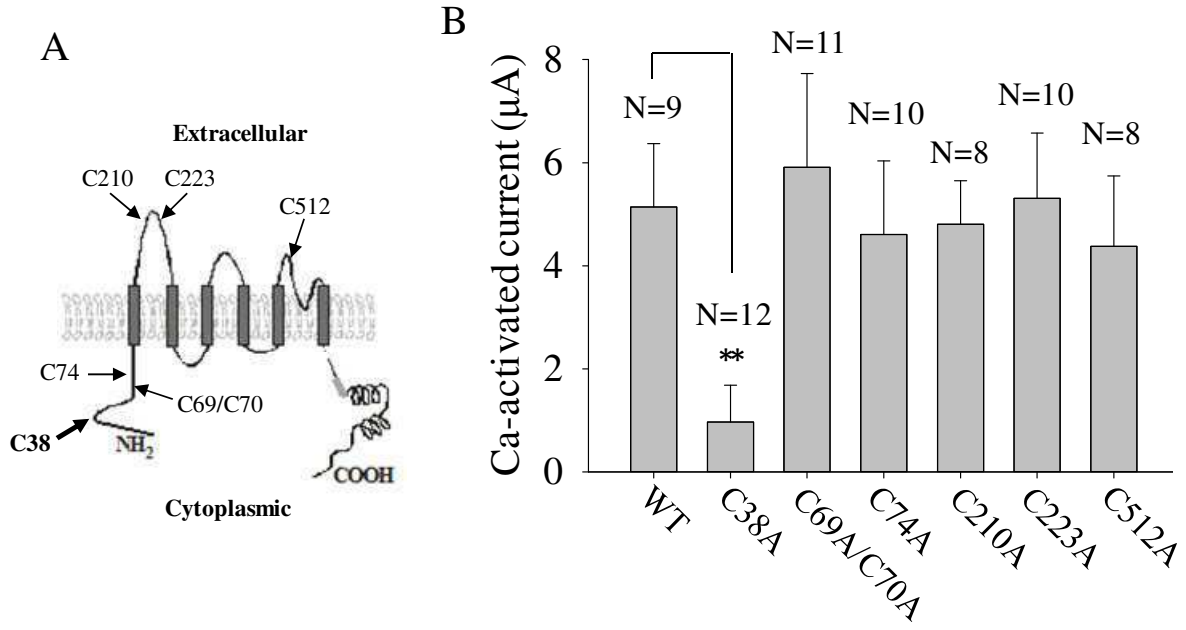

C

C38

Human	21	PHGTLRV**C**TISSTGP	45
Mouse	21	PNRTLRI**C**TVSSVAL	45
Rat	21	PNGTPRI**C**TVSSVAL	45
Monkey	21	PHGTLRV**C**TISSTGP	45
Pig	21	PQEMLRI**C**TISTAAL	45
Rabbit	21	PHGTLRI**C**TISNPVT	45
Cat	21	PHGTLRI**C**TISSVMP	45
Dog	352	PRGTLKI**C**TISSAMP	366

D

CSS-Palm v4.0	Peptide	Position	Score
TRPP3 N-terminus	PHGTLRV**C**TISSTGP	38	8.51
	YRTQVSS**C**CLHICQG	69	5.048
	RTQVSSC**C**LHICQGI	70	5.292
	SSCCLHI**C**QGIRGLW	74	1.676

Fig. 5-3. Characterization of the TRPP3 other intracellular or extracellular cysteine residues and prediction of candidate palmitoylation residues. (**A**) Schematic illustration of all intracellular or extracellular cysteine residues in human TRPP3. (**B**) Averaged Ca-activated

currents obtained at -50 mV from oocytes expressing TRPP3 WT or an indicated mutant. Currents were averaged from three independent experiments with indicated total numbers of tested oocytes. '**' indicates $p < 0.01$. (**C**) Amino acid sequence alignment of TRPP3 N-terminal fragments containing C38 or the corresponding cysteine from indicated species. National Center for Biotechnology Information accession number for sequences used here are NP_057196 (human), NP_852087 (mouse), NP_001099822 (rat), XP_001168415 (monkey), XP_012999134 (pig), XP_002718661 (rabbit), XP_006938169 (cat) and XP_005637930 (dog). Potential phosphorylation sites near the cysteine residue are marked with '•' (**D**) Palmitoylation scores for cysteine residues in the human TRPP3 N-terminus predicted by a CSS-palm v4.0 algorithm (http://csspalm.biocuckoo.org/online.php). A higher score value indicates a higher probability.

Recently, more and more ion channel proteins, such as the large conductance voltage-gated (BK) potassium channel and TRPML1, have been reported to be post-translationally modified by palmitoylation at cysteine residues to regulate channel trafficking and/or function [31-33]. We then investigated whether TRPP3 C38 is a palmitoylation site. First we used palmitoylation prediction program CSS-Palm v4.0 and found that C38 has the highest palmitoylation score compared with the other N-terminal cysteine residues, C69, C70 and C74 (Fig. 5-3D). We then treated TRPP3-expressing oocytes with widely used palmitoylation inhibitor 2-bromopalmitate (2BP) [31] overnight at various concentrations from 1 μM to 50 μM, according to a previous report [39]. TRPP3 channel currents measured at -50 mV and other membrane potentials were indeed reduced by 2BP in a dose-dependent manner (Fig. 5-4A-C). Because immunofluorescence assays found that 2BP treatment has no effect on the TRPP3 plasma membrane expression (Fig. 5-4D), our data showed that 2BP treatment results in an inhibition of TRPP3 channel function in oocytes. To verify the specificity of the 2BP effect on TRPP3 channel function, we wonder whether the inhibitory effect of 2BP on TRPP3 channel function can be competitively rescued by palmitic acid (PA), the natural substrate of the palmitoylation catalyzed by DHHC enzymes. For this, we treated TRPP3-expressing oocytes overnight with increasing concentrations of PA, from 0 to 20 μM, in the presence of 20 μM 2BP

which inhibited 80% of TRPP3 channel activity (Fig. 5-4B). Indeed, the inhibition of TRPP3 channel activity (measured at -50 mV or other membrane potentials) by 2BP was rescued by PA in a dose-dependent manner (Fig. 5-5A-C). Again, we confirmed that TRPP3 surface membrane localization is not affected by these treatments, as shown by immunofluorescence data in oocytes (Fig. 5-5D). Thus, our rescue experiments using PA supported a specific effect of 2BP on TRPP3

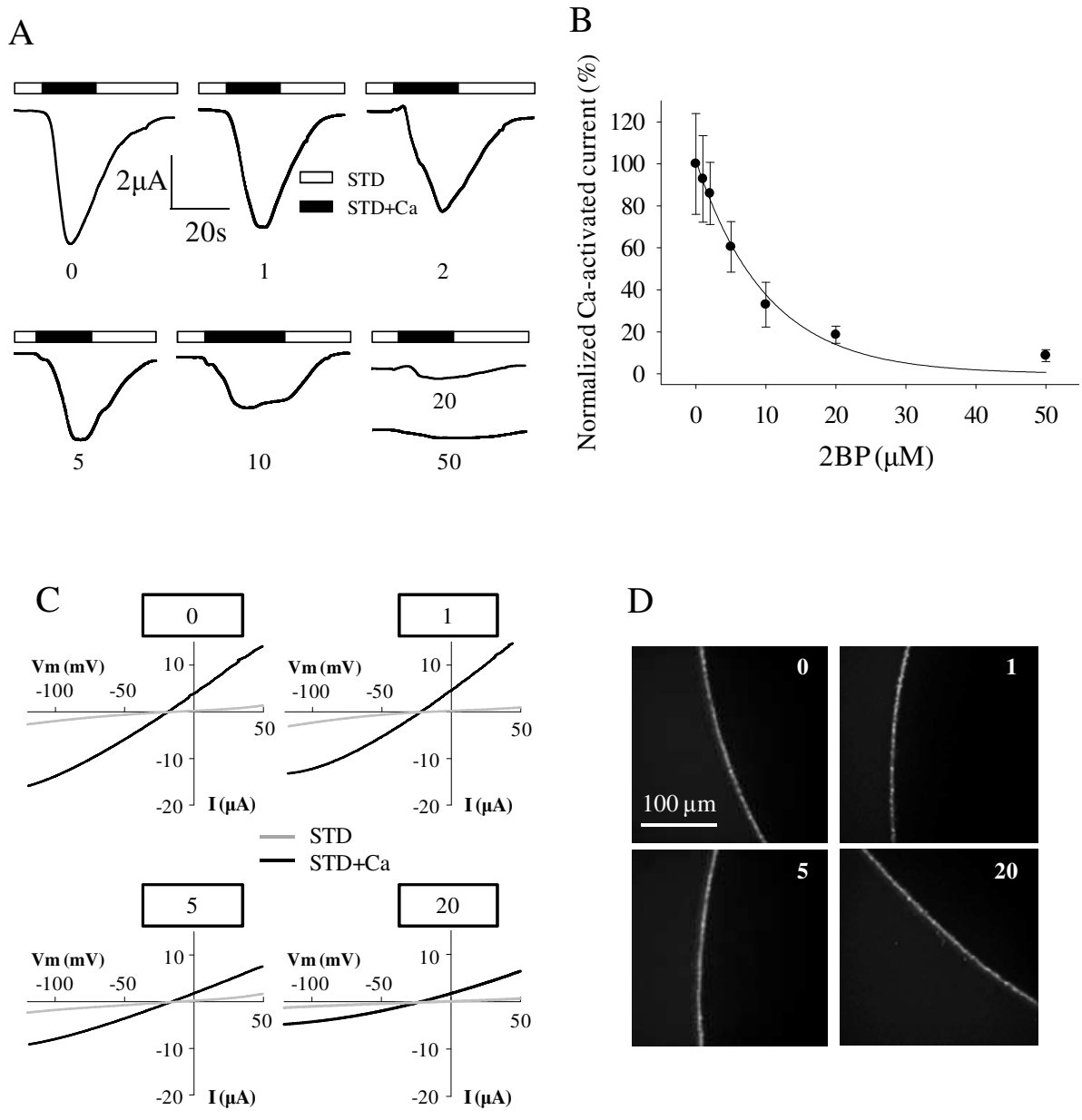

Fig. 5-4. Effect of palmitoylation inhibitor 2-bromopalmitate (2BP) on TRPP3 channel activity. (**A**) Representative whole-cell current traces obtained at -50 mV from oocytes expressing TRPP3, treated with DMSO (0.05% in Barth's solution) dissolving different concentrations of 2BP (in μM, 0, 1, 2, 5, 10, 20 and 50) overnight before current measurements with the TEVC. (**B**) Averaged Ca-activated currents obtained at -50 mV from oocytes expressing TRPP3 under similar treatments as those in panel A to show concentration dependent inhibition of Ca-activated TRPP3 channel activity by 2BP. Currents were averaged from three independent experiments and normalized to that of TRPP3-expressing oocytes without 2BP treatment. (**C**) Representative current-voltage relationship curves obtained using a voltage ramp protocol before (STD) and after (STD+Ca) addition of 5 mM $CaCl_2$. Oocytes expressing TRPP3 were incubated with indicated concentrations of 2BP. (**D**) Representative whole-mount immunofluorescence data showing the PM expression of TRPP3 WT in oocytes treated with indicated concentrations of 2BP.

channel function. We also treated TRPP3-expressing oocytes overnight with PA alone, from 1 μM to 20 μM, but found no effect on TRPP3 channel activity (Fig. 5-5E), which suggests that there may be saturated amount of endogenous PA or its equivalent in oocytes. Taken together, these data strongly indicated that TRPP3 is modified by palmitoylation which is important for TRPP3 channel function, but not trafficking, in *Xenopus* oocytes.

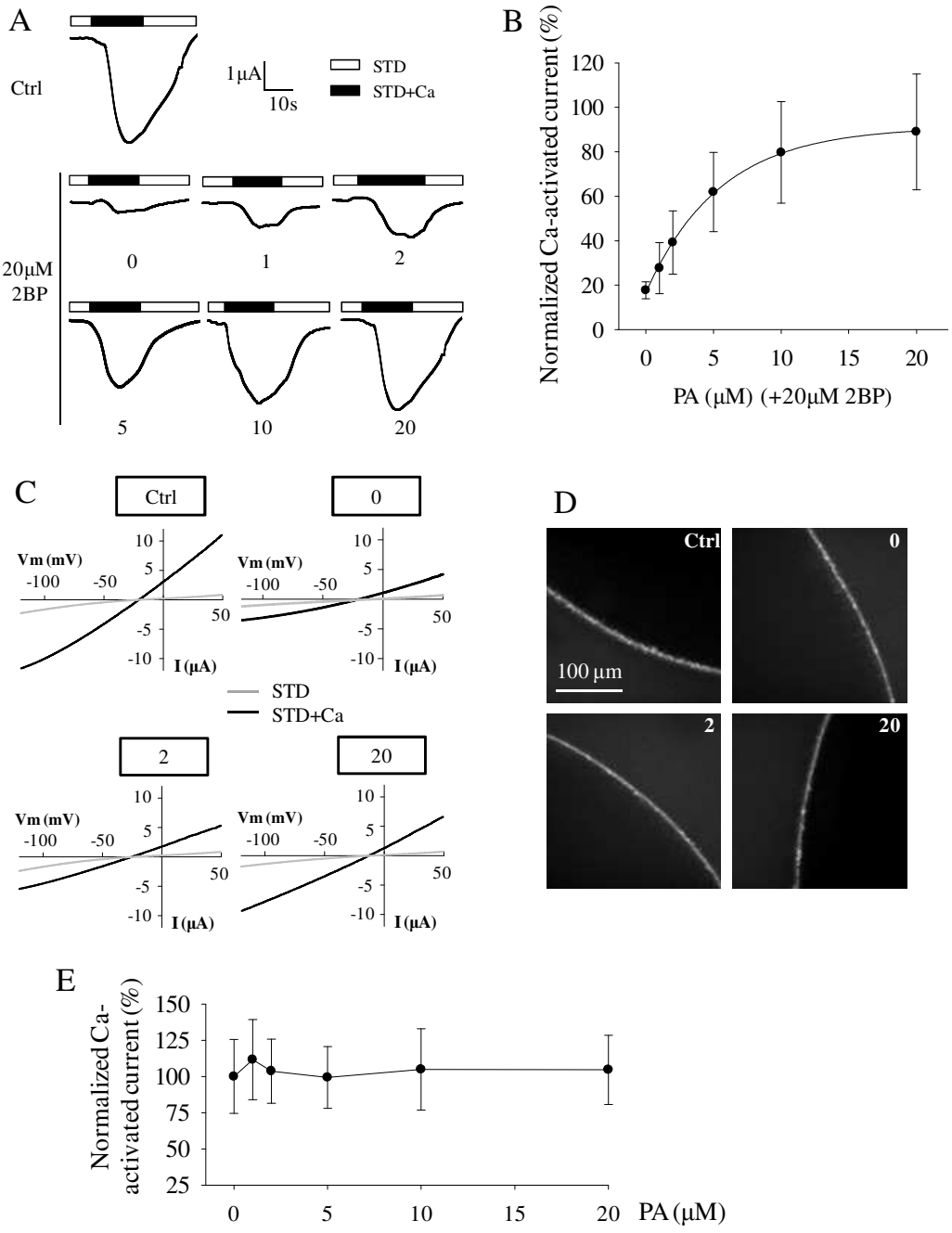

Fig. 5-5. Rescuing effect of palmitic acid (PA) on 2BP-mediated TRPP3 channel activity inhibition. (**A**) Representative whole-cell current traces obtained at -50 mV from oocytes expressing TRPP3, treated with different concentrations of PA (in μM, 0, 1, 2, 5, 10 and 20) in the presence of 20 μM 2BP overnight before current measurements with TEVC technique. The TRPP3-expressing oocytes treated with DMSO (0.1% in Barth's solution) were designated as Ctrl. (**B**) Averaged Ca-activated currents obtained at -50 mV from oocytes expressing TRPP3 under similar treatments as those in panel A to show concentration-dependent rescue of 2BP-elicited TRPP3 channel activity inhibition by PA. Currents were averaged from three

independent experiments and normalized to that of Ctrl (0.1% DMSO in Barth's solution). (**C**) Representative current-voltage relationship curves obtained using a voltage ramp protocol before (STD) and after (STD+Ca) addition of 5 mM $CaCl_2$. Oocytes expressing TRPP3 were similarly treated as in panel A. (**D**) Representative whole-mount immunofluorescence data showing the PM expression of TRPP3 in oocytes similarly treated as in panel A. (**E**) Effect of PA on TRPP3 channel activity. Oocytes expressing TRPP3 were treated with different concentrations of PA (in μM, 0, 1, 2, 5, 10 and 20) overnight before current measurement. Currents were normalized to the values with 0 PA.

We next wanted to provide further documents on the TRPP3 C38 palmitoylation. It is known that palmitoylation of a transmembrane domain containing protein allows its cytosolic domains to anchor to the plasma membrane [40]. We thus examined whether C38 confers palmitoylation and attachment of the N-terminal domain of TRPP3 to the plasma membrane. For this, we over-expressed EGFP-fused human TRPP3 N-terminus, M1-L95 (EGFP-TRPP3NT) in HEK cells and detected EGFP epifluorescence to determine TRPP3NT cellular localization using confocal microscopy. We found that EGFP-TRPP3NT indeed shows plasma membrane expression while EGFP-TRPP3CT (a TRPP3 C-terminal fragment, E706-S805, as a negative control) exhibits intracellular distribution only (Fig. 5-6A). As expected, EGFP-N-Ras (a positive control), a well-known palmitoylated oncoprotein, also attached to the plasma membrane in our experimental condition (Fig. 5-6A), consistent with its previously reported plasma membrane localization in COS-7 cells [41]. To determine whether the plasma membrane expression of EGFP-TRPP3NT is due to palmitoylation, we attempted to disrupt palmitoylation by starving HEK cells in a fatty acid-free medium or treating cells with the palmitoylation inhibitor 2BP (100 μM) overnight, as previously reported [41]. Under both conditions, EGFP-TRPP3NT was found to stay in the cytoplasm (Fig. 5-6B), indicating that palmitoylation is required for the plasma membrane targeting of TRPP3NT. Similar results were also obtained for EGFP-N-Ras (Fig. 5-6B), which is consistent with the previous report using COS-7 cells [41].

Furthermore, C38A mutation also resulted in stay of EGFP-TRPP3NT in the cytoplasm (Fig. 5-6B).

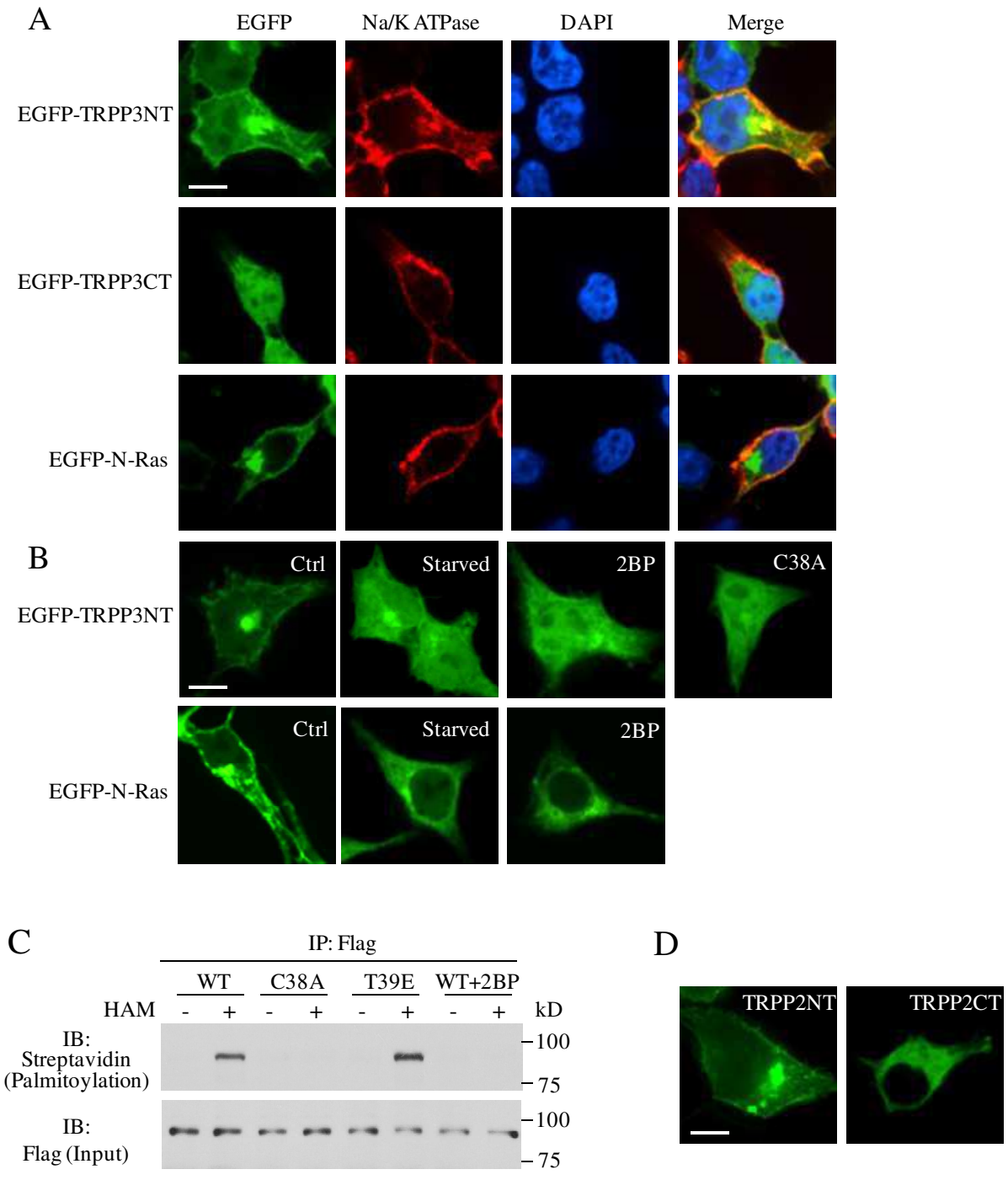

Fig. 5-6. Effects of 2BP and mutation C38A on the plasma membrane anchorage of TRPP3NT and palmitoylation of TRPP3 at C38. (**A**) Representative confocal images showing

subcellular localization of EGFP-TRPP3NT (EGFP fused the TRPP3 N-terminus, M1-L95), EGFP-TRPP3CT (EGFP fused the TRPP3 C-terminal fragment E706-S805, as a negative control) and EGFP-N-Ras (EGFP fused with human N-Ras, as a positive control) in HEK cells. Scale Bar = 10 μm. (**B**) Subcellular localization of EGFP-TRPP3NT and EGFP-N-Ras in HEK cells without (Ctrl) or with fatty acid starvation, with 100 μM 2BP treatment overnight, or with the C38A mutation. Scale Bar = 10 μm. (**C**) Palmitoylation of Flag-TRPP3 in HEK cells detected by immunoprecipitation - acyl-biotin exchange assays. See Experimental Procedures for method details. Cells were transfected with WT Flag-tagged TRPP3, mutant C38A or T39E. 2BP treatment was as in panel B. Palmitoylated TRPP3 proteins were detected with streptavidin-HRP antibody and total immunoprecipitated TRPP3 proteins (Input) were detected with Flag antibody. Shown are representative immunoblots from three independent experiments. (**D**) Representative confocal images showing subcellular localization of EGFP-TRPP2NT (EGFP fused the TRPP2 N-terminus, M1-K215) and EGFP-TRPP2CT (EGFP fused theTRPP2 C-terminus, D682-V968) in HEK cells. Scale Bar = 10 μm.

We next performed acyl-biotin exchange assay to directly determine whether TRPP3 is palmitoylated. For this we transiently transfected Flag-tagged TRPP3 WT and mutants C38A and T39E in HEK cells. TRPP3 was first immunoprecipitated with a rabbit anti-Flag antibody and protein G-coated sepharose beads. Immunoprecipitated TRPP3 proteins were then treated either with hydroxylamine (HAM) to remove palmitate, or with Tris base as a negative control. The exposed cysteine thiol groups were labelled with a thiol-reactive biotinylation reagent, biotin-BMCC. The streptavidin-HRP antibody was then used to detect the palmitoylated TRPP3 and a mouse anti-Flag antibody to detect total immunoprecipitated TRPP3. We indeed found that TRPP3 and mutant T39E, but not mutant C38A, are modified by palmitoylation (Fig. 5-6C). Furthermore, the TRPP3 palmitoylation was abolished by 2BP treatment overnight at concentration of 100 μM (Fig. 5-6C). These data together demonstrated that TRPP3 is indeed palmitoylated at C38, which accounts for our observation that the plasma membrane targeting of TRPP3NT requires palmitoylation at C38. Interestingly, the N-terminus of TRPP2 (EGFP-TRPP2NT, M1-K215) that possesses four cysteine residues also targeted to the plasma membrane when over-expressed in HEK cells while the C-terminus of TRPP2 (EGFP-

TRPP2CT, D682-V968) showed a cytosolic distribution (Fig. 5-6D), suggesting that the N-terminal palmitoylation is a shared mechanism by TRPP3 and TRPP2.

Phosphorylation of TRPP3 at T39

Since there have been reports about an interplay between palmitoylation and phosphorylation at a nearby site [40,42,43], we next examined potential phosphorylation sites near C38. Five candidate phosphorylation sites, T34, T39, S41, S42 and T43 are predicted in human TRPP3 by GPS 3.0 program (Fig. 5-3C). First, mutating any of these five sites to alanine did not affect channel function [34], suggesting either that these sites are not important or that expressed TRPP3 channels are predominantly de-phosphorylated channel at one of these sites in *Xenopus* oocytes. We then mutated each of them to E, to mimic phosphorylation and found that only mutation T39E significantly affects (substantially reduces) the channel function, while no mutation significantly alters the surface membrane localization (Fig. 5-7A and B). Together with our observation that mutant T39D, compared with T39E, exhibited similarly impaired channel function and similar surface membrane localization (Fig. 5-7A and B), our data suggest that T39 is a functionally important phosphorylation site, which is consistent with the fact that T39 is conserved among different species (Fig. 5-3C).

We next further examined T39 phosphorylation by Western blotting using human TRPP3NT with an N-terminal HA tag. When HA-TRPP3NT was transiently expressed in HEK cells, double bands were observed (Fig. 5-7C, left panel). The upper band disappeared following treatment by lambda phosphatase (λPP) (Fig. 5-7C, left panel), which removes all phosphate groups from serine, threonine and tyrosine residues. As a positive control, we found that human TRPP2NT, previously reported to be phosphorylated at S76 [23], also displays double bands under

our experimental conditions and that the upper band disappears by λPP treatment (Fig. 5-7C, right panel). Furthermore, mutation of T39 to A, but not S41 to A, eliminated the upper band of TRPP3NT (Fig. 5-7D). Taken together, our data indicate that TRPP3 is phosphorylated at N-terminal T39.

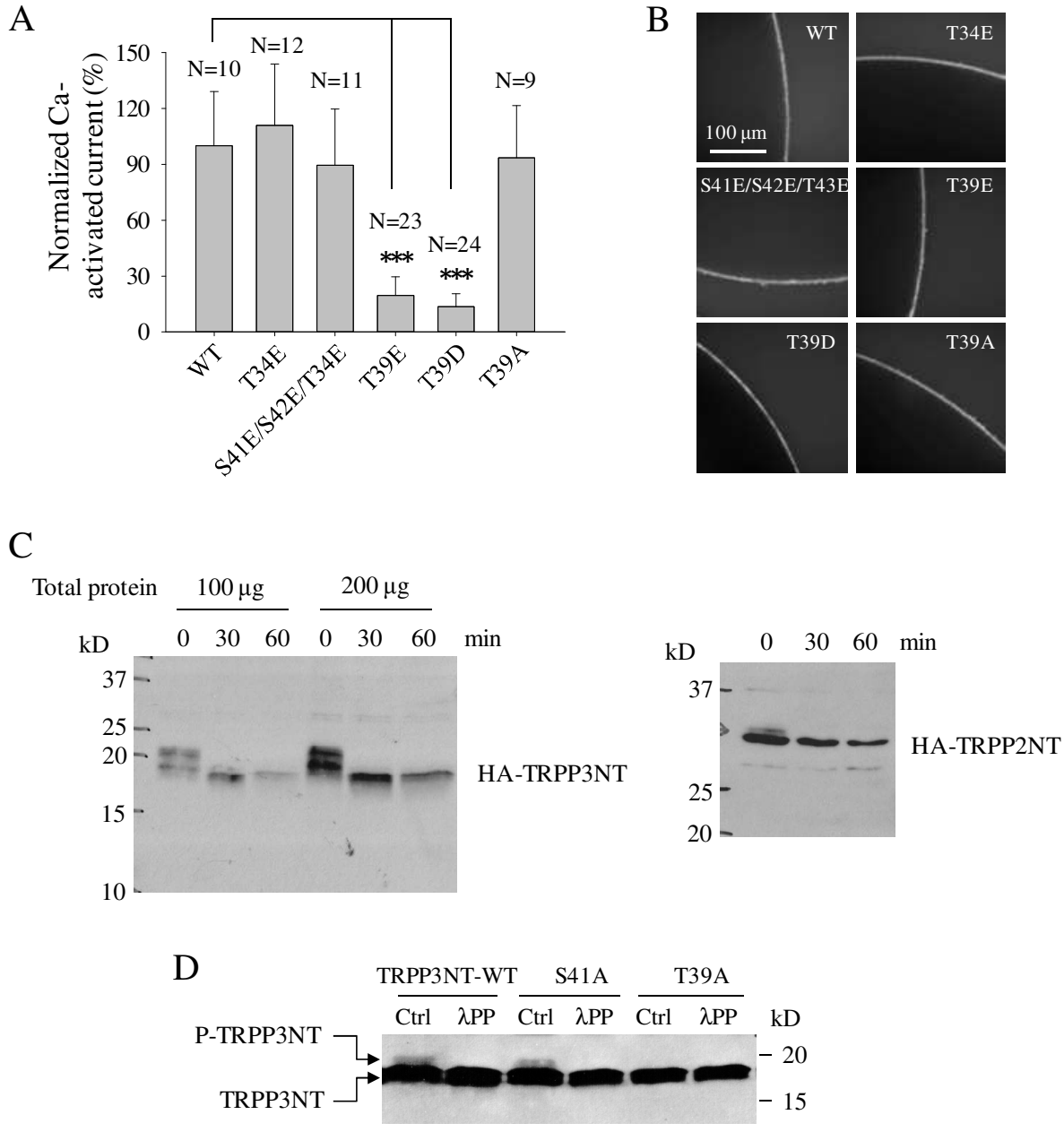

Fig. 5-7. Roles of T39 and its phosphorylation in regulating TRPP3 channel function. (**A**) Averaged currents obtained from oocytes expressing TRPP3 WT, T34E, S41E/S42E/T43E

(triple S41E, S42E and T43E mutations), T39E, T39D or T39A. Currents at -50 mV were averaged from three independent experiments with indicated total numbers of tested oocytes and normalized to that of TRPP3 WT. '***' indicates $p < 0.001$. (**B**) Representative whole-mount immunofluorescence data showing the PM expression of TRPP3 WT or a mutant in oocytes. (**C**) Phosphorylation state of the TRPP3 N-terminus assessed by lambda phosphatase (λPP) treatment. HA-tagged TRPP3NT and TRPP2NT (as a positive control) were transfected into HEK cells of which cell lysates were treated with λPP for indicated periods of time. Shown are representative blots from three independent experiments. (**D**) Phosphorylation of TRPP3NT WT and TRPP3NT containing the S41A or T39A mutation. These three constructs were transfected into HEK cells, and resulting cell lysates were treated without (Ctrl) or with λPP for 30 min. Shown are representative blots from three independent experiments.

Relationship between palmitoylation at C38 and phosphorylation at T39

We next investigated whether there is a correlation between palmitoylation at C38 and phosphorylation at T39 of TRPP3, given the presence of an interplay between these two types of post-translational modifications in some membrane proteins [31,42-44]. For this we examined whether the C38A mutation or de-palmitoylation reduces TRPP3 channel activity through increasing phosphorylation at T39. First, introduction of the C38A mutation to the WT and T39A mutant channels resulted in similar reduction of channel activity (Fig. 5-8A). Second, treatment of oocytes expressing mutant T39A or WT TRPP3 with 20 μM 2BP resulted in similar reduction of channel activity (Fig. 5-8A). As these mutations and 2BP treatments did not significantly affect surface membrane expression (Fig. 5-8B), we concluded that reduction of TRPP3 channel activity by de-palmitoylation is not through increasing phosphorylation at T39. This conclusion was supported by our observation that C38A has little effect on the upper band of TRPP3NT (Fig. 5-8C).

Conversely, we examined whether the T39E mutation, which mimics phosphorylation at T39, reduces TRPP3 channel activity through decreasing palmitoylation at C38. Introduction of the T39E mutation to C38A mutant that cannot be palmitoylated further significantly reduced

TRPP3 channel activity (Fig. 5-8D) without affecting plasma membrane expression (Fig. 5-8B), indicating that inhibition of TRPP3 channel function by phosphorylation at T39 is not through decreasing palmitoylation at C38. Furthermore, the T39E mutation had little effect on the plasma membrane localization of TRPP3NT (Fig. 5-8E) and palmitoylation of full-length TRPP3 at C38 (Fig. 5-6C). Taken together, these data showed that TRPP3 channel activity is regulated by palmitoylation at C38 and phosphorylation at T39 rather independently.

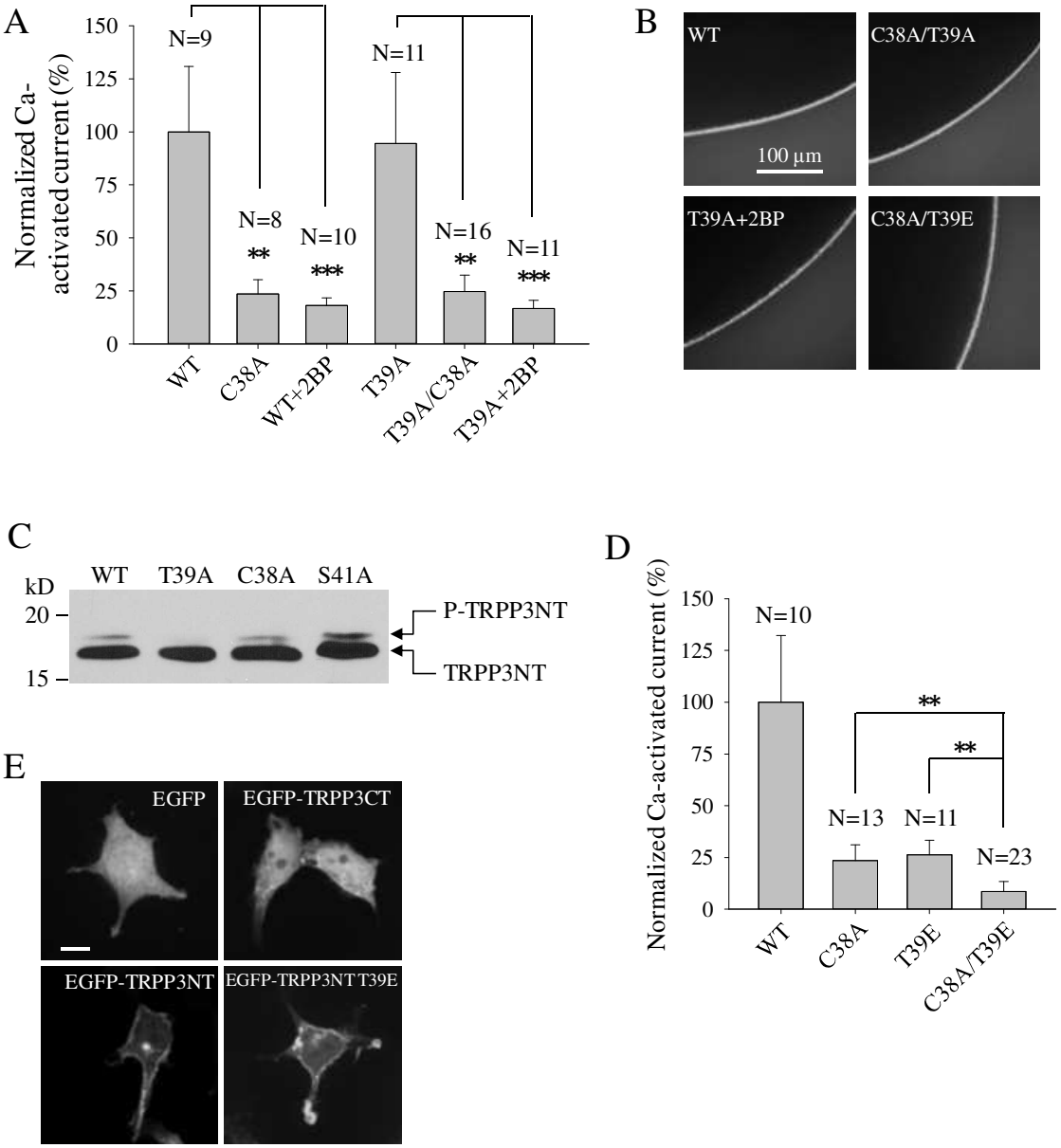

Fig. 5-8. Relationship between palmitoylation at C38 and phosphorylation at T39. (A) Averaged Ca-activated currents obtained at -50 mV from oocytes expressing TRPP3 WT without or with 20 μM 2BP treatment (WT+2BP), C38A, T39A without or with 20 μM 2BP treatment (T39A+2BP), or C38A/T39A (double C38A and T39A mutations). Currents were averaged from three independent experiments with indicated total numbers of tested oocytes and normalized to that of TRPP3 WT. '**' and '***' indicates $p < 0.01$ and 0.001, respectively. (**B**) Representative whole-mount immunofluorescence data showing the PM expression of TRPP3 WT, C38A/T39A, C38A/T39E and T39A with 20 μM 2BP treatment (T39A+2BP). (**C**) Phosphorylation of TRPP3NT WT, and TRPP3NT with the T39A, C38A or S41A mutation in HEK cells. (**D**) Averaged and normalized currents obtained at -50 mV from oocytes expressing TRPP3 WT, C38A, T39E or C38A/T39E. Currents were averaged from three independent experiments with indicated total numbers of tested oocytes and normalized to that of TRPP3 WT. '**' indicates $p < 0.01$. (**E**) Representative confocal images showing subcellular localization of EGFP, EGFP-TRPP3CT, EGFP-TRPP3NT and EGFP-TRPP3NT T39E in HEK cells. Scale Bar = 10 μm.

5.5 DISCUSSION

Not much have so far been known about TRPP3 post-translational modifications although its homologue TRPP2 was reported to undergo phosphorylation, glycosylation and disulfide bond formation [22,24,38]. In this study, we found that TRPP3 is modified by palmitoylation and phosphorylation at the N-terminal cysteine 38 and threonine 39, respectively, and showed that these two post-translational modifications independently regulate TRPP3 channel function.

Palmitoylation is a dynamic post-translational modification that was first described 35 years ago in a transmembrane glycoprotein of vesidular stomatitis virus [45]. 8 years later in 1987, the first palmitoylated ion channel, rodent voltage-gated Na^+ channel, was characterized [46]. Since then, more than 50 different ion channels have been experimentally demonstrated to be palmitoylated [31]. Increasing evidence has so far indicated that palmitoylation may regulate either the channel's membrane density or single channel activity [31]. In the case of TRPP3, palmitoylation at C38 had little effect on its plasma membrane expression, at least in *Xenopus* oocytes (Fig. 5-2F), but dramatically reduced its channel activity (Fig. 5-2D) by a to-be-identified mechanism that is independent of phosphorylation at T39. A surprising characteristic of TRP channels is that they can be activated by a wide variety of environmental stimuli. A shared mechanism underlying gating of TRPs by seemingly disparate activators was recently proposed by Montell based on the discovery that a phospholipase C-dependent signaling cascade activates TRP channels in *Drosophila* photoreceptor cells through generation of force in lipid bilayer [47]. According to this theory, besides known mechano-sensitive TRP channels, other TRPs are also activated through mechanical forces formed by architectural changes in the cell membrane in response to different stimuli [47]. TRPP2 was known to be co-localized with PKD1 in

primary cilia of kidney cells where it is believed to act as part of a mechanical sensor [48]. On the other hand, TRPP3 was reported to be co-localized with PKD1L1 in cilia [20] even though it remains unclear as to whether it is mechano-sensitive. It is generally assumed that palmitoylation facilitates the association of the protein to the membrane. Therefore, it is possible that TRPP3 palmitoylation has an interplay with the mechanical force exercised on the cell membrane with respect to channel gating. Alternatively, it remains to be determined whether palmitoylation regulates TRPP3 channel activity through facilitating an intramolecular interaction between its N-terminal pre-S1 and C-terminal TRP domains. This type of interaction was suggested to occur in TRPV1, TRPV2, TRPA1 and TRPV6 based on structural information revealed using cryo-EM or crystallography [3-6].

TRPP3 is expressed in the brain [14] and a recent study using TRPP3 knockout mice found that disruption of TRPP3 causes hippocampal and thalamocortical hyperexcitability and increases susceptibility to pentylenetatrazol-induced seizure [49]. Interestingly, several neural proteins, including various G-protein- coupled receptors and ion channels which control the excitability of neurons, have now been reported to be dynamically regulated by palmitoylation [50]. It would be interesting to see whether palmitoylation of TRPP3 at C38 represents a mechanism underlying the control of TRPP3 channel activity in neurons with respect to neuronal excitability. On the other hand, TRPP3 was also found to interact with β2-adrenoceptor (β2AR) and co-localize with β2AR in the brain [49]. Binding of agonist isoproterenol to β2AR was reported to markedly reduce the palmitoylation of the associated $G\alpha_s$ [51]. Thus, it is possible that β2AR regulates TRPP3 palmitoylation through physical binding. Further, β2AR itself is also palmitoylated and agonist-stimulated de-palmitoylation of β2AR was reported to promote its phosphorylation and β-arrestin-mediated receptor internalization [28]. Therefore, it would be

interesting to see whether there is an interplay between TRPP3 palmitoylation and β2AR, and how this interplay is regulated and whether it is involved in the control of neuronal excitability.

Post-translational modifications of TRP channels, such as glycosylation, phosphorylation, and covalent/reversible binding of an activator to a cysteine residue, mainly affect their subcellular trafficking or channel activity [52]. To date, within the TRP superfamily only TRPML1 is known to be palmitoylated, both in a heterologous expression system and native stomach tissue, for regulation of its endocytosis [32,33]. Thus, TRPP3 represent the first TRP member whose channel function is regulated by palmitoylation. It would thus be important to examine whether the function of other TRPs is also regulated by palmitoylation and to investigate the physiological implications of this type of post-translational modification. Palmitoylation is mostly mediated by a family of 23 (human) DHHC motif-containing palmitoyltransferases with unclear substrate specificities [40]. De-palmitoylation, on the other hand, is mediated by acylprotein thioesterases (APTs) including APT1, APT2 and APT-like [40]. Future studies would have to determine which DHHC enzyme(s) and APT(s) are involved in TRPP3 palmitoylation and de-palmitoylation.

Phosphorylation at C-terminal S812 of TRPP2 by casein kinase II regulates its channel function while phosphorylation at N-terminal S76 by glycogen synthase kinase 3 regulates its subcellular localization [22,23]. Although phosphorylation of TRPP3 at N-terminal T39 abolishes its channel function, we still don't know which kinase is involved. Prediction by GPS 3.0 program suggests that a PKC kinase phosphorylates TRPP3 at T39. Of note, the fact that mutant T39A displayed a similar functional activity as the WT channel suggests that TRPP3 channels in oocytes are mostly de-phosphorylated, which is consistent with our data obtained from Western blotting experiments (Fig. 5-7D). It is also interesting to determine whether TRPP3 is

phosphorylated at other sites and, if any, what are the corresponding functional roles. Further, although palmitoylation at C38 and phosphorylation at T39, the only phosphorylation site proximate to C38, are both functionally important for TRPP3, our experiments showed that they are not linked to each other. This is in contrast to previously reported ion channels with respect to an interplay between the two modifications. Eg, large conductance Ca^{2+}- and voltage-gated K^{+} channels were found to be inhibited by PKA phosphorylation of a C-terminal serine residue, immediately upstream of a conserved palmitoylated cysteine residue, through reducing palmitoylation to disrupt the anchorage of their C-terminus to the plasma membrane [42]. Thus, it could be that TRPP3 palmitoylation at C38 is not linked to any phosphorylation or to a phosphorylation that is not close to C38, which would suggest that TRPP3 palmitoylation may represent a novel and yet-to-be determined way of functional regulation. Since both phosphorylation and palmitoylation are of dynamic and reversible regulation mechanisms, it would be important to elucidate how the function of other TRPs is regulated by the two modifications and examine potential cross-talk between them.

In summary, our current study has identified N-terminal C38 as a palmitoylation site that mediates anchorage of the N-terminus to the surface membrane and regulates TRPP3 channel function. We have also identified N-terminal T39 as a phosphorylation site critical for TRPP3 channel function. Further, we have shown that the palmitoylation and phosphorylation independently regulate TRPP3 channel function, which we think may represent a novel mechanism of regulation that deserves further studies.

5.6 REFERENCES

1. Clapham, D. E. TRP channels as cellular sensors. *Nature.* **426**, 517-524 (2003).

2. Venkatachalam, K. & Montell, C. TRP channels. *Annu. Rev. Biochem.* **76:387-417.**, 387-417 (2007).

3. Liao, M., Cao, E., Julius, D. & Cheng, Y. Structure of the TRPV1 ion channel determined by electron cryo-microscopy. *Nature.* **504**, 107-112 (2013).

4. Paulsen, C. E., Armache, J. P., Gao, Y., Cheng, Y. & Julius, D. Structure of the TRPA1 ion channel suggests regulatory mechanisms. *Nature.* **520**, 511-517 (2015).

5. Zubcevic, L. *et al.* Cryo-electron microscopy structure of the TRPV2 ion channel. *Nat. Struct. Mol. Biol.* **23**, 180-186 (2016).

6. Saotome, K., Singh, A. K., Yelshanskaya, M. V. & Sobolevsky, A. I. Crystal structure of the epithelial calcium channel TRPV6. *Nature* **534**, 506-511 (2016).

7. Mochizuki, T. *et al.* PKD2, a gene for polycystic kidney disease that encodes an integral membrane protein. *Science.* **272**, 1339-1342 (1996).

8. Huang, A. L. *et al.* The cells and logic for mammalian sour taste detection. *Nature.* **442**, 934-938 (2006).

9. Ishimaru, Y. *et al.* Transient receptor potential family members PKD1L3 and PKD2L1 form a candidate sour taste receptor. *Proc. Natl. Acad. Sci. U. S. A.* **103**, 12569-12574 (2006).

10. Lopezjimenez, N. D. *et al.* Two members of the TRPP family of ion channels, Pkd1l3 and Pkd2l1, are co-expressed in a subset of taste receptor cells. *J. Neurochem.* **98**, 68-77 (2006).

11. Horio, N. *et al.* Sour taste responses in mice lacking PKD channels. *PLoS. One.* **6**, e20007 (2011).

12. Djenoune, L. *et al.* Investigation of spinal cerebrospinal fluid-contacting neurons expressing PKD2L1: evidence for a conserved system from fish to primates. *Front Neuroanat.* **8:26. doi: 10.3389/fnana.2014.00026. eCollection@2014.**, 26 (2014).

13. Orts-Del'Immagine, A. *et al.* Morphology, distribution and phenotype of polycystin kidney disease 2-like 1-positive cerebrospinal fluid contacting neurons in the brainstem of adult mice. *PLoS. One.* **9**, e87748 (2014).

14. Nomura, H. *et al.* Identification of PKDL, a novel polycystic kidney disease 2-like gene whose murine homologue is deleted in mice with kidney and retinal defects. *J. Biol. Chem.* **273**, 25967-25973 (1998).

15. Chen, X. Z. *et al.* Polycystin-L is a calcium-regulated cation channel permeable to calcium ions. *Nature.* **401**, 383-386 (1999).

16. Zheng, W. *et al.* A novel PKD2L1 C-terminal domain critical for trimerization and channel function. *Sci. Rep.* **5:9460. doi: 10.1038/srep09460.**, 9460 (2015).

17. Li, Q. *et al.* Direct binding of alpha-actinin enhances TRPP3 channel activity. *J. Neurochem.* **103**, 2391-2400 (2007).

18. Murakami, M. *et al.* Genomic organization and functional analysis of murine PKD2L1. *J. Biol. Chem.* **280**, 5626-5635 (2005).

19. Inada, H. *et al.* Off-response property of an acid-activated cation channel complex PKD1L3-PKD2L1. *EMBO Rep.* **9**, 690-697 (2008).

20. DeCaen, P. G., Delling, M., Vien, T. N. & Clapham, D. E. Direct recording and molecular identification of the calcium channel of primary cilia. *Nature.* **504**, 315-318 (2013).

21. Delling, M., DeCaen, P. G., Doerner, J. F., Febvay, S. & Clapham, D. E. Primary cilia are specialized calcium signalling organelles. *Nature.* **504**, 311-314 (2013).

22. Cai, Y. *et al.* Calcium dependence of polycystin-2 channel activity is modulated by phosphorylation at Ser812. *J. Biol. Chem.* **279**, 19987-19995 (2004).

23. Streets, A. J., Moon, D. J., Kane, M. E., Obara, T. & Ong, A. C. Identification of an N-terminal glycogen synthase kinase 3 phosphorylation site which regulates the functional localization of polycystin-2 in vivo and in vitro. *Hum. Mol. Genet.* **15**, 1465-1473 (2006).

24. Cai, Y. *et al.* Identification and characterization of polycystin-2, the PKD2 gene product. *J. Biol. Chem.* **274**, 28557-28565 (1999).

25. Yeste-Velasco, M., Linder, M. E. & Lu, Y. J. Protein S-palmitoylation and cancer. *Biochim. Biophys. Acta.* **1856**, 107-120 (2015).

26. Tsutsumi, R., Fukata, Y. & Fukata, M. Discovery of protein-palmitoylating enzymes. *Pflugers Arch.* **456**, 1199-1206 (2008).

27. Fernandez-Hernando, C. *et al.* Identification of Golgi-localized acyl transferases that palmitoylate and regulate endothelial nitric oxide synthase. *J. Cell Biol.* **174**, 369-377 (2006).

28. Moffett, S., Rousseau, G., Lagace, M. & Bouvier, M. The palmitoylation state of the beta(2)-adrenergic receptor regulates the synergistic action of cyclic AMP-dependent protein kinase and beta-adrenergic receptor kinase involved in its phosphorylation and desensitization. *J. Neurochem.* **76**, 269-279 (2001).

29. Loisel, T. P. *et al.* Activation of the beta(2)-adrenergic receptor-Galpha(s) complex leads to rapid depalmitoylation and inhibition of repalmitoylation of both the receptor and Galpha(s). *J. Biol. Chem.* **274**, 31014-31019 (1999).

30. Moffett, S. *et al.* Palmitoylated cysteine 341 modulates phosphorylation of the beta2-adrenergic receptor by the cAMP-dependent protein kinase. *J. Biol. Chem.* **271**, 21490-21497 (1996).

31. Shipston, M. J. Ion channel regulation by protein S-acylation. *J. Gen. Physiol.* **143**, 659-678 (2014).

32. Vergarajauregui, S. & Puertollano, R. Two di-leucine motifs regulate trafficking of mucolipin-1 to lysosomes. *Traffic.* **7**, 337-353 (2006).

33. Chandra, M. *et al.* A role for the Ca2+ channel TRPML1 in gastric acid secretion, based on analysis of knockout mice. *Gastroenterology* **140**, 857-867 (2011).

34. Yang, J. *et al.* Receptor for activated C kinase 1 (RACK1) inhibits function of transient receptor potential (TRP)-type channel Pkd2L1 through physical interaction. *J. Biol. Chem.* **287**, 6551-6561 (2012).

35. Li, Q., Liu, Y., Zhao, W. & Chen, X. Z. The calcium-binding EF-hand in polycystin-L is not a domain for channel activation and ensuing inactivation. *FEBS Lett.* **516**, 270-278 (2002).

36. Brigidi, G. S. & Bamji, S. X. Detection of protein palmitoylation in cultured hippocampal neurons by immunoprecipitation and acyl-biotin exchange (ABE). *J. Vis. Exp.* (2013).

37. Ishimaru, Y. *et al.* Interaction between PKD1L3 and PKD2L1 through their transmembrane domains is required for localization of PKD2L1 at taste pores in taste cells of circumvallate and foliate papillae. *FASEB J.* **24**, 4058-4067 (2010).

38. Feng, S., Rodat-Despoix, L., Delmas, P. & Ong, A. C. A single amino acid residue constitutes the third dimerization domain essential for the assembly and function of the tetrameric polycystin-2 (TRPP2) channel. *J. Biol. Chem.* **286**, 18994-19000 (2011).

39. Bosmans, F., Milescu, M. & Swartz, K. J. Palmitoylation influences the function and pharmacology of sodium channels. *Proc. Natl. Acad. Sci. U. S. A* **108**, 20213-20218 (2011).

40. Blaskovic, S., Blanc, M. & van der Goot, F. G. What does S-palmitoylation do to membrane proteins? *FEBS J.* **280**, 2766-2774 (2013).

41. Lin, D. T. & Conibear, E. ABHD17 proteins are novel protein depalmitoylases that regulate N-Ras palmitate turnover and subcellular localization. *Elife.* **4**, (2015).

42. Tian, L. *et al.* Palmitoylation gates phosphorylation-dependent regulation of BK potassium channels. *Proc. Natl. Acad. Sci. U. S. A* **105**, 21006-21011 (2008).

43. Moritz, A. E. *et al.* Reciprocal Phosphorylation and Palmitoylation Control Dopamine Transporter Kinetics. *J. Biol. Chem.* **290**, 29095-29105 (2015).

44. Gauthier-Kemper, A. *et al.* Interplay between phosphorylation and palmitoylation mediates plasma membrane targeting and sorting of GAP43. *Mol. Biol. Cell* **25**, 3284-3299 (2014).

45. Schmidt, M. F. & Schlesinger, M. J. Fatty acid binding to vesicular stomatitis virus glycoprotein: a new type of post-translational modification of the viral glycoprotein. *Cell.* **17**, 813-819 (1979).

46. Schmidt, J. W. & Catterall, W. A. Palmitylation, sulfation, and glycosylation of the alpha subunit of the sodium channel. Role of post-translational modifications in channel assembly. *J. Biol. Chem.* **262**, 13713-13723 (1987).

47. Liu, C. & Montell, C. Forcing open TRP channels: Mechanical gating as a unifying activation mechanism. *Biochem. Biophys. Res. Commun.* **460**, 22-25 (2015).

48. Nauli, S. M. *et al.* Polycystins 1 and 2 mediate mechanosensation in the primary cilium of kidney cells. *Nat. Genet.* **33**, 129-137 (2003).

49. Yao, G. *et al.* Disruption of polycystin-L causes hippocampal and thalamocortical hyperexcitability. *Hum. Mol. Genet.* **25**, 448-458 (2016).

50. el-Husseini, A. & Bredt, D. S. Protein palmitoylation: a regulator of neuronal development and function. *Nat. Rev. Neurosci.* **3**, 791-802 (2002).

51. Wedegaertner, P. B. & Bourne, H. R. Activation and depalmitoylation of Gs alpha. *Cell* **77**, 1063-1070 (1994).

52. Voolstra, O. & Huber, A. Post-Translational Modifications of TRP Channels. *Cells* **3**, 258-287 (2014).

CHAPTER 6

RESULTS #5

Unconventional double-residue pore gates in transient receptor potential channels

6.1 ABSTRACT

Mammalian TRP channels from six subfamilies respond to remarkably diverse stimuli which may act to open common or distinct gates. Here we identified hydrophobic gates in TRPV6/P3/P2/M8/C4, using *Xenopus* oocyte electrophysiology, by systematically substituted hydrophobic residues within pore-lining helix S6 with hydrophilic residues. We found that channel activity drastically increases when TRPV6-Ala616, -Met617, TRPP3-Leu557 or -Ala558, but not any proximate residue, were substituted with hydrophilic residues. Channel activities strongly correlated with the hydrophilicity and inversely with the size of residues at these sites, suggesting that consecutive TRPV6-Ala616/-Met617 and TRPP3-Leu557/-Ala558 forms a double-residue gate in each channel. By the same strategy we identified conventional single-residue gates in TRPP2 (Leu677), TRPM8 (Val976) and TRPC4 (Iso617). The double-residue gate channels were more sensitive to small changes in the gate's hydrophobicity or size than single-residue gate channels, suggesting association with stimuli triggering small gate conformational changes. Our results reveal a unique double-residue gating mechanism.

6.2 INTRODUCTION

With few exceptions, mammalian transient receptor potential (TRP) channels are a superfamily of non-selective cation channels found in almost all cell types [1]. They are divided into six subfamilies named after the first described member of each subfamily, “vanilloid” (TRPV), “polycystin” (TRPP). “canonical” (TRPC), “melastatin” (TRPM), “ankyrin” (TRPA), and “mucolipin” (TRPML). TRP channels are tetramers in which each subunit has six transmembrane segments (S1-S6) and cytosolic amino- and carboxy-termini [2]. S5, S6, and the S5-S6 pore loop of each subunit form the central pore module surrounded by S1 to S4 [3]. Although sharing similar structural arrangements with voltage-gated cation channels, TRP channels respond to remarkably diverse stimuli that include pH, temperature, touch, osmolarity, pheromones, and noxious chemicals [1,4-8]. Numerous studies have established that TRP channels fulfill salient roles in sensory physiology such as sensations of pain, hotness, warmth and coldness, tastes, pressure, and vision [5-8]. Mutations in TRP genes have been linked to an inherited pain syndrome, skeletal dysplasia, kidney disorders, and, likely, cancer [9-11]. Although TRP channels have recently been among the most intensively pursued drug targets [12], our understanding of their gating mechanisms and of the way they respond to such diverse types of stimulatory inputs lags far behind and requires a systematic correlation of their structure and function.

Ion channels control ion flow by opening or closing an activation gate, the region preventing ions passing through the channel’s pore in the closed state. Structural determination of TRPV1, TRPV2, TRPV6, TRPA1 and TRPP2 revealed that the ion permeation pore in TRP channels, like that of voltage-gated cation channels, is characterized by the presence of a selectivity filter, sometimes called an upper gate, formed by the four intervening S5-S6 loops and

a constriction, the pore gate or lower gate, formed by the cytoplasmic end of each of the four pore-lining S6 helices [3,13-17]. Voltage-gated sodium and calcium channels have been shown to possess an evolutionarily conserved hydrophobic lower gate in the pore-lining transmembrane helix [18,19]. In voltage-gated potassium channels, a highly conserved Pro-Val-Pro (PVP) motif in S6 is thought to form a tight hydrophobic seal [19,20], because changing these residues to hydrophilic residues opens the channel at resting voltages [21,22]. In comparison, the nature and the location of TRP channels gates have remained more elusive. Despite of a shared transmembrane topology and tetrameric conformation, TRP channels possess little overall amino acid sequence identity. Structures of rat TRPV1 in closed and open states revealed isoleucine (I) at position 679 (I679) as the gate residue [3,23], but leucine (L) at position 681 (L681), two amino acids distal of I679, has been identified by the substituted cysteine accessibility method (SCAM) as the gate residue that obstructs the ion conduction pathway [24]. Structures of rabbit TRPV2 and rat TRPV6 in putative closed states identified a conserved methionine (M) at positions 643 and 577, respectively, as the gate residue [13,14]; the two sites align with each other but represent one amino acid distal of the L681 in TRPV1. Despite of the variant locations of the gate residues identified by these studies, they all supported their hydrophobic nature.

Based on the hydrophobic gate theory [25], a hydrophobic gate allows to close the pore through the so-called liquid-vapor transition of water molecules within the gate region rather than through physical steric occlusion of the pore. These transient vapor states are ‘dewetted’, i.e., effectively devoid of water molecules within the hydrophobic gate region, thus leading to an energetic barrier to ion conduction. Molecular dynamics simulations on model nanopores showed that the hydration rate is close to zero when the gate region has a physical diameter of less than 9 Å (closed state) and dramatically increases to the maximum when it reaches 12-13 Å

(open state) in a strong sigmoidal dependence [25]. In this dynamic range of the gate region (9-13 Å), the ion conduction (∝ hydration rate × pore surface area) could increase substantially without a drastic gain of the pore surface area, which explains well the observed pore sizes of crystallized bacterial small conductance mechano-sensitive channel MscS in closed (8 Å) and open (13 Å) states [26,27]. In fact, the open-state pore sizes of several TRP channels were all found to be within the 11-13 Å range [28-32]. On the other hand, simulation studies also showed that replacement of the hydrophobic gate by a hydrophilic residue drastically increases the pore hydration rate and consequently, ion flow [25]. Thus, channels can be opened by increasing either the pore diameter defined by the gate (e.g., via conformational changes induced by stimuli) or the hydrophilicity of the gate residue (e.g., via mutations) [25]. The latter procedure has led to identification of a hydrophobic barrier deep within the inner pore of the TWIK-1 K2P potassium channel responsible for its low levels of functional activity [33].

The distal amino acid sequence of the pore-lining helix S6 is one of the very few sequences shared by most of the TRP channels and contains a cluster of four conserved hydrophobic residues, leucine-isoleucine-alanine-methionine, the 'LIAM' motif (Fig. 6-S1). The recently resolved structures of several TRP channels identified gate residues within or around this motif [3,13,14,16,17], but they did not always find the same or corresponding gate residues as sequence homology would predict (Fig. 6-1A). In this study, we systematically substituted residues in the distal part of the S6 helix in five members from four TRP subfamilies, TRPV6, TRPP3, TRPP2, TRPM8, and TRPC4, with hydrophilic residues and studied the effects on channel function, using the two-electrode voltage clamp in *Xenopus laevis* oocytes, biotinylation, and immunofluorescence, to identify the relevant lower gate residues. We reasoned that the gate residue in TRP channels, but not the adjacent residue, would give rise to constitutive channel

opening when its hydrophilicity is increased. We discussed our data in view of available TRP structures and SCAM studies, compared characteristic differences between single- and double-residue gates, and proposed mechanistic models to illustrate distinct pore gating through S6 helix twisting.

6.3 METHODS

Plasmids, mutants and antibodies

Human TRPP3 cDNA (accession #: NM_016112) was subcloned into vector pCHGF [34] for *Xenopus laevis* oocyte expression. Flag tag was then inserted 5' of the TRPP3 coding region for detection. Human TRPV6 (NM_018646) and mouse TRPC4 (NM_001253682) cDNAs were subcloned into oocyte expression vectors pBSMXT-MCS and pSGEM, respectively. HA-tagged human TRPP2 (NM_000297) plasmid [35] was a kind gift of Dr. Yong Yu (St. John's University, NY). Rat TRPM8 (NM_134371) plasmid was kindly provided by Dr. David Julius (University of California at San Francisco, CA). All mutations were made with QuikChange Lightning Site-Directed Mutagenesis kit (Agilent Technologies, La Jolla, CA) and confirmed by sequencing. Rabbit antibodies against FLAG (D-8), HA (Y-11) and mouse antibodies against β-actin (C-4) were purchased from Santa Cruz Biotechnology (Santa Cruz, CA). Rabbit antibodies against TRPC4 (ab83689) and TRPM8 (ab3243) were purchased from Abcam (Cambridge, MA). Rabbit antibody against TRPV6 was custom generated previously [36]. Secondary antibodies were purchased from GE Healthcare (Waukesha, WI).

Xenopus oocyte expression

Capped synthetic RNA of TRPP3, TRPP2, TRPV6, TRPC4 and TRPM8 were synthesized by *in vitro* transcription with mMESSAGE mMACHINE kit (Ambion, Austin, TX) and injected (25-50 ng per oocyte) into *Xenopus laevis* oocytes prepared as described [37]. Equal volumes of water were injected into control oocytes. Experiments were performed 1-3 days after injection. The present study was approved by the Ethical Committee for Animal Experiments of the University of Alberta, and was carried out in accordance with the Guidelines for Research

with Experimental Animals of the University of Alberta and the Guide for the Care and Use of Laboratory Animals (NIH Guide) revised in 1996.

Electrophysiology

Two-electrode voltage clamp experiments were performed as described previously [34]. Briefly, the two electrode (Capillary pipettes, Warner Instruments, Hamden, CT) impaling an oocyte were filled with 3 M KCl to form a tip resistance of 0.3-2 MΩ. Unless otherwise indicated, whole-cell currents of oocytes were recorded at room temperature in standard extracellular solution containing 100 mM NaCl, 2 mM KCl, 1 mM $MgCl_2$ and 10 mM HEPES (pH 7.5) with or without 5 mM $CaCl_2$. Duration of application of Ca^{2+} solution was indicated in time course recordings. Currents were recorded using a Geneclamp 500B amplifier and Digidata 1322A AD/DA converter (Molecular Devices, Union City, CA). The pClamp 9 software (Axon Instruments, Union City, CA) was employed for data acquisition and analysis. Currents and voltage were digitally recorded at 200 μs/sample and filtered at 2 kHz through a Bessel filter. SigmaPlot 12 (Systat Software, San Jose, CA) was used for data fitting and plotting.

Western blotting and surface protein biotinylation

Xenopus oocytes were washed 3 times with ice-cold PBS solution followed by incubation with 0.5 mg/ml sulfo-NHS-SS-Biotin (Pierce, Rockford, IL) for 30 min at room temperature. 1 M NH_4Cl was used to quench the non-reacted biotin. Oocytes were then washed with ice-cold PBS solution and harvested in ice-cold CelLytic M lysis buffer (Sigma, St. Louis, MO) supplemented with proteinase inhibitor mixture (Thermo Scientific, Waltham, MA). Lysates were incubated at 4˚C overnight with gentle shaking upon addition of 100 μl streptavidin

(Pierce). The surface protein absorbed by streptavidin was resuspended in SDS loading buffer and subjected to SDS-PAGE.

Immunofluorescence

Whole mount immunofluorescence assays using oocytes were performed as previously described [37]. Briefly, *Xenopus* oocytes were washed in PBS, fixed in 4% paraformaldehyde for 15 min, washed 3 times in PBS plus 50 mM NH_4Cl, and then permeabilized with 0.1% Triton X-100 for 4 min. Oocytes were then blocked in PBS plus 3% skim milk for 30 min, and then incubated overnight with indicated primary antibodies, followed by incubation with a secondary AlexaFluor 488-conjugated donkey anti-rabbit antibody (Jackson ImmunoResearch Laboratories, West Grove, PA) for 30 min. Oocytes were then mounted in Vectashield (Vector Labs, Burlington, ON) and examined on an AIVI spinning disc confocal microscopy (Cell Imaging Facility, Faculty of Medicine and Dentistry, University of Alberta). The surface expression was assessed by quantifying the plasma membrane immunofluorescence using Volocity 6.2 (Perkin Elmer, Waltham, MA).

Statistical analysis

Data were analyzed and plotted using SigmaPlot 12 (Systat Software), and expressed as mean ± SEM (standard error of the mean).

6.4 RESULTS

We replaced each of the nine human TRPV6 hydrophobic residues in the S6 fragment M610-G619 encompassing the LIAM motif (Fig. 6-1A) by the hydrophilic asparagine (N) and assessed activities of the mutant channels. We measured steady-state currents at -50 mV induced by addition of 5 mM extracellular Ca^{2+}, which follows a large, transient Cl^- current mediated by native Ca^{2+}-activated Cl^- channels (Fig. 6-1B), as described before [38,39]. We indeed found that, compared with wild-type (WT) TRPV6, mutants A616N and M617N exhibit drastic 211 ± 22 and 174 ± 19 fold increases, respectively, in the channel activities, while other mutant channels behaved like WT or had revealed lower activities (Fig. 6-1B and C). In particular, based on rat TRPV6 crystal structure the methionine at position 618 (M618) was reported to be the gate residue [14], but the activities of the mutant M618N and WT channels were similar. By immunofluorescence and biotinylation, we found that these mutations do not significantly affect their plasma membrane targeting (Fig. 6-1C, D and E). When we next replaced each of them by the hydroxyl-containing serine (S) we found a similar activity pattern (Fig. 6-1F and G). Thus, these data together indicated that A616 and M617, rather than the M618, are crucial gate residues.

We next replaced A616 by 12 amino acid residues of different hydrophobicities and/or sizes, and found that mutation to a bulky and hydrophobic amino acid (V, I, F, Y or W) abolishes the channel function while replacement by a small or hydrophilic amino acid (G, T, S, Q, N, E or K) tremendously increases the channel function (Fig. 6-1H). Replacement of M617 by different amino acids in general produced similar results as obtained for A616 (Fig. 6-1I). These mutations at the positions of A616 and M617 do not affect TRPV6 targeting to the surface membrane (Fig. 6-1J and Fig. 6-S2A) as assayed by biotinylation and immunofluorescence. So

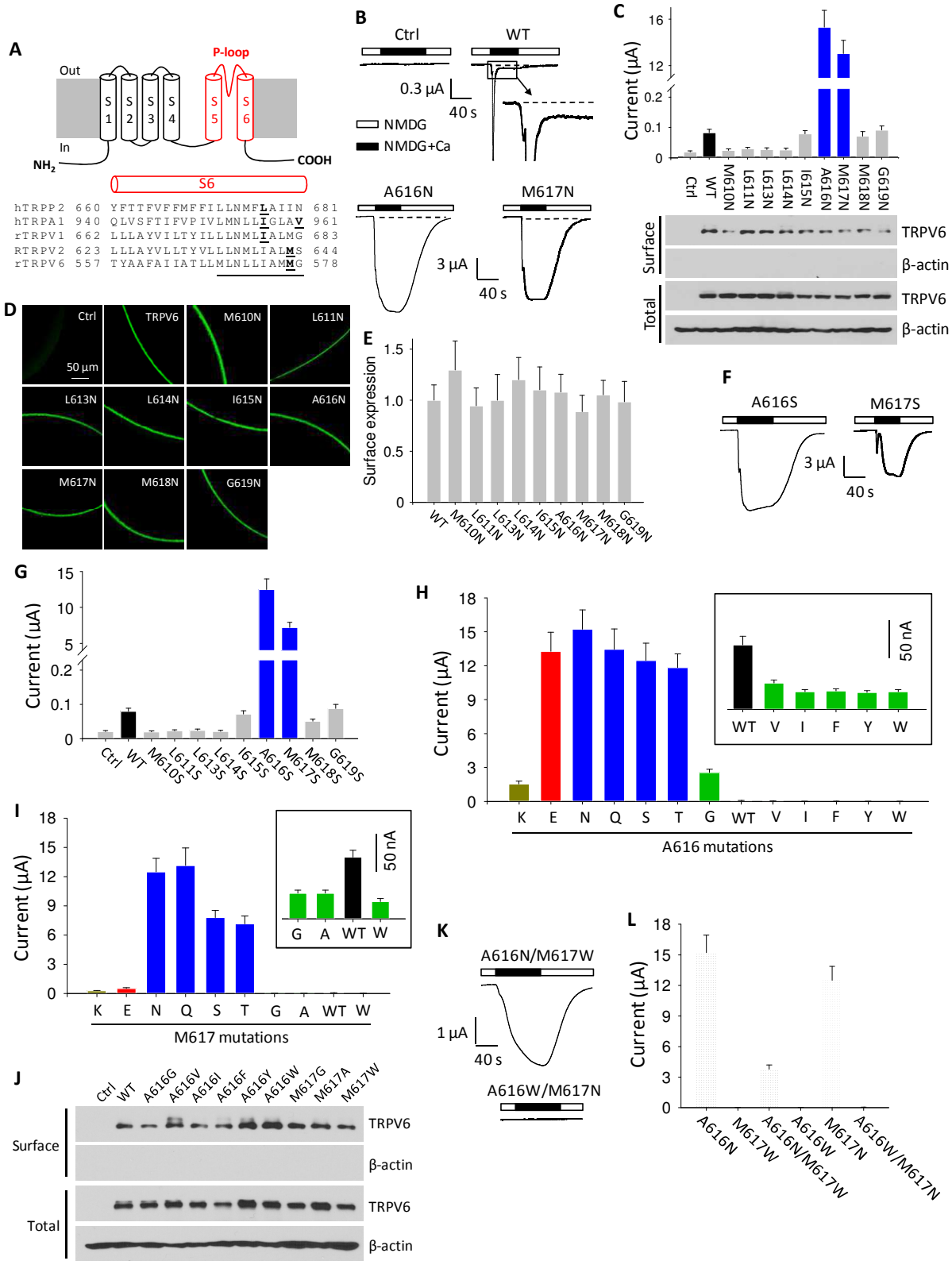
A
Out
In
P-loop
S1
S2
S3
S4
S5
S6
NH2
COOH
S6
hTRPP2 660 YFTTFVFFMFFILLNMFLAIIN 681
hTRPA1 940 QLVSFTIFVPIVLMNLLIGLAV 961
rTRPV1 662 LLLAYVILTYILLNMLIALMG 683
RTRPV2 623 LLLAYVLLTYVLLNMLIALMS 644
rTRPV6 557 TYAAFAIIATLLMLNLLIAMMG 578
B
Ctrl
WT
0.3 μA
40 s
NMDG
NMDG+Ca
A616N
M617N
3 μA
40 s
C
Current (μA)
Ctrl
WT
M610N
L611N
L613N
L614N
I615N
A616N
M617N
M618N
G619N
Surface
Total
TRPV6
β-actin
TRPV6
β-actin
D
Ctrl
TRPV6
M610N
L611N
50 μm
L613N
L614N
I615N
A616N
M617N
M618N
G619N
E
Surface expression
WT
M610N
L611N
L613N
L614N
I615N
A616N
M617N
M618N
G619N
F
A616S
M617S
3 μA
40 s
G
Current (μA)
Ctrl
WT
M610S
L611S
L613S
L614S
I615S
A616S
M617S
M618S
G619S
H
Current (μA)
50 nA
WT V I F Y W
K E N Q S T G WT V I F Y W
A616 mutations
I
Current (μA)
50 nA
G A WT W
K E N Q S T G A WT W
M617 mutations
J
Ctrl
WT
A616G
A616V
A616I
A616F
A616Y
A616W
M617G
M617A
M617W
Surface
Total
TRPV6
β-actin
TRPV6
β-actin
K
A616N/M617W
1 μA
40 s
A616W/M617N
L
Current (μA)
A616N
M617W
A616N/M617W
A616W
M617N
A616W/M617N

Fig. 6-1. Functional characterization of human TRPV6 point mutants around the putative lower gate region. (**A**) Membrane topology of a single TRP protein and amino acid (aa) sequence alignment of the S6 helix of the five TRP channels whose structures were recently solved (TRPV6 [14], TRPV2 [13], TRPV1 [3], TRPP2 [17], and TRPA1 [16]) (r, rat; h, human; R, rabbit). The residues assumed to form the lower gate are marked bold and underlined. Each single underlined aa of TRPV6 was mutated to asparagine (N). (**B**) Representative membrane currents recorded in voltage clamped oocytes at -50 mV injected with cRNA of human TRPV6 wild-type (WT) or mutants A616N or M617N. Water-injected oocytes were used as control (Ctrl). The extracellular solution contained (in mM): 100 N-methyl-D-glucamine (NMDG)-Cl, 2 KCl, 1 $MgCl_2$, 10 HEPES at pH 7.5 (NMDG), or the NMDG solution including 5 mM $CaCl_2$ (NMDG+Ca). Dashed lines are the baselines from which plateau current values were determined. (**C**) *Upper panel,* averaged plateau current amplitudes obtained from oocytes injected with the cRNA of WT or mutant channel, or from water-injected oocytes (Ctrl), like in 1B (mean ± SEM; n = 15 - 21). Oocytes were from at least three batches. *Lower panel*, representative Western blot of surface biotinylated (Surface) and total TRPV6 proteins (Total), as indicated. β-actin was used as a control. (**D**) Representative whole-mount immunofluorescence using the anti-TRPV6 antibody showing the oocyte surface expression of the mutants from panel C. (**E**) Averaged surface membrane expression of TRPV6 mutants normalized to that of TRPV6 WT (n = 4 - 7). (**F**) Representative membrane currents measured at -50 mV in oocytes expressing A616S or M617S. (**G**) Similar to panel C, averaged currents for the indicated single mutants (n = 14 - 21). (**H**) A616 was replaced by the aa as indicated and the averaged currents obtained with these mutants are shown (n = 17 - 20 oocytes from at least three batches). Inset: bar graph with a different current scale. (**I**) M617 was replaced by different aa, as indicated; the resulting membrane currents from different mutants were recorded and averaged (n = 15 - 20). Inset: bar graph with a different current scale. (**J**) Western blot of surface biotinylated and total TRPV6 as in panel C. (**K**) Representative current traces obtained at -50 mV in oocytes injected with the TRPV6 double mutant A616N/M617W or A616W/M617N. (**L**) Averaged currents at -50 mV of the mutants indicated.

far our results show that both A616 and M617 act as the gate residues. A noticeable difference between the two sites is that replacement of M617 by G, A, E or K did not produce comparable activity increases as the corresponding replacements at A616, suggesting that, compared with M617, A616 is a more primary gate residue. Next, we examined double mutants carrying two 'opposing' mutations (to N and W), A616N/M617W and A616W/M617N, and found that mutant A616N/M617W still exhibits a substantial activity increase while A616W/M617N was non-functional (Fig. 6-1K and L), even though they both exhibit similar surface membrane expression (Fig. 6-S2B and C). In other words, the pore can be closed at site 616 (by changing to

W), regardless of what happens at site 617, but not vice versa. This result is in strong support to a hierarchical arrangement with A616 acting as the primary and M617 being rather the secondary gate residue.

To identify residues responsible for the lower gate in TRPP3, we examined roles of eight hydrophobic residues in the S6 fragment L552-I560 (Fig. 6-2A) through replacing each of them by N and found that L557N and A558N produce largest, substantial increases (6.9 - 9.1 folds) in the basal channel activity assessed by Na^+ currents at -50 mV, which is comparable with the WT channel activity activated by 5 mM extracellular Ca^{2+} (Fig. 6-2A and B). Their neighbor sites, F556 and I559, also gave rise to significant increases (about 2 folds) when mutated to N, but not of a comparable size to L557 or A558. Similar results were obtained when currents were measured at other membrane potentials using a ramp protocol (Fig. 6-2C). We also found that the plasma membrane densities of these mutants were all similar to that of the WT channel (Fig. 6-2D and E). We then replaced A558 by 12 different amino acids and found a similar pattern of channel activity changes as those of TRPV6 A616 and M617 (Fig. 6-2F), with exceptions that TRPP3 A558G and A558T did not exhibit any activity increase at -50 mV compared to WT channel (Fig. 6-2F). Examination of the channel activity at other membrane potentials revealed that A558G and A558T (as well as A558S) in fact exhibit strong outward rectification and increase the channel activity by 5 folds at +80 mV as compared with the WT channel (Fig. 6-2G and H), although the exact reason underlying the rectification remains unaccounted for. Removal of Mg^{2+} from extracellular solutions had little effect on the rectification (Fig. 6-S3A), excluding the possibility of a blockade of inward currents by extracellular Mg^{2+} as a cause of the rectification. On the other hand, site L557 also gave rise to a similar pattern of the activity

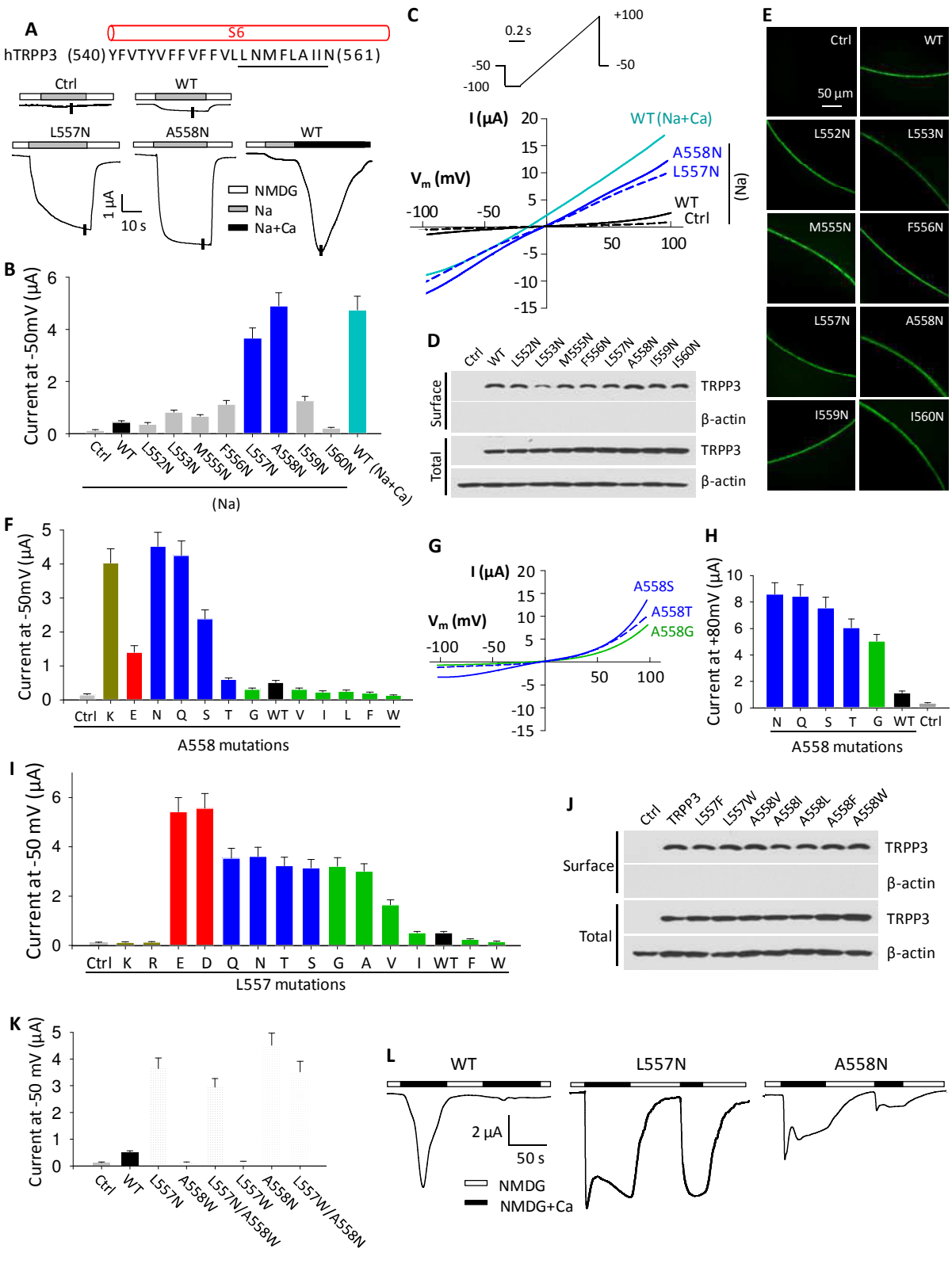
A
S6
hTRPP3 (540) YFVTYVFFVFFVLLNMFLAIIN (561)
Ctrl
WT
L557N
A558N
WT
1 μA
10 s
NMDG
Na
Na+Ca
B
Current at -50mV (μA)
Ctrl WT L552N L553N M555N F556N L557N A558N I559N I560N WT (Na+Ca)
(Na)
C
0.2 s
+100
-50
-100
-50
I (μA)
WT (Na+Ca)
A558N
L557N
WT
Ctrl
Vm (mV)
(Na)
D
Ctrl WT L552N L553N M555N F556N L557N A558N I559N I560N
Surface
Total
TRPP3
β-actin
E
Ctrl
WT
50 μm
L552N
L553N
M555N
F556N
L557N
A558N
I559N
I560N
F
Current at -50mV (μA)
Ctrl K E N Q S T G WT V I L F W
A558 mutations
G
I (μA)
A558S
A558T
A558G
Vm (mV)
H
Current at +80mV (μA)
N Q S T G WT Ctrl
A558 mutations
I
Current at -50 mV (μA)
Ctrl K R E D Q N T S G A V I WT F W
L557 mutations
J
Ctrl TRPP3 L557F L557W A558V A558I A558L A558F A558W
Surface
Total
TRPP3
β-actin
K
Current at -50 mV (μA)
Ctrl WT L557N A558W L557N/A558W L557W A558N L557W/A558N
L
WT
L557N
A558N
2 μA
50 s
NMDG
NMDG+Ca

Fig. 6-2. Scanning mutagenesis of human TRPP3 S6 helix around the putative lower gate region and functional characterization of point mutants. (**A**) Each single underlined aa of TRPP3 was mutated to asparagine (N). Representative current traces were obtained from oocytes injected with WT or a mutant (L557N or A558N) TRPP3 cRNA, or water (Ctrl). Oocytes were voltage clamped at -50 mV in the presence of NMDG- or Na-containing solution (equimolar Na^+ substituting NMDG), or Na+Ca solution (Na-containing solution supplemented with 5 mM $CaCl_2$). (**B**) Averaged currents as the difference between NMDG- and Na- or Na+Ca-containing solutions obtained at -50 mV, as in panel A, in oocytes expressing the single mutants, as indicated. For each mutant, currents were averaged from 17 - 20 oocytes of at least three batches. (**C**) Representative I-V curves from Ctrl (water-injected oocyte), TRPP3 WT, L557N or A558N expressing oocytes using a ramp protocol, as indicated, were obtained at peak current points indicated by the vertical bars in the traces in panel A. **(D**) Western blot of surface biotinylated and total TRPP3 WT or indicated mutants. **(E**) Whole-mount immunofluorescence using the Flag antibody showing the oocyte surface expression of the mutants from panel D. (**F**) TRPP3 A558 was replaced by different aa, as indicated. Shown are averaged currents obtained under the same experimental conditions as in panel A (n = 14 - 23). (**G**) Representative I-V curves for three indicated A558 mutants generated under the same experimental condition as in panel C. (**H**) Averaged outward currents at +80 mV for A558 mutants (n = 13 - 18). (**I**) TRPP3 L557 was replaced by different aa, as indicated. Shown are averaged currents obtained under the same experimental conditions as in A (n = 18 - 25). **(J**) Western blot of surface biotinylated and total protein of TRPP3 WT or indicated mutants. **(K**) L557 and A558 were replaced by W or N. Shown are averaged current at -50 mV for single or double mutants, as indicated (n = 12 - 15). (**L**) Representative current traces in oocytes expressing TRPP3 WT, L557N or A558N mutant, in the presence of the NMDG-containing solution (NMDG) or with addition of 5 mM $CaCl_2$ (NMDG+Ca).

increase when mutated to 14 different amino acids (Fig. 6-2I), but note that outward rectification was not observed in the corresponding mutants (L557G, L557T and L557S) (Fig. 6-S3B). The mutations at L557 and A558 did not affect TRPP3 targeting to the surface membrane as shown by biotinylation and immunofluorescence data (Fig. 6-2J and Fig. 6-S3C). Thus, similar to TRPV6, our data indicate that both L557 and A558 serve as the gate residues in TRPP3.

Nevertheless, double mutants with two 'opposing' mutations (L557N/A558W and L557W/A558N) still exhibited large increases of the channel activity (Fig. 6-2K), indicating that the pore can be opened from either site, regardless of the other site, which is distinct from the

properties of the corresponding double mutants of TRPV6. However, we found that L557 is more sensitive than A558 with respect to small changes in the amino acid hydrophobicity and size through substitutions among A, V and L (Fig. 6-2F and I), suggesting that L557 acts as the primary gate residue. While WT TRPP3 was reported to exhibit inactivation and have a recovery time of 8-10 min after Ca^{2+}-induced activation [40], gate mutant L557N or A558N did not display inactivation and can be re-activated immediately (Fig. 6-2L), indicating that the two gate sites are involved in both the activation and inactivation, which is in contrast to voltage-gated sodium channels in which inactivation is accomplished by an intracellular fragment [41].

We then wondered whether human TRPP2 has identical gate residues as its close homologue TRPP3 because their 10 amino acids around the TRPP3 gate are identical (LLNMF**LA**IIN). TRPP2 is mutated in 15% of autosomal dominant polycystic kidney disease, one of the most common genetic diseases in humans [42,43]. Functional studies of TRPP2 channel have been impeded by the lack of an effective readout and by unknown channel agonists. We reasoned that an appropriate mutation to the gate residue(s) must open the channel and produce detectable currents. For this we first replaced each of the hydrophobic residues in the F676-I679 fragment (that contains the TRPP3 gate) (Fig. 6-3A) by N and found that only the L677N mutant exhibits substantially increased channel activity which was comparable to that of the previously reported gain-of-function mutant F604P [35] (see below) (Fig. 6-3A and B). We next focused on L677 by substituting it with different amino acids and found that replacement of L677 by N, S or G, but not by charged or large hydrophobic residues, indeed produces large currents (Fig. 6-3C). Since A678 corresponds to the TRPP3 A558, one of the two TRPP3 gate residues, we examined the effects of replacing it by other hydrophilic residues, to provide further documentations. Replacement of A678 by any of N, Q, S and T, did not show any appreciable current over the

background signal (Fig. 6-3D), in support of the concept that A678 is not a gate residue. By surface biotinylation and immunofluorescence we found that the plasma membrane targeting of mutants A678N, -Q, -S and -T, L677N, or F604P is similar to that of the WT proteins (Fig. 6-3D, Fig. 6-S4A and B). Thus these functional data support that L677, but not A678, serves as the single-residue gate.

Because how TRPP2 is activated has remained unclear or debatable, we made use of human TRPP2 mutant F604P which was recently reported to display substantially increased channel activity compared to the WT channel, presumably because it is somehow trapped in a constitutive open state [35]. Expression of mutant F604P in oocytes indeed produced large currents at various membrane voltages, which were comparable to currents produced by L677N (Fig. 6-3A and B). When examining the effect of L677 gate mutations using the F604P mutant, which produces double mutants, we found that, compared to the F604P single mutant, replacement of L677 by the small residue G further increases the activity while replacements by charged or large hydrophobic residues substantially or significantly reduce the activity (Fig. 6-3E and F), further supporting that L677 serves as the channel gate. The identified gate residue (L677) is in agreement with the known structure of TRPP2 [17,44,45], which thus validates our methodology. In summary, although TRPP2 and TRPP3 have identical amino acids in their distal half of S6, TRPP3 adapts a doublet gate (LA) while TRPP2 uses a single-residue gate (L).

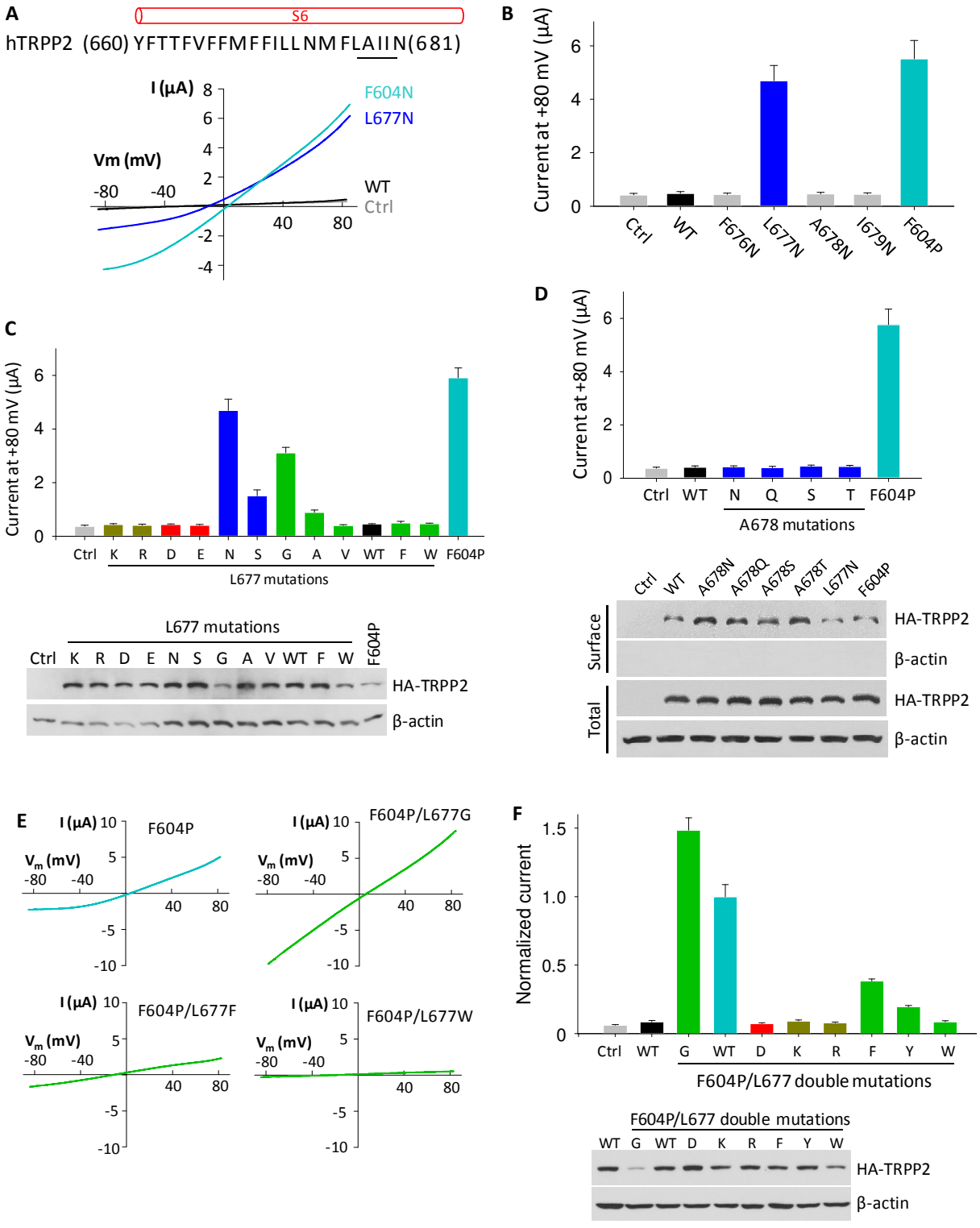

Fig. 6-3. Characterization of human TRPP2 point mutants at and adjacent to the putative gate region in S6. (**A**) Each single underlined aa of TRPP2 was mutated to asparagine (N). Representative I-V curves were obtained in oocytes expressing WT or a mutant TRPP2, as

indicated, in the presence of the Mg^{2+}-free Na-containing solution (in mM): 100 NaCl, 2 KCl, 10 HEPES at pH 7.5. The gain-of function mutant F604P serves as a positive control and water-injected oocytes were used as negative control (Ctrl). (**B)** Averaged currents at +80 mV obtained under the same experimental conditions as in panel A in expressing or control oocytes, as indicated. Currents were averaged from 12 - 18 oocytes of at least three batches. (**C**) *Upper panel*, the TRPP2 L677 was replaced by different aa as indicated. Shown are averaged currents obtained as in panel A including F604P currents as a positive control (n = 19 - 23). *Lower panel*, Western blot showing total protein of TRPP2 WT and the indicated mutants present in the injected oocytes. (**D**) *Upper panel*, averaged currents for WT, A678 mutants, or F604P obtained as in panel A (n = 15 - 19). *Lower panel*, Western blot of surface biotinylated and total protein of TRPP2 WT or indicated mutants. (**E**) Representative I-V curves for F604P/L677 double mutants, as indicated, under the same condition as in panel A. (**F**) *Upper panel*, averaged normalized currents at +80 mV recorded from oocytes injected with cRNA of the indicated F604P/L677 double mutants (n = 16 - 20). Ctrl, water-injected oocyte; WT, wild-type TRPP2; F604P/L677 WT, single F604P mutant. *Lower panel*, Western blot showing total protein of TRPP2 present in the injected oocytes.

To study whether members of the TRPM and TRPC subfamilies possess a single- or double-residue gate, we examined TRPM8 and TRPC4. TRPM8 is a cold-sensitive channel and is activated by cooling agents like menthol [46]. In oocytes, TRPM8 produced distinct voltage-dependent activation currents with pronounced outward rectification (Fig. 6-4A), in line with previous report that TRPM8 is closed by a voltage-dependent mechanism at negative membrane potentials [47]. We reasoned that mutation of the gate residue(s) must constitutively open the pore and thus give rise to detectable currents at negative voltages. Based on the S6 alignment (Fig. 6-S1), we mutated each of the nine individual hydrophobic residues between L971 and G980 to serine (Fig. 6-4A), and found that in the absence of menthol V976S, but not the WT or any other mutant channels, produces robust currents at negative voltages, which is comparable to menthol-activated currents (Fig. 6-4A and B). Consistently, mutant channel V976S also gave rise to substantially increased currents at positive voltages, similar to those induced by menthol (Fig. 6-4A and B). Biotinylation assays showed that all tested TRPM8 mutants have similar surface expression as WT (Fig. 6-4C). Replacing V976 by Q produced comparable large activities as

V976S (Fig. 6-4D and E), but replacements by large hydrophobic residues or by D abolished the channel activity (Fig. 6-4E), which is similar to TRPP2 (Fig. 6-3E and F). Changing V976 to R produced significantly increased currents at negative voltages (Fig. 6-4D and E). In summary, our studies show that V976 acts as the single-residue gate of TRPM8.

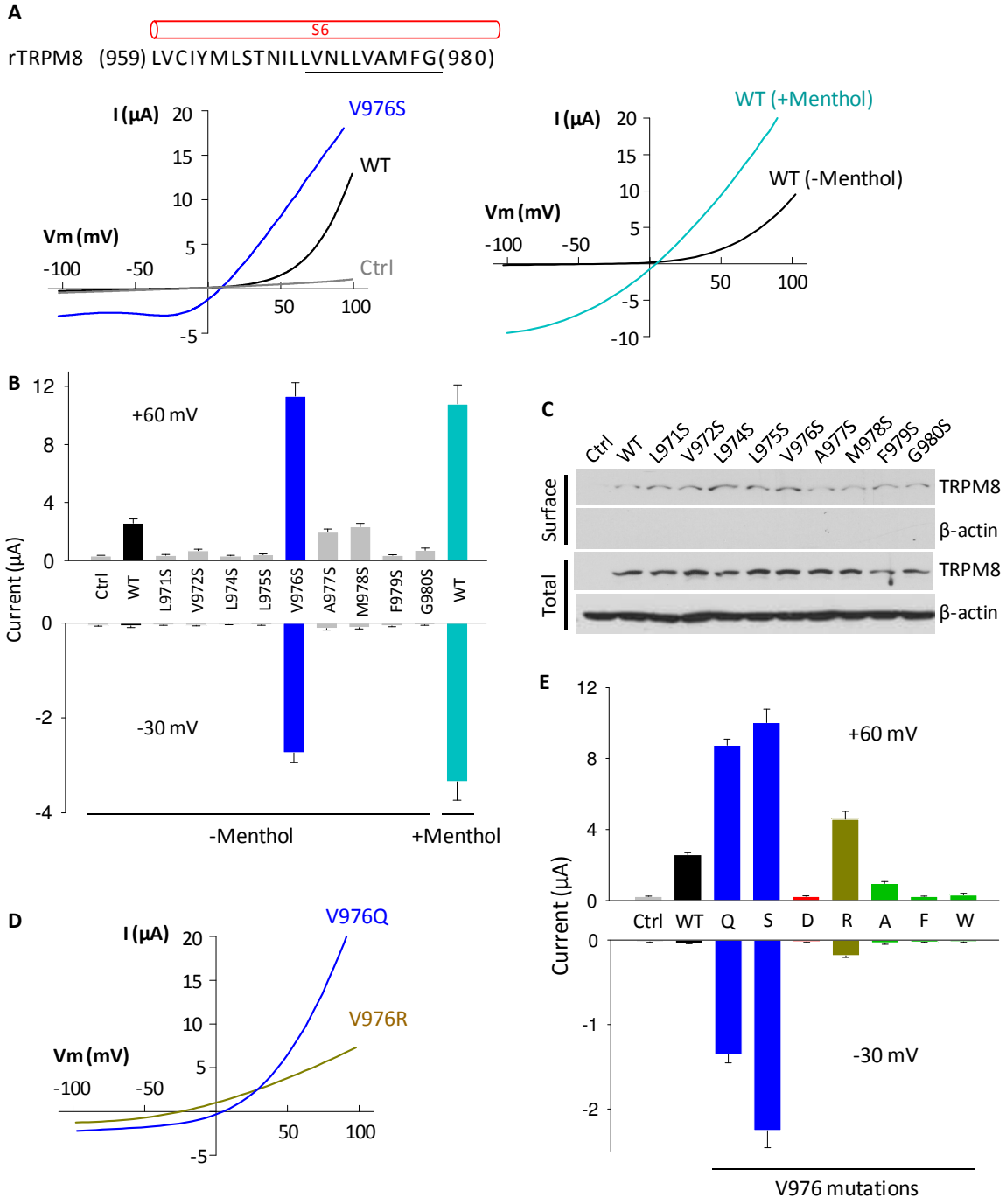

Fig. 6-4. Characterization of rat TRPM8 point mutants around the putative gate region in S6. (**A**). Each single underlined aa of TRPM8 was replaced by serine (S). Representative I-V curves were obtained in oocytes expressing TRPM8 or its mutant V976S, or water-injected oocytes (Ctrl) in the absence of the agonist menthol at room temperature (*left panel*), or oocytes expressing WT TRPM8 in the absence or presence of 0.5 mM extracellular menthol at room temperature (*right panel*). The Na-containing solution was used in these experiments. (**B**). Averaged currents were obtained at -30 and +60 mV for oocytes expressing TRPM8 WT or single mutants, or water-injected oocytes (Ctrl), as indicated (n = 16 - 21). (**C**). Western blot of surface biotinylated and total protein of TRPM8 WT or indicated mutants. (**D**). Representative I-V curves obtained from oocytes expressing TRPM8 V976Q or V976R in the absence of menthol. (**E**). Averaged currents at -30 and +60 mV in oocytes expressing TRPM8 WT or V976, as indicated, in the absence of menthol (n = 18 - 22).

Endogenously and heterologously expressed TRPC4 is activated by stimulation of G-protein-coupled receptors and the resulting currents are doubly (outwardly and inwardly) rectifying [48]. We reasoned that an appropriate mutation to the gate residue(s) must constitutively open the channel and produce detectable currents without receptor activation. We replaced each of the nine residues around the putative gate residue(s), L612-M620 (Fig. 6-5A), by N in mouse TRPC4 and studied their channel activities under voltage clamp conditions in oocytes. We found that mutant I617N, but not WT or any other mutant channels, produces large currents (Fig. 6-5A and B), suggesting the presence of a single-residue gate. By immunofluorescence and biotinylation, we found that the plasma membrane localization of these mutants is similar to that of the WT channel (Fig. 6-5C and D). It was reported that the G503S mutation in mouse TRPC4 renders the channel in a constitutively activated state [49]. Expression of this mutant in oocytes indeed produced a typical doubly rectified I-V curve and large Na^+ currents comparable to those by I617N at +100 mV (Fig. 6-5A and B). The I-V curves for the two mutant channels were characteristically different, which should be understandable given that they are apparently opened by two different ways. Replacement of I617 by D, K, G, A, F or W did not result in any appreciable current (Fig. 6-5E). Further, on top of the G503S mutation, replacement of I617 by

any of the charged or large hydrophobic residues D, K, F and W, but not by A, were able to completely or substantially inhibit the channel activity (Fig. 6-5F and G). All the data together indicated that, like TRPP2 and TRPM8, TRPC4 also possesses a single-residue gate I617.

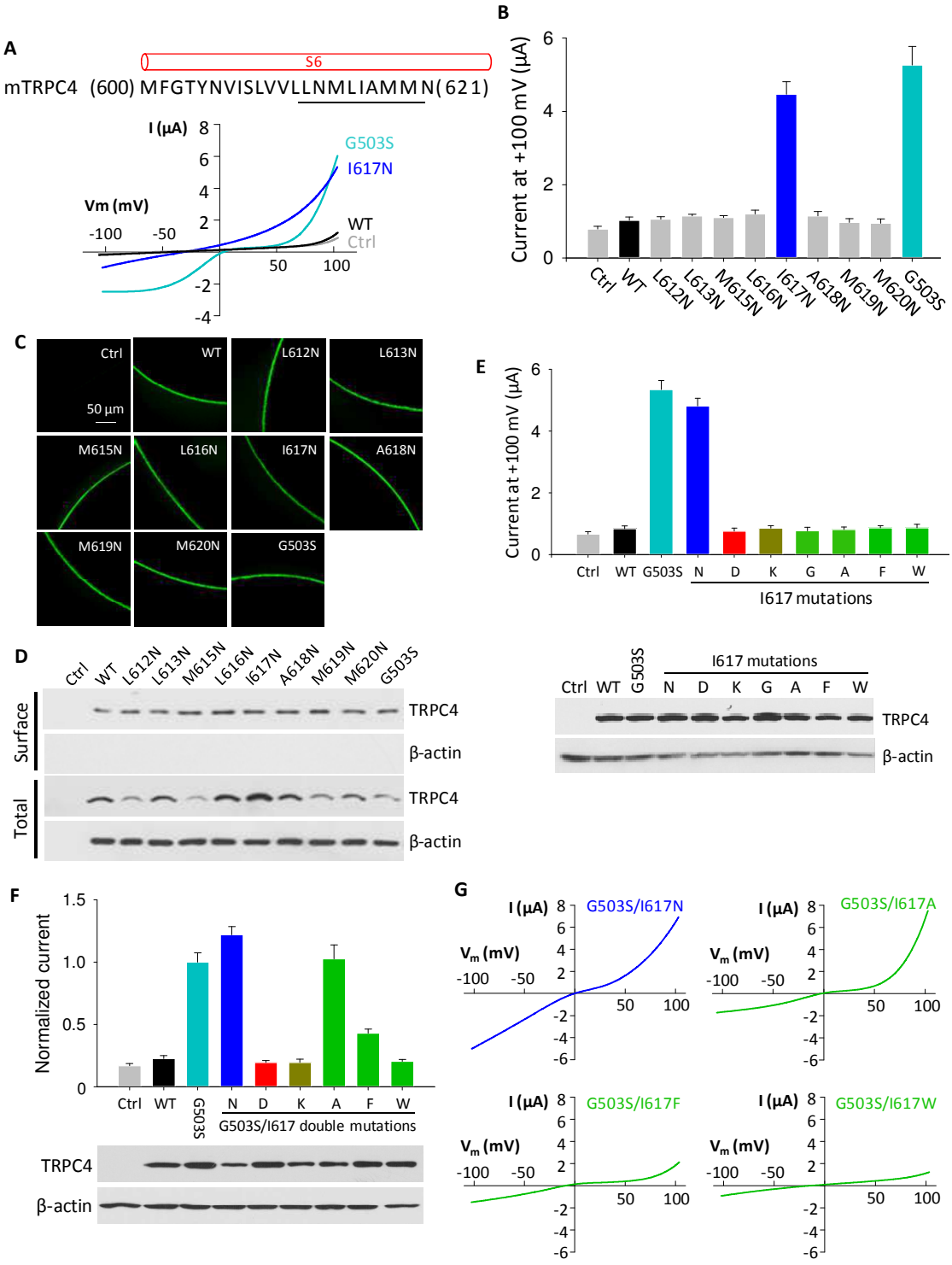

Fig. 6-5. Characterization of mouse TRPC4 point mutants around the putative gate region in S6. (**A**). Each single underlined aa of TRPC4 was mutated to asparagine (N). Representative I-V curves were obtained in oocytes expressing TRPC4 WT, mutants I617N or G503S, or water-injected oocytes (Ctrl), in the presence of the Na-containing solution. The gain-of-function mutant G503S (within the S4-S5-linker) serves as a positive control. (**B**). Averaged currents obtained at +100 mV under the same condition as in panel A for oocytes expressing one of the asparagine mutants, as indicated (n = 18 - 21). (**C**). Whole-mount immunofluorescence using the antibody for mouse TRPC4 showing the oocyte surface expression of TRPC4 WT or mutants from panel B. (**D**). Western blot of surface biotinylated and total protein of TRPC4 WT or mutants from panel B. (**E**). *Upper panel*, averaged currents for TRPC4 WT, G503S and I617 mutants, as indicated (n = 15 - 21). *Lower panel*, Western blot showing total protein of TRPC4 WT or indicated mutants present in the injected oocytes. (**F**). Averaged normalized currents at +100 mV for different G503S/I617 double mutants (*Upper panel*), as indicated (n = 14 - 20), and Western blot showing total protein of indicated mutants present in the injected oocytes (*Lower panel*). (**G**). Representative I-V curves for various G503S/I617 double mutants, obtained in the presence of the Na-containing solution.

6.5 DISCUSSION

Although high resolution structures of TRPA1, TRPV1, TRPV2, TRPV6 and TRPP2 are now available [3,13-17,23], the precise identity and position of residues defining the lower pore gate in TRP channels have still to be defined by functional studies. Also, whether different TRP channels share common or distinct gate residue/site has yet to be shown. In this study, we performed electrophysiological measurements in *Xenopus* oocytes on five TRP channels from the four major TRP subfamilies by focusing on hydrophobic amino acids proximate to, and including, candidate gate residues in the distal half of S6. While in TRPP2, TRPM8, and TRPC4 we identified a conventional single amino-acid gate residue, as anticipated, we found that in TRPV6 and TRPP3 two consecutive amino acids together form a double-residue gate. We found that all the seven identified gate residues are hydrophobic and are within the gate motif "L(F)I(L/V)AM(L/I)" (see Fig. 6-S1) (Fig. 6-6A). In fact, they were located at the "LIAM" sites with a "0-4-2-1 (L-I-A-M)" pattern, i.e., none (0), 4, 2 and 1 of them were located at the four sites (left-to-right) of "LIAM" (Fig. 6-6A). Thus, our study showed that TRP channels exhibit some degree of shared or conserved gate residues/sites. In comparison, the results from structural analyses and SCAM suggested a "0-3-0-1-2-1 (L-I-A-M-X-X)" pattern (Fig. 6-6A). Interestingly, the "I" in "L**I**AM" has been identified as a gate site in more than half of all the reported studies [3,13,14,16,17,24] including our present results.

Gate residues M618 in TRPV6 [14] and M645 in TRPV2 [13] identified by structural analysis align well with each other but are one to three amino acids distal from the TRPV6 gate A616-M617 identified by our current functional studies and the TRPV1 gate I679 predicted by the structure [3] (Fig. 6-6A). In contrast, the TRPV1 gate L681 identified by the functional SCAM [24] corresponds exactly to the secondary TRPV6 M617 gate identified in our study, i.e. the "M" in

A **Gate residues identified in this study**

```
hTRPV6  598 TYAAFAIIATLLMLNLLIAMMG 619
hTRPP3  540 YFVTYVFFVFFVLLNMFLAIIN 561
hTRPP2  660 YFTTFVFFMFFILLNMFLAIIN 681
rTRPM8  959 LVCIYMLSTNILLVNLLVAMFG 980
mTRPC4  600 MFGTYNVISLVVLLNMLIAMMN 621
                          Gate motif
```

Reported gate residues

```
rTRPV6  557 TYAAFAIIATLLMLNLLIAMMG 578
RTRPV2  623 LLLAYVLLTYVLLLNMLIALMS 644
rTRPV1  662 LLLAYVILTYILLLNMLIALMG 683
hTRPP2  660 YFTTFVFFMFFILLNMFLAIIN 681
hTRPA1  940 QLVSFTIFVPIVLMNLLIGLAV 961
```

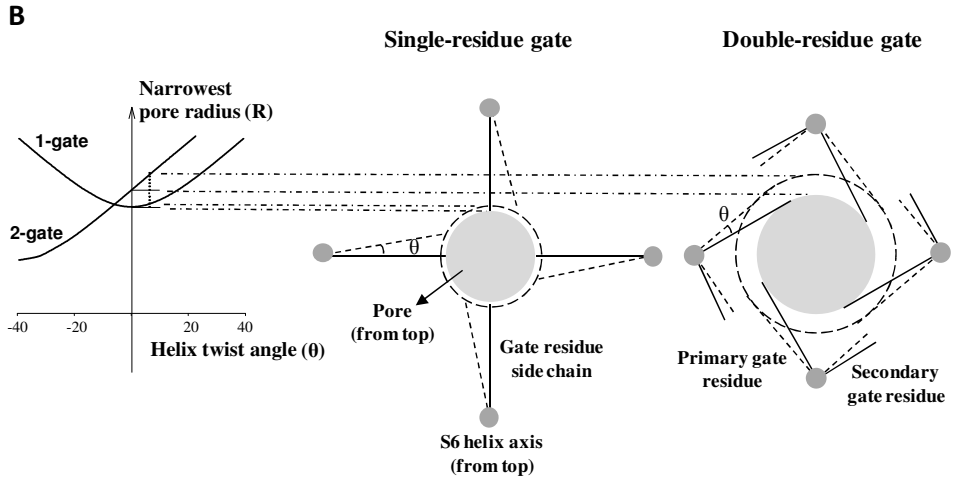

Fig. 6-6. Summary of identified pore gate residues and pore gate models. (**A**). *Upper panel*, alignment of the S6 helix sequences of the five TRP channels studied here. Identified gate residues are bold and underlined with the "LIAM" motif indicated. *Lower panel*, alignment of the S6 helix sequences of the five TRP channels whose structures were recently solved (TRPV6 [14], TRPV2 [13], TRPV1 [3], TRPP2 [17], and TRPA1 [16]). Identified gate residues are bold and underlined. The gate residue identified by SCAM in TRPV1 is bold and double underlined [24]. h, human; m, mouse; r, rat; R, rabbit. First and last amino acid numbers are indicated. (**B**). Pore size changes in single- and double-residue gate models, following helix twist. *Left panel*, narrowest pore radius (R, arbitrary unit) as a function of the helix twist angle (θ) according to $R = Sqrt[R_0^2 + 2A(A+R_0)(1-\cos\theta)] = Sqrt[9+176*(1-\cos\theta)]$, where R_0 and A, the initial pore radius (when $\theta = 0$) and gate amino acid length, were assumed to be 3 and 8 nm, respectively. This relationship holds true when twist angles remain small so that only the (primary) gate residue is involved in defining the pore size. *Middle panel*, schematic illustration of a single-residue gate model in which pore size increases when helices twist in a small counter-clock angle. S6 helix axes are

marked by small grey circles. Large grey and dashed line circles represent the narrowest pore before and after twisting, respectively. Gate residue side chains before and after twisting are indicated by solid and dashed lines, respectively. *Right panel*, double-residue gate model in which the primary and secondary gate amino acids are respectively indicted by long and short lines which were assumed in the drawing to form an angle of 40 and 60 degrees, respectively, with the line linking the helix centre and pore centre.

the LIA**M** motif. Apparently, TRPV configurations under experimental conditions in the functional studies may be different from those in structural analyses. The fact that the TRPV1, TRPV2 and TRPV6 lower gates predicted from the structures do not align could be caused by distinct properties of the three highly homologous but not identical proteins or the experimental conditions used to elucidate the structures, e.g. conditions used in cryo-EM (TRPV1, TRPV2) or crystallography (TRPV6). In contrast, the same residue L677 of TRPP2 was identified as the lower gate by our functional study and recent structural analyses [17,44,45]; it also aligns with the lower gate of TRPV1 (I679) [3] and TRPA1 (I957) [16] (Fig. 6-6A). Of note, the TRPP2 structural analysis combined cryo-EM and nanodisc technology, which mimics a native lipid bilayer environment [17].

While the concept of single-residue gate has been generally accepted, some bacterial ion channels were reported to possess a double-residue gate in which the two residues are one turn away from each other [26,27], which is similar to the TRPA1 gate indicated by structural study [16] (Fig. 6-6A). For TRPP2, TRPM8 and TRPC4 channels, the single gate residue presumably faces the pore. We proposed a model in which the four gate residues in a tetramer define the narrowest pore constriction (Fig. 6-6B, middle panel). In contrast, for TRPV6 and TRPP3 that possess a double-residue gate, either of the two gate residues would face away from the pore centre (Fig. 6-6B, right panel). In this model, the primary gate residue was drawn to face slightly more towards the pore centre than the secondary gate residue, to reflect their different sensitivities to

small changes in the residue hydrophobicity and size. In fact, unlike primary gate residues, substitutions of a secondary gate residue in TRPV6 and TRPP3 or a single gate residue in TRPM8, TRPC4 and TRPP2 to an amino acid among A, V, I, and L did not give rise to appreciable changes in the channel activity (Fig. 6-1K and L, Fig. 6-2F and I, Fig. 6-3F, Fig. 6-4D and Fig. 6-5F). These results together suggest that replacements of a gate residue by hydrophobic amino acids of various sizes represent reasonable mimics of pore size changes under physiological conditions. Thus, we wonder whether under physiological conditions TRP channels with a double-residue gate are associated with smaller gate conformational changes as compared to those with a single-residue gate. On the other hand, because secondary gate residues in TRPP3 and TRPV6 seemed to require stronger mutations for their channel activity to be significantly affected, it remains to be determined as to whether under physiological conditions, besides 'pushing' the primary gate residue away from facing the pore centre, they are actually involved in controlling channel opening/closing.

Gating of an ion channel may involve complex protein conformational changes, which may include a combination of S6 splaying, twisting and bending. Unlike potassium channels that possess a canonical S6 PVP motif to allow helix bending [25], TRP channels do not have a similar PVP motif in their S6 and thus do not likely involve a S6 bending movement. Interestingly, by a SCAM analysis using extracellular thiol-modifying compounds the TRPV5 upper gate (selectivity filter) was shown to undergo pH-dependent twisting [32]. We here propose models to illustrate pore opening and closing through twisting of the four S6 helices around their axis in TRP channels with a single- or double-residue gate (Fig. 6-6B). In these models, we can see that a double-residue gate allows much more efficient changes in the pore size than a single-residue gate through twisting of the same angle (Fig. 6-6B), which represents a unique characteristic of a

double-residue gate channel. Interestingly, based on these models, if TRPP3 S6 twists a certain angle so that L557 faces more towards, while at the same time A558 more away from, the pore centre, then TRPP3 would become a single-residue gate (i.e. L557) channel, like TRPP2. Because these two homologous channels have an almost identical S6 sequence, we wonder whether their sequence differences elsewhere would be translated into two distinct protein conformations that show an apparently twisted S6 of one channel relative to the S6 of the other.

In summary, we have identified distinct amino acid residues within the LIAM motif of the distal part of the pore-lining S6 helix, which form the most constricted sites of the lower gate in TRPV6, TRPP3 (double-residue gate) and TRPP2, TRPM8, TRPC4 (single-residue gate). We have found that a double-residue gate channel is more sensitive than a single-residue gate channel to small changes in the hydrophobicity and size of the gating residues, as is to S6 helix twisting. We assume that single- and double-residue gating may have been evolutionarily adapted by TRP channels to respond to a variety of physiological stimuli that induce distinct gate conformational changes associated with channel opening and closing.

6.6 REFERENCES

1. Clapham, D. E. TRP channels as cellular sensors. *Nature.* **426**, 517-524 (2003).

2. Julius, D. TRP channels and pain. *Annu. Rev. Cell Dev. Biol.* **29**, 355-384 (2013).

3. Liao, M., Cao, E., Julius, D. & Cheng, Y. Structure of the TRPV1 ion channel determined by electron cryo-microscopy. *Nature.* **504**, 107-112 (2013).

4. Venkatachalam, K. & Montell, C. TRP channels. *Annu. Rev. Biochem.* **76**, 387-417 (2007).

5. Clapham, D. E., Runnels, L. W. & Strubing, C. The TRP ion channel family. *Nat. Rev. Neurosci.* **2**, 387-396 (2001).

6. Montell, C. The TRP superfamily of cation channels. *Sci. STKE.* **2005**, re3 (2005).

7. Ishimaru, Y. & Matsunami, H. Transient receptor potential (TRP) channels and taste sensation. *J. Dent. Res.* **88**, 212-218 (2009).

8. Eijkelkamp, N., Quick, K. & Wood, J. N. Transient receptor potential channels and mechanosensation. *Annu. Rev. Neurosci.* **36**, 519-546 (2013).

9. Nilius, B., Owsianik, G., Voets, T. & Peters, J. A. Transient receptor potential cation channels in disease. *Physiol Rev.* **87**, 165-217 (2007).

10. Nilius, B., Voets, T. & Peters, J. TRP channels in disease. *Sci. STKE.* **2005**, re8 (2005).

11. Shapovalov, G., Ritaine, A., Skryma, R. & Prevarskaya, N. Role of TRP ion channels in cancer and tumorigenesis. *Semin. Immunopathol.* **38**, 357-369 (2016).

12. Moran, M. M., McAlexander, M. A., Biro, T. & Szallasi, A. Transient receptor potential channels as therapeutic targets. *Nat. Rev. Drug Discov.* **10**, 601-620 (2011).

13. Zubcevic, L. *et al.* Cryo-electron microscopy structure of the TRPV2 ion channel. *Nat. Struct. Mol. Biol.* **23**, 180-186 (2016).

14. Saotome, K., Singh, A. K., Yelshanskaya, M. V. & Sobolevsky, A. I. Crystal structure of the epithelial calcium channel TRPV6. *Nature* **534**, 506-511 (2016).

15. Huynh, K. W. *et al.* Structure of the full-length TRPV2 channel by cryo-EM. *Nat. Commun.* **7**, 11130 (2016).

16. Paulsen, C. E., Armache, J. P., Gao, Y., Cheng, Y. & Julius, D. Structure of the TRPA1 ion channel suggests regulatory mechanisms. *Nature.* **520**, 511-517 (2015).

17. Shen, P. S. *et al.* The Structure of the Polycystic Kidney Disease Channel PKD2 in Lipid Nanodiscs. *Cell* **167**, 763-773 (2016).

18. Oelstrom, K. & Chanda, B. Congruent pattern of accessibility identifies minimal pore gate in a non-symmetric voltage-gated sodium channel. *Nat. Commun.* **7**, 11608 (2016).

19. Oelstrom, K., Goldschen-Ohm, M. P., Holmgren, M. & Chanda, B. Evolutionarily conserved intracellular gate of voltage-dependent sodium channels. *Nat. Commun.* **5**, 3420 (2014).

20. del, C. D. & Yellen, G. Tight steric closure at the intracellular activation gate of a voltage-gated K(+) channel. *Neuron* **32**, 649-656 (2001).

21. Kitaguchi, T., Sukhareva, M. & Swartz, K. J. Stabilizing the closed S6 gate in the Shaker Kv channel through modification of a hydrophobic seal. *J. Gen. Physiol* **124**, 319-332 (2004).

22. Sukhareva, M., Hackos, D. H. & Swartz, K. J. Constitutive activation of the Shaker Kv channel. *J. Gen. Physiol* **122**, 541-556 (2003).

23. Cao, E., Liao, M., Cheng, Y. & Julius, D. TRPV1 structures in distinct conformations reveal activation mechanisms. *Nature* **504**, 113-118 (2013).

24. Salazar, H. *et al.* Structural determinants of gating in the TRPV1 channel. *Nat. Struct. Mol. Biol.* **16**, 704-710 (2009).

25. Aryal, P., Sansom, M. S. & Tucker, S. J. Hydrophobic gating in ion channels. *J. Mol. Biol.* **427**, 121-130 (2015).

26. Wang, W. *et al.* The structure of an open form of an E. coli mechanosensitive channel at 3.45 A resolution. *Science* **321**, 1179-1183 (2008).

27. Bass, R. B., Strop, P., Barclay, M. & Rees, D. C. Crystal structure of Escherichia coli MscS, a voltage-modulated and mechanosensitive channel. *Science* **298**, 1582-1587 (2002).

28. Jeon, J. P. *et al.* Activation of TRPC4beta by Galphai subunit increases Ca2+ selectivity and controls neurite morphogenesis in cultured hippocampal neuron. *Cell Calcium* **54**, 307-319 (2013).

29. Gees, M., Colsoul, B. & Nilius, B. The role of transient receptor potential cation channels in Ca2+ signaling. *Cold Spring Harb. Perspect. Biol.* **2**, a003962 (2010).

30. Chen, J. *et al.* Pore dilation occurs in TRPA1 but not in TRPM8 channels. *Mol. Pain* **5**, 3 (2009).

31. Chung, M. K., Guler, A. D. & Caterina, M. J. TRPV1 shows dynamic ionic selectivity during agonist stimulation. *Nat. Neurosci.* **11**, 555-564 (2008).

32. Yeh, B. I., Kim, Y. K., Jabbar, W. & Huang, C. L. Conformational changes of pore helix coupled to gating of TRPV5 by protons. *EMBO J.* **24**, 3224-3234 (2005).

33. Aryal, P., bd-Wahab, F., Bucci, G., Sansom, M. S. & Tucker, S. J. A hydrophobic barrier deep within the inner pore of the TWIK-1 K2P potassium channel. *Nat. Commun.* **5**, 4377 (2014).

34. Yang, J. *et al.* Receptor for activated C kinase 1 (RACK1) inhibits function of transient receptor potential (TRP)-type channel Pkd2L1 through physical interaction. *J. Biol. Chem.* **287**, 6551-6561 (2012).

35. Arif, P. M. *et al.* Function and regulation of TRPP2 ion channel revealed by a gain-of-function mutant. *Proc. Natl. Acad. Sci. U. S. A* **113**, E2363-E2372 (2016).

36. Fecher-Trost, C. *et al.* The in vivo TRPV6 protein starts at a non-AUG triplet, decoded as methionine, upstream of canonical initiation at AUG. *J. Biol. Chem.* **288**, 16629-16644 (2013).

37. Zheng, W. *et al.* A novel PKD2L1 C-terminal domain critical for trimerization and channel function. *Sci. Rep.* **5:9460. doi: 10.1038/srep09460.**, 9460 (2015).

38. Courjaret, R., Hubrack, S., Daalis, A., Dib, M. & Machaca, K. The Xenopus TRPV6 homolog encodes a Mg(2+) -permeant channel that is inhibited by interaction with TRPC1. *J. Cell Physiol* **228**, 2386-2398 (2013).

39. Peng, J. B. *et al.* Molecular cloning and characterization of a channel-like transporter mediating intestinal calcium absorption. *J. Biol. Chem.* **274**, 22739-22746 (1999).

40. Chen, X. Z. *et al.* Polycystin-L is a calcium-regulated cation channel permeable to calcium ions. *Nature.* **401**, 383-386 (1999).

41. Catterall, W. A. Structure and function of voltage-gated sodium channels at atomic resolution. *Exp. Physiol* **99**, 35-51 (2014).

42. Harris, P. C. & Torres, V. E. Polycystic kidney disease. *Annu. Rev. Med.* **60**, 321-337 (2009).

43. Wu, G. & Somlo, S. Molecular genetics and mechanism of autosomal dominant polycystic kidney disease. *Mol. Genet. Metab* **69**, 1-15 (2000).

44. Grieben, M. *et al.* Structure of the polycystic kidney disease TRP channel Polycystin-2 (PC2). *Nat. Struct. Mol. Biol.* (2016).

45. Wilkes, M. *et al.* Molecular insights into lipid-assisted Ca2+ regulation of the TRP channel Polycystin-2. *Nat. Struct. Mol. Biol.* (2017).

46. Bharate, S. S. & Bharate, S. B. Modulation of thermoreceptor TRPM8 by cooling compounds. *ACS Chem. Neurosci.* **3**, 248-267 (2012).

47. Voets, T. *et al.* The principle of temperature-dependent gating in cold- and heat-sensitive TRP channels. *Nature* **430**, 748-754 (2004).

48. Freichel, M., Tsvilovskyy, V. & Camacho-Londono, J. E. TRPC4- and TRPC4-Containing Channels. *Handb. Exp. Pharmacol.* **222**, 85-128 (2014).

49. Beck, A. *et al.* Conserved gating elements in TRPC4 and TRPC5 channels. *J. Biol. Chem.* **288**, 19471-19483 (2013).

6.7 SUPPLEMENTARY MATERIALS

Fig. 6-S1. Amino acid sequence alignment of the S6 helices of the human TRP channels from the six subfamilies present in mammals, of the N-subfamily only present in fly, frog, worm and fish, and of the Y-subfamily from yeast. The first and last amino acid numbers are indicated. The Universal Protein Resource accession number for sequences used here are

Q8NER1 (hV1), Q9Y5S1 (hV2), Q8NET8 (hV3), Q9HBA0 (hV4), Q9NQA5 (hV5), Q9H1D0 (hV6), P48995 (hC1), Q9R244 (mC2), Q13507 (hC3), Q9UBN4 (hC4), Q9UL62 (hC5), Q9Y210 (hC6), Q9HCX4 (hC7), Q7Z4N2 (hM1), O94759 (hM2), Q9HCF6 (hM3), Q8TD43 (hM4), Q9NZQ8 (hM5), Q9BX84 (hM6), Q96QT4 (hM7), Q7Z2W7 (hM8), Q13563 (hP2), Q9P0L9 (hP3), Q9NZM6 (hP5), Q9GZU1 (hML1), Q8IZK6 (hML2), Q8TDD5 (hML3), O75762 (hA1), Q7KIQ2 (TRPN, fruit fly), Q9GRV5 (TRPN, *C. elegans* or worm), Q4A520 (TRPN, frog), Q7T1G6 (TRPN, zebrafish), and H0GNL1 (TRPY, yeast). Human TRPC2 is a pseudogene and mouse TRPC2 was used instead. Putative gate motif 'LIAM' is highlighted grey.

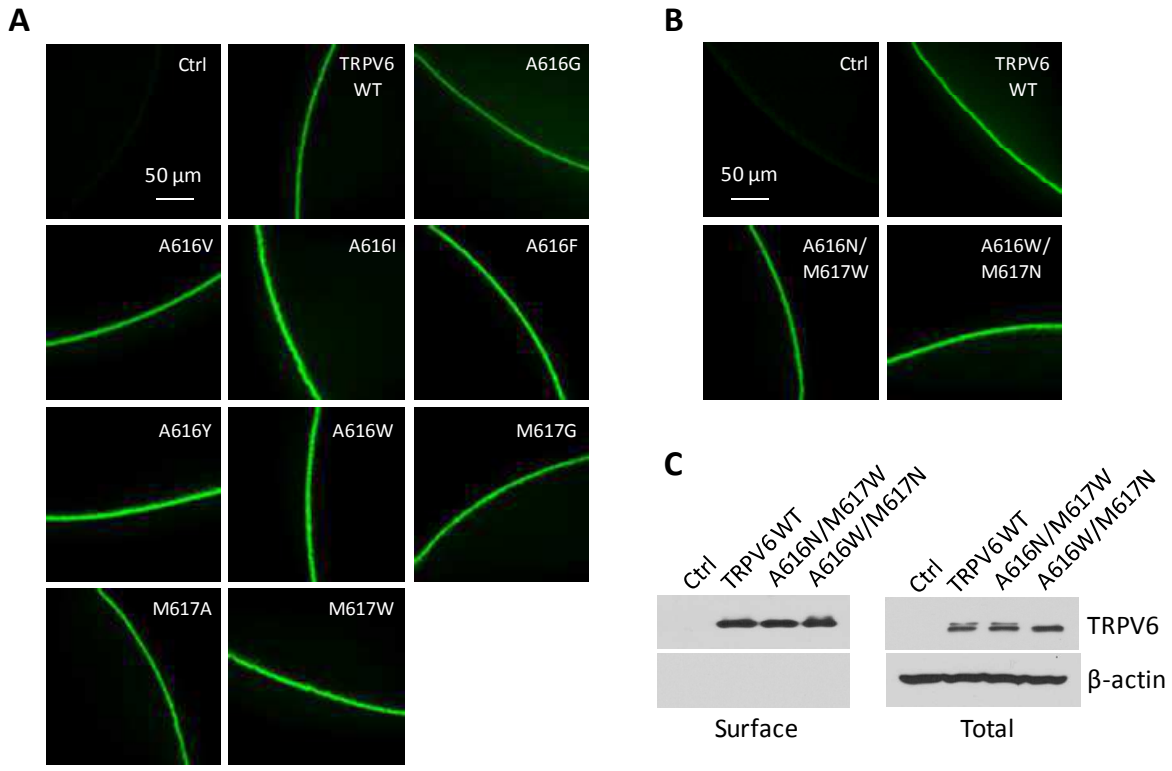

Fig. 6-S2. Surface and total expression of human TRPV6 in oocytes. (**A** and **B**). Whole-mount immunofluorescence using the anti-TRPV6 antibody showing the oocyte surface expression of indicated mutants; Ctrl, water injected oocytes; WT, wild-type). (**C**). Western blot of surface biotinylated and total protein ofTRPV6 WT, mutant A616N/M617W or A616W/M617N.

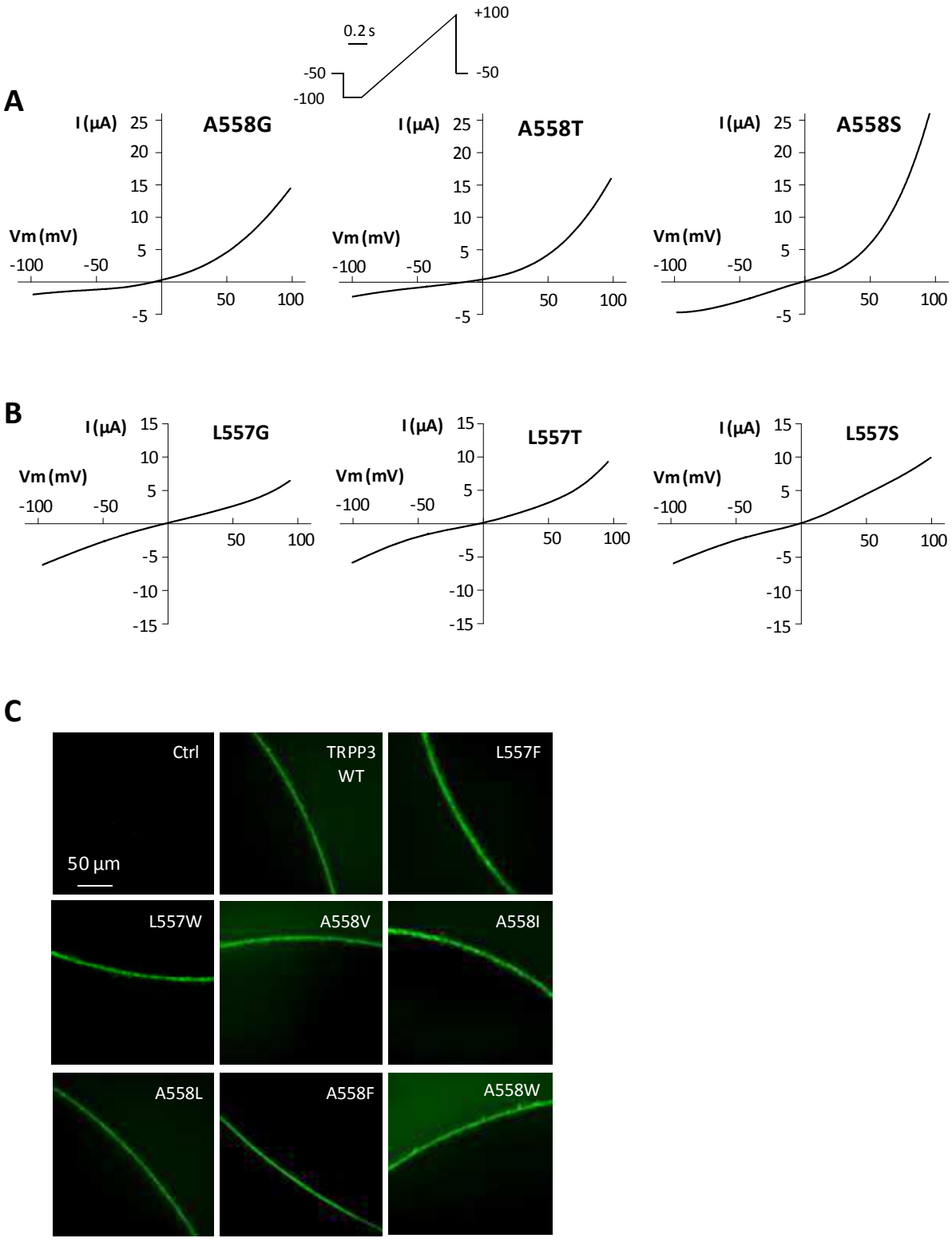

Fig. 6-S3. I-V curves and surface expression of human WT or mutant TRPP3 in oocytes. (**A**). Representative I-V curves obtained from TRPP3 A558G, A558T or A558S expressing

oocytes using a ramp protocol in the presence of Mg^{2+}-free Na-containing solution (in mM): 100 NaCl, 2 KCl, 10 HEPES, pH 7.5. (**B**). Representative I-V curves obtained from human TRPP3 L557G, L557T or L557S expressing oocytes in the presence of the Na-containing solution. (**C**). Whole-mount immunofluorescence using the antibody for the Flag-tag showing the oocyte surface expression of the TRPP3 WT or indicated mutants; Ctrl, water injected oocytes.

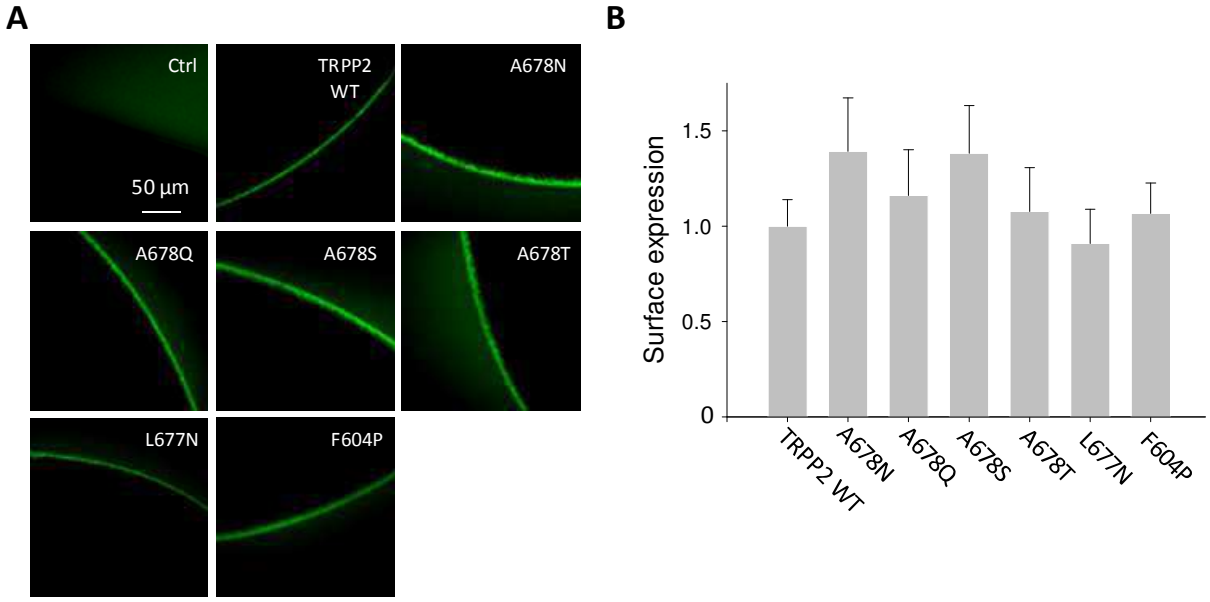

Fig. 6-S4. Surface and total expression of human TRPP2 in oocytes. (**A**). Whole-mount immunofluorescence using the antibody for the HA-tag showing the oocyte surface expression of the TRPP2 WT or indicated mutants; Ctrl, water injected oocytes. (**B**). Averaged surface membrane expression of the TRPP2 mutants normalized to that of TRPP2 WT; n = 4 – 7.

CHAPTER 7

GENERAL DISCUSSION

7.1 A threshold model of cystogenesis in ADPKD

Cyst formation in ADPKD is thought to initiate following a 'second hit' resulting in reduction of functional PC1 or TRPP2 protein level below the cystogenic threshold [202]. The 'second hit' may be either somatic mutation leading to inactivation of the unaffected allele or environmental factors resulting in down-regulation of PC1 or TRPP2 protein level. However, somatic mutations were only identified in 20-43% of the analyzed *PKD1* or *PKD2* renal cysts [83-86]. Over the past decade, evidence has been accumulated to support a "dosage" model that suggests renal cystogenesis can be initiated when the functional PC1 or TRPP2 protein level is reduced below a threshold level in the absence of a somatic mutation [87-89]. Studies about how TRPP2 is regulated are limited. MicroRNA-17 binds to the 3'UTR of TRPP2 mRNA and down-regulates the stability of TRPP2 mRNA and its translation. Further, *Xenopus* and mice showed cystic phenotype and down-regulated TRPP2 mRNA with knockin of microRNA-17 [110]. Bicc1, a RNA-binding protein, up-regulates TRPP2 expression through competing with microRNA-17 for binding to the same site in TRPP2 mRNA 3'UTR, and consistently, mice with *Bicc1* mutation exhibit reduced TRPP2 protein levels [111]. In this study, we identified two additional factors, ER stress and FUBP1, to positively and negatively regulate TRPP2 protein translation, respectively.

Ischemia-reperfusion (I/R) injury in rat kidney was previously shown to dramatically enhance TRPP2 expression [106]. I/R injury will generally induce various cellular stresses, such as oxidative stress and ER stress [238] which is involved in diverse renal diseases [145]. Although we found that TRPP2 is rapidly up-regulated during ER stress, sustained ER stress was previously shown to down-regulate TRPP2 protein level through ER-associated degradation [239]. How this transition occurs remains to be determined. More importantly, it needs to examine whether and how this regulation is involved in the pathogenesis of ADPKD.

FUBP1 was initially identified as a DNA-binding protein to promote *c-Myc* transcription and plays a critical role in embryonic development [166]. FUBP1 was also shown to reduce transcription of TNFα [169]. Interestingly, c-Myc and TNFα leves are both elevated in cystic tissues of various PKD models [95]. Moreover, c-Myc transgenic mice and application of TNFα to in vitro cultured kidney both developed cysts [240]. Thus, although FUBP1 altered the expression of three cystogenic proteins TRPP2 (down), TNFα (down) and c-Myc (up), whether and how FUBP1 is implicated in cystogenesis remains to be determined.

Considering that recent clinical trials aiming to slow the growth of cysts based on reported aberrant signaling pathways in ADPKD are not successful, it is important to unveil novel mechanisms of dosage regulation of PC1 and TRPP2, and identify new therapeutic targets and approaches. In fact, the identified translationally regulatory pathways of TRPP2 would allow the design of molecules that increase the dosage, hence the function, of TRPP2 to correct the reduced TRPP2 function in individuals only with a TRPP2 pathogenic germline mutation in one of the two allelse, i.e., before the 'second hit' and cyst initiation. For those already with occurred 'second hit' in the other allele, i.e., in a cystic disease state, as long as their germline or somatic TRPP2 mutant remains partially functional a therapeutic strategy targeting these pathways should still work, i.e., by increasing the mutants' dosage to compensate for the partial loss of function.

7.2 TRPP3 homo- and hetero-tetramer assemblies

Similar to voltage-gated potassium channels, TRP channels were predicted to function as tetramers, which was confirmed by recently published TRPV1, -2, -6, TRPA1 and TRPP2 structures [44,47,48,50,51]. TRPP2 and TRPP3 are also assumed to assemble into homo-tetramers to be functional. Different from other TRP members, TRPP2 and TRPP3 are also found to form hetero-tetramers with PKD1 and PKD1L3, respectively, with 3:1 stoichiometry [194,201]. Therefore, one would ask whether the homo- and hetero-tetramer of TRPP2 or TRPP3 share a trimer/monomer assembly model. Critical evidence to support this hypothesis would be identification of a trimerization domain in TRPP2 and TRPP3. Indeed, a conserved trimerization domain, CC2, was identified later in C-terminus of TRPP2 and TRPP3 [186]. However, a previous study and our current study found that TRPP3 truncation mutants lacking CC2 exhibit similar channel function as WT TRPP3 [187], suggesting that CC2 is not necessary for functional TRPP3 assembly. We identified, for the first time, C1 domain, which is not overlapped with CC2, to be critical for both TRPP3 trimerization and channel function. Moreover, C1 peptide expression is able to block TRPP3/PKD1L3 channel function, indicating the involvement of C1 in assembly of TRPP3/PKD1L3 channel complex. Therefore, it could be that C1 is the sharing the trimerzation domain for both TRPP3 homotetramers and TRPP3/PKD1L3 heterotetramers. It would be interesting to see whether TRPP2 contains a similar functionally important trimerization domain. Since recently published high-resolution TRPP2 structure lacks both N- and C-termini [51], it provides little insight into its oligomeric assembly. Another interesting question is that whether the trimerization process is unique to TRPP3 and TRPP2 or also exists in other TRP members which are generally speculated to form functional channels through dimerization of two homodimers.

7.3 Regulation of TRPP3 by post-translational modifications

Post-translational modifications play critical roles in regulation of ion channel activity. To date, various post-translational modifications have been reported for TRP channels, such as phosphorylation, glycosylation, disulfide bond, and covalently adding chemicals to specific cysteine residues. These post-translational modifications can regulate a variety of aspects of TRP channels ranging from trafficking, single channel kinetics and channel gating [241]. As TRPP3 homologue, TRPP2 was shown to undergo several post-translational modifications. For example, casein kinase II phosphorylates TRPP2 at C-terminal Ser-812 [242] and glycogen synthase kinase phosphorylates it at N-terminal Ser-76 [243]. These phosphorylations modulate either trafficking or channel activity of TRPP2. Additionally, TRPP2 was also reported to undergo glycosylation which was proposed to regulate TRPP2 trafficking and maturation [74]. Although TRPP3 was predicted to be able to be modified by phosphorylation, glycosylation, and palmitoylation, little information is available so far as to whether and how it is regulated by post-translational modifications. For the first time, we reported that TRPP3 is palmitoyated at C38 and phosphorylated at T39. These two types of modifications have no effect on TRPP3 trafficking in Xenopus oocytes, but modulate its channel activity. Since palmitoylation and phosphorylation are both reversible, they may represent important dynamic ways to regulate TRPP3 channel function. It is yet to be determined whether and how these post-translational modifications are involved in regulation of TRPP3 physiological function *in vivo*. Also, future studies are needed to identify DHHC enzymes and kinases responsible for TRPP3 palmitoylation and phosphorylation.

7.4 Pore gates in TRP channels

Ion channels control ion flow by opening or closing an activation gate and this process is called gating. Voltage-gated sodium and calcium channels have been shown to possess an evolutionarily conserved hydrophobic gate composed of four residues with each from one pore-lining helix. In TRP channels, except for the conventional single-residue gate, we also identified gates composed of double consecutive residues from each pore-lining helix in TRPV6 and TRPP3. What makes double-residue gate unique? One is that channels with double-residue gate, such as TRPV6 and TRPP3, show high sensitivity to the gate residue substitutions with closely related amino acids. In other words, a relatively small conformational change would be enough to open the channels with a double-residue gate, but not the ones with single-residue gate. This unique property may be in line with the nature of their physiological activators that only induce small conformational changes *in vivo*. Considering both TRPV6 and TRPP3 are supposed to be responsive to fluid flow [244-247] and the bacterial mechano-sensitive channel MscS also possesses a double-residue gate although the two residues are three amino acids apart [227,228], it is possible that mechanical force is a such physiological stimuli that correspond to small conformational changes, which can be accomplished by ion channels with a double-residue gate. In contrast, TRPM8 and TRPC4 did not show any activity increase when the gate residue was similarly substituted (V976A and V976G in TRPM8 and I617A and I617G in TRPC4), suggesting that large conformational change at the gate region is required to open these two channels. Compared with voltage-gated sodium and calcium channels which contain only single-residue gate and mainly respond to one type of activator, membrane potential, TRP channels respond to a remarkably wide range of stimuli. We thus hypothesize that single- and double-residue gating may have been evolutionarily adapted by TRP channels to respond to a variety of physiological

stimuli that induce distinct gate conformational changes associated with channel opening and closing.

7.5 Future directions

In terms of translational regulations of TRPP2 mediated by its 5'UTR and 3'UTR, it would be interesting to see whether these pathways identified *in vitro* can really regulate TRPP2 expression *in vivo* (e.g., in mice) and TRPP2-deficient induced phenotypes. Since salubrinal treatment increases TRPP2 expression in cell cultures, it would be intriguing to examine whether it can slow the renal cyst progression in $PKD2^{+/-}$ mice. $FUBP1^{-/-}$ mice die at E13.5 while $FUBP1^{+/-}$ mice exhibit the same FUBP1 protein expression level as WT mice, so these mice cannot be used to check the effects of FUBP1 knockout or knockdown on cyst formation in $PKD2^{+/-}$ mice by cross-breeding. *In vivo* knockdown through siRNA injection would be practical way in this regard.

As for palmitoylation and phosphorylation of TRPP3, future studies are needed to examine the effects of these two types of post-translational modifications on TRPP3 function in more *in vivo* models, such as primarily cultured renal tubule epithelial cells. Since we showed that C38 palmitoylation and T39 phosphorylation regulate TRPP3 channel function independently, further studies are required to elucidate the underlying individual mechanism. Also, it is needed to identify the DHHC enzyme responsible for C38 palmitoylation and the kinase responsible for T39 phosphorylation.

We identified double-residue gate in TRPV6 (A616/M617), which is different from the one (M618) revealed by TRPV6 cyrstal structure. The difference may come from different experimental conditions of these two studies in which TRPV6 protein is not lipid bilayer

environment during crystallization. It would be interesting to see whether double-residue gate can be observed if TRPV6 structure is determined with cryo-EM combined with nanodisc technique which was successfully used in the structure determination of TRPP2. Another interesting question is whether activations of TRP channels involve rotation movement of gate region, which can be examined by cysteine substituted accessibility assays. The strategy we developed to force TRP channel open without agonists would be very useful to study those TRP channels with no detectable activity, such as TRPC1 and TRPP5. Besides, since mice deficient with most individual TRP channels show no obvious phenotype, the gate mutants which show increased channel activity and are still gatable would be good candidates for generation of knockin mice models to investigate physiological functions of TRP channels.

8. REFERENCES

1. Cosens, D. J. & Manning, A. Abnormal electroretinogram from a Drosophila mutant. *Nature* **224**, 285-287 (1969).

2. Montell, C. & Rubin, G. M. Molecular characterization of the Drosophila trp locus: a putative integral membrane protein required for phototransduction. *Neuron* **2**, 1313-1323 (1989).

3. Venkatachalam, K. & Montell, C. TRP channels. *Annu. Rev. Biochem.* **76**, 387-417 (2007).

4. Clapham, D. E. TRP channels as cellular sensors. *Nature.* **426**, 517-524 (2003).

5. Nilius, B., Owsianik, G., Voets, T. & Peters, J. A. Transient receptor potential cation channels in disease. *Physiol Rev.* **87**, 165-217 (2007).

6. Nilius, B. & Owsianik, G. Transient receptor potential channelopathies. *Pflugers Arch.* **460**, 437-450 (2010).

7. Julius, D. TRP channels and pain. *Annu. Rev. Cell Dev. Biol.* **29**, 355-384 (2013).

8. Nilius, B. TRP channels in disease. *Biochim. Biophys. Acta* **1772**, 805-812 (2007).

9. Montell, C. The TRP superfamily of cation channels. *Sci. STKE.* **2005**, re3 (2005).

10. Moiseenkova-Bell, V. & Wensel, T. G. Functional and structural studies of TRP channels heterologously expressed in budding yeast. *Adv. Exp. Med. Biol.* **704**, 25-40 (2011).

11. Latorre, R., Zaelzer, C. & Brauchi, S. Structure-functional intimacies of transient receptor potential channels. *Q. Rev. Biophys.* **42**, 201-246 (2009).

12. Wu, L. J., Sweet, T. B. & Clapham, D. E. International Union of Basic and Clinical Pharmacology. LXXVI. Current progress in the mammalian TRP ion channel family. *Pharmacol. Rev.* **62**, 381-404 (2010).

13. Nilius, B. & Owsianik, G. The transient receptor potential family of ion channels. *Genome Biol.* **12**, 218 (2011).

14. Nilius, B., Owsianik, G. & Voets, T. Transient receptor potential channels meet phosphoinositides. *EMBO J.* **27**, 2809-2816 (2008).

15. Rohacs, T., Lopes, C. M., Michailidis, I. & Logothetis, D. E. PI(4,5)P2 regulates the activation and desensitization of TRPM8 channels through the TRP domain. *Nat. Neurosci.* **8**, 626-634 (2005).

16. Perraud, A. L. *et al.* ADP-ribose gating of the calcium-permeable LTRPC2 channel revealed by Nudix motif homology. *Nature* **411**, 595-599 (2001).

17. Nadler, M. J. *et al.* LTRPC7 is a Mg.ATP-regulated divalent cation channel required for cell viability. *Nature* **411**, 590-595 (2001).

18. Runnels, L. W., Yue, L. & Clapham, D. E. TRP-PLIK, a bifunctional protein with kinase and ion channel activities. *Science* **291**, 1043-1047 (2001).

19. Earley, S. & Brayden, J. E. Transient receptor potential channels in the vasculature. *Physiol Rev.* **95**, 645-690 (2015).

20. Cheng, W., Sun, C. & Zheng, J. Heteromerization of TRP channel subunits: extending functional diversity. *Protein Cell* **1**, 802-810 (2010).

21. Strubing, C., Krapivinsky, G., Krapivinsky, L. & Clapham, D. E. Formation of novel TRPC channels by complex subunit interactions in embryonic brain. *J. Biol. Chem.* **278**, 39014-39019 (2003).

22. Hofmann, T., Schaefer, M., Schultz, G. & Gudermann, T. Subunit composition of mammalian transient receptor potential channels in living cells. *Proc. Natl. Acad. Sci. U. S. A* **99**, 7461-7466 (2002).

23. Hellwig, N., Albrecht, N., Harteneck, C., Schultz, G. & Schaefer, M. Homo- and heteromeric assembly of TRPV channel subunits. *J. Cell Sci.* **118**, 917-928 (2005).

24. Li, M., Jiang, J. & Yue, L. Functional characterization of homo- and heteromeric channel kinases TRPM6 and TRPM7. *J. Gen. Physiol* **127**, 525-537 (2006).

25. Venkatachalam, K., Hofmann, T. & Montell, C. Lysosomal localization of TRPML3 depends on TRPML2 and the mucolipidosis-associated protein TRPML1. *J. Biol. Chem.* **281**, 17517-17527 (2006).

26. Ramsey, I. S., Delling, M. & Clapham, D. E. An introduction to TRP channels. *Annu. Rev. Physiol.* **68:619-47.**, 619-647 (2006).

27. Zimmermann, K. *et al.* Transient receptor potential cation channel, subfamily C, member 5 (TRPC5) is a cold-transducer in the peripheral nervous system. *Proc. Natl. Acad. Sci. U. S. A* **108**, 18114-18119 (2011).

28. Vriens, J. *et al.* TRPM3 is a nociceptor channel involved in the detection of noxious heat. *Neuron* **70**, 482-494 (2011).

29. Venkatachalam, K., Zheng, F. & Gill, D. L. Regulation of canonical transient receptor potential (TRPC) channel function by diacylglycerol and protein kinase C. *J. Biol. Chem.* **278**, 29031-29040 (2003).

30. Hofmann, T. *et al.* Direct activation of human TRPC6 and TRPC3 channels by diacylglycerol. *Nature* **397**, 259-263 (1999).

31. Li, M. *et al.* Molecular determinants of Mg2+ and Ca2+ permeability and pH sensitivity in TRPM6 and TRPM7. *J. Biol. Chem.* **282**, 25817-25830 (2007).

32. Li, M., Jiang, J. & Yue, L. Functional characterization of homo- and heteromeric channel kinases TRPM6 and TRPM7. *J. Gen. Physiol* **127**, 525-537 (2006).

33. Launay, P. *et al.* TRPM4 is a Ca2+-activated nonselective cation channel mediating cell membrane depolarization. *Cell* **109**, 397-407 (2002).

34. Prawitt, D. *et al.* TRPM5 is a transient Ca2+-activated cation channel responding to rapid changes in [Ca2+]i. *Proc. Natl. Acad. Sci. U. S. A* **100**, 15166-15171 (2003).

35. Du, J., Xie, J. & Yue, L. Intracellular calcium activates TRPM2 and its alternative spliced isoforms. *Proc. Natl. Acad. Sci. U. S. A* **106**, 7239-7244 (2009).

36. Zurborg, S., Yurgionas, B., Jira, J. A., Caspani, O. & Heppenstall, P. A. Direct activation of the ion channel TRPA1 by Ca2+. *Nat. Neurosci.* **10**, 277-279 (2007).

37. Hara, Y. *et al.* LTRPC2 Ca2+-permeable channel activated by changes in redox status confers susceptibility to cell death. *Mol. Cell* **9**, 163-173 (2002).

38. Sano, Y. *et al.* Immunocyte Ca2+ influx system mediated by LTRPC2. *Science* **293**, 1327-1330 (2001).

39. Perraud, A. L. *et al.* ADP-ribose gating of the calcium-permeable LTRPC2 channel revealed by Nudix motif homology. *Nature* **411**, 595-599 (2001).

40. Vriens, J. *et al.* TRPM3 is a nociceptor channel involved in the detection of noxious heat. *Neuron* **70**, 482-494 (2011).

41. Grimm, C., Kraft, R., Schultz, G. & Harteneck, C. Activation of the melastatin-related cation channel TRPM3 by D-erythro-sphingosine [corrected]. *Mol. Pharmacol.* **67**, 798-805 (2005).

42. Lee, N. *et al.* Expression and characterization of human transient receptor potential melastatin 3 (hTRPM3). *J. Biol. Chem.* **278**, 20890-20897 (2003).

43. Grimm, C., Kraft, R., Sauerbruch, S., Schultz, G. & Harteneck, C. Molecular and functional characterization of the melastatin-related cation channel TRPM3. *J. Biol. Chem.* **278**, 21493-21501 (2003).

44. Liao, M., Cao, E., Julius, D. & Cheng, Y. Structure of the TRPV1 ion channel determined by electron cryo-microscopy. *Nature.* **504**, 107-112 (2013).

45. Cao, E., Liao, M., Cheng, Y. & Julius, D. TRPV1 structures in distinct conformations reveal activation mechanisms. *Nature* **504**, 113-118 (2013).

46. Gao, Y., Cao, E., Julius, D. & Cheng, Y. TRPV1 structures in nanodiscs reveal mechanisms of ligand and lipid action. *Nature* **534**, 347-351 (2016).

47. Paulsen, C. E., Armache, J. P., Gao, Y., Cheng, Y. & Julius, D. Structure of the TRPA1 ion channel suggests regulatory mechanisms. *Nature.* **520**, 511-517 (2015).

48. Zubcevic, L. *et al.* Cryo-electron microscopy structure of the TRPV2 ion channel. *Nat. Struct. Mol. Biol.* **23**, 180-186 (2016).

49. Huynh, K. W. *et al.* Structure of the full-length TRPV2 channel by cryo-EM. *Nat. Commun.* **7**, 11130 (2016).

50. Saotome, K., Singh, A. K., Yelshanskaya, M. V. & Sobolevsky, A. I. Crystal structure of the epithelial calcium channel TRPV6. *Nature* **534**, 506-511 (2016).

51. Shen, P. S. *et al.* The Structure of the Polycystic Kidney Disease Channel PKD2 in Lipid Nanodiscs. *Cell* **167**, 763-773 (2016).

52. Winn, M. P. *et al.* A mutation in the TRPC6 cation channel causes familial focal segmental glomerulosclerosis. *Science* **308**, 1801-1804 (2005).

53. Igarashi, P. & Somlo, S. Genetics and pathogenesis of polycystic kidney disease. *J. Am. Soc. Nephrol.* **13**, 2384-2398 (2002).

54. uer-Grumbach, M. *et al.* Alterations in the ankyrin domain of TRPV4 cause congenital distal SMA, scapuloperoneal SMA and HMSN2C. *Nat. Genet.* **42**, 160-164 (2010).

55. Kaneko, Y. & Szallasi, A. Transient receptor potential (TRP) channels: a clinical perspective. *Br. J. Pharmacol.* **171**, 2474-2507 (2014).

56. Desai, B. N. & Clapham, D. E. TRP channels and mice deficient in TRP channels. *Pflugers Arch.* **451**, 11-18 (2005).

57. Wilson, P. D. Polycystic kidney disease. *N. Engl. J. Med.* **350**, 151-164 (2004).

58. Gabow, P. A. Autosomal dominant polycystic kidney disease. *N. Engl. J. Med.* **329**, 332-342 (1993).

59. Gabow, P. A. Autosomal dominant polycystic kidney disease--more than a renal disease. *Am. J. Kidney Dis.* **16**, 403-413 (1990).

60. Mochizuki, T. *et al.* PKD2, a gene for polycystic kidney disease that encodes an integral membrane protein. *Science* **272**, 1339-1342 (1996).

61. The polycystic kidney disease 1 gene encodes a 14 kb transcript and lies within a duplicated region on chromosome 16. The European Polycystic Kidney Disease Consortium. *Cell* **78**, 725 (1994).

62. Peters, D. J. & Sandkuijl, L. A. Genetic heterogeneity of polycystic kidney disease in Europe. *Contrib. Nephrol.* **97**, 128-139 (1992).

63. Tan, Y. C., Blumenfeld, J. & Rennert, H. Autosomal dominant polycystic kidney disease: genetics, mutations and microRNAs. *Biochim. Biophys. Acta* **1812**, 1202-1212 (2011).

64. Nims, N., Vassmer, D. & Maser, R. L. Transmembrane domain analysis of polycystin-1, the product of the polycystic kidney disease-1 (PKD1) gene: evidence for 11 membrane-spanning domains. *Biochemistry* **42**, 13035-13048 (2003).

65. Qian, F. *et al.* Cleavage of polycystin-1 requires the receptor for egg jelly domain and is disrupted by human autosomal-dominant polycystic kidney disease 1-associated mutations. *Proc. Natl. Acad. Sci. U. S. A* **99**, 16981-16986 (2002).

66. Qian, F. *et al.* PKD1 interacts with PKD2 through a probable coiled-coil domain. *Nat. Genet.* **16**, 179-183 (1997).

67. Lal, M. *et al.* Polycystin-1 C-terminal tail associates with beta-catenin and inhibits canonical Wnt signaling. *Hum. Mol. Genet.* **17**, 3105-3117 (2008).

68. Low, S. H. *et al.* Polycystin-1, STAT6, and P100 function in a pathway that transduces ciliary mechanosensation and is activated in polycystic kidney disease. *Dev. Cell* **10**, 57-69 (2006).

69. Vassilev, P. M. *et al.* Polycystin-2 is a novel cation channel implicated in defective intracellular Ca(2+) homeostasis in polycystic kidney disease. *Biochem. Biophys. Res. Commun.* **282**, 341-350 (2001).

70. Koulen, P. *et al.* Polycystin-2 is an intracellular calcium release channel. *Nat. Cell Biol.* **4**, 191-197 (2002).

71. Torres, V. E. & Harris, P. C. Autosomal dominant polycystic kidney disease: the last 3 years. *Kidney Int.* **76**, 149-168 (2009).

72. Foggensteiner, L. *et al.* Cellular and subcellular distribution of polycystin-2, the protein product of the PKD2 gene. *J. Am. Soc. Nephrol.* **11**, 814-827 (2000).

73. Ong, A. C. *et al.* Coordinate expression of the autosomal dominant polycystic kidney disease proteins, polycystin-2 and polycystin-1, in normal and cystic tissue. *Am. J. Pathol.* **154**, 1721-1729 (1999).

74. Cai, Y. *et al.* Identification and characterization of polycystin-2, the PKD2 gene product. *J. Biol. Chem.* **274**, 28557-28565 (1999).

75. Wilson, P. D., Geng, L., Li, X. & Burrow, C. R. The PKD1 gene product, "polycystin-1," is a tyrosine-phosphorylated protein that colocalizes with alpha2beta1-integrin in focal clusters in adherent renal epithelia. *Lab Invest* **79**, 1311-1323 (1999).

76. Yoder, B. K., Hou, X. & Guay-Woodford, L. M. The polycystic kidney disease proteins, polycystin-1, polycystin-2, polaris, and cystin, are co-localized in renal cilia. *J. Am. Soc. Nephrol.* **13**, 2508-2516 (2002).

77. Pazour, G. J., San Agustin, J. T., Follit, J. A., Rosenbaum, J. L. & Witman, G. B. Polycystin-2 localizes to kidney cilia and the ciliary level is elevated in orpk mice with polycystic kidney disease. *Curr. Biol.* **12**, R378-R380 (2002).

78. Nauli, S. M. *et al.* Polycystins 1 and 2 mediate mechanosensation in the primary cilium of kidney cells. *Nat. Genet.* **33**, 129-137 (2003).

79. Ong, A. C. & Wheatley, D. N. Polycystic kidney disease--the ciliary connection. *Lancet* **361**, 774-776 (2003).

80. Raj, A., Rifkin, S. A., Andersen, E. & van, O. A. Variability in gene expression underlies incomplete penetrance. *Nature* **463**, 913-918 (2010).

81. Ong, A. C. *et al.* Polycystin-1 expression in PKD1, early-onset PKD1, and TSC2/PKD1 cystic tissue. *Kidney Int.* **56**, 1324-1333 (1999).

82. Qian, F., Watnick, T. J., Onuchic, L. F. & Germino, G. G. The molecular basis of focal cyst formation in human autosomal dominant polycystic kidney disease type I. *Cell* **87**, 979-987 (1996).

83. Cornec-Le, G. E., Audrezet, M. P., Le, M. Y., Chen, J. M. & Ferec, C. Genetics and pathogenesis of autosomal dominant polycystic kidney disease: 20 years on. *Hum. Mutat.* **35**, 1393-1406 (2014).

84. Koptides, M., Hadjimichael, C., Koupepidou, P., Pierides, A. & Constantinou, D. C. Germinal and somatic mutations in the PKD2 gene of renal cysts in autosomal dominant polycystic kidney disease. *Hum. Mol. Genet.* **8**, 509-513 (1999).

85. Brasier, J. L. & Henske, E. P. Loss of the polycystic kidney disease (PKD1) region of chromosome 16p13 in renal cyst cells supports a loss-of-function model for cyst pathogenesis. *J. Clin. Invest* **99**, 194-199 (1997).

86. Pei, Y. *et al.* Somatic PKD2 mutations in individual kidney and liver cysts support a "two-hit" model of cystogenesis in type 2 autosomal dominant polycystic kidney disease. *J. Am. Soc. Nephrol.* **10**, 1524-1529 (1999).

87. Jiang, S. T. *et al.* Defining a link with autosomal-dominant polycystic kidney disease in mice with congenitally low expression of Pkd1. *Am. J. Pathol.* **168**, 205-220 (2006).

88. Lantinga-van, L., I *et al.* Lowering of Pkd1 expression is sufficient to cause polycystic kidney disease. *Hum. Mol. Genet.* **13**, 3069-3077 (2004).

89. Kim, I. *et al.* Polycystin-2 expression is regulated by a PC2-binding domain in the intracellular portion of fibrocystin. *J. Biol. Chem.* **283**, 31559-31566 (2008).

90. Fedeles, S. V. *et al.* A genetic interaction network of five genes for human polycystic kidney and liver diseases defines polycystin-1 as the central determinant of cyst formation. *Nat. Genet.* **43**, 639-647 (2011).

91. Raphael, K. L. *et al.* Inactivation of Pkd1 in principal cells causes a more severe cystic kidney disease than in intercalated cells. *Kidney Int.* **75**, 626-633 (2009).

92. Piontek, K., Menezes, L. F., Garcia-Gonzalez, M. A., Huso, D. L. & Germino, G. G. A critical developmental switch defines the kinetics of kidney cyst formation after loss of Pkd1. *Nat. Med.* **13**, 1490-1495 (2007).

93. Hopp, K. *et al.* Functional polycystin-1 dosage governs autosomal dominant polycystic kidney disease severity. *J. Clin. Invest* **122**, 4257-4273 (2012).

94. Happe, H. & Peters, D. J. Translational research in ADPKD: lessons from animal models. *Nat. Rev. Nephrol.* **10**, 587-601 (2014).

95. Lanoix, J., D'Agati, V., Szabolcs, M. & Trudel, M. Dysregulation of cellular proliferation and apoptosis mediates human autosomal dominant polycystic kidney disease (ADPKD). *Oncogene* **13**, 1153-1160 (1996).

96. Woo, D. Apoptosis and loss of renal tissue in polycystic kidney diseases. *N. Engl. J. Med.* **333**, 18-25 (1995).

97. Nadasdy, T. *et al.* Proliferative activity of cyst epithelium in human renal cystic diseases. *J. Am. Soc. Nephrol.* **5**, 1462-1468 (1995).

98. Harris, P. C. & Torres, V. E. Polycystic kidney disease. *Annu. Rev. Med.* **60**, 321-337 (2009).

99. Shillingford, J. M. *et al.* The mTOR pathway is regulated by polycystin-1, and its inhibition reverses renal cystogenesis in polycystic kidney disease. *Proc. Natl. Acad. Sci. U. S. A* **103**, 5466-5471 (2006).

100. Boca, M. *et al.* Polycystin-1 induces resistance to apoptosis through the phosphatidylinositol 3-kinase/Akt signaling pathway. *J. Am. Soc. Nephrol.* **17**, 637-647 (2006).

101. Yamaguchi, T. *et al.* Cyclic AMP activates B-Raf and ERK in cyst epithelial cells from autosomal-dominant polycystic kidneys. *Kidney Int.* **63**, 1983-1994 (2003).

102. Bhunia, A. K. *et al.* PKD1 induces p21(waf1) and regulation of the cell cycle via direct activation of the JAK-STAT signaling pathway in a process requiring PKD2. *Cell* **109**, 157-168 (2002).

103. Arnould, T. *et al.* The polycystic kidney disease 1 gene product mediates protein kinase C alpha-dependent and c-Jun N-terminal kinase-dependent activation of the transcription factor AP-1. *J. Biol. Chem.* **273**, 6013-6018 (1998).

104. Markowitz, G. S. *et al.* Polycystin-2 expression is developmentally regulated. *Am. J. Physiol.* **277**, F17-F25 (1999).

105. Obermuller, N. *et al.* Altered expression pattern of polycystin-2 in acute and chronic renal tubular diseases. *J. Am. Soc. Nephrol.* **13**, 1855-1864 (2002).

106. Zhao, Y., Haylor, J. L. & Ong, A. C. Polycystin-2 expression is increased following experimental ischaemic renal injury. *Nephrol. Dial. Transplant.* **17**, 2138-2144 (2002).

107. Prasad, S., McDaid, J. P., Tam, F. W., Haylor, J. L. & Ong, A. C. Pkd2 dosage influences cellular repair responses following ischemia-reperfusion injury. *Am. J. Pathol.* **175**, 1493-1503 (2009).

108. Lantinga-van, L., I *et al.* Common regulatory elements in the polycystic kidney disease 1 and 2 promoter regions. *Eur. J. Hum. Genet.* **13**, 649-659 (2005).

109. Sun, H. *et al.* MicroRNA-17 post-transcriptionally regulates polycystic kidney disease-2 gene and promotes cell proliferation. *Mol. Biol. Rep.* **37**, 2951-2958 (2010).

110. Patel, V. *et al.* miR-17~92 miRNA cluster promotes kidney cyst growth in polycystic kidney disease. *Proc. Natl. Acad. Sci. U. S. A* **110**, 10765-10770 (2013).

111. Tran, U. *et al.* The RNA-binding protein bicaudal C regulates polycystin 2 in the kidney by antagonizing miR-17 activity. *Development.* **137**, 1107-1116 (2010).

112. Araujo, P. R. *et al.* Before It Gets Started: Regulating Translation at the 5' UTR. *Comp. Funct. Genomics.* **2012:475731. Epub@2012 May 28.**, 475731 (2012).

113. Gebauer, F. & Hentze, M. W. Molecular mechanisms of translational control. *Nat. Rev. Mol. Cell Biol.* **5**, 827-835 (2004).

114. Sonenberg, N. & Hinnebusch, A. G. Regulation of translation initiation in eukaryotes: mechanisms and biological targets. *Cell.* **136**, 731-745 (2009).

115. Jackson, R. J., Hellen, C. U. & Pestova, T. V. The mechanism of eukaryotic translation initiation and principles of its regulation. *Nat. Rev. Mol. Cell Biol.* **11**, 113-127 (2010).

116. Conne, B., Stutz, A. & Vassalli, J. D. The 3' untranslated region of messenger RNA: A molecular 'hotspot' for pathology? *Nat. Med.* **6**, 637-641 (2000).

117. Pesole, G. *et al.* Structural and functional features of eukaryotic mRNA untranslated regions. *Gene.* **276**, 73-81 (2001).

118. Matsui, M., Yachie, N., Okada, Y., Saito, R. & Tomita, M. Bioinformatic analysis of post-transcriptional regulation by uORF in human and mouse. *FEBS. Lett.* **581**, 4184-4188 (2007).

119. Vogel, C. *et al.* Sequence signatures and mRNA concentration can explain two-thirds of protein abundance variation in a human cell line. *Mol. Syst. Biol.* **6:400.**, 400 (2010).

120. Calvo, S. E., Pagliarini, D. J. & Mootha, V. K. Upstream open reading frames cause widespread reduction of protein expression and are polymorphic among humans. *Proc. Natl. Acad. Sci. U. S. A.* **106**, 7507-7512 (2009).

121. Mueller, P. P. & Hinnebusch, A. G. Multiple upstream AUG codons mediate translational control of GCN4. *Cell.* **45**, 201-207 (1986).

122. Hinnebusch, A. G. Translational regulation of GCN4 and the general amino acid control of yeast. *Annu. Rev. Microbiol.* **59:407-50.**, 407-450 (2005).

123. Lohse, I., Reilly, P. & Zaugg, K. The CPT1C 5'UTR contains a repressing upstream open reading frame that is regulated by cellular energy availability and AMPK. *PLoS. One.* **6**, e21486 (2011).

124. Lee, Y. Y., Cevallos, R. C. & Jan, E. An upstream open reading frame regulates translation of GADD34 during cellular stresses that induce eIF2alpha phosphorylation. *J. Biol. Chem.* **284**, 6661-6673 (2009).

125. Palam, L. R., Baird, T. D. & Wek, R. C. Phosphorylation of eIF2 facilitates ribosomal bypass of an inhibitory upstream ORF to enhance CHOP translation. *J. Biol. Chem.* **286**, 10939-10949 (2011).

126. Vattem, K. M. & Wek, R. C. Reinitiation involving upstream ORFs regulates ATF4 mRNA translation in mammalian cells. *Proc. Natl. Acad. Sci. U. S. A* **101**, 11269-11274 (2004).

127. Holcik, M. & Sonenberg, N. Translational control in stress and apoptosis. *Nat. Rev. Mol. Cell Biol.* **6**, 318-327 (2005).

128. Gallie, D. R. A tale of two termini: a functional interaction between the termini of an mRNA is a prerequisite for efficient translation initiation. *Gene.* **216**, 1-11 (1998).

129. Varani, G. Delivering messages from the 3' end. *Proc. Natl. Acad. Sci. U. S. A.* **98**, 4288-4289 (2001).

130. Gingras, A. C., Raught, B. & Sonenberg, N. eIF4 initiation factors: effectors of mRNA recruitment to ribosomes and regulators of translation. *Annu. Rev. Biochem.* **68:913-63.**, 913-963 (1999).

131. Mazumder, B. & Fox, P. L. Delayed translational silencing of ceruloplasmin transcript in gamma interferon-activated U937 monocytic cells: role of the 3' untranslated region. *Mol. Cell Biol.* **19**, 6898-6905 (1999).

132. Mazumder, B., Seshadri, V., Imataka, H., Sonenberg, N. & Fox, P. L. Translational silencing of ceruloplasmin requires the essential elements of mRNA circularization:

poly(A) tail, poly(A)-binding protein, and eukaryotic translation initiation factor 4G. *Mol. Cell Biol.* **21**, 6440-6449 (2001).

133. Ostareck, D. H., Ostareck-Lederer, A., Shatsky, I. N. & Hentze, M. W. Lipoxygenase mRNA silencing in erythroid differentiation: The 3'UTR regulatory complex controls 60S ribosomal subunit joining. *Cell.* **104**, 281-290 (2001).

134. Ostareck, D. H. *et al.* mRNA silencing in erythroid differentiation: hnRNP K and hnRNP E1 regulate 15-lipoxygenase translation from the 3' end. *Cell.* **89**, 597-606 (1997).

135. Kong, J. & Lasko, P. Translational control in cellular and developmental processes. *Nat. Rev. Genet.* **13**, 383-394 (2012).

136. Schroder, M. & Kaufman, R. J. ER stress and the unfolded protein response. *Mutat. Res.* **569**, 29-63 (2005).

137. Fewell, S. W., Travers, K. J., Weissman, J. S. & Brodsky, J. L. The action of molecular chaperones in the early secretory pathway. *Annu. Rev. Genet.* **35**, 149-191 (2001).

138. Kornfeld, R. & Kornfeld, S. Assembly of asparagine-linked oligosaccharides. *Annu. Rev. Biochem.* **54**, 631-664 (1985).

139. Ellgaard, L., Molinari, M. & Helenius, A. Setting the standards: quality control in the secretory pathway. *Science* **286**, 1882-1888 (1999).

140. Shen, X., Zhang, K. & Kaufman, R. J. The unfolded protein response--a stress signaling pathway of the endoplasmic reticulum. *J. Chem. Neuroanat.* **28**, 79-92 (2004).

141. Schroder, M. & Kaufman, R. J. The mammalian unfolded protein response. *Annu. Rev. Biochem.* **74**, 739-789 (2005).

142. Wang, S. & Kaufman, R. J. The impact of the unfolded protein response on human disease. *J. Cell Biol.* **197**, 857-867 (2012).

143. Doyle, K. M. *et al.* Unfolded proteins and endoplasmic reticulum stress in neurodegenerative disorders. *J. Cell Mol. Med.* **15**, 2025-2039 (2011).

144. Dickhout, J. G., Carlisle, R. E. & Austin, R. C. Interrelationship between cardiac hypertrophy, heart failure, and chronic kidney disease: endoplasmic reticulum stress as a mediator of pathogenesis. *Circ. Res.* **108**, 629-642 (2011).

145. Kitamura, M. Endoplasmic reticulum stress and unfolded protein response in renal pathophysiology: Janus faces. *Am. J. Physiol Renal Physiol* **295**, F323-F334 (2008).

146. Minamino, T. & Kitakaze, M. ER stress in cardiovascular disease. *J. Mol. Cell Cardiol.* **48**, 1105-1110 (2010).

147. Ron, D. & Walter, P. Signal integration in the endoplasmic reticulum unfolded protein response. *Nat. Rev. Mol. Cell Biol.* **8**, 519-529 (2007).

148. Bertolotti, A., Zhang, Y., Hendershot, L. M., Harding, H. P. & Ron, D. Dynamic interaction of BiP and ER stress transducers in the unfolded-protein response. *Nat. Cell Biol.* **2**, 326-332 (2000).

149. Scheuner, D. & Kaufman, R. J. The unfolded protein response: a pathway that links insulin demand with beta-cell failure and diabetes. *Endocr. Rev.* **29**, 317-333 (2008).

150. Harding, H. P., Zhang, Y., Bertolotti, A., Zeng, H. & Ron, D. Perk is essential for translational regulation and cell survival during the unfolded protein response. *Mol. Cell* **5**, 897-904 (2000).

151. Ron, D. Translational control in the endoplasmic reticulum stress response. *J. Clin. Invest* **110**, 1383-1388 (2002).

152. Harding, H. P., Zhang, Y. & Ron, D. Protein translation and folding are coupled by an endoplasmic-reticulum-resident kinase. *Nature* **397**, 271-274 (1999).

153. Wang, X. Z. *et al.* Cloning of mammalian Ire1 reveals diversity in the ER stress responses. *EMBO J.* **17**, 5708-5717 (1998).

154. Tirasophon, W., Welihinda, A. A. & Kaufman, R. J. A stress response pathway from the endoplasmic reticulum to the nucleus requires a novel bifunctional protein kinase/endoribonuclease (Ire1p) in mammalian cells. *Genes Dev.* **12**, 1812-1824 (1998).

155. Yoshida, H., Matsui, T., Yamamoto, A., Okada, T. & Mori, K. XBP1 mRNA is induced by ATF6 and spliced by IRE1 in response to ER stress to produce a highly active transcription factor. *Cell* **107**, 881-891 (2001).

156. Haze, K., Yoshida, H., Yanagi, H., Yura, T. & Mori, K. Mammalian transcription factor ATF6 is synthesized as a transmembrane protein and activated by proteolysis in response to endoplasmic reticulum stress. *Mol. Biol. Cell* **10**, 3787-3799 (1999).

157. Cao, S. S. & Kaufman, R. J. Unfolded protein response. *Curr. Biol.* **22**, R622-R626 (2012).

158. Nishitoh, H. *et al.* ASK1 is essential for endoplasmic reticulum stress-induced neuronal cell death triggered by expanded polyglutamine repeats. *Genes Dev.* **16**, 1345-1355 (2002).

159. Urano, F. *et al.* Coupling of stress in the ER to activation of JNK protein kinases by transmembrane protein kinase IRE1. *Science* **287**, 664-666 (2000).

160. Ron, D. & Walter, P. Signal integration in the endoplasmic reticulum unfolded protein response. *Nat. Rev. Mol. Cell Biol.* **8**, 519-529 (2007).

161. Kaufman, R. J. Orchestrating the unfolded protein response in health and disease. *J. Clin. Invest* **110**, 1389-1398 (2002).

162. vis-Smyth, T., Duncan, R. C., Zheng, T., Michelotti, G. & Levens, D. The far upstream element-binding proteins comprise an ancient family of single-strand DNA-binding transactivators. *J. Biol. Chem.* **271**, 31679-31687 (1996).

163. Weber, A. *et al.* The FUSE binding proteins FBP1 and FBP3 are potential c-myc regulators in renal, but not in prostate and bladder cancer. *BMC. Cancer* **8**, 369 (2008).

164. Lu, J. Y. & Schneider, R. J. Tissue distribution of AU-rich mRNA-binding proteins involved in regulation of mRNA decay. *J. Biol. Chem.* **279**, 12974-12979 (2004).

165. Duncan, R. *et al.* A sequence-specific, single-strand binding protein activates the far upstream element of c-myc and defines a new DNA-binding motif. *Genes Dev.* **8**, 465-480 (1994).

166. Zhang, J. & Chen, Q. M. Far upstream element binding protein 1: a commander of transcription, translation and beyond. *Oncogene* **32**, 2907-2916 (2013).

167. Irwin, N., Baekelandt, V., Goritchenko, L. & Benowitz, L. I. Identification of two proteins that bind to a pyrimidine-rich sequence in the 3'-untranslated region of GAP-43 mRNA. *Nucleic Acids Res.* **25**, 1281-1288 (1997).

168. Bettegowda, C. *et al.* Mutations in CIC and FUBP1 contribute to human oligodendroglioma. *Science* **333**, 1453-1455 (2011).

169. Rabenhorst, U. *et al.* Overexpression of the far upstream element binding protein 1 in hepatocellular carcinoma is required for tumor growth. *Hepatology* **50**, 1121-1129 (2009).

170. Malz, M. *et al.* Overexpression of far upstream element binding proteins: a mechanism regulating proliferation and migration in liver cancer cells. *Hepatology* **50**, 1130-1139 (2009).

171. Zubaidah, R. M. *et al.* 2-D DIGE profiling of hepatocellular carcinoma tissues identified isoforms of far upstream binding protein (FUBP) as novel candidates in liver carcinogenesis. *Proteomics.* **8**, 5086-5096 (2008).

172. Kim, M. J. *et al.* Downregulation of FUSE-binding protein and c-myc by tRNA synthetase cofactor p38 is required for lung cell differentiation. *Nat. Genet.* **34**, 330-336 (2003).

173. Williams, B. Y., Hamilton, S. L. & Sarkar, H. K. The survival motor neuron protein interacts with the transactivator FUSE binding protein from human fetal brain. *FEBS Lett.* **470**, 207-210 (2000).

174. Liu, J. *et al.* The FUSE/FBP/FIR/TFIIH system is a molecular machine programming a pulse of c-myc expression. *EMBO J.* **25**, 2119-2130 (2006).

175. Braddock, D. T., Louis, J. M., Baber, J. L., Levens, D. & Clore, G. M. Structure and dynamics of KH domains from FBP bound to single-stranded DNA. *Nature* **415**, 1051-1056 (2002).

176. Benjamin, L. R. *et al.* Hierarchical mechanisms build the DNA-binding specificity of FUSE binding protein. *Proc. Natl. Acad. Sci. U. S. A* **105**, 18296-18301 (2008).

177. Liu, J. *et al.* The FBP interacting repressor targets TFIIH to inhibit activated transcription. *Mol. Cell* **5**, 331-341 (2000).

178. Valverde, R., Edwards, L. & Regan, L. Structure and function of KH domains. *FEBS J.* **275**, 2712-2726 (2008).

179. Kusik, B. W., Hammond, D. R. & Udvadia, A. J. Transcriptional regulatory regions of gap43 needed in developing and regenerating retinal ganglion cells. *Dev. Dyn.* **239**, 482-495 (2010).

180. Nishizawa, K. & Okamoto, H. Mutation analysis of the role for the carboxy-terminus encoding region in NGF-induced stabilization of GAP-43 mRNA. *Biochem. Biophys. Res. Commun.* **205**, 1380-1385 (1994).

181. Colombo, E., Alcalay, M. & Pelicci, P. G. Nucleophosmin and its complex network: a possible therapeutic target in hematological diseases. *Oncogene* **30**, 2595-2609 (2011).

182. Grisendi, S. *et al.* Role of nucleophosmin in embryonic development and tumorigenesis. *Nature* **437**, 147-153 (2005).

183. Olanich, M. E., Moss, B. L., Piwnica-Worms, D., Townsend, R. R. & Weber, J. D. Identification of FUSE-binding protein 1 as a regulatory mRNA-binding protein that represses nucleophosmin translation. *Oncogene* **30**, 77-86 (2011).

184. Chien, H. L., Liao, C. L. & Lin, Y. L. FUSE binding protein 1 interacts with untranslated regions of Japanese encephalitis virus RNA and negatively regulates viral replication. *J. Virol.* **85**, 4698-4706 (2011).

185. Molland, K. L., Paul, L. N. & Yernool, D. A. Crystal structure and characterization of coiled-coil domain of the transient receptor potential channel PKD2L1. *Biochim. Biophys. Acta.* **1824**, 413-421 (2012).

186. Molland, K. L., Narayanan, A., Burgner, J. W. & Yernool, D. A. Identification of the structural motif responsible for trimeric assembly of the C-terminal regulatory domains of polycystin channels PKD2L1 and PKD2. *Biochem. J.* **429**, 171-183 (2010).

187. Li, Q., Liu, Y., Zhao, W. & Chen, X. Z. The calcium-binding EF-hand in polycystin-L is not a domain for channel activation and ensuing inactivation. *FEBS Lett.* **516**, 270-278 (2002).

188. Chen, X. Z. *et al.* Polycystin-L is a calcium-regulated cation channel permeable to calcium ions. *Nature.* **401**, 383-386 (1999).

189. Inada, H. *et al.* Off-response property of an acid-activated cation channel complex PKD1L3-PKD2L1. *EMBO Rep.* **9**, 690-697 (2008).

190. Ishimaru, Y. *et al.* Transient receptor potential family members PKD1L3 and PKD2L1 form a candidate sour taste receptor. *Proc. Natl. Acad. Sci. U. S. A.* **103**, 12569-12574 (2006).

191. Horio, N. *et al.* Sour taste responses in mice lacking PKD channels. *PLoS. One.* **6**, e20007 (2011).

192. Nelson, T. M. *et al.* Taste function in mice with a targeted mutation of the pkd1l3 gene. *Chem. Senses.* **35**, 565-577 (2010).

193. Fujimoto, C. *et al.* The single pore residue Asp523 in PKD2L1 determines Ca2+ permeation of the PKD1L3/PKD2L1 complex. *Biochem. Biophys. Res. Commun.* **404**, 946-951 (2011).

194. Yu, Y. *et al.* Molecular mechanism of the assembly of an acid-sensing receptor ion channel complex. *Nat. Commun.* **3**, 1252 (2012).

195. Li, Q. *et al.* Direct binding of alpha-actinin enhances TRPP3 channel activity. *J. Neurochem.* **103**, 2391-2400 (2007).

196. Basora, N. *et al.* Tissue and cellular localization of a novel polycystic kidney disease-like gene product, polycystin-L. *J. Am. Soc. Nephrol.* **13**, 293-301 (2002).

197. Lopezjimenez, N. D. *et al.* Two members of the TRPP family of ion channels, Pkd1l3 and Pkd2l1, are co-expressed in a subset of taste receptor cells. *J. Neurochem.* **98**, 68-77 (2006).

198. Huang, A. L. *et al.* The cells and logic for mammalian sour taste detection. *Nature.* **442**, 934-938 (2006).

199. Huque, T. *et al.* Sour ageusia in two individuals implicates ion channels of the ASIC and PKD families in human sour taste perception at the anterior tongue. *PLoS. One.* **4**, e7347 (2009).

200. Hussein, S. *et al.* Acid-induced off-response of PKD2L1 channel in Xenopus oocytes and its regulation by Ca(2.). *Sci. Rep.* **5**, 15752 (2015).

201. Yu, Y. *et al.* Structural and molecular basis of the assembly of the TRPP2/PKD1 complex. *Proc. Natl. Acad. Sci. U. S. A.* **106**, 11558-11563 (2009).

202. Ong, A. C. & Harris, P. C. A polycystin-centric view of cyst formation and disease: the polycystins revisited. *Kidney Int.* 10 (2015).

203. Ishimaru, Y. *et al.* Interaction between PKD1L3 and PKD2L1 through their transmembrane domains is required for localization of PKD2L1 at taste pores in taste cells of circumvallate and foliate papillae. *FASEB J.* **24**, 4058-4067 (2010).

204. Fukata, Y. & Fukata, M. Protein palmitoylation in neuronal development and synaptic plasticity. *Nat. Rev. Neurosci.* **11**, 161-175 (2010).

205. Baekkeskov, S. & Kanaani, J. Palmitoylation cycles and regulation of protein function (Review). *Mol. Membr. Biol.* **26**, 42-54 (2009).

206. Linder, M. E. & Deschenes, R. J. Palmitoylation: policing protein stability and traffic. *Nat. Rev. Mol. Cell Biol.* **8**, 74-84 (2007).

207. el-Husseini, A. & Bredt, D. S. Protein palmitoylation: a regulator of neuronal development and function. *Nat. Rev. Neurosci.* **3**, 791-802 (2002).

208. Yeste-Velasco, M., Linder, M. E. & Lu, Y. J. Protein S-palmitoylation and cancer. *Biochim. Biophys. Acta.* **1856**, 107-120 (2015).

209. Raymond, F. L. *et al.* Mutations in ZDHHC9, which encodes a palmitoyltransferase of NRAS and HRAS, cause X-linked mental retardation associated with a Marfanoid habitus. *Am. J. Hum. Genet.* **80**, 982-987 (2007).

210. Blaskovic, S., Blanc, M. & van der Goot, F. G. What does S-palmitoylation do to membrane proteins? *FEBS J.* **280**, 2766-2774 (2013).

211. Shipston, M. J. Ion channel regulation by protein S-acylation. *J. Gen. Physiol.* **143**, 659-678 (2014).

212. Roth, A. F. *et al.* Global analysis of protein palmitoylation in yeast. *Cell* **125**, 1003-1013 (2006).

213. Nadolski, M. J. & Linder, M. E. Molecular recognition of the palmitoylation substrate Vac8 by its palmitoyltransferase Pfa3. *J. Biol. Chem.* **284**, 17720-17730 (2009).

214. Varner, A. S. *et al.* Characterization of human palmitoyl-acyl transferase activity using peptides that mimic distinct palmitoylation motifs. *Biochem. J.* **373**, 91-99 (2003).

215. Ohno, Y., Kihara, A., Sano, T. & Igarashi, Y. Intracellular localization and tissue-specific distribution of human and yeast DHHC cysteine-rich domain-containing proteins. *Biochim. Biophys. Acta* **1761**, 474-483 (2006).

216. Tomatis, V. M., Trenchi, A., Gomez, G. A. & Daniotti, J. L. Acyl-protein thioesterase 2 catalyzes the deacylation of peripheral membrane-associated GAP-43. *PLoS. One.* **5**, e15045 (2010).

217. Zeidman, R., Jackson, C. S. & Magee, A. I. Protein acyl thioesterases (Review). *Mol. Membr. Biol.* **26**, 32-41 (2009).

218. Siegel, G. *et al.* A functional screen implicates microRNA-138-dependent regulation of the depalmitoylation enzyme APT1 in dendritic spine morphogenesis. *Nat. Cell Biol.* **11**, 705-716 (2009).

219. Duncan, J. A. & Gilman, A. G. A cytoplasmic acyl-protein thioesterase that removes palmitate from G protein alpha subunits and p21(RAS). *J. Biol. Chem.* **273**, 15830-15837 (1998).

220. Rusch, M. *et al.* Identification of acyl protein thioesterases 1 and 2 as the cellular targets of the Ras-signaling modulators palmostatin B and M. *Angew. Chem. Int. Ed Engl.* **50**, 9838-9842 (2011).

221. Tian, L., McClafferty, H., Knaus, H. G., Ruth, P. & Shipston, M. J. Distinct acyl protein transferases and thioesterases control surface expression of calcium-activated potassium channels. *J. Biol. Chem.* **287**, 14718-14725 (2012).

222. Schmidt, J. W. & Catterall, W. A. Palmitylation, sulfation, and glycosylation of the alpha subunit of the sodium channel. Role of post-translational modifications in channel assembly. *J. Biol. Chem.* **262**, 13713-13723 (1987).

223. Rasaiah, J. C., Garde, S. & Hummer, G. Water in nonpolar confinement: from nanotubes to proteins and beyond. *Annu. Rev. Phys. Chem.* **59**, 713-740 (2008).

224. Beckstein, O. & Sansom, M. S. Liquid-vapor oscillations of water in hydrophobic nanopores. *Proc. Natl. Acad. Sci. U. S. A* **100**, 7063-7068 (2003).

225. Hummer, G., Rasaiah, J. C. & Noworyta, J. P. Water conduction through the hydrophobic channel of a carbon nanotube. *Nature* **414**, 188-190 (2001).

226. Aryal, P., Sansom, M. S. & Tucker, S. J. Hydrophobic gating in ion channels. *J. Mol. Biol.* **427**, 121-130 (2015).

227. Bass, R. B., Strop, P., Barclay, M. & Rees, D. C. Crystal structure of Escherichia coli MscS, a voltage-modulated and mechanosensitive channel. *Science* **298**, 1582-1587 (2002).

228. Wang, W. *et al.* The structure of an open form of an E. coli mechanosensitive channel at 3.45 A resolution. *Science* **321**, 1179-1183 (2008).

229. Jeon, J. P. *et al.* Activation of TRPC4beta by Galphai subunit increases Ca2+ selectivity and controls neurite morphogenesis in cultured hippocampal neuron. *Cell Calcium* **54**, 307-319 (2013).

230. Yeh, B. I., Kim, Y. K., Jabbar, W. & Huang, C. L. Conformational changes of pore helix coupled to gating of TRPV5 by protons. *EMBO J.* **24**, 3224-3234 (2005).

231. Chen, J. *et al.* Pore dilation occurs in TRPA1 but not in TRPM8 channels. *Mol. Pain* **5**, 3 (2009).

232. Gees, M., Colsoul, B. & Nilius, B. The role of transient receptor potential cation channels in Ca2+ signaling. *Cold Spring Harb. Perspect. Biol.* **2**, a003962 (2010).

233. Chung, M. K., Guler, A. D. & Caterina, M. J. TRPV1 shows dynamic ionic selectivity during agonist stimulation. *Nat. Neurosci.* **11**, 555-564 (2008).

234. Aryal, P., bd-Wahab, F., Bucci, G., Sansom, M. S. & Tucker, S. J. A hydrophobic barrier deep within the inner pore of the TWIK-1 K2P potassium channel. *Nat. Commun.* **5**, 4377 (2014).

235. Yoshimura, K., Batiza, A., Schroeder, M., Blount, P. & Kung, C. Hydrophilicity of a single residue within MscL correlates with increased channel mechanosensitivity. *Biophys. J.* **77**, 1960-1972 (1999).

236. Ou, X., Blount, P., Hoffman, R. J. & Kung, C. One face of a transmembrane helix is crucial in mechanosensitive channel gating. *Proc. Natl. Acad. Sci. U. S. A* **95**, 11471-11475 (1998).

237. Reeders, S. T. Multilocus polycystic disease. *Nat. Genet.* **1**, 235-237 (1992).

238. Matsui, Y. *et al.* Molecular mechanisms and physiological significance of autophagy during myocardial ischemia and reperfusion. *Autophagy.* **4**, 409-415 (2008).

239. Liang, G. *et al.* Polycystin-2 is regulated by endoplasmic reticulum-associated degradation. *Hum. Mol. Genet.* **17**, 1109-1119 (2008).

240. Li, X. *et al.* A tumor necrosis factor-alpha-mediated pathway promoting autosomal dominant polycystic kidney disease. *Nat. Med.* 14, 863-868 (2008).

241. Voolstra, O. & Huber, A. Post-Translational Modifications of TRP Channels. *Cells* 3, 258-287 (2014).

242. Cai, Y. *et al.* Calcium dependence of polycystin-2 channel activity is modulated by phosphorylation at Ser812. *J. Biol. Chem.* 279, 19987-19995 (2004).

243. Streets, A. J., Moon, D. J., Kane, M. E., Obara, T. & Ong, A. C. Identification of an N-terminal glycogen synthase kinase 3 phosphorylation site which regulates the functional localization of polycystin-2 in vivo and in vitro. *Hum. Mol. Genet.* 15, 1465-1473 (2006).

244. Miura, S., Sato, K., Kato-Negishi, M., Teshima, T. & Takeuchi, S. Fluid shear triggers microvilli formation via mechanosensitive activation of TRPV6. *Nat. Commun.* 6, 8871 (2015).

245. DeCaen, P. G., Delling, M., Vien, T. N. & Clapham, D. E. Direct recording and molecular identification of the calcium channel of primary cilia. *Nature.* 504, 315-318 (2013).

246. Delling, M., DeCaen, P. G., Doerner, J. F., Febvay, S. & Clapham, D. E. Primary cilia are specialized calcium signalling organelles. *Nature* 504, 311-314 (2013).

247. Shimizu, T., Janssens, A., Voets, T. & Nilius, B. Regulation of the murine TRPP3 channel by voltage, pH, and changes in cell volume. *Pflugers Arch.* 457, 795-807 (2009).